# RADICAL-SAM ENZYMES WITH TWO IRON-SULFUR CLUSTERS: COFACTOR COMPOSITION AND SPECTROSCOPIC STUDIES OF *ESCHERICHIA COLI* AND *BACILLUS SUBTILIS* BIOTIN SYNTHASE, HUMAN MOCS1A, AND *THERMOTOGA MARITIMA* MIAB

by

HEATHER LOUISE HERNÁNDEZ

(Under the Direction of Michael Kenneth Johnson)

## ABSTRACT

A new class of Fe-S proteins, termed radical-SAM enzymes, catalyzes radical reactions in a variety of biosynthetic processes. These [4Fe-4S]$^{2+,+}$ cluster-containing enzymes initiate radical enzymatic reactions via reductive cleavage of *S*-adenosyl-L-methionine (SAM) to yield methionine and an extremely reactive 5'-deoxyadenosyl radical. A growing number of radical-SAM enzymes have recently been discovered to contain a second Fe-S cluster of unknown function, although possible roles include acting as sacrificial S-donor or anchoring and possibly activating the substrate. The combination of analytical and spectroscopic studies, including EPR, Mössbauer, UV-visible absorption/circular dichroism/variable temperature magnetic circular dichroism, and resonance Raman, have been used to investigate the cofactor composition and properties of the two cluster containing radical-SAM enzymes *Escherichia coli* and *Bacillus subtilis* biotin synthase (BioB), human MOCS1A, and *Thermotoga maritima* MiaB. These enzymes are involved in crucial steps in the biosynthesis of biotin and molybdopterin, and in the thiomethylation of tRNA. *E. coli* and *B. subtilis* BioB are shown to house a radical-SAM [4Fe-4S] cluster and a [2Fe-2S] cluster in separate binding sites. The function and relevance of the [2Fe-2S] cluster, which has been suggested to be the S-donor to biotin, is addressed. In *E. coli* BioB, the most active form of the enzyme contains a 1:1 ratio of [2Fe-2S]/[4Fe-4S] clusters and the [2Fe-2S] cluster degrades during turnover. However, Mössbauer studies of *E. coli* BioB show that [2Fe-2S] cluster degradation is at least an order of magnitude faster than the initial rate of biotin formation and *B. subtilis* BioB exhibits comparable activity in samples depleted in the [2Fe-2S] cluster. Taken together, these results suggest that a [2Fe-2S] cluster degradation product may be the physiologically relevant S-donor. Both MOCS1A and *T. maritima* MiaB are characterized and shown to contain a radical-SAM [4Fe-4S] cluster as well as a second [4Fe-4S] cluster. In MOCS1A, the second cluster now appears to play a role in anchoring the 5'-GTP substrate. In *T. maritima* MiaB, the second cluster does not appear to interact with the tRNA substrate and may function as a S-donor in the thiomethylation reaction.

INDEX WORDS: Radical-SAM superfamily, SAM, iron-sulfur cluster, radical generation, biotin synthase, MOCS1A, MiaB, electron paramagnetic resonance, resonance Raman, magnetic circular dichroism, Mössbauer

# RADICAL-SAM ENZYMES WITH TWO IRON-SULFUR CLUSTERS: COFACTOR COMPOSITION AND SPECTROSCOPIC STUDIES OF *ESCHERICHIA COLI* AND *BACILLUS SUBTILIS* BIOTIN SYNTHASE, HUMAN MOCS1A, AND *THERMOTOGA MARITIMA* MIAB

by

HEATHER LOUISE HERNÁNDEZ

B.S., Michigan State University, 1998

A Dissertation Submitted to the Graduate Faculty of The University of Georgia in Partial Fulfillment of the Requirements for the Degree

DOCTOR OF PHILOSOPHY

ATHENS, GEORGIA

2006

© 2006

Heather Louise Hernández

All Rights Reserved

# RADICAL-SAM ENZYMES WITH TWO IRON-SULFUR CLUSTERS: COFACTOR COMPOSITION AND SPECTROSCOPIC STUDIES OF *ESCHERICHIA COLI* AND *BACILLUS SUBTILIS* BIOTIN SYNTHASE, HUMAN MOCS1A, AND *THERMOTOGA MARITIMA* MIAB

by

HEATHER LOUISE HERNÁNDEZ

| | |
|---|---|
| Major Professor: | Michael K. Johnson |
| Committee: | Michael W. W. Adams<br>Robert A. Scott |

Electronic Version Approved:

Maureen Grasso
Dean of the Graduate School
The University of Georgia
December 2006

# DEDICATION

To my husband, Noé, our daughter, Nora, and

my parents, Leonard and Joanne,

for their unwavering love and support.

# ACKNOWLEDGEMENTS

I would like to thank my advisor, Professor Michael K. Johnson, for his tutelage, direction and time. I greatly appreciated that your door was always open and you were always eager to discuss science or whatever else was on our minds. Thank you for also understanding your students have lives outside of lab (as long as we are producing enough data!).

Thank you to my entire advisory committee, Professors Michael W. W. Adams, Marly K. Eidsness, Donald M. Kurtz, Jr. and Robert A. Scott. Our discussions were thought provoking and your time was appreciated.

Thanks to all the lab mates that I have had the pleasure of working with during my time in the Johnson lab. Each of you has helped make life in the lab most enjoyable. Mostly, I would like to thank (in alphabetical order) Kala Chandramouli, Michele Mader Cosper, and Elizabeth Mengelt Walters for being such great friends and for providing so much encouragement and support throughout the years. You helped make the not so good times bearable and the good times great.

Last, but certainly not least, thank you to my parents, Leonard and Joanne Sackett, and my husband, Noé. Thanks mom and dad for teaching me that the skies not even the limit and that I can accomplish anything that I put my mind to. Nobody could wish for better parents than the two of you. And to my husband, thank you for always being there and always being willing to "do what it takes." I appreciate you so much. And of course to my beautiful, happy baby, Nora, thank you for being you. Your precious smiles make the rest of the world melt away.

# TABLE OF CONTENTS

Page

ACKNOWLEDGEMENTS .......... v

LIST OF TABLES .......... ix

LIST OF SCHEMES .......... x

LIST OF FIGURES .......... xi

CHAPTER

1 Introduction .......... 1

- Structure and Function of Iron-Sulfur Proteins .......... 1
- Radical-SAM Enzymes .......... 6
- References .......... 21

2 Characterization of the Cofactor Composition of *Escherichia coli* Biotin Synthase .......... 54

- Abstract .......... 56
- Introduction .......... 57
- Materials and Methods .......... 61
- Results .......... 67
- Discussion .......... 81
- References .......... 87

3 Role of the [2Fe-2S] Cluster in Recombinant *Escherichia coli* Biotin Synthase .......... 115

- Abstract .......... 117
- Introduction .......... 118

Materials and Methods ....................................................................................121

Results ..............................................................................................................123

Discussion ........................................................................................................135

References .........................................................................................................140

4 Cofactor Composition, Spectroscopic Properties and Activity Studies of *Bacillus subtilis* Biotin Synthase ..........................................................................................161

Abstract .............................................................................................................163

Introduction .......................................................................................................164

Materials and Methods ....................................................................................167

Results ..............................................................................................................172

Discussion ........................................................................................................183

References .........................................................................................................188

5 Characterization of MOCS1A, an Oxygen-sensitive Iron-Sulfur Protein Involved in Human Molybdenum Cofactor Biosynthesis .......................................................216

Abstract .............................................................................................................218

Introduction .......................................................................................................219

Experimental Procedures..................................................................................221

Results ..............................................................................................................224

Discussion ........................................................................................................239

References .........................................................................................................245

6 MiaB Protein from *Thermotoga maritima*: Characterization of an Extremely Thermophilic tRNA-Methylthiotransferase .........................................................267

Abstract .............................................................................................................269

Introduction ....................................................................................................270

Materials and Methods .......................................................................................272

Results ..............................................................................................................278

Discussion .........................................................................................................285

References .........................................................................................................291

7 MiaB, a bifunctional radical-*S*-adenosylmethionine enzyme involved in the thiolation and methylation of tRNA, contains two [4Fe-4S] clusters ..................................315

Abstract ............................................................................................................317

Introduction ......................................................................................................318

Materials and Methods .......................................................................................320

Results and Discussion .......................................................................................322

References .........................................................................................................329

# LIST OF TABLES

Page

Table 1.1: Distances Between the Unique Iron of the radical-SAM cluster and SAM .................32

Table 2.1: Cluster Composition, Absorption Properties, Mössbauer Parameters, and Activity of [2Fe-2S], [4Fe-4S], and [2Fe-2S]/[4Fe-4S] Forms of *E. coli* BioB ...............................94

Table 2.2: Assay of *E. coli* $[4Fe\text{-}4S]^{2+}$ BioB and His-Tagged IscS for Cysteine Desulfurase Activity ..........................................................................................................95

Table 3.1: Mössbauer Percent Absorption and Quantification of $^{57}Fe$ Species in $[2^{57}Fe\text{-}2S]/[4Fe\text{-}4S]$ BioB during Single Turnover .......................................................................145

Table 4.1: Cluster content, UV-visible absorption properties, and Mössbauer parameters of as purified and reconstituted forms of *B. subtilis* and *E. coli* BioB .................................192

# LIST OF SCHEMES

Page

Table 2.1: Conversion of biotin from dethiobiotin ........................................................................96

Table 3.1: Conversion of biotin from dethiobiotin ......................................................................146

Table 4.1: Conversion of biotin from dethiobiotin ......................................................................193

Table 7.1: Biosynthesis of $ms^2i^6A$-37 ...........................................................................................333

# LIST OF FIGURES

Page

Figure 1.1: Crystallographically defined structures of the four basic iron-sulfur clusters in biology .................................................................................................33

Figure 1.2: Ground state spin (*S*) and valence-delocaliztion schemes of the fundamental types of Fe-S clusters. ..........................................................................................35

Figure 1.3: Ranges of midpoint potentials (mV verses NHE) for biological Fe-S centers ...........37

Figure 1.4: Summary of the types of cluster transformation that have been observed in Fe-S proteins ..............................................................................................39

Figure 1.5: Reactions catalyzed by radical-SAM enzymes ..........................................................41

Figure 1.6: Crystal structures of the coordination of SAM to the [4Fe-4S] cluster......................44

Figure 1.7: Proposed mechanism for the reductive cleavage of SAM .........................................46

Figure 1.8: The primary reaction steps common to all radical-SAM enzymes ............................48

Figure 1.9: Crystal structures of radical-SAM protein monomers containing co-factor(s) and substrate(s).........................................................................................50

Figure 1.10: Crystal structures of the active sites of radical-SAM enzymes................................52

Figure 2.1: UV-visible absorption and resonance Raman spectra of *E. coli* BioB.......................97

Figure 2.2: Mössbauer spectra of [2Fe-2S], [4Fe-4S], and [2Fe-2S]/[4Fe-4S] *E. coli* BioB ........99

Figure 2.3: Resonance Raman spectra of [4Fe-4S] BioB during oxygen-induced cluster degradation and of aerobically reconstituted BioB ....................................................101

Figure 2.4: Resonance Raman spectra of [2Fe-2S]/[4Fe-4S] BioB after exposure to air for 10 minutes ....................103

Figure 2.5: Resonance Raman spectra of *E. coli* BioB samples in the presence of a 10-fold stoichiometric excess of SAM....................105

Figure 2.6: The effect of SAM on the Mössbauer spectrum of [2Fe-2S]/[4$^{57}$Fe-4S] BioB.........107

Figure 2.7: Mössbauer spectra of anaerobically grown $^{57}$Fe-enriched whole cells of *E. coli* with and without overexpression of BioB....................109

Figure 2.8: UV-visible absorption spectra of *E. coli* [4Fe-4S] BioB, *E. coli* [2Fe-2S] BioB, and *E. coli* IscS-his$_6$ ....................111

Figure 2.9: Summary of cluster-bound forms, cluster reconstitutions, and O$_2$-induced cluster conversions in *E. coli* BioB....................113

Figure 3.1: Mössbauer spectra of as-prepared [2$^{57}$Fe-2S]/[4Fe-4S] BioB ....................147

Figure 3.2: Time-dependent Mössbauer spectra of $^{57}$Fe-enriched [2Fe-2S]/[4Fe-4S] BioB during single turnover....................149

Figure 3.3: Mössbauer spectrum prepared from the spectrum shown in Figure 2A by removing the contribution of the SAM-bound [4Fe-4S]$^{2+}$ cluster....................151

Figure 3.4: [2Fe-2S]$^{2+}$ cluster degradation and biotin production during BioB single turnover.153

Figure 3.5: Mössbauer spectrum of a control sample of [2$^{57}$Fe-2S]/[4Fe-4S] BioB, which was incubated anaerobically for 3.5 h in a solution identical to that used in the turnover experiment but without the presence of DTB ....................155

Figure 3.6: EPR spectrum of a natural abundance [2Fe-2S]/[4Fe-4S] BioB sample taken at 15 minutes reaction time during the single turnover reaction of the enzyme ....................157

Figure 3.7: EPR spectra of a natural abundance [2Fe-2S]/[4Fe-4S] BioB sample taken at the indicated time periods during the single turnover reaction of the enzyme.................159

Figure 4.1: Mössbauer spectra of anaerobically grown $^{57}$Fe-enriched wholes cells of *E. coli* with and without overexpression of *B. subtilis* BioB ........................................................194

Figure 4.2: Comparison of the UV-visible absorption (upper panel) and CD (lower panel) spectra of his-tagged as-purified *B. subtilis* BioB (black) and his-tagged as-purified *E. coli* BioB (red)............................................................................................................196

Figure 4.3: Mössbauer spectra (hatched marks) of as-purified and reconstituted forms of his-tagged *B. subtilis* BioB..............................................................................................198

Figure 4.4: Comparison of the low-temperature resonance Raman spectra of as-purified *B. subtilis* BioB (left panel) and as-purified *E. coli* BioB (right panel) using 458-, 488-, and 514-nm excitation....................................................................................................200

Figure 4.5: UV-visible absorption spectra of as-purified and reconstituted forms of his-tagged *B. subtilis* BioB (left panel) and wild-type *E. coli* BioB (right panel) ............................202

Figure 4.6: Comparison of low-temperature resonance Raman spectra for equivalent forms of *B. subtilis* BioB (left panel) and *E. coli* BioB (right panel)............................................204

Figure 4.7: Time dependent CD and UV/visible absorption spectra of an IscS mediated reconstitution of as-purified *B. subtilis* BioB.............................................................206

Figure 4.8: Mössbauer spectra of $^{57}$Fe-enriched as-purified *B. subtilis* BioB before and after reconstitution for 6 hours with a 10-fold excess of $^{56}FeCl_3$ and $Na_2S$ ........................208

Figure 4.9: X-band EPR spectrum of his-tagged *B. subtilis* BioB reconstituted for 6 hours, repurified and reduced with a 10-fold excess dithionite .............................................210

Figure 4.10: Effect of SAM on the low-temperature resonance Raman spectra of the $[4Fe\text{-}4S]^{2+}$ clusters in reconstituted *B. subtilis* BioB (left panel) and *E. coli* [4Fe-4S] BioB (right panel). ....212

Figure 4.11: Activity assays comparing biotin production as a function of time by samples of *B. subtilis* and *E. coli* BioB ....214

Figure 5.1: Multiple sequence alignments of the N- (*A*) and C-terminal (*B*) cysteine motifs of MOCS1A ....249

Figure 5.2: UV-visible absorption spectra of MOCS1A ....251

Figure 5.3: Resonance Raman spectra of MOCS1A ....253

Figure 5.4: X-band EPR spectra of MOCS1A ....255

Figure 5.5: Perpendicular and parallel mode X-band EPR spectra of anaerobically purified MOCS1A ....257

Figure 5.6: VTMCD spectra of MOCS1A ....259

Figure 5.7: VTVH MCD saturation magnetization plots of MOCS1A ....261

Figure 5.8: Mössbauer spectra of MOCS1A ....263

Figure 5.9: Functional and UV-visible absorption characterization of MOCS1A and single Cys→ Ser mutants ....265

Figure 6.1: Biosynthesis of $ms^2i^6A$-37 ....295

Figure 6.2: Amino acid alignments of MiaB proteins from *T. maritima* (*Tm*), *E. coli* (*Ec*), *Salmonella typhimurium* (*St*), *Yersinia pestis* (*Yp*), *Vibrio cholerae* (*Vc*), and *Aquifex aeolicus* (*Aa*) ....297

Figure 6.3: HPLC chromatogram of modified tRNA nucleosides from *T. maritima* ....299

Figure 6.4: Purification of MiaBTM ....301

Figure 6.5: HPLC chromatograms of tRNA hydrolyastes for the *in vivo* complementation of miaB$^-$ TX3346 *E. coli* strain transformed with pT7-MiaBTm at 37 ˚C (*A*) and 45 ˚C (*B*)..........303

Figure 6.6: UV-visible absorption spectra of purified MiaBTM..........305

Figure 6.7: EPR spectra of MiaBTm..........307

Figure 6.8: Low temperature resonance Raman spectra of MiaBTm as isolated (*a*), reconstituted from the apoprotein (*b*), and reconstituted from the as-isolated form before (*c*), and after (*d*) exposure to air for 30 min..........309

Figure 6.9: VTMCD spectra of reconstituted MiaBTm reduced with a 6-fold excess of sodium dithionite..........311

Figure 6.10: Square wave voltammogram of reconstituted MiaBTm..........313

Figure 7.1: UV/visible absorption spectra of reconstituted wild-type (black) and C150/154/157A (red) *T. maritima* MiaB...........334

Figure 7.2: Resonance Raman spectra of reconstituted wild-type (black) and C150/154/157A (red) *T. maritima* MiaB...........336

Figure 7.3: Mössbauer spectra (hatched marks) of reconstituted wild-type and C150/154/157A *T. maritima* MiaB...........338

Figure 7.4: X-band EPR spectra of reconstituted wild-type (black) and C150/154/157A (red) *T. maritima* MiaB..........340

Figure 7.5: Resonance Raman (*left panel*) and EPR (*right panel*) spectra of reconstituted C150/154/157A MiaB in the absence (a) and presence (b) of a 6-fold excess of the $i^6$A-37-tRNA substrate...........342

# CHAPTER 1

# INTRODUCTION

## Background of Structure and Function of Iron-Sulfur Proteins

Iron-sulfur containing proteins are essential to life as we know it. Moreover, almost all life forms are dependant on iron-sulfur proteins, from ancient microscopic archaea to the most advanced eukaryotes. Deletions or mutations in iron-sulfur proteins have been shown to cause severe sickness and death in organisms, including humans. Hence, the study of iron-sulfur containing proteins is crucial to understanding our natural world.

Iron-sulfur proteins are broadly defined as proteins containing at least one Fe with at least partial S coordination. Most biological iron-sulfur centers correspond to one of four basic types: mononuclear Fe centers, [2Fe-2S], cubane-type [3Fe-4S], and [4Fe-4S] clusters, see figure 1.1. Since the first detection of Fe-S clusters, approximately 40 years ago, Fe-S clusters have been shown to exhibit extremely versatile roles in biology. Fe-S clusters have been shown to mediate electron transfer, coupled electron and proton transfer, substrate binding and activation, Fe storage, structural regulation of gene expression and enzyme activity, radical generation, disulfide reduction and sulfur donation. Hence several recent review articles and books have been published describing Fe-S cluster structure and function (*1-8*).

Various spectroscopic and physical methods have been employed to characterize biological Fe-S centers including x-ray absorption (XAS), electron paramagnetic resonance (EPR), electron-nuclear double resonance (ENDOR), electron spin-echo envelope modulation (ESEEM), Mössbauer, UV-visible absorption/circular dichroism (CD)/variable temperature magnetic circular dichroism (VTMCD), resonance Raman, nuclear magnetic resonance (NMR), saturation magnetization, and x-ray crystallography. Together, these methods have provided detailed information concerning the electronic, magnetic, structural and functional properties of biological Fe-S centers.

Mononuclear Fe-S centers consist of Fe coordinated in a highly conserved roughly tetrahedral cysteinyl S environment, see figure 1.1a, typically involving two Cys–$X_2$–Cys motifs or one Cys–$X_2$–Cys and one Cys–Cys motif, and function as high-potential electron-transfer mediators in bacterial proteins (*3;6;9*). These centers, otherwise known as Rd-type centers, are found in rubredoxin (Rd) and desulforedoxin (Dx). Rd-type Fe-S centers cycle between high-spin Fe(III) ($S$ = 5/2) and high-spin Fe(II) ($S$ = 2), see figure 1.2, with redox potentials ranging from +281 mV to −87 mV, see figure 1.3.

The majority of [2Fe-2S] clusters have complete cysteinyl coordination, but they can also be coordinated by two cysteines at one Fe site and two histidines at the other Fe site, known as Rieske-type centers (*10*), and there have been a few reports of [2Fe-2S] clusters containing one aspartate or arginine ligand (*11-13*). Spectroscopic and crystallographic studies indicate approximate tetrahedral coordination at each Fe site and the $Fe_2(\mu_2\text{-}S)_2$ core is roughly planer (*9;11;13-18*), see figure 1.1b. These clusters serve primarily as electron transfer mediators (*3;6;10*), but there have been reports that they may play a regulatory role in some proteins (*18-22*) and there has been one report of a [2Fe-2S] cluster acting as a sulfur donor (*11;23*). Under physiologically relevant conditions, [2Fe-2S] clusters cycle between oxidized, +2 (two $S$ = 5/2 FeIII), and reduced, +1 (one $S$ = 2 FeII and one $S$ = 5/2 FeIII), oxidation states, where the two high-spin Fe atoms are antiferromagnetically coupled yielding ground states of $S$ = 0 and $S$ = 1/2 respectively, see figure 1.2. Redox potentials of $[2Fe\text{-}2S]^{2+,+}$ clusters range from +380 mV to

−150 mV for Rieske-type centers and from +100 mV to −460 mV for [2Fe-2S] centers with complete cysteinyl ligation, see figure 1.3. The primary sequence of coordinating cysteinyl residues that bind [2Fe-2S] centers with complete cysteinyl ligation are not represented by one highly conserved motif, but the observed spacing between cysteinyl residues can be summarized as $\text{Cys–X}_{4\text{-}12}\text{–Cys–X}_{2\text{-}35}\text{–Cys–X}_{3\text{-}37}\text{–Cys}$ (*24;25*). The motif for histidine and cysteine residues that ligate Rieske-type clusters is more highly conserved and can be summarized as $\text{Cys–X–His–X}_{15\text{-}47}\text{–Cys–X}_2\text{–His}$ (*10*).

When first discovered [3Fe-4S] clusters were thought to be an artifact of aerobic protein purification (*26*). However, although there are numerous examples of [4Fe-4S] clusters that degrade to [3Fe-4S] clusters upon aerial oxidative damage, it has since been discovered that [3Fe-4S] clusters are intrinsic components of a variety of Fe-S proteins and are usually bound by a $\text{Cys–X}_{2\text{-}7}\text{–Cys}$ motif with the third cysteine more remotely located (*9*). Although [3Fe-4S] clusters occur in cubane and linear forms (*27;28*), only the cubane-type clusters appears to be biologically relevant and are best described as a cubane [4Fe-4S] cluster lacking one Fe, with the remaining three Fe atoms retaining approximately tetrahedral coordination and complete cysteinyl ligation (*13;29;30*), see figure 1.1c. To date, the only known physiological role of cubane-type [3Fe-4S] clusters is electron transfer and electrochemical studies indicate that the clusters have physiologically relevant oxidation states of +1 and 0 with potentials ranging from +90 mV to −460 mV (*29*), see figure 1.3. The −2 oxidation state is also observed and occurs with the addition of three protons, but is not considered biologically relevant due to a non-physiological redox potential of −700 mV for the 0/−2 redox couple at pH 7 (*31*). The three $S$ = 5/2 FeIII ions of the cubane-type $[3\text{Fe-4S}]^+$ cluster are antiferromagnetically coupled giving rise to a $S$ = 1/2 ground state, see figure 1.2. One-electron reduction yields the $[3\text{Fe-4S}]^0$ cluster which comprises a valence-delocalized *S* = 9/2 FeIII/FeII pair and a valence-localized *S* = 5/2 FeIII site, which interacts antiferromagnetically giving rise to a *S* = 2 ground state, see figure 1.2.

Cubane-type [4Fe-4S] clusters are the most prevalent electron transfer centers in biology. Although [4Fe-4S] clusters are known to have numerous different primary sequence arrangements of cysteine residues, they are most commonly found ligated by a Cys–$X_2$–Cys–$X_2$–Cys motif, with the fourth cysteine more remotely located (*3;6;9*). The majority of [4Fe-4S] clusters have all cysteinyl-S ligation, figure 1.1d, but there are a few instances of electron-transfer [4Fe-4S] clusters with one non-cysteinyl ligand, such as aspartate (*32*) or histidine (*16;33;34*). While the primary role of [4Fe-4S] clusters is electron transfer, these clusters have proven extremely versatile. They have been shown to play catalytic roles in binding and activating substrates (*16;21;35-38*) and cleaving active-site disulfides (*39-41*), as well as regulatory (*20;21;42*), structural (*43;44*), and storage roles (*45;46*). To facilitate catalytic roles, a unique Fe site is generated by the absence of an amino acid ligand in (de)hydratases (*47*) and radical-SAM enzymes (*48;49*), creating a site for substrate binding and activation. Biological cubane-type [4Fe-4S] clusters are most often found in the +3, +2, and +1 core oxidation states and undergo one-electron redox cycling between either the +2/+1 states in Fd-type centers, with midpoint potentials ranging from +80 to -715 mV, or the +3/+2 states as found in high-potential iron-proteins (HiPIPs), with midpoint potentials between +50 and 500 mV, see figures 1.2 and 1.3. The magnetic properties of [4Fe-4S] cluster are best described in terms of antiferromagnetic coupling between two ferromagnetically coupled [2Fe-2S] fragments, see figure 1.2. The $[4Fe\text{-}4S]^{+}$ cluster most commonly exhibits a *S* = 1/2 ground state that results from antiferromagnetic coupling of a valence-delocalized FeII/FeIII pair (*S* = 9/2) and a FeII/FeII pair (*S* = 4). The $[4Fe\text{-}4S]^{2+}$ cluster invariably exhibits a diamagnetic *S* = 0 ground state as a result of antiferromagnetic coupling between two valence-delocalized FeII/FeIII pairs ($S$ = 9/2). Finally, the $[4Fe\text{-}4S]^{3+}$ cluster exhibits a $S$ = 1/2 ground state as a result of antiferromagnetic coupling between a FeIII/FeIII pair ($S$ = 5) and a valence-delocalized FeII/FeIII pair ($S$ = 9/2).

An interesting aspect of Fe-S cluster chemistry is the ability of some clusters to convert or degrade from one cluster type to another, most commonly [4Fe-4S] ↔ [3Fe-4S] and [4Fe-4S] ↔ [2Fe-2S] conversions/degradations. Figure 1.4 summarizes the cluster conversions that have been observed in Fe-S proteins. These changes are generally caused by $O_2$ or NO exposure, oxidizing or reducing agents, pH changes or mutations of cluster binding residues. Interestingly, there is increasing evidence that cluster conversions can also act as sensory mechanisms in protein regulation (*4*).

Proteins containing [4Fe-4S] clusters with incomplete cysteinyl ligation, such as aconitase and MOCS1A, a radical-SAM enzyme involved in molybdenum cofactor biosynthesis, have been observed to degrade to a $[3Fe\text{-}4S]^{+,0}$ clusters during purification or oxygen exposure (*21;50*). Under reducing conditions, $[3Fe\text{-}4S]^{0}$ clusters readily pick up Fe to reform the active $[4Fe\text{-}4S]^{2+,+}$ cluster. [4Fe-4S] clusters with complete cysteinyl ligation also can undergo this conversion albeit under more oxidizing conditions. A cubane $[3Fe\text{-}4S]^{+}$ to a linear $[3Fe\text{-}4S]^{+}$ cluster conversion has been well characterized in aconitase (*27;28*). The linear cluster is formed at alkaline pH (> 9.5) and reduction of this cluster in the presence of Fe results in formation of a $[4Fe\text{-}4S]^{2+,+}$ cluster. [4Fe-4S] or [3Fe-4S] cluster to [2Fe-2S] cluster conversions have been observed in several systems under oxidative or denaturing conditions and are often reversible under reducing conditions in the presence of Fe and S. Clusters in the radical-SAM family of enzymes undergo degradation from a $[4Fe\text{-}4S]^{2+}$ cluster to a semi-stable $[2Fe\text{-}2S]^{2+}$ cluster when exposed to oxygen (*51*), in some cases by way of a $[3Fe\text{-}4S]^{+}$ cluster intermediate (*50;52;53*).

Oxygen exposed fumarate-nitrate reduction (FNR) regulatory protein is also converted from a $[4Fe\text{-}4S]^{2+}$ to a $[2Fe\text{-}2S]^{2+}$ cluster via a $[3Fe\text{-}4S]^{+}$ intermediate. In this instance, the conversion is believed to constitute an $O_2$-sensing mechanism prompting the change from anaerobic to aerobic *E. coli* growth (*54-56*). Finally, under certain conditions, the subunit-bridging [4Fe-4S] cluster in the nitrogenase Fe protein has been observed to convert from a $[4Fe\text{-}4S]^{2+}$ to $[2Fe\text{-}2S]^{2+}$ cluster (*57*), and a novel cluster conversion has been observed with a mimic of the nucleotide-bound form (*58*). Under oxidizing conditions and in the presence of glycerol, crystallographic and spectroscopic studies have shown that the reduced [4Fe-4S] cluster can be reversibly cleaved into two [2Fe-2S] units separated by approximately 5 Å. Such transformations are likely to mimic the final step in [4Fe-4S] cluster biosynthesis (*59;60*).

## Radical-SAM Enzymes

The objective of the research described in this dissertation was to understand the role of Fe-S clusters in an emerging class of Fe-S enzymes that catalyze a wide range of radical reactions. Over the past decade evidence has accumulated for $[4Fe\text{-}4S]^{2+,+}$ clusters initiating radical enzymatic reactions via reductive cleaving of *S*-adenosylmethionine (SAM) into methionine and an extremely reactive 5'-deoxyadenosyl radical. This new class of Fe-S proteins, termed radical-SAM enzymes, catalyzes radical reactions in a vast variety of biosynthetic processes. Traditionally, SAM has primarily been known as a biological methyl donor but also serves as a methylene, amino, ribosyl, and aminopropyl group donor (*61*). Prior to the discovery of SAM as a 5'-deoxyadenosyl radical generator, adenosylcobalamin ($B_{12}$) was the only known biological generator of this species (*62*), although the latter is responsible for a much less diverse variety of reactions. The 5'-deoxyadenosyl radical generated from SAM is used in an assortment of diverse reactions including the biosynthesis of DNA precursors, vitamins, cofactors, antibiotics, herbicides, among many others. Consequently it is not surprising that radical-SAM enzymes have emerged as the most prolific growth area of Fe-S protein research. The research described in this dissertation has provided key insights into the roles of the Fe-S clusters in three radical-SAM enzymes involved in crucial steps in the biosynthesis of biotin (Chapters 2 – 4) and molybdopterin (Chapter 5), and the thiomethylation of tRNA (Chapters 6 and 7). To understand the importance of these results in the context of the current understanding of structure/function relationships in radical-SAM enzymes, an up-to-date summary of the research progress on the entire class of radical-SAM enzymes is presented below.

In 1970, Barker and coworkers reported the purification and properties of lysine-2,3-aminomutase (KAM), an enzyme that as isolated contained iron and pyridoxal 5′-phosphate (PLP), but required additional Fe, SAM, and anaerobic incubation with a reducing agent for activity (*63*). However, 20 years lapsed before the presence of the [4Fe-4S] cluster in KAM was established and a role for this cluster in reductive cleavage of SAM was suggested (*64;65*). Over the next several years a small group of proteins, consisting of pyruvate formate lyase-activating enzyme (PFL-AE), biotin synthase (BioB), anaerobic ribonucleotide reductase-activating enzyme (aRNR-AE), spore photoproduct lyase (SP-lyase), benzylsuccinate synthase activating enzyme (BssD-AE) and lipoic acid synthase (LipA) (*48;66*), see figure 1.5, were also revealed to require an oxygen sensitive [4Fe-4S] cluster and SAM for activity (*67-74*). A major breakthrough occurred in 2001, when Sofia and coworkers used a bioinformatics approach to demonstrate that the radical-SAM family of proteins was actually a protein superfamily possibly consisting of almost 650 unique sequences, spanning all three domains of life (*75*). To date, at least half have unknown function and, while the list is growing, only a handful have begun to be characterized, including most recently HemN, AtsB, MoaA, HydE/G, and the focus of this work, MiaB, MOCS1A along with BioB see figure 1.5. The slow discovery and characterization of this superfamily is in large part due to the lability of the [4Fe-4S] clusters. The clusters are extremely sensitive to oxygen and require strict anaerobic conditions for assembly and *in vitro* activity.

Although the proteins in the radical-SAM superfamily perform a wide variety of different radical reactions, they share a common radical initiation step involving a unique type of redox-active $[4Fe\text{-}4S]^{2+,+}$ cluster that is responsible for binding and mediating reductive cleavage of SAM.

### *The CxxxCxxC motif binds a [4Fe-4S] cluster*

Initially, the most noticeable similarity among radical-SAM proteins is the presence of a rigorously conserved CxxxCxxC cysteine motif. The motif is most commonly found near the N-terminus but may also be found elsewhere in the protein. Mutagenesis studies of several radical-SAM proteins have shown that the three cysteines in this motif coordinate three of the four iron sites of the [4Fe-4S] cluster responsible for the reductive cleavage of SAM (*70;76;77*). Subsequent crystallographic studies have confirmed these findings, see figure 1.6 (*11;49;78;79*). This [4Fe-4S] cluster binding motif is unusual as most [4Fe-4S] clusters are bound by four amino acid residues from the protein backbone, usually cysteines, rather than three. The fourth iron, known as the unique iron, is presumably left open to accommodate the binding of a molecule of SAM (*80*) and the presence of this unique iron is most likely the cause of the lability of the cluster. When exposed to air, the [4Fe-4S] cluster readily breaks down to a quasi stable $[2Fe\text{-}2S]^{2+}$ cluster, sometimes via a $[3Fe\text{-}4S]^{+}$ cluster and when purified aerobically, the cluster is invariably in the $[2Fe\text{-}2S]^{2+}$ or $[3Fe\text{-}4S]^{+}$ form, or not present at all (*51;53*). The research presented in this dissertation provides spectroscopic and analytical characterization of the radical-SAM cluster housed in *E. coli* and *B. subtilis* BioB (Chapters 2-4), human MOCS1A (Chapter 5) and *T. maritima* MiaB (Chapter 6).

### *Binding and cleavage of SAM at the unique iron site*

Spectroscopic studies of KAM, PFL-AE and BioB provided the first evidence that in the presence of SAM, the $[4Fe\text{-}4S]^{2+,+}$ cluster is not only perturbed, but is directly coordinated by SAM at the unique iron site.

Via selenium x-ray absorption spectroscopy (Se-XAS), Cosper et al. were the first to provided experimental evidence that SAM is coordinated directly to the $[4Fe\text{-}4S]^{2+}$ cluster of KAM, a radical-SAM and PLP-dependant enzyme responsible for the interconversion between L-α-lysine and L-ß-lysine (*81*). By using selenomethionine (Se-M), one of the reductive cleavage products of Se-adenosylmethionine (Se-SAM), the authors were able to determine that the Se was weakly bound to the open iron of the cluster at distance of 2.7 Å. However, there was no evidence of interaction between Fe and Se in the presence of Se-SAM. ENDOR studies of cryoreduced KAM subsequently revealed N and O ligation by the α-amino and α-carboxyl groups of SAM at the unique iron of the $[4Fe\text{-}4S]^{2+}$ cluster (*82*). The authors rationalize that these results are congruent with the observation that in KAM, SAM is regenerated each turnover and is therefore a catalytic cofactor and not a substrate (*83*). This has led to the proposed mechanism involving SAM binding to the unique iron of the $[4Fe\text{-}4S]^{2+}$ cluster via its α-amino and α-carboxyl groups. Following one-electron reduction, inner sphere electron transfer occurs from the $[4Fe\text{-}4S]^{+}$ cluster to the sulfonium of SAM while simultaneously the sulfur of SAM also binds to the unique iron of the cluster and the S-C bond is homolytically cleaved forming the 5'-deoxyadenosyl radical. The recent 2.1 Å resolution crystal structure of Se-SAM bound KAM supports the above mentioned spectroscopic data, see figure 1.6d (*79*). The crystal structure reveals that the Se in Se-SAM, presumably analogous to the S in SAM, is positioned 3.2 Å away from the unique iron indicating that the Se is readily available to bind to the unique iron upon electron transfer and formation of the radical, thereby anchoring the methionine for regeneration of SAM (*84*). To date, spore photoproduct lyase (SP-lyase) is the only other radical-SAM enzyme believed to reversibly generate the adenosyl radical (*85*).

Similar studies were performed on PFL-AE, a radical-SAM activating enzyme responsible for generating a stable glycyl radical on PFL, and BioB, the radical-SAM enzyme responsible for forming biotin from dethiobiotin, with slightly different results. Mössbauer studies of PFL-AE and BioB revealed that SAM is coordinated to the unique iron of the $[4Fe-4S]^{2+}$ cluster (*51;80;86*). Direct evidence for the mode of SAM binding to the [4Fe-4S] cluster was provided by ENDOR experiments on PFL-AE using various forms of isotopically labeled SAM (*87;88*). These experiments were the first to demonstrate that SAM is bound at the unique iron by the α-amino and α-carboxyl groups. However, in contrast to KAM, these experiments revealed that the S of SAM is 4 Å from the nearest iron in PFL-AE and is more closely associated with a $\mu_3$-bridging sulfide of the [4Fe-4S] cluster. Se-XAS experiments analogous to those performed on KAM were also performed on PFL-AE and BioB (*84*). In accord with ENDOR results there was no evidence of an Fe-Se interaction. The crystal structure of BioB as well as the crystal structures of HemN and MoaA confirmed the above experimental data in terms of the mode of SAM binding to the cluster, see figure 1.6a-c (*11;49;78;89*). The differences seen in BioB and PFL-AE verses KAM are rationalized by the slightly dissimilar role of SAM, as that of a consumable substrate, rather than a reusable cofactor, resulting in a slightly different mechanism of SAM cleavage. It is suggested that inner-sphere electron transfer occurs from the active [4Fe-4S]$^+$ cluster to the sulfonium of SAM via a sulfide-sulfonium interaction enabling the reductive cleavage into cluster bound methionine and the active 5'-deoxyadenosyl radical (*87*).

Thus the [4Fe-4S]$^{2+,+}$ cluster bound by the CxxxCxxC motif has two distinct and crucial roles in the radical-SAM superfamily. The [4Fe-4S]$^{2+}$ cluster is responsible for anchoring SAM via ligation of α-amino and α-carboxyl groups at the unique iron site. This brings the sulfonium ion close enough to the cluster to effect reductive cleavage to yield methionine and the 5'-deoxyadenosyl radical upon one-electron reduction of the cluster. A generalized scheme for the reductive cleavage of SAM is illustrated in figure 1.7.

### *Common mechanism among radical-SAM proteins*

Despite the amazingly diverse reactions catalyzed by radical-SAM enzymes, the preliminary reaction steps, see figure 1.8, including the initial radical generation step depicted in figure 1.7, appears to be common to all members of the radical-SAM superfamily. In some *E. coli* radical-SAM enzymes cluster reduction has been shown to be mediated by a flavodoxin/flavodoxin reductase system (*90-92*), whereas in plant BioB, adrenodoxin is believed to be the immediate electron donor (*93*). The active [4Fe-4S]$^+$ cluster then transfers an electron to the cluster bound SAM, inducing the reductive cleavage of the carbon-sulfonium bond forming methionine and the extremely reactive 5'-deoxyadenosyl radical (*94-100*). To date, the radical has not been experimentally observed in any system due to its highly reactive nature.

The 5’-deoxyadenosyl radical then abstracts a hydrogen from the carbon of a nearby substrate producing a substrate based radical as in KAM and BioB (*101;102*) or from a protein based glycine, creating a protein based radical as in PFL-AE and aRNR-AE (*103*). The substrate based radicals seem to be quite reactive as only one has been directly observed in KAM via EPR (*74;101*). Studies on SP-lyase and BioB where $^2$H or $^3$H was incorporated into 5’-dexoyadenosine from labeled substrate offers indirect evidence of the formation of a substrate based radical (*85;102*). On the other hand, glycine based protein radicals seem relatively stable and have been directly observed with EPR (*103-105*). Interestingly, some substrates require two hydrogen abstraction steps to form product, as is the case with BioB, HemN, MiaB and LipA, and therefore two molecules of SAM are believed to be required per turnover (*76;89;106*). After the hydrogen atom abstraction step(s) the chemistry that takes place is unique to each enzyme, see figure 1.5.

### *Crystal structures of radical-SAM enzymes*

Recently, the crystal structures of four different radical-SAM enzymes, HemN (*78*), BioB (*11*), MoaA (*49*), and KAM (*79*), have been solved, see figures 1.6, 1.9 and 1.10. These structures have been extremely beneficial for understanding the fundamental similarities and differences among radical-SAM proteins. All of the proteins were crystallized with intact [4Fe-4S] clusters bound to the CxxxCxxC motif and with SAM (or Se-SAM in the case of KAM) coordinated to the unique iron of the radical-SAM cluster, see figure 1.6. Distances between the specific SAM atoms and the unique iron of the cluster are summarized in table 1.1.

The structure of HemN, the enzyme responsible for the oxygen independent oxidative decarboxylation of coproporphyrinogen III to protoporphyrinogen IX in heme and chlorophyll biosynthesis, was resolved at 2.1 Å as a monomer with a ¾ triosephosphate isomerase (TIM)-barrel structure (*78*), see figure 1.9a. Two molecules of SAM were located in the structure, one bound to the radical-SAM [4Fe-4S] cluster and another located close by, see figure 1.10a. The authors speculate that although the second SAM molecule could be a crystallization artifact, it may be relevant due to HemN's requirement for two molecules of SAM per turnover.

The BioB structure was resolved at 3.4 Å as a homodimeric ¾-TIM-barrel, see figure 1.9b, with a [2Fe-2S] cluster and substrate, dethiobiotin, present in addition to the radical-SAM cluster and SAM (*11*), see figure 1.10b. The cluster was bound by 3 rigorously conserved cysteine residues and the fourth ligand was identified as an arginine; the first example of arginine ligation of biological Fe-S cluster. Edge to edge, the clusters are positioned 12.7 Å away from one another with dethiobiotin situated between them. Notably, the first substrate carbon believed to be activated by a 5'-deoxyadenosyl radical is positioned 4.6 Å away from the bridging sulfur of the [2Fe-2S] cluster, a location consistent with the transfer of this sulfur into substrate to form biotin.

MoaA was solved as a ¾-TIM barrel homodimer at 2.2 Å resolution, see figure 1.9c (*49*). Like BioB, MoaA has a second cluster in addition to the SAM-bound radical-SAM [4Fe-4S] cluster, but in this case the second cluster is a [4Fe-4S] cluster as predicted based on spectroscopic studies (50), see figure 1.10c. Edge to edge, the two clusters were found to be 16 Å apart. A subsequent crystal structure contained the bound 5'-GTP substrate (*107*). The structure positions the purine N1 nitrogen and the exocyclic amino-group of 5'-GTP at 2.8 Å and 2.4 Å, respectively, from the unique Fe site of the second cluster, suggesting the role of the second cluster may be to position the substrate for attack by the 5'-deoxyadenosyl radical.

Lastly, the KAM structure has been solved at 2.1 Å again revealing a homotetrameric ¾-TIM barrel, see figure 1.9d (*79*). Each monomer contained the PLP cofactor and substrate L-α-lysine bound together as a lysyl-PLP external aldimine, a zinc atom that is thought to help hold together domain-swapped dimmers and, due to bacterial growth conditions, Se-SAM was coordinated to the unique iron of the radical-SAM cluster in lieu of SAM, see figure 1.10d. The authors note that after reductive cleavage of SAM, the radical would be in an excellent position to perform the abstraction step (< 4 Å away from the H to be removed).

### *Emergence of second clusters - A new subclass of radical-SAM enzymes*

Much of the focus of this dissertation revolves around the recent discovery of a second Fe-S cluster, in addition to the radical-SAM [4Fe-4S] cluster, in several radical-SAM enzymes. The second cluster is bound by rigorously conserved cysteines unique to each individual protein. In our laboratory, a second cluster has thus far been observed and characterized in BioB, MOCS1A/MoaA, HydE and MiaB. A second cluster has also been characterized in LipA (*76*). In this work, Chapters 2, 3, and 4 characterize and address the function of the second cluster in *E. coli* and *B. subtilis* BioB. Chapter 5 focuses on MOCS1A and the characterization and function of both of its clusters and finally, the characterization of the second cluster in MiaB is discussed in Chapter 7. While the role of these second clusters has yet to be fully elucidated, possible functions include S-donor, substrate anchor or activator, or perhaps as suggested in the case of BioB, merely an artifact due to recombinant growth conditions. Although this dissertation focuses on BioB, MOCS1A, and MiaB, all radical-SAM enzymes containing a second cluster are briefly summarized below in order to fully appreciate similarities and differences among this newly emerging subclass.

BioB, the enzyme responsible for converting dethiobiotin to biotin by inserting a S between two unactivated carbons of the substrate (figure 1.5) was the first radical-SAM enzyme found to contain two clusters. Jarrett and coworkers were the first to establish that BioB contained two distinct iron-sulfur binding sites, the second or non-radical-SAM cluster being a $[2Fe\text{-}2S]^{2+}$ cluster (*108;109*). This cluster is air stable, but breaks down under reducing conditions (*69*). The functional form of BioB under anaerobic conditions is proposed to contain one $[4Fe\text{-}4S]^{2+,+}$ and one $[2Fe\text{-}2S]^{2+}$ cluster in distinct binding sites, with [2Fe-2S] cluster presumably bound by the three other rigorously conserved cysteines plus an arginine (*11*). On the basis of changes in the absorption, the rate destruction of the $[2Fe\text{-}2S]^{2+}$ cluster was reported to parallel sulfur insertion into the substrate in single turnover experiments, suggesting that the role of this second cluster is that of a sacrificial S-donor (*110*). In Chapter 2 a detailed spectroscopic and analytical characterization of the Fe-S clusters in *E. coli* BioB is presented (*51*). The results confirmed the presence of [4Fe-4S] and [2Fe-2S] clusters in separate binding sites and established the cluster transformations that occur on reduction or exposure to oxygen. This set the stage for a detailed study of the role of the $[2Fe\text{-}2S]^{2+}$ cluster during enzymatic turnover using EPR and Mössbauer spectroscopies, which is presented in Chapter 3 (*23*). In contrast to the findings of Jarrett and coworkers the initial decay of the $[2Fe\text{-}2S]^{2+}$ cluster was found to be approximately 1 order of magnitude faster than the initial rate of biotin formation, indicating that if this second cluster is the immediate S-donor, insertion of S into the substrate is not be the rate-limiting step. This result also leaves open the possibility that a cluster breakdown product rather than the [2Fe-2S] cluster itself is the immediate S-donor to DTB and raises the possibility that the [2Fe-2S] cluster may be an artifact of recombinant overexpression. Both this hypothesis and the hypothesis proposed by Jarrett and coworkers can explain the observation of

Se or $^{34}$S incorporation into biotin using BioB containing [2Fe-2Se] or [2Fe-2$^{34}$S] clusters (*111;112*). The 3.4 Å crystal structure of BioB which appeared in 2004 confirmed the presence of two clusters in BioB, see figures 1.9b and 1.10b (*11*), and showed that a S of the [2Fe-2S] is positioned close to S-insertion site on DTB. However, the buried nature of the [2Fe-2S] cluster raised serious concerns over the ability to reconstitute the [2Fe-2S] cluster and thereby enable enzymatic turnover. Indeed the possibility that BioB is a substrate or suicide enzyme was raised, although recent evidence indicates that it is capable of multiple turnovers *in vivo* (*113*).

In order to further address the role of the [2Fe-2S]$^{2+}$ cluster in BioB, Chapter 4 reports purification and detailed spectroscopic and analytical characterization of BioB from *Bacillus subtilis*. In common with the *E. coli* enzyme, *B. subtilis* BioB was found to accommodate [2Fe-2S] and [4Fe-4S] clusters in separate binding sites. However, the spectroscopic properties and stability of the [2Fe-2S] center in *B. subtilis* BioB are distinct from those in *E. coli* BioB and activity studies indicate that a full complement of [2Fe-2S] clusters is not required for optimal activity. The results further question the role of the [2Fe-2S] cluster, however, more conclusive work needs to be done in order to establish the precise role of the second cluster in BioB.

Lipoic acid synthase (LipA), the enzyme responsible for converting octanoic acid into lipoic acid by inserting two S atoms into the substrate, see figure 1.5, has also been recently implicated to contain a second cluster; an essential [4Fe-4S] cluster bound by a C-$X_4$-C-$X_5$-C motif unique to LipA (*76*). The second [4Fe-4S]$^{2+,+}$ cluster was observed by absorption, EPR and Mössbauer in a LipA triple variant in which each of the three cysteines of the radical-SAM [4Fe-4S] cluster binding motif were mutated to alanine. Moreover, the presence of the second cluster appears to correlate with activity, with maximal activity corresponding to one turnover as in the case of BioB, and both sulfur atoms inserted into octanoic acid have been found to originate from the same polypeptide (*114*). Hence the second cluster has been implicated to serve as the immediate S-donor and the difference in the nature of the second cluster in BioB and LipA, $[2Fe\text{-}2S]^{2+}$ verses $[4Fe\text{-}4S]^{2+}$ clusters respectively, has been suggested to relate to the number of sulfur atoms needed for product formation, one sulfur in BioB and two in LipA.

HydE and HydG are both radical-SAM enzymes that are involved in the maturation of the Fe-only hydrogenase active site, see figure 1.5 (*115;115;116*). While specific roles have yet to be established, it seems likely that one or both the enzymes is involved with biosynthesis of the bridging di(thiomethyl)amine ligand. For example, one may catalyze sulfur insertion into dimethylamine to form di(thiomethyl)amine ligand, see figure 1.5. EPR, resonance Raman and Mössbauer studies of both the wild-type and a triple variant form of HydE, in which the SAM binding cluster cysteines were mutated to alanine, have recently confirmed the presence of a second $[4Fe\text{-}4S]^{2+,+}$ cluster (*116*) (H. L. Hernández, S. Subramanian, and M. K. Johnson, unpublished observations). The role of this cluster has yet to be determined, but by analogy to LipA, it may serve as the source of sulfur atoms for the bridging ligand of Fe-only hydrogenase (*116*).

As discussed in Chapter 6, MiaB has been shown to be involved in thiomethylation of tRNA modification, more specifically, the conversion of (N6-isopentenyl)-adenosine-37 ($i^6A$-37) to (2-methylthio-N6-isopentenyl)-adenosine-37 ($ms^2i^6A$-37) during the complicated process of tRNA maturation. The reaction involves H-atom abstraction at position 2 of the base moiety and then the activated carbon is thiolated and methylated, see figure 1.5 (*117*). Interestingly, MiaB has been shown to use two molecules of SAM in an unprecedented manner. The first SAM is used for radical generation and carbon activation via H-atom abstraction by the mechanism common to all radical-SAM enzymes, while the second SAM is utilized in the more traditional role as a methyl donor (*117*). In Chapter 6, MiaB was initially characterized as a radical-SAM enzyme containing only the SAM-activating [4Fe-4S] cluster (*52*). Chapter 7 reports subsequent spectroscopic and analytical studies of wild-type MiaB, reconstituted under improved conditions, and a triple variant in which the three cysteines of the CxxxCxxC motif were all mutated to alanine residues. The results reveal that MiaB contains two [4Fe-4S] clusters per monomer. When MiaB was reconstituted with $Se^{2-}$ rather than $S^{2-}$ in order to generate [4Fe-4Se] clusters, Se was found to be incorporated into the tRNA substrate instead of S, indicating that the sulfur atom introduced into the substrate is inserted into the protein during Fe-S cluster reconstitution and can be mobilized under turnover conditions (*117*). Hence MiaB may also use a [4Fe-4S] cluster as a S-donor under single turnover conditions.

The human enzyme MOCS1A characterized in Chapter 5 and its bacterial ortholog, MoaA, are radical-SAM enzymes that in conjunction with MoaC/MOCS1B are responsible for the conversion of 5'-GTP to precursor Z, in the first step of molybdopterin biosynthesis, see figure 1.5 (*49;50*). Spectroscopic work presented in Chapter 5 and subsequent crystallographic studies have recently revealed that MoaA/MOCS1A contains two oxygen sensitive $[4Fe\text{-}4S]^{2+,+}$ clusters, one ligated by the cysteines in the radical-SAM binding motif and another bound by three rigorously conserved cysteines closer to the C-terminus, see figures 1.9c and 1.10c (*49;50*). In contrast to the above mentioned radical-SAM enzymes, MoaA/MOCSIA is not implicated to be involved in a sulfur insertion step. Preliminary EPR and resonance Raman studies of MOCS1A indicated that the guanine moiety of the 5'-GTP substrate interacts at the unique Fe site of the C-terminal [4Fe-4S] cluster (H. L. Hernández and M. K. Johnson, unpublished results), suggesting a role in positioning or activating the substrate for H-abstraction. The recent 2.3 Å resolution crystal structure of MoaA complexed with 5'-GTP confirmed this observation

(*107*). MoaA binds 5'-GTP with high affinity and the crystal structure shows that 5'-GTP interacts with the C-terminal [4Fe-4S] cluster via the guanine N1 and N2 atoms, in a yet uncharacterized binding mode. The purine N1 nitrogen and the exocyclic N2 amino-group are 2.8 Å and 2.4 Å from the unique Fe of the C-terminal cluster, while the phosphate groups are tightly anchored within the hydrophilic channel by 12 hydrogen bonding interactions. $^{14}N/^{15}N$ ENDOR studies of MoaA and MOCS1A in collaboration with Professor Hoffman's group at Northwestern University are currently in progress to more precisely define the GTP-binding mode.

In summary, major advances in characterizing and understanding the mechanisms of radical-SAM enzymes have occurred over the past decade and the work presented in this dissertation has contributed significantly to the field. The emergence of a subclass of radical-SAM enzymes containing a second Fe-S cluster is an exciting development and much of the work presented in this dissertation constitutes pioneering attempts to characterize the role and properties of these clusters. Some of the second clusters discussed above have been shown to easily degrade and all have incomplete cysteinyl ligation making a purely structural or electron transfer role very unlikely. It is also clear that key components are likely missing from *in vitro* assays of radical-SAM enzymes with second clusters as none have been shown to be capable of more than one turnover. To date, *in vitro* assays of BioB, LipA, and MiaB do not catalyze multiple turnovers and the substrates for HydE and HydG have yet to be identified. Maximally, BioB produces 1 biotin per 1 monomer of BioB after 24 hours at 25 ˚C (*51*) and 50 μM LipA produces 18 μM lipoic acid over 30 min at 37 ˚C (*118*). While the substrate of HydE has not yet been determined, the enzyme cleaves SAM at a slow rate of 1 mol AdoH per mol protein per hour, indicating slow substrate turnover (*116*) and the MiaB reaction ceases after production of about 0.18 ms$^2$i$^6$Adenosine per MiaB polypeptide (*117*). While it is tempting to suggest that the second cluster has a direct role as a sulfur donor in radical-SAM enzymes involved in S-insertion reactions, it may be premature to ascribe such a function without evidence for multiple turnovers and the emerging evidence for a role in substrate binding and activation in MOCS1A/MoaA.

References

1. *Iron-Sulfur Proteins*, Advances in Inorganic Chemistry, Vol. 47, (Sykes, A. G. and Cammack, R., Eds.) Academic Press, San Diego (1999).

2. Beinert, H., Holm, R. H., and Münck, E. (1997) Iron-sulfur clusters; Nature's modular, multipurpose structures, *Science 277*, 653-659.

3. Beinert, H. (2000) Iron-sulfur proteins: ancient structures, still full of surprises, *JBIC, J. Biol. Inorg. Chem. 5*, 2-15.

4. Beinert, H. (2003) Iron-sulfur proteins: Properties and functions, in *Cellular Implications of Redox Signaling* (Gitler, C. and Danon, A., Eds.) pp 47-72, Imperial College Press, London.

5. Broderick, J. B. (2004) Iron-sulfur clusters in enzyme catalysis, in *Comprehensive Coordination Chemistry II, Vol. 8* (McCleverty, J. A. and Meyer, T. J., Eds.) pp 739-757, Elsevier, Oxford.

6. Johnson, M. K. (1994) Iron-sulfur proteins, in *Encyclopedia of inorganic chemistry* (King, R. B., Ed.) 1 ed., pp 1896-1915, John Wiley & Sons, Chichester.

7. Rees, D. C. (2002) Great Metalloclusters in Enzymology, *Annu. Rev. Biochem. 71*, 221-246.

8. Johnson, M. K. and Smith, A. D. (2005) Iron-sulfur proteins, in *Encyclopedia of inorganic chemistry* (King, R. B., Ed.) 2 ed., pp 2589-2619, John Wiley & Sons, Chichester.

9. Sticht, H. and Rösch, P. (1998) The structure of iron-sulfur proteins, *Prog. Biophys. Mol. Biol. 70*, 95-136.

10. Link, T. A. (1999) The structures of Rieske and Rieske-type proteins, *Adv. Inorg. Chem. 47*, 83-157.

11. Berkovitch, F., Nicolet, Y., Wan, J. T., Jarrett, J. T., and Drennan, C. L. (2004) Crystal structure of biotin synthase, an *S*-adenosylmethionine-dependent radical enzyme, *Science 303*, 76-79.

12. Hagen, W. R., Silva, P. J., Amorim, M. A., Hagedoorn, P. L., Wassink, H., Haaker, H., and Robb, F. T. (2000) Novel structure and redox chemistry of the prosthetic groups of the iron-sulfur flavoprotein sulfide dehydrogenase from *Pyrococcus furiosus*; evidence for a [2Fe-2S] cluster with Asp(Cys)$_3$ ligands, *J. Biol. Inorg. Chem. 5*, 527-534.

13. Yankovskaya, V., Horsefield, R., Törnroth, S., Luna-Chavez, C., Miyoshi, H., Léger, C., Byrne, B., Cecchini, G., and Iwata, S. (2003) Architecture of succinate dehydrogenase and reactive oxygen species generation, *Science 299*, 700-704.

14. Cecchini, G., Schröder, I., Gunsalus, R. P., and Maklashina, E. (2002) Succinate dehydrogenase and fumarate reductase from *Escherichia coli*, *Biochim. Biophys. Acta 1553*, 140-157.

15. Hunsicker-Wang, L. M., Heine, A., Chen, Y., Luna, E. P., Todaro, T., Zhang, Y. M., Williams, P. A., McRee, D. E., Hirst, J., Stout, C. D., and Fee, J. A. (2003) High-resolution structure of the soluble, respiratory-type Rieske protein from *Thermus thermophilus*: Analysis and comparison, *Biochemistry 42*, 7303-7217.

16. Peters, J. W., Lanzilotta, W. N., Lemon, B. J., and Seefeldt, L. C. (1998) X-ray crystal structure of the Fe-only hydrogenase (Cp1) from *Clostridium pasteurianum* to 1.8 Angstrom resolution, *Science 282*, 1853-1858.

17. Romao, M. J., Archer, M., Moura, I., Moura, J. J. G., LeGall, J., Engh, R., Schneider, M., Hof, P., and Huber, R. (1995) Crystal structure of the xanthine oxidase-related aldehyde oxido-reductase from *D. gigas*, *Science 270*, 1170-1176.

18. Wu, C. K., Dailey, H. A., Rose, J. P., Burden, A., Sellers, V. M., and Wang, B. C. (2001) The 2.0 Å structure of human ferrochelatase, the terminal enzyme of heme biosynthesis, *Nature Struct. Biol. 8*, 156-160.

19. Hidalgo, E. and Demple, B. (1994) An iron-sulfur center essential for transcriptional activation by the redox-sensing SoxR protein, *EMBO J. 13*, 138-146.

20. Kiley, P. J. and Beinert, H. (1998) Oxygen sensing by the global regulator, FNR: The role of the iron-sulfur cluster, *FEMS Microbiol. Rev. 22*, 341-352.

21. Beinert, H., Kennedy, M. C., and Stout, C. D. (1996) Aconitase as iron-sulfur protein, enzyme, and iron-regulatory protein, *Chem. Rev. 96*, 2335-2373.

22. Schwartz, C. J., Giel, J. L., Patschkowski, T., Luther, C., Ruzicka, F. J., Beinert, H., and Kiley, P. J. (2001) IscR, an Fe-S cluster-containing transcription factor, represses expression of *Escherichia coli* genes encoding Fe-S cluster assembly proteins, *Proc. Natl. Acad. Sci. USA 98*, 14895-14900.

23. Jameson, G. N. L., Cosper, M. M., Hernández, H. L., Johnson, M. K., and Huynh, B. H. (2004) Role of the [2Fe-2S] cluster in recombinant *Escherichia coli* biotin synthase, *Biochemistry 43*, 2022-2031.

24. Fukuyama, K. (2004) Structure and function of plant-type ferredoxins, *Photosyn. Res. 81*, 289-301.

25. Meyer, J. (2001) Ferredoxins of the third kind, *FEBS Lett. 509*, 1-5.

26. Beinert, H. and Thomson, A. J. (1983) Three-iron clusters in iron-sulfur proteins, *Arch. Biochem. Biophys. 222*, 333-361.

27. Kennedy, M. C., Kent, T. A., Emptage, M. H., Merkle, H., Beinert, H., and Münck, E. (1984) Evidence for the formation of a linear [3Fe-4S] cluster in partially unfolded aconitase, *J. Biol. Chem. 259*, 14463-14471.

28. Richards, A. J. M., Thomson, A. J., Holm, R. H., and Hagen, K. S. (1990) The magnetic circular dichroism spectra of the linear trinuclear clusters $[Fe_3S_4(SR)_4]^{3-}$ in purple aconitase and in a synthetic model, *Spectrochim. Acta 46A*, 987-993.

29. Johnson, M. K., Duderstadt, R. E., and Duin, E. C. (1999) Biological and synthetic $[Fe_3S_4]$ clusters, *Adv. Inorg. Chem. 47*, 1-82.

30. Schipke, C. G., Goodin, D. B., McRee, D. E., and Stout, C. D. (1999) Oxidized and reduced *Azotobacter vinelandii* ferredoxin I at 1.4 Å resolution: conformational change of surface residues without significant change in the $[3Fe\text{-}4S]^{+/0}$ cluster, *Biochemistry 38*, 8228-8239.

31. Duff, J. L. C., Breton, J. L., Butt, J. N., Armstrong, F. A., and Thomson, A. J. (1996) Novel redox chemistry of the [3Fe-4S] clusters: Electrochemical characterization of the all-Fe(II) form of the [3Fe-4S] cluster generated reversibly in various proteins and its spectroscopic investigation in *Sulfolobus acidocaldarius* ferredoxin, *J. Am. Chem. Soc. 118*, 8593-8603.

32. Calzolai, L., Gorst, C. M., Zhou, Z.-H., Teng, Q., Adams, M. W. W., and La Mar, G. N. (1995) $^1$H-NMR investigation of the electronic and molecular structure of the 4-iron cluster ferredoxin from the hyperthermophile *Pyrococcus furiosus* - identification of Asp-14 as a cluster ligand in each of the 4 redox states, *Biochemistry 34*, 11373-11384.

33. Volbeda, A., Charon, M.-H., Piras, C., Hatchikian, E. C., Frey, M., and Fontecilla-Camps, J. C. (1995) Crystal structure of the nickel-iron hydrogenase from *Desulfovibrio gigas*, *Nature 373*, 580-587.

34. Bertero, M. G., Rothery, R. A., Palak, M., Hou, C., Lim, D., Blasco, F., Weiner, J. H., and Strynadka, N. C. (2003) Insights into the respiratory electron transfer pathway from the structure of nitrate reductase A, *Nat. Struct. Biol. 10*, 681-687.

35. Marsh, E. N. G., Patwardhan, A., and Huhta, M. S. (2004) *S*-adenosylmethionine radical enzymes, *Bioorg. Chem. 32*, 326-340.

36. Crane, B. R., Siegel, L. M., and Getzoff, E. D. (1997) Structures of the siroheme- and [4Fe-4S]-containing active center of sulfite reductase in different states of oxidation: Heme activation via reduction-gated exogenous ligand exchange, *Biochemistry 36*, 12101-12119.

37. Dobbek, H., Svetlitchnyi, V., Gremer, L., Huber, R., and Meyer, O. (2001) Crystal structure of carbon monoxide dehydrogenase reveals a [Ni-4Fe-5S] cluster, *Science 293*, 1281-1285.

38. Doukov, T. I., Iverson, T. M., Seravalli, J., Ragsdale, S. W., and Drennan, C. L. (2002) A Ni-Fe-Cu center in a bifunctional carbon monoxide dehydrogenase/acetyl-CoA synthase, *Science 298*, 567-572.

39. Dai, S., Schwendtmayer, C., Johansson, K., Ramaswamy, S., Schürmann, P., and Eklund, H. (2000) How does light regulate chloroplast enzymes? Structure-function studies of the ferredoxin/thioredoxin system, *Quart. Rev. Biophys. 33*, 67-108.

40. Walters, E. M. and Johnson, M. K. (2004) Ferredoxin:thioredoxin reductase: disulfide reduction catalyzed via novel site-specific [4Fe-4S] cluster chemistry, *Photosynth. Res. 79*, 249-264.

41. Duin, E. C., Madadi-Kahkesh, S., Hedderich, R., Clay, M. D., and Johnson, M. K. (2002) Heterodisulfide reductase from *Methanothermobacter marburgensis* contains an active-site [4Fe-4S] cluster that is directly involved in mediating heterodisulfide reduction, *FEBS Lett. 512*, 263-268.

42. Grandoni, J. A., Switzer, R. L., Marakoff, C. A., and Zalkin, H. (1989) Evidence that the iron-sulfur cluster of *Bacillus subtilis* glutamine phosphoribosylpyrophosphate amidotransferase determines stability of the enzyme to degradation *in vivo*, *J. Biol. Chem. 264*, 6058-6064.

43. Cunningham, R. P., Asahara, H., Bank, J. F., Scholes, C. P., Salerno, J. C., Surerus, K. K., Münck, E., McCracken, J., Peisach, J., and Emptage, M. H. (1989) Endonuclease III is an iron-sulfur protein, *Biochemistry 28*, 4450-4455.

44. Porello, S. L., Cannon, M. J., and David, S. S. (1998) A substrate recognition role for the $[4Fe\text{-}4S]^{2+}$ cluster of the DNA repair glycosylase MutY, *Biochemistry 37*, 6465-6475.

45. Thauer, R. K. and Schönheit, P. (1982) Iron-sulfur complexes of ferredoxin as a storage form of iron in *Clostridium pasteurianum*, in *Iron-Sulfur Proteins* (Spiro, T. G., Ed.) pp 329-341, Wiley, New York.

46. Reeve, J. N., Beckler, G. S., Cram, D. S., Hamilton, P. T., Brown, J. W., Krzycki, J. A., Kolodziej, A. F., Alex, L. A., Orme-Johnson, W. H., and Walsh, C. T. (1989) A hydrogenase-linked gene in *Methanobacterium thermoautotrophicum* strain ΔH encodes a polyferredoxin, *Proc. Natl. Acad. Sci. USA 86*, 3031-3035.

47. Flint, D. H. and Allen, R. M. (1996) Iron-sulfur proteins with non-redox functions, *Chem. Rev. 96*, 2315-2334.

48. Jarrett, J. T. (2003) The generation of 5'-deoxyadenosyl radicals by adenosylmethionine-dependent radical enzymes, *Curr. Opin. Chem. Biol. 7*, 174-182.

49. Hänzelmann, P. and Schindelin, H. (2004) Crystal structure of the *S*-adenosylmethionine-dependent enzyme MoaA and its implications for molybdenum cofactor deficiency in humans, *Proc. Natl. Acad. Sci. USA 101*, 12870-12875.

50. Hänzelmann, P., Hernández, H., Menzel, C., Garcìa-Serres, R., Huynh, B. H., Johnson, M. K., Mendel, R. R., and Schindelin, H. (2004) Characterization of MOCS1A, an oxygen-sensitive iron-sulfur protein involved in human molybdenum cofactor biosynthesis, *J. Biol. Chem. 279*, 34721-34732.

51. Cosper, M. M., Krebs, B., Hernandez, H., Jameson, G., Eidsness, M. K., Huynh, B. H., and Johnson, M. K. (2004) Characterization of the cofactor content of *Escherichia coli* biotin synthase, *Biochemistry 43*, 2007-2021.

52. Pierrel, F., Hernández, H., Johnson, M. K., Fontecave, M., and Atta, M. (2003) MiaB protein from *Thermotoga maritima*: Characterization of an extremely thermophilic tRNA-methylthiotransferase, *J. Biol. Chem. 278*, 29515-29524.

53. Broderick, J. B., Henshaw, T. F., Cheek, J., Wojtuszewski, K., Smith, S. R., Trojan, M. R., McGhan, R. M., Kopf, A., Kibbey, M., and Broderick, W. E. (2000) Pyruvate formate-lyase-activating enzyme: Strictly anaerobic isolation yields active enzyme containing a $[3Fe\text{-}4S]^+$ cluster, *Biochem. Biophys. Res. Commun. 269*, 451-456.

54. Popescu, C., Bates, D. M., Beinert, H., Münck, E., and Kiley, P. J. (1998) Mössbauer spectroscopy as a tool for the study of activation/inactivation of the transcription regulator FNR in whole cells of *Escherichia coli*, *Proc. Natl. Acad. Sci. USA 95*, 13431-13435.

55. Kiley, P. J. and Beinert, H. (2003) The role of Fe-S proteins in sensing and regulation in bacteria, *Curr. Opin. Microbiol. 6*, 181-185.

56. Crack, J., Green, J., and Thomson, A. J. (2004) Mechanism of oxygen sensing by the bacterial transcriptional factor fumarate-nitrate reduction (FNR), *J. Biol. Chem. 279*, 9278-8286.

57. Anderson, G. L. and Howard, J. B. (1984) Reactions of the oxidized iron protein of *Azotobacter vinelandii* nitrogenase: Formation of a 2Fe center, *Biochemistry 23*, 2118-2122.

58. Sen, S., Igarashi, R., Smith, A. D., Johnson, M. K., Seefeldt, L. C., and Peters, J. W. (2004) A conformational mimic of the MgATP-bound "on state" of the nitrogenase iron protein, *Biochemistry 43*, 1787-1797.

59. Johnson, D., Dean, D. R., Smith, A. D., and Johnson, M. K. (2005) Structure, function and formation of biological iron-sulfur clusters, *Annu. Rev. Biochem. 74*, 247-281.

60. Agar, J. N., Krebs, B., Frazzon, J., Huynh, B. H., Dean, D. R., and Johnson, M. K. (2000) IscU as a scaffold for iron-sulfur cluster biosynthesis: Sequential assembly of [2Fe-2S] and [4Fe-4S] clusters in IscU, *Biochemistry 39*, 7856-7862.

61. Fontecave, M., Atta, M., and Mulliez, E. (2004) *S*-adenosylmethionine: Nothing goes to waste, *Trends Biochem. Sci. 29*, 243-249.

62. Marsh, E. N. G. (1999) Coenzyme B12 (cobalamin)-dependent enzymes, *Essays Biochem. 34*, 139-154.

63. Chirpich, T. P., Zappa, V., Costilow, R. N., and Barker, H. A. (1970) Lysine 2,3-aminomutase: Purification and properties of a pyridoxal phosphate and *S*-adenosylmethionine-activated enzyme, *J. Biol. Chem. 245*, 1778-1789.

64. Petrovich, R. M., Ruzicka, F. J., Reed, G. H., and Frey, P. A. (1991) Metal cofactors of lysine 2,3-aminomutase, *J. Biol. Chem. 266*, 7656-7660.

65. Petrovich, R. M., Ruzicka, F. J., Reed, G. H., and Frey, P. A. (1992) Characterization of iron-sulfur cluster in lysine 2,3-aminomutase by electron paramagnetic resonance spectroscopy, *Biochemistry 31*, 10774-10781.

66. Frey, P. A. and Magnusson, O. Th. (2003) *S*-adenosylmethionine: A wolf in sheep's clothing, or a rich man's adenosylcobalamin, *Chem. Rev. 103*, 2129-2148.

67. Knappe, J., Neugebauer, F. A., Blaschkowski, H. P., and Gänzler, M. (1984) Post-translational activation introduces a free radical into pyruvate formate-lyase, *Proc. Natl. Acad. Sci. USA 81*, 1332-1335.

68. Frey, P. A. and Moss, M. L. (1987) *S*-adenosylmethionine and the mechanism of hydrogen transfer in the lysine 2,3-aminomutase reaction, *Cold Spring Harbor Symp. Quant. Biol. 52*, 571-577.

69. Duin, E. C., Lafferty, M. E., Crouse, B. R., Allen, R. M., Sanyal, I., Flint, D. H., and Johnson, M. K. (1997) [2Fe-2S] to [4Fe-4S] cluster conversion in *Escherichia coli* biotin synthase, *Biochemistry 36*, 11811-11820.

70. Külzer, R., Pils, T., Kappl, R., Hüttermann, J., and Knappe, J. (1998) Reconstitution and characterization of the polynuclear iron-sulfur cluster in pyruvate formate-lyase-activating enzyme. Molecular properties of the holoenzyme form, *J. Biol. Chem. 273*, 4897-4903.

71. Ollagnier, S., Meier, C., Mulliez, E., Gaillard, J., Schuenemann, V., Trautwein, A. X., Mattioli, T., Lutz, M., and Fontecave, M. (1999) Assembly of 2Fe-2S and 4Fe-4S clusters in the anaerobic ribonucleotide reductase from *Escherichia coli*, *J. Am. Chem. Soc. 121*, 6344-6350.

72. Miller, J. R., Busby, R. W., Jordan, S. W., Cheek, J., Henshaw, T. F., Ashley, G. W., Broderick, J. B., Cronan, J. E., and Marletta, M. A. (2000) *Escherichia coli* LipA is a lipoyl synthase: *in vitro* biosynthesis of lipoylated pyruvate dehydrogenase complex from octanoyl-acyl carrier protein, *Biochemistry 39*, 15166-15178.

73. Ollagnier-de-Choudens, S., Sanakis, Y., Hewitson, K. S., Roach, P., Baldwin, J. E., Münck, E., and Fontecave, M. (2000) Iron-sulfur center of biotin synthase and lipoate synthase, *Biochemistry 39*, 4165-4173.

74. Wu, W., Booker, S. J., Lieder, K. W., Bandarian, V., Reed, G. H., and Frey, P. A. (2000) Lysine 2,3-aminomutase and trans-4.5-dehydrolysine: Characterization of an allylic analogue of a substrate-based radical in the catalytic mechanism, *Biochemistry 39*, 9561-9570.

75. Sofia, H. J., Chen, G., Hetzler, B. G., Reyes-Spindola, J. F., and Miller, N. E. (2001) Radical SAM, a novel protein superfamily linking unresolved steps in familiar biosynthetic pathways with radical mechanisms: Functional characterization using new analysis and information visualization methods, *Nucleic Acids Res. 29*, 1097-1106.

76. Cicchillo, R. M., Lee, K.-H., Baleanu-Gogonea, C., Nesbitt, N. M., Krebs, C., and Booker, S. J. (2004) *Escherichia coli* lipoyl synthase binds two distinct [4Fe-4S] clusters per polypeptide, *Biochemistry 43*, 11770-11781.

77. Tamarit, J., Gerez, C., Meier, C., Mulliez, E., Trautwein, A. X., and Fontecave, M. (2000) The activating component of the anaerobic ribonucleotide reductase from *Escherichia coli*: An iron-sulfur center with only three cysteines, *J. Biol. Chem. 275*, 15669-15675.

78. Layer, G., Moser, J., Heinz, D. W., Jahn, D., and Schubert, W. D. (2003) Crystal structure of coproporphyrinogen III oxidase reveals cofactor geometry of Radical SAM enzymes, *EMBO J. 22*, 6214-6224.

79. Lepore, B. W., Ruzicka, F. J., Frey, P. A., and Ringe, D. (2005) The x-ray crystal structure of lysine-2,3-aminomutase from *Clostridium subterminale*, *Proc. Natl. Acad. Sci. USA 102*, 13819-13824.

80. Krebs, C., Broderick, W. E., Henshaw, T. F., Broderick, J. B., and Huynh, B. H. (2002) Coordination of adenosylmethionine to a unique iron site of the [4Fe-4S] cluster of pyruvate formate-lyase activating enzyme: a Mössbauer spectroscopic study, *J. Am. Chem. Soc. 124*, 912-913.

81. Cosper, N. J., Booker, S. J., Ruzicka, F. J., Frey, P. A., and Scott, R. A. (2000) Direct FeS cluster involvement in generation of a radical in lysine 2,3-aminomutase, *Biochemistry 39*, 15668-15673.

82. Chen, D. W., Walsby, C. J., Hoffman, B. M., and Frey, P. A. (2003) Coordination and mechanism of reversible cleavage of *S*-adenosylmethionine by the [4Fe-4S] center in lysine 2,3-aminomutse, *J. Am. Chem. Soc. 125*, 11788-11789.

83. Moss, M. and Frey, P. A. (1987) The role of *S*-adenosylmethionine in the lysine 2,3-aminomutase reaction, *J. Biol. Chem. 262*, 14859-14862.

84. Cosper, M. M., Cosper, N. J., Hong, W., Shokes, J. E., Broderick, W. E., Broderick, J. B., Johnson, M. K., and Scott, R. A. (2003) Structural studies of the interaction of *S*-adenosylmethionine with the [4Fe-4S] clusters in biotin synthase and pyruvate formate-lyase activating enzyme, *Protein Science 12*, 1573-1577.

85. Cheek, J. and Broderick, J. B. (2002) Direct H atom abstraction from spore photoproduct C-6 initiates DNA repair in the reaction catalyzed by spore photoproduct lyase: Evidence for a reversibly generated adenosyl radical intermediate, *J. Am. Chem. Soc. 124*, 2860-2861.

86. Cosper, M. M., Jameson, G. N. L., Davydov, R., Eidsness, M. K., Hoffman, B. M., Huynh, B. H., and Johnson, M. K. (2002) The $[4Fe\text{-}4S]^{2+}$ cluster in reconstituted biotin synthase binds *S*-adenosylmethionine, *J. Am. Chem. Soc. 124*, 14006-14007.

87. Walsby, C. J., Hong, W., Broderick, W. E., Cheek, J., Ortillo, D., Broderick, J. B., and Hoffman, B. M. (2002) Electron-nuclear double resonance spectroscopic evidence that *S*-adenosylmethionine binds in contact with the catalytically active $[4Fe\text{-}4S]^{+}$ cluster in pyruvate formate-lyase activating enzyme, *J. Am. Chem. Soc. 124*, 3143-3151.

88. Walsby, C. J., Ortillo, D., Broderick, W. E., Broderick, J. B., and Hoffman, B. M. (2002) An anchoring role for FeS clusters: Chelation of the amino acid moiety of *S*-adenosylmethionine to the unique iron site of the [4Fe-4S] cluster of pyruvate formate-lyase activating enzyme, *J. Am. Chem. Soc. 124*, 11270-11271.

89. Layer, G., Kervio, E., Morlock, G., Heinz, D. W., Jahn, D., Retey, J., and Schubert, W.-D. (2005) Structural and functional comparison of HemN to other radical SAM enzymes, *Biol. Chem. 386*, 971-980.

90. Volker Wagner, A. F., Frey, M., Neugebauer, F. A., Schafer, W., and Knappe, J. (1992) The free radical in pyruvate formate-lyase is located on glycine-734, *Proc. Natl. Acad. Sci. USA 89*, 996-1000.

91. Bianchi, V., Eliasson, R., Fontecave, M., Mulliez, E., Hoover, D. M., Matthews, R. G., and Reichard, P. (1993) Flavodoxin is required for the activation of the anaerobic ribonucleotide reductase, *Biochem. Biophys. Res. Commun. 197*, 792-797.

92. Mulliez, E., Padovani, D., Atta, M., Alcouffe, C., and Fontecave, M. (2001) Activation of class III ribonucleotide reductase by flavodoxin: A protein radical-driven electron transfer to the iron-sulfur center, *Biochemistry 40*, 3730-3736.

93. Picciocchi, A., Douce, R., and Alban, C. (2003) The plant biotin synthase reaction: Identification and characterization of essential mitochondrial accessory protein components, *J. Biol. Chem. 278*, 24966-24975.

94. Ollagnier-de-Choudens, S., Sanakis, Y., Hewitson, K. S., Roach, P. L., Münck, E., and Fontecave, M. (2002) Reductive cleavage of *S*-adenosylmethionine by biotin synthase from *Escherichia coli*, *J. Biol. Chem. 277*, 13449-13454.

95. Henshaw, T. F., Cheek, J., and Broderick, J. B. (2000) The $[4Fe\text{-}4S]^{1+}$ cluster of pyruvate formate-lyase activating enzyme generates the glycyl radical on pyruvate formate-lyase: EPR-detected single turnover, *J. Am. Chem. Soc. 122*, 8331-8332.

96. Padovani, D., Thomas, F., Trautwein, A. X., Mulliez, E., and Fontecave, M. (2001) Activation of class III ribonucleotide reductase from *E. coli*. The electron transfer from the iron-sulfur center to *S*-adenosylmethionine, *Biochemistry 40*, 6713-6719.

97. Moss, M. L. and Frey, P. A. (1990) Activation of lysine 2,3-aminomutase by *S*-adenosylmethionine, *J. Biol. Chem. 265*, 18112-18115.

98. Frey, M., Rothe, M., Volker Wagner, A. F., and Knappe, J. (1994) Adenosylmethionine-dependent synthesis of the glycyl radical in pyruvate formate-lyase by abstraction of the glycine C-2 pro-S hydrogen atom, *J. Biol. Chem. 269*, 12432-12437.

99. Ollagnier, S., Mulliez, E., Schmidt, P. P., Eliasson, R., Gaillard, J., Deronzier, C., Bergman, T., Reichard, P., and Fontecave, M. (1997) Activation of the anaerobic ribonucleotide reductase from *Escherichia coli*: The essential role of the iron-sulfur center for *S*-adenosylmethionine reduction, *J. Biol. Chem. 272*, 24216-24223.

100. Rebeil, R. and Nicholson, W. L. (2001) The subunit structure and catalytic mechanism of the *Bacillus subtilis* DNA repair enzyme spore photoproduct lyase, *Proc. Natl. Acad. Sci. USA 98*, 9038-9043.

101. Ballinger, M. D., Reed, G. H., and Frey, P. A. (1992) An organic radical in the lysine 2,3-aminomutase reaction, *Biochemistry 31*, 949-953.

102. Escalettes, F., Florentin, D., Tse Sum Bui, B., Lesage.D., and Marquet, A. (1999) Biotin synthase mechanism: Evidence for hydrogen transfer from the substrate into deoxyadenosine, *J. Am. Chem. Soc. 121*, 3571-3578.

103. Duboc-Toia, C., Hassan, A. K., Mulliez, E., Ollagnier-de Choudens, S., Fontecave, M., Leutwein, C., and Heider, J. (2003) Very high-field EPR study of glycyl radical enzymes, *J. Am. Chem. Soc. 125*, 38-39.

104. Knappe, J. and Wagner, A. F. V. (2001) Stable glycyl radical form pyruvate formate-lyase and ribonucleotide reductase (III), *Adv. Protein Chem. 58*, 277-315.

105. Verfürth, K., Pierik, A. J., Leutwein, C., Zorn, S., and Heider, J. (2004) Substrate specificities and electron paramagnetic resonance properties of benzylsuccinate synthases in anaerobic toluene and m-xylene metabolism, *Arch. Microbiol. 181*, 155-162.

106. Ugulava, N. B., Frederick, K. K., and Jarrett, J. T. (2003) Control of adenosylmethionine-dependent radical generation in biotin synthase: A kinetic and thermodynamic analysis of substrate binding to active and inactive forms of BioB, *Biochemistry 42*, 2708-2719.

107. Hänzelmann, P. and Schindelin, H. (2006) Binding of 5'-GTP to the C-terminal FeS cluster of the radical *S*-adenosylmethionine enzyme MoaA provides insights into mechanism, *Proc. Natl. Acad. Sci. USA 103*, 6829-6834.

108. Ugulava, N. B., Gibney, B. R., and Jarrett, J. T. (2001) Biotin synthase contains two distinct iron-sulfur cluster binding sites: Chemical and spectroelectrochemical analysis of iron-sulfur cluster interconversions, *Biochemistry 40*, 8343-8351.

109. Ugulava, N. B., Surerus, K. K., and Jarrett, J. T. (2003) Evidence from Mössbauer spectroscopy for distinct $[2Fe\text{-}2S]^{2+}$ and $[4Fe\text{-}4S]^{2+}$ cluster binding sites in biotin synthase from *Escherichia coli*, *J. Am. Chem. Soc. 124*, 9050-9051.

110. Ugulava, N. B., Sacanell, C. J., and Jarrett, J. T. (2001) Spectroscopic changes during a single turnover of biotin synthase: Destruction of a [2Fe-2S] cluster accompanies sulfur insertion, *Biochemistry 40*, 8352-8358.

111. Tse Sum Bui, B., Florentin, D., Fournier, F., Ploux, O., Méjean, A., and Marquet, A. (1998) Biotin synthase mechanism: On the origin of sulfur, *FEBS Lett. 440*, 226-230.

112. Tse Sum Bui, B., Mattioli, T., Florentin, D., Bolbach, G., and Marquet, A. (2006) *Escherichia coli* biotin synthase produces selenobiotin. Further evidence of the involvement of the $[2Fe\text{-}2S]^{2+}$ cluster in the sulfur insertion step, *Biochemistry 45*, 3824-3834.

113. Choi-Rhee, E. and Cronan, J. E. (2005) Biotin synthase is catalytic in vivo, but catalysis endangers destruction of the protein, *Chemistry and Biology 12*, 461-468.

114. Cicchillo, R. M. and Booker, S. J. (2005) Mechanistic investigations of lipoic acid biosynthesis in *Escherichia coli*: Both sulfur atoms in lipoic acid are contributed by the same lipoyl synthase polypeptide, *J. Am. Chem. Soc. 127*, 2860-2861.

115. Posewitz, M. C., King, P. W., Smolinski, S. L., Zhang, L., Seibert, M., and Ghirardi, M. L. (2004) Discovery of two novel radical *S*-adenosylmethionine proteins required for the assemble of an active [Fe] hydrogenase, *J. Biol. Chem. 279*, 25711-25720.

116. Rubach, J. K., Brazzolotto, X., Gaillard, J., and Fontecave, M. (2005) Biochemical characterization of the HydE and HydG iron-only hydrogenase maturation enzymes from *Thermotoga maritima*, *FEBS Lett. 579*, 5055-5060.

117. Pierrel, F., Douki, T., Fontecave, M., and Atta, M. (2004) MiaB protein is a bifunctional radical-*S*-adenosylmethionine enzyme involved in thiolation and methylation of tRNA, *Biochemistry 46*, 47555-47563.

118. Cicchillo, R. M., Iwig, D. F., Jones, A. D., Nesbitt, N. M., Baleanu-Gogonea, C., Souder, M. G., Tu, L., and Booker, S. J. (2004) Lipoyl synthase requires two equivalents of *S*-adenosylmethionine to synthesize one equivalent of lipoic acid, *Biochemistry 43*, 6378-6386.

119. Dauter, Z., Sieker, L. C., and Wilson, K. S. (1992) Refinement of rubredoxin from *Desulfovibrio vulgaris* at 1.0 Å with and without restraints, *Acta Crystallogr. 48*, 42-59.

120. Jacobson, B. L., Chae, Y. K., Markley, J. L., Rayment, I., and Holden, H. M. (1993) Molecular structure of the oxidized, recombinant, heterocyst [2Fe-2S] ferredoxin from Anabaena 7120 determined to 1.7-Å resolution, *Biochemistry 32* 6788-6793.

121. Surerus, K. K., Münck, E., Moura, I., Moura, J. J. G., and LeGall, J. (1987) Evidence for the formation of a $ZnFe_3S_4$ cluster in *Desulfovibio gigas* ferredoxin II, *J. Am. Chem. Soc. 109*, 3805-3807.

122. Breton, J. L., Duff, J. L. C., Butt, J. N., Armstrong, F. A., George, S. J., Petillot, Y., Forest, E., Schafer, G., and Thomson, A. J. (1995) Identification of the iron-sulfur clusters in a ferredoxin from the archaeon *Sulfolobus acidocaldarius*: Evidence for a reduced [3Fe-4S] cluster with pH-dependent electronic properties, *Eur. J. Biochem. 233*, 937-946.

123. Crouse, B. R., Meyer, J., and Johnson, M. K. (1995) Spectroscopic evidence for a reduced $Fe_2S_2$ cluster with a $S = 9/2$ ground state in mutant forms of *Clostridium pasteurianum* 2Fe ferredoxin, *J. Am. Chem. Soc. 117*, 9612-9613.

124. Achim, C., Golinelli, M.-P., Bominaar, E. L., Meyer, J., and Münck, E. (1996) Mössbauer study of Cys56Ser mutant 2Fe ferredoxin from *Clostridium pasteurianum*: Evidence for double exchange in an $[Fe_2S_2]^+$ cluster, *J. Am. Chem. Soc. 118*, 8168-8169.

125. Johnson, M. K., Duin, E. C., Crouse, B. R., Golinelli, M.-P., and Meyer, J. (1998) Valence-delocalized $[Fe_2S_2]^+$ clusters, in *Spectroscopic methods in bioinorganic chemistry* (Solomon, E. I. and Hodgson, K. O., Eds.) pp 286-301, American Chemical Society, Washington, D.C.

**Table 1.1** Distances between the unique iron of the radical-SAM cluster and SAM.

| | Structure resolution (Å) | $Fe_{unique}$-$SAM_N$ (Å) | $Fe_{unique}$-$SAM_O$ (Å) | $Fe_{unique}$-$SAM_{S/Se}$ (Å) | $Fe_{unique}$-$SAM_{CH_3}$ (Å) |
|---|---|---|---|---|---|
| HemN | 2.1 | 2.6 | 2.3 | 3.6 | 4.3 |
| BioB | 3.4 | 2.4 | 2.5 | 4.0 | 5.4 |
| MoaA | 2.2 | 2.3 | 2.0 | 3.2 | 4.4 |
| KAM | 2.1 | 2.0 | 2.0 | 3.2 | 4.5 |

HemN from *E. coli*, PDB ID# 1OLT (*78*);BioB from *E. coli*, PDB ID# 1R30 (*11*); MoaA from *S. aureus*, PDB ID# 1TV8 (*49*); KAM from *C. subterminale*, PDB ID# 2A5H (*79*).

**Figure 1.1** Crystallographically defined structures of the four basic iron-sulfur clusters in biology. Shown with all cysteinyl ligation. Structures were taken from coordinates deposited in the Protein Data Bank: a. Fe Rd, PDB ID# 8RXN, rubredoxin from *Desulfovibrio vulgaris* (*119*); b.[2Fe-2S], PDB ID# 1FRD, *Anabaena* pcc7120 Fd (*120*); c. [3Fe-4S], PDB ID# 6FDR, *Azotobacter vinelandii* FdI (*30*); d. [4Fe-4S], PDB ID# 6FDR, *Azotobacter vinelandii* FdI (*30*). Color code: pink, iron; yellow, sulfur. Adapted from (*8*).

a

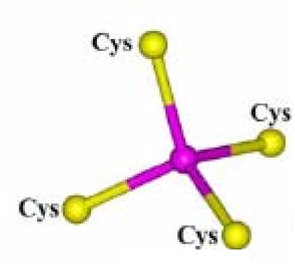
Cys
Cys
Cys
Cys

Fe Rd

b

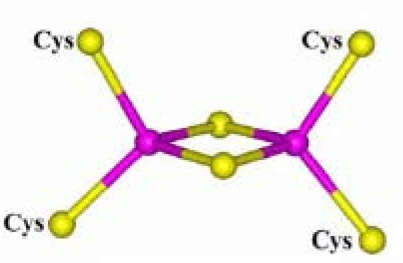
Cys
Cys
Cys
Cys

[2Fe-2S]

c

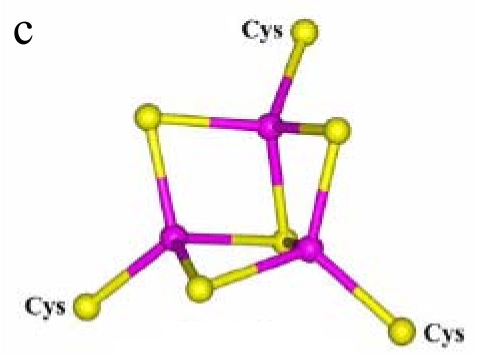

[3Fe-4S]

d

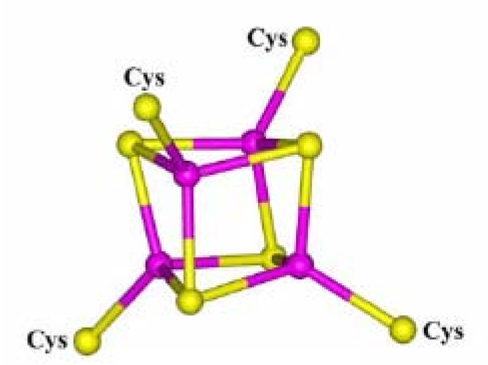
Cys
Cys
Cys
Cys

[4Fe-4S]

**Figure 1.2** Ground state spin (*S*) and valence-delocalization schemes of the fundamental types of Fe-S clusters. Discrete $[3Fe\text{-}4S]^-$ centers are shown in brackets as they have not been observed in any protein, but have been identified as fragments of heterometallic cubane clusters (*121*). The three electron reduction of $[3Fe\text{-}4S]^+$ clusters to yield $[3Fe\text{-}4S]^{2-}$ clusters occurs with the concomitant addition of three proteins (*122*). Valance-delocalized $[2Fe\text{-}2S]^+$ clusters have only been observed in the C56S and C60S variants of *C. pasteurianum* 2Fe Fd (*123-125*). Color code: $Fe^{3+}$, red; $Fe^{2+}$, blue; $Fe^{2.5+}$, green; S, yellow; O, white (*8*).

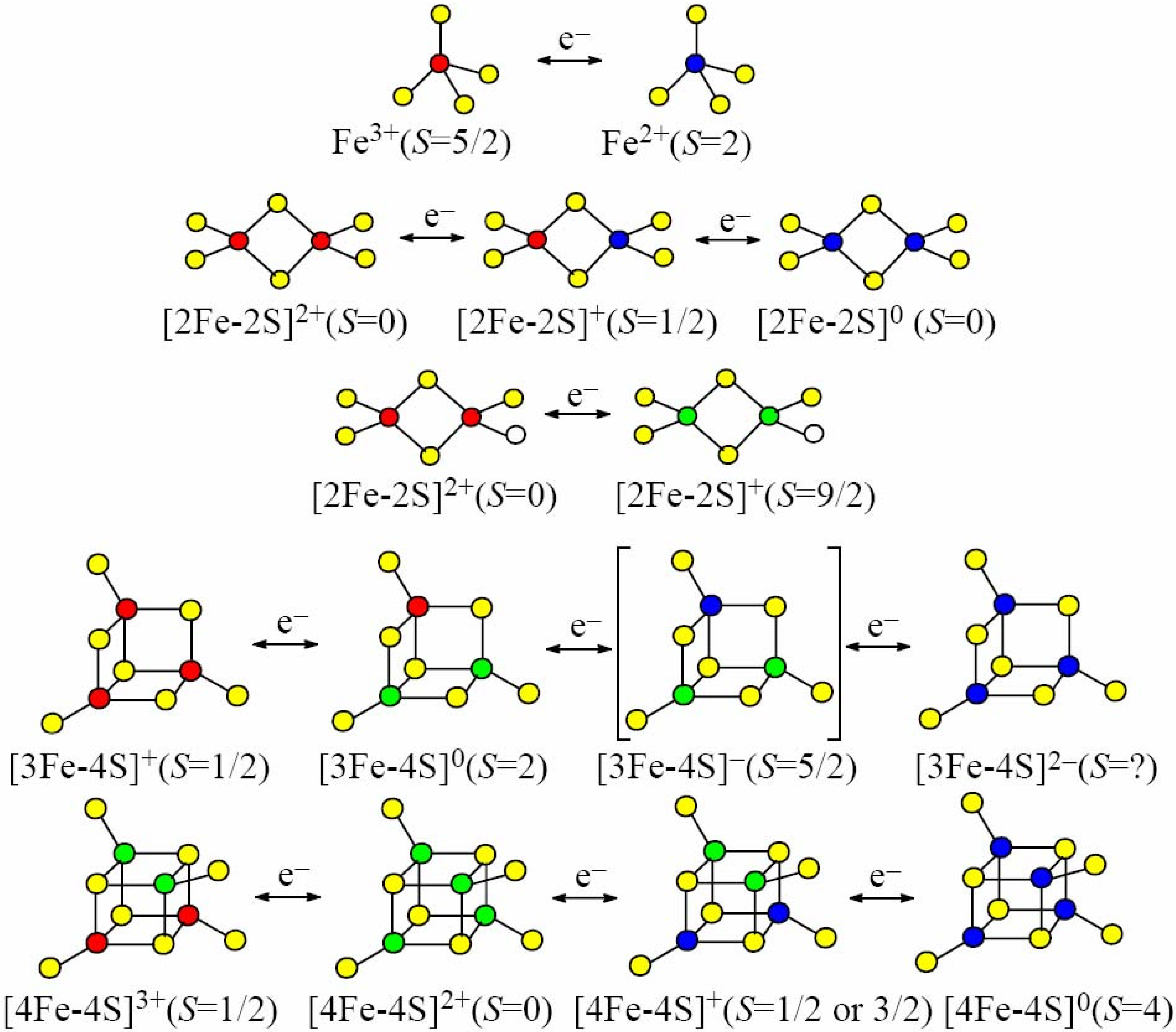
e⁻
Fe3+(S=5/2)
Fe2+(S=2)
e⁻
e⁻
[2Fe-2S]2+(S=0)
[2Fe-2S]+(S=1/2)
[2Fe-2S]0 (S=0)
e⁻
[2Fe-2S]2+(S=0)
[2Fe-2S]+(S=9/2)
e⁻
e⁻
e⁻
[3Fe-4S]+(S=1/2)
[3Fe-4S]0(S=2)
[3Fe-4S]−(S=5/2)
[3Fe-4S]2−(S=?)
e⁻
e⁻
e⁻
[4Fe-4S]3+(S=1/2)
[4Fe-4S]2+(S=0)
[4Fe-4S]+(S=1/2 or 3/2)
[4Fe-4S]0(S=4)

**Figure 1.3** Ranges of midpoint potentials (mV verses NHE) for biological Fe-S centers. $[2Fe-2S]^{2+,+}{}_R$, Rieske-type Fe-S center (*8*).

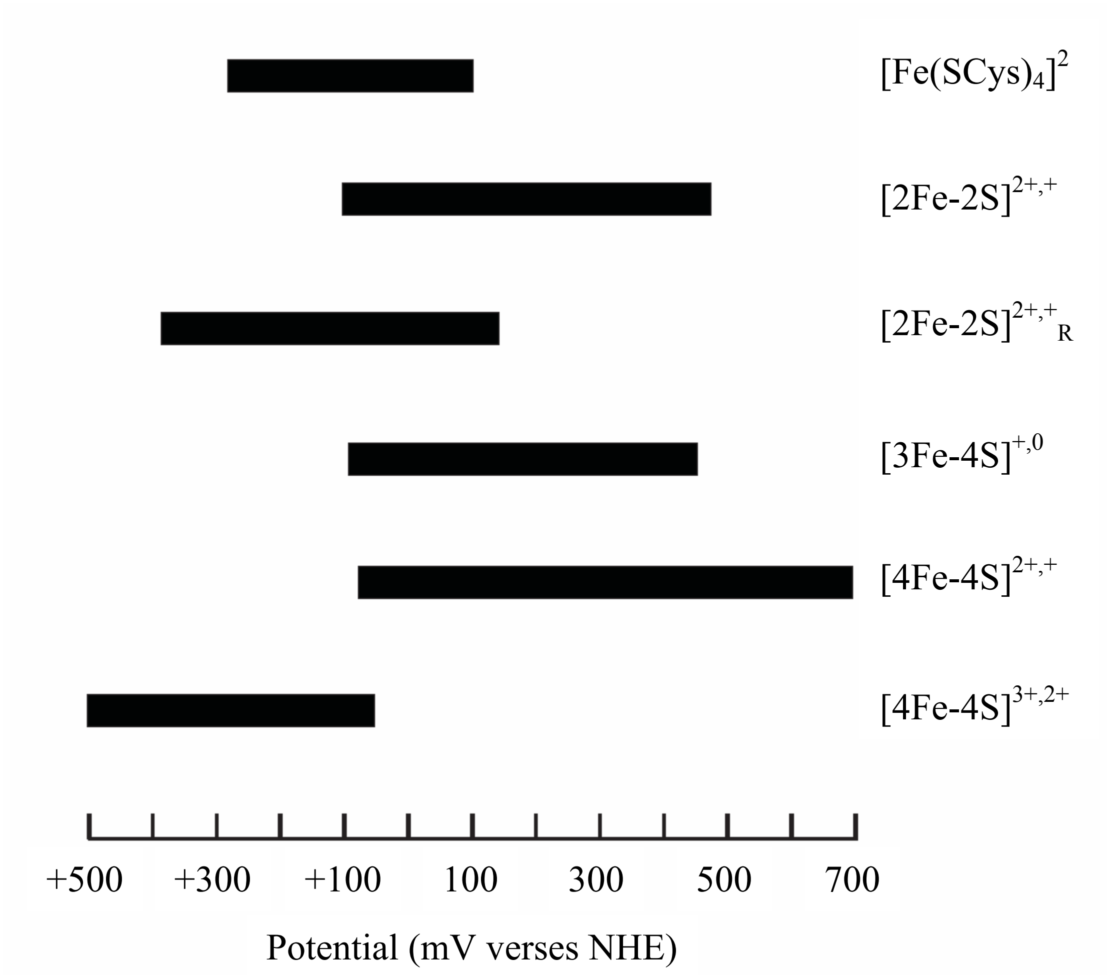
[Fe(SCys)4]2
[2Fe-2S]2+,+
[2Fe-2S]2+,+R
[3Fe-4S]+,0
[4Fe-4S]2+,+
[4Fe-4S]3+,2+
+500
+300
+100
100
300
500
700
Potential (mV verses NHE)

**Figure 1.4** Summary of the types of cluster transformations that have been observed in Fe-S proteins. $M^+$ = $Cu^+$ and $Tl^+$; $M^{2+}$ = $Cr^{2+}$, $Mn^{2+}$, $Co^{2+}$, $Ni^{2+}$, $Zn^{2+}$, $Cd^{2+}$ (*8*).

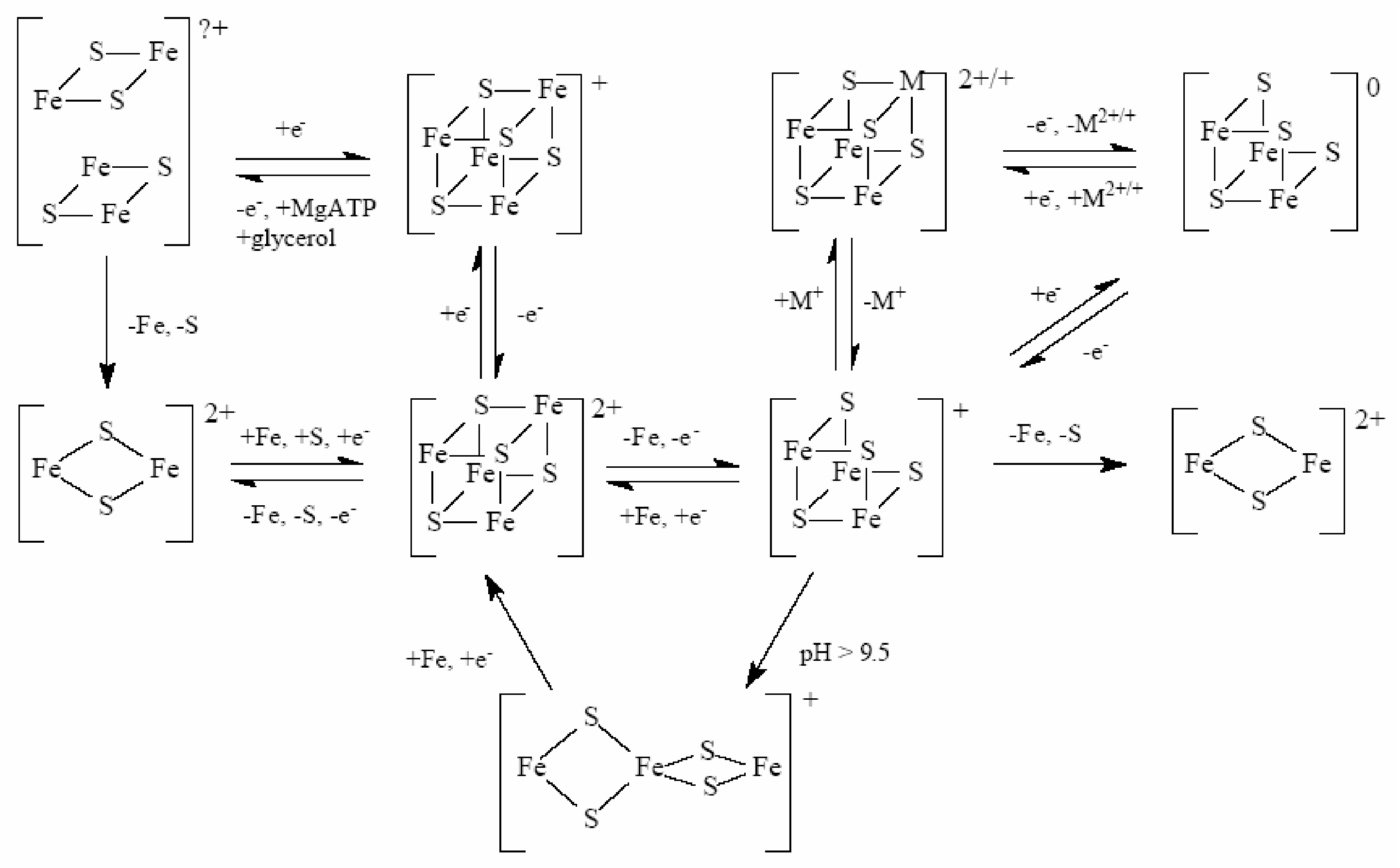
?+
+e-
-e-, +MgATP
+glycerol
+
2+/+
-e-, -M2+/+
+e-, +M2+/+
0
-Fe, -S
+e-
-e-
+M+
-M+
+e-
-e-
2+
+Fe, +S, +e-
-Fe, -S, -e-
2+
-Fe, -e-
+Fe, +e-
+
-Fe, -S
2+
+Fe, +e-
pH > 9.5
+

**Figure 1.5** Reactions catalyzed by radical-SAM enzymes. All reactions require a reduced radical-SAM $[4Fe\text{-}4S]^+$ cluster and one or two molecules of SAM. Those requiring two molecules of SAM are indicated by (2) following SAM above the arrow. The nature of additional cofactors and/or the second Fe-S cluster (if any) is indicated below the arrow.

KAM

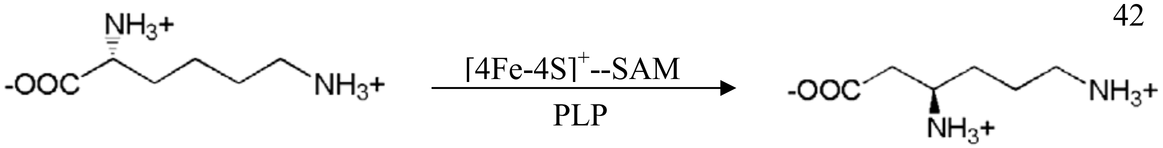

NH3+
-OOC
NH3+
[4Fe-4S]+--SAM
PLP
-OOC
NH3+
NH3+

L-α-lysine

L-ß-lysine

PFL-AE
RNR-AE
BssD-AE

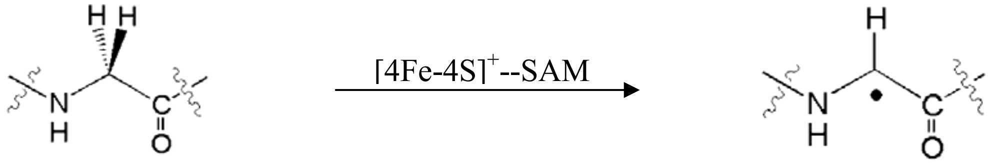

H H
N
H
C
O
[4Fe-4S]+--SAM
H
N
H
C
O

glycine of PFL, RNR or BssD

glycine radical

BioB

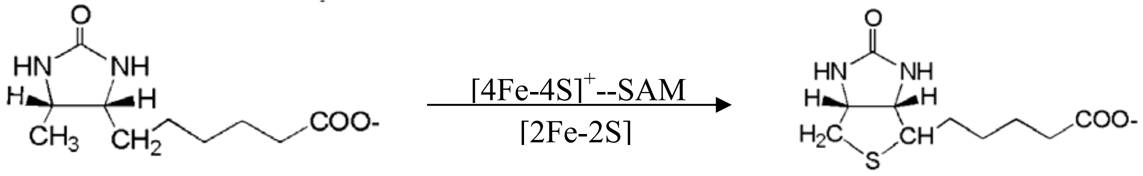

O
HN
NH
H
H
CH3
CH2
COO-
[4Fe-4S]+--SAM
[2Fe-2S]
O
HN
NH
H
H
H2C
CH
S
COO-

dethiobiotin

biotin

SP-lyase

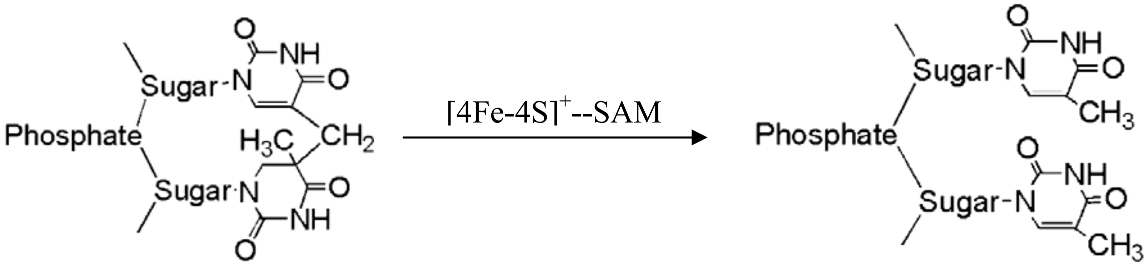

Sugar-N
NH
O
O
Phosphate
H3C
CH2
Sugar-N
O
NH
O
[4Fe-4S]+--SAM
Sugar-N
NH
O
O
CH3
Phosphate
Sugar-N
NH
O
O
CH3

thymine dimer

two thymidines

LipA

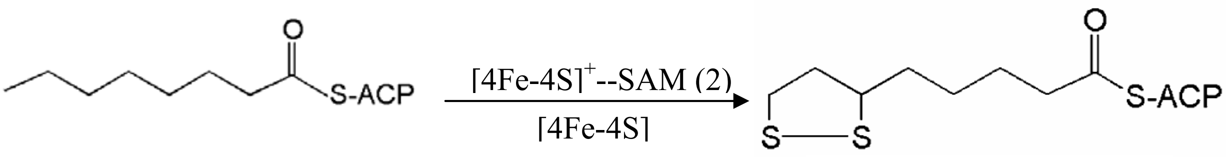

O
S-ACP
[4Fe-4S]+--SAM (2)
[4Fe-4S]
O
S-ACP
S
S

octanoyl acyl carrier protein

lipoyl acyl carrier protein

HemN

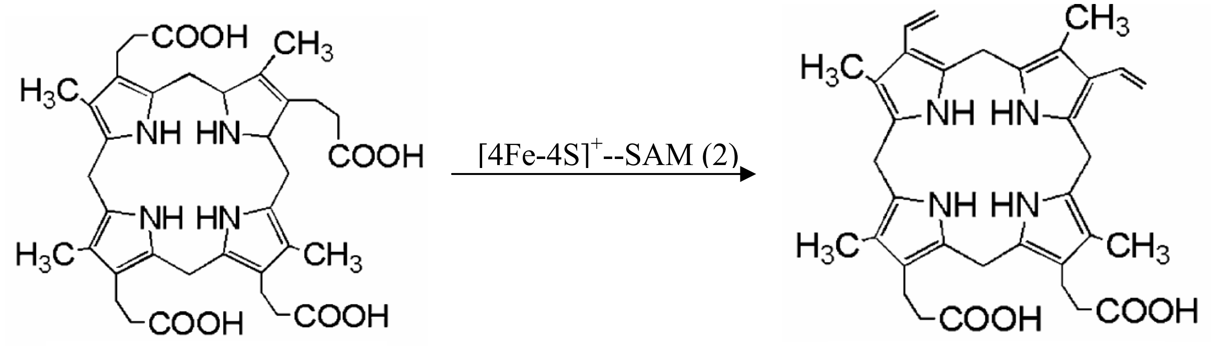

COOH
CH3
H3C
NH HN
COOH
NH HN
H3C
CH3
COOH
COOH
[4Fe-4S]+--SAM (2)
CH3
H3C
NH HN
NH HN
H3C
CH3
COOH
COOH

coproporphyrinogen III

protoporphyrinogen IX

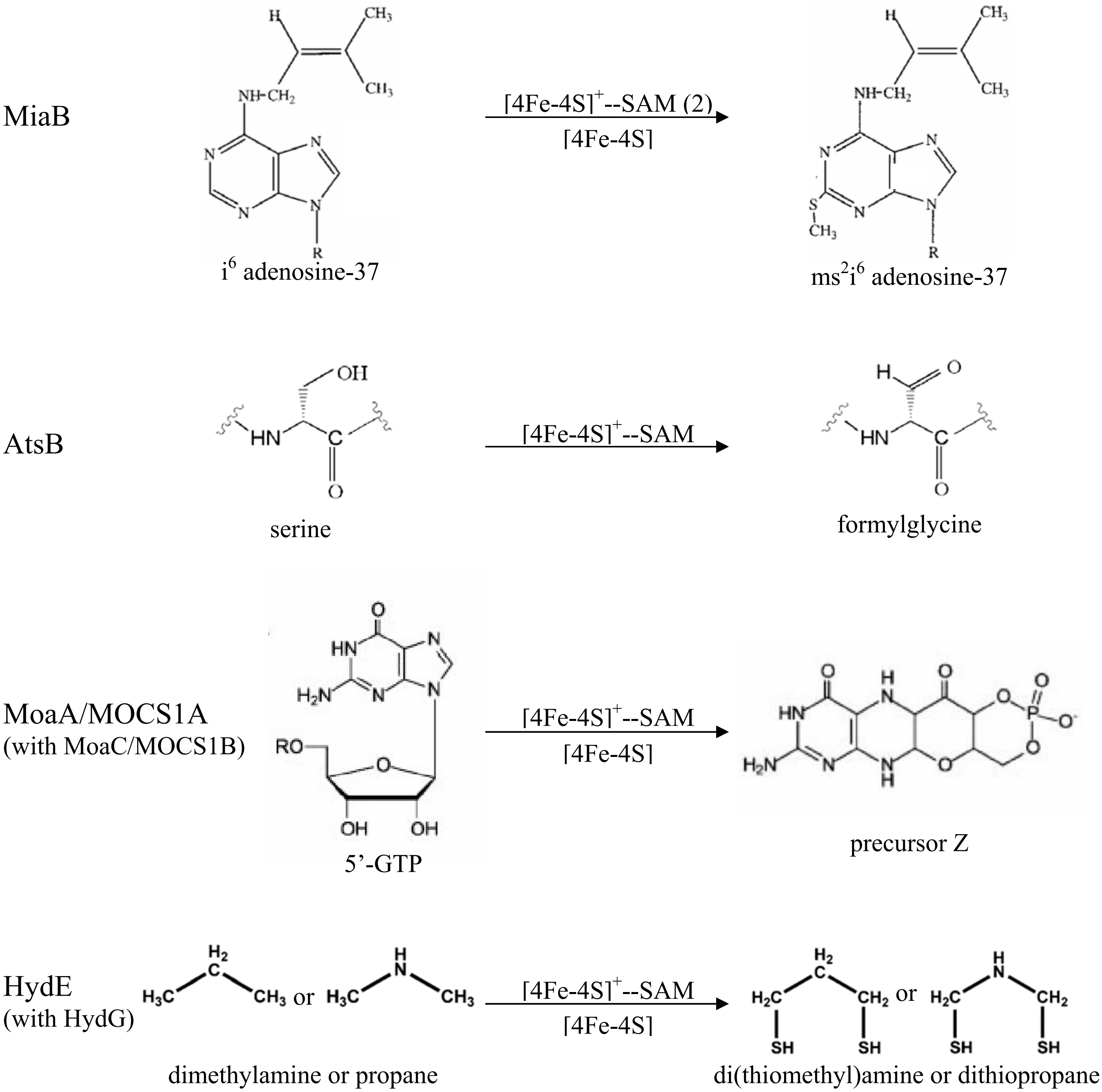
MiaB
[4Fe-4S]+--SAM (2)
[4Fe-4S]
i6 adenosine-37
ms2i6 adenosine-37
AtsB
[4Fe-4S]+--SAM
serine
formylglycine
MoaA/MOCS1A
(with MoaC/MOCS1B)
[4Fe-4S]+--SAM
[4Fe-4S]
5'-GTP
precursor Z
HydE
(with HydG)
or
[4Fe-4S]+--SAM
[4Fe-4S]
or
dimethylamine or propane
di(thiomethyl)amine or dithiopropane

**Figure 1.6** Crystal structures of the coordination of SAM to the [4Fe-4S] cluster bound by the CxxxCxxC motif are compared. a, HemN from *E. coli*, PDB ID# 1OLT (*78*); b, BioB from *E. coli*, PDB ID# 1R30 (*11*); c, MoaA from *S. aureus*, PDB ID# 1TV8 (*49*); d, KAM from *C. subterminale*, PDB ID# 2A5H (*79*).

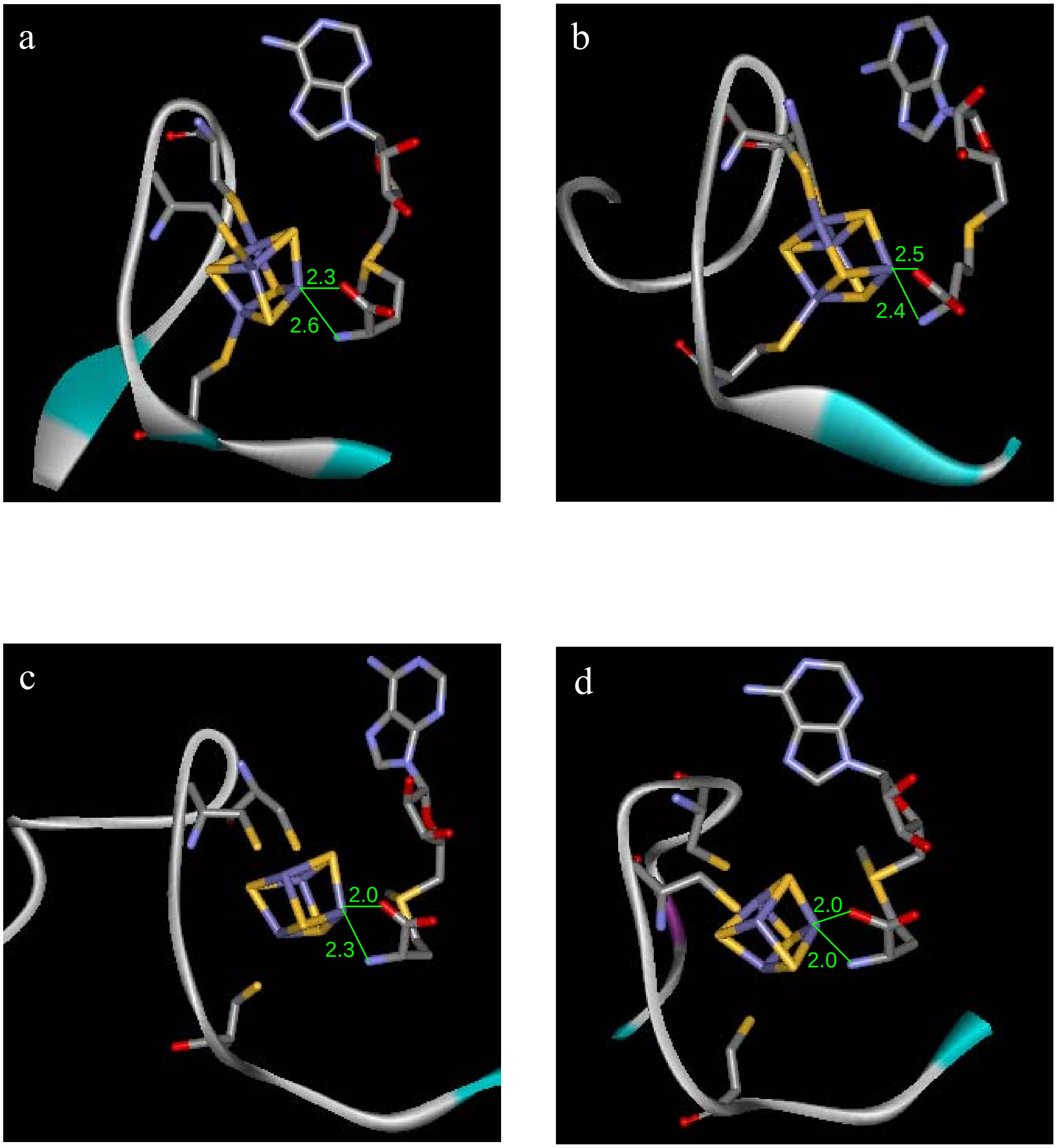
a
2.3
2.6
b
2.5
2.4
c
2.0
2.3
d
2.0
2.0

**Figure 1.7** Proposed mechanism for the reductive cleavage of SAM**.** Once the $[4Fe\text{-}4S]^{2+}$ cluster is reduced via electron transfer from reduced flavodoxin, the SAM bound active $[4Fe\text{-}4S]^{+}$ cluster transfers an electron to the sulfonium of SAM, inducing the reductive cleavage of the carbon-sulfonium bond forming methionine and the extremely reactive 5'-deoxyadenosyl radical.

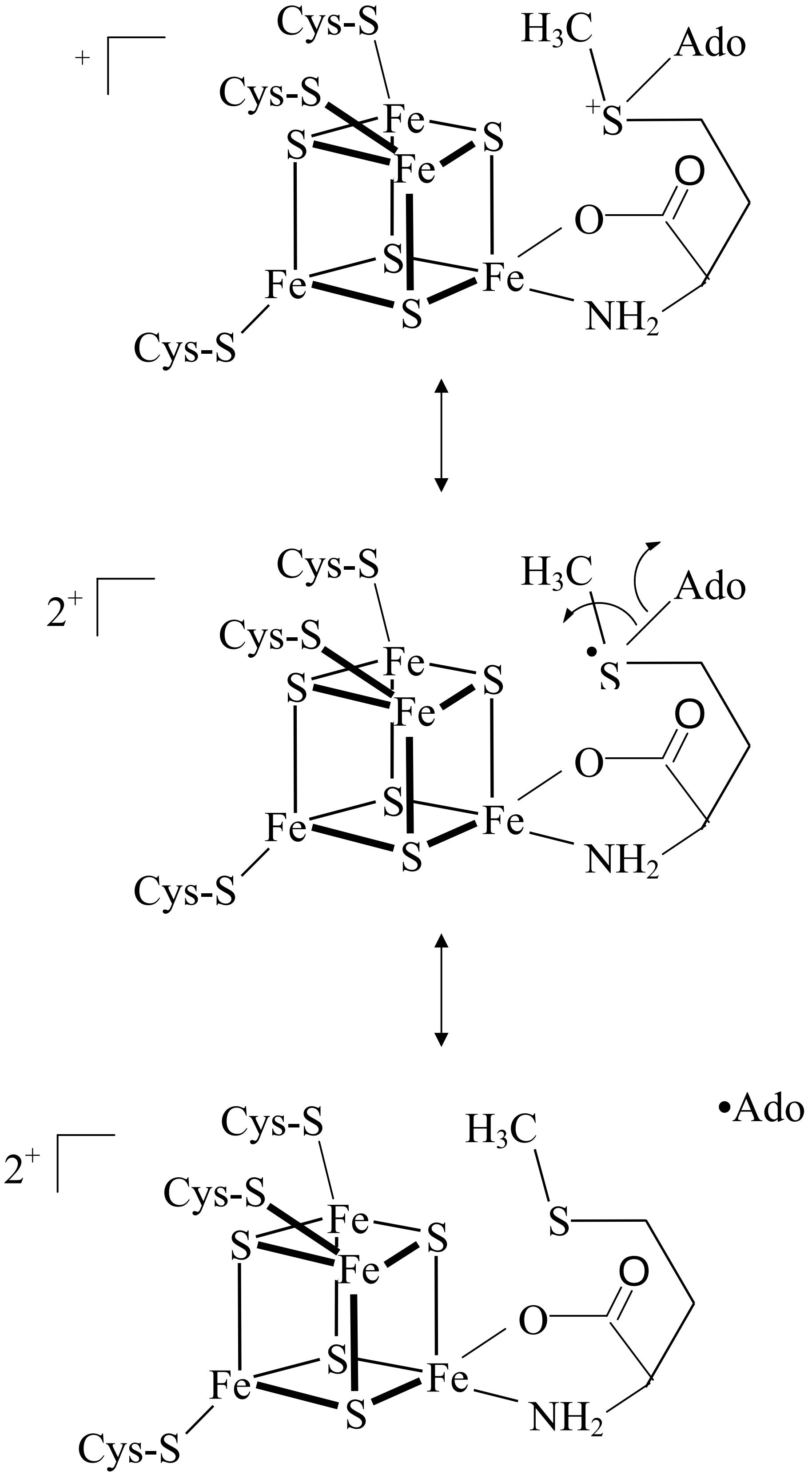
+
Cys-S
Cys-S
Fe
S
Fe
S
S
Fe
Fe
S
Cys-S
H3C
Ado
+S
O
O
NH2
2+
•S
•Ado

**Figure 1.8** The primary reaction steps common to all radical-SAM enzymes. 1) an external electron donor (usually flavodoxin) reduces the $[4Fe\text{-}4S]^{2+}$ cluster to the $[4Fe\text{-}4S]^{+}$ cluster. 2) The reduced cluster transfers an electron to SAM causing cleavage into methionine and the 5'-deoxyadenosyl radical. 3) The 5'-deoxyadenosyl radical abstracts a hydrogen from an appropriately place substrate creating a substrate based radical.

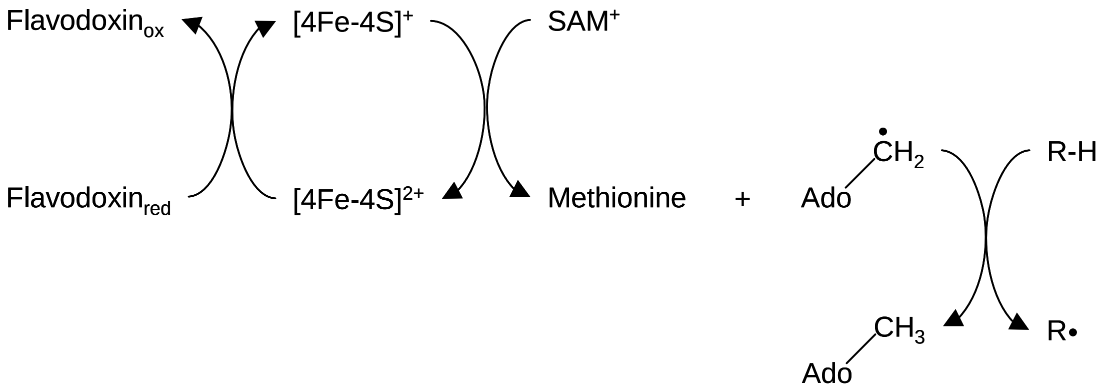
Flavodoxin$_{ox}$
[4Fe-4S]$^{+}$
SAM$^{+}$
Flavodoxin$_{red}$
[4Fe-4S]$^{2+}$
Methionine
+
Ado
$\dot{C}H_2$
R-H
Ado
$CH_3$
R•

**Figure 1.9** Crystal structures of radical-SAM protein monomers containing co-factor(s) and substrate(s). a, HemN from *E. coli*, PDB ID# 1OLT (*78*); b, BioB from *E. coli*, PDB ID# 1R30 (*11*); c, MoaA from *S. aureus*, PDB ID# 1TV8 (*49*); d, KAM from *C. subterminale*, PDB ID# 2A5H (*79*).

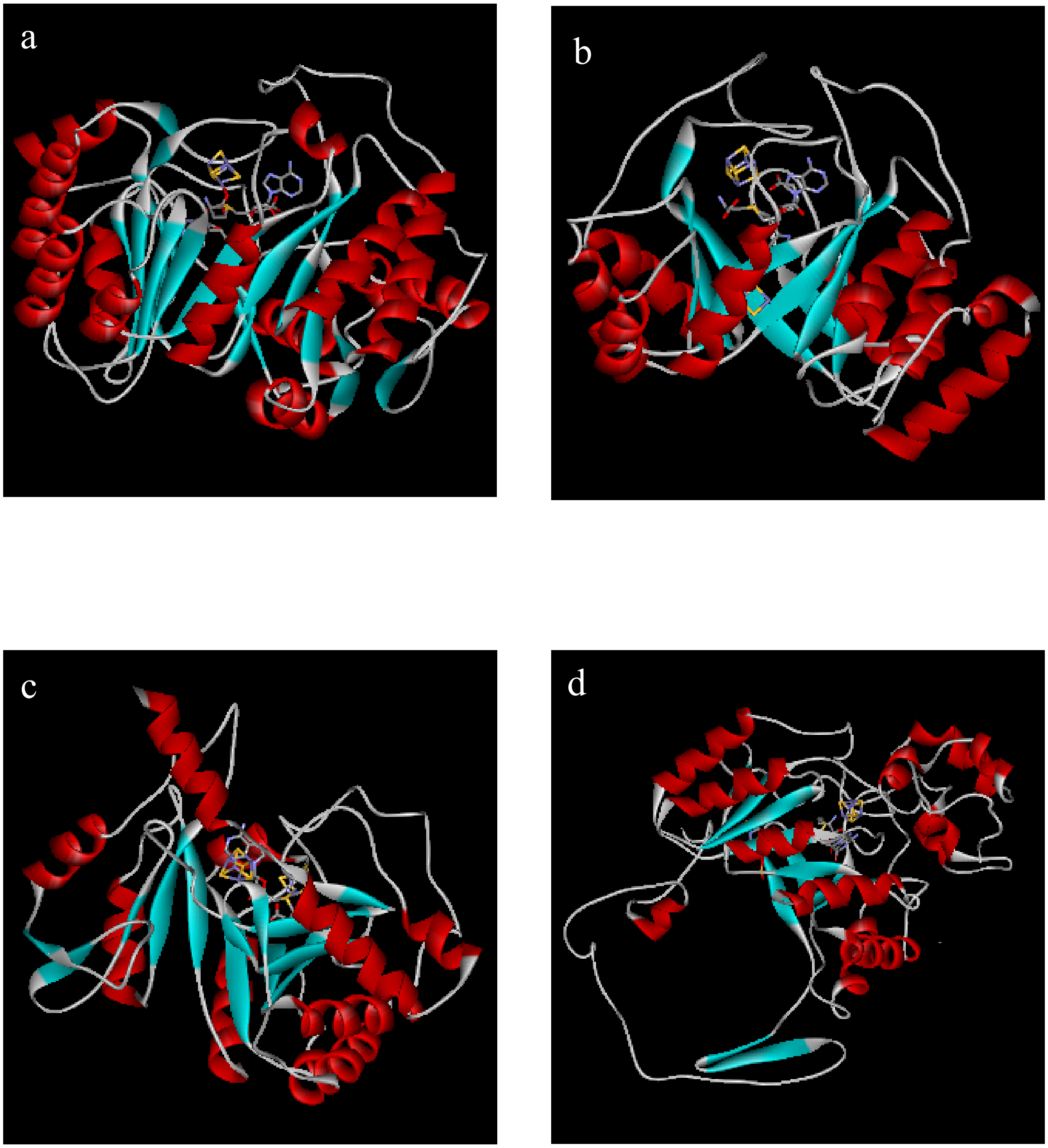
a
b
c
d

**Figure 1.10** Crystal structures of the active sites of radical-SAM enzymes are compared. a, HemN from *E. coli*, PDB ID# 1OLT (*78*); b, BioB from *E. coli*, PDB ID# 1R30 (*11*); c, MoaA from *S. aureus*, PDB ID# 1TV8 (*49*); d, KAM from *C. subterminale*, PDB ID# 2A5H (*79*).

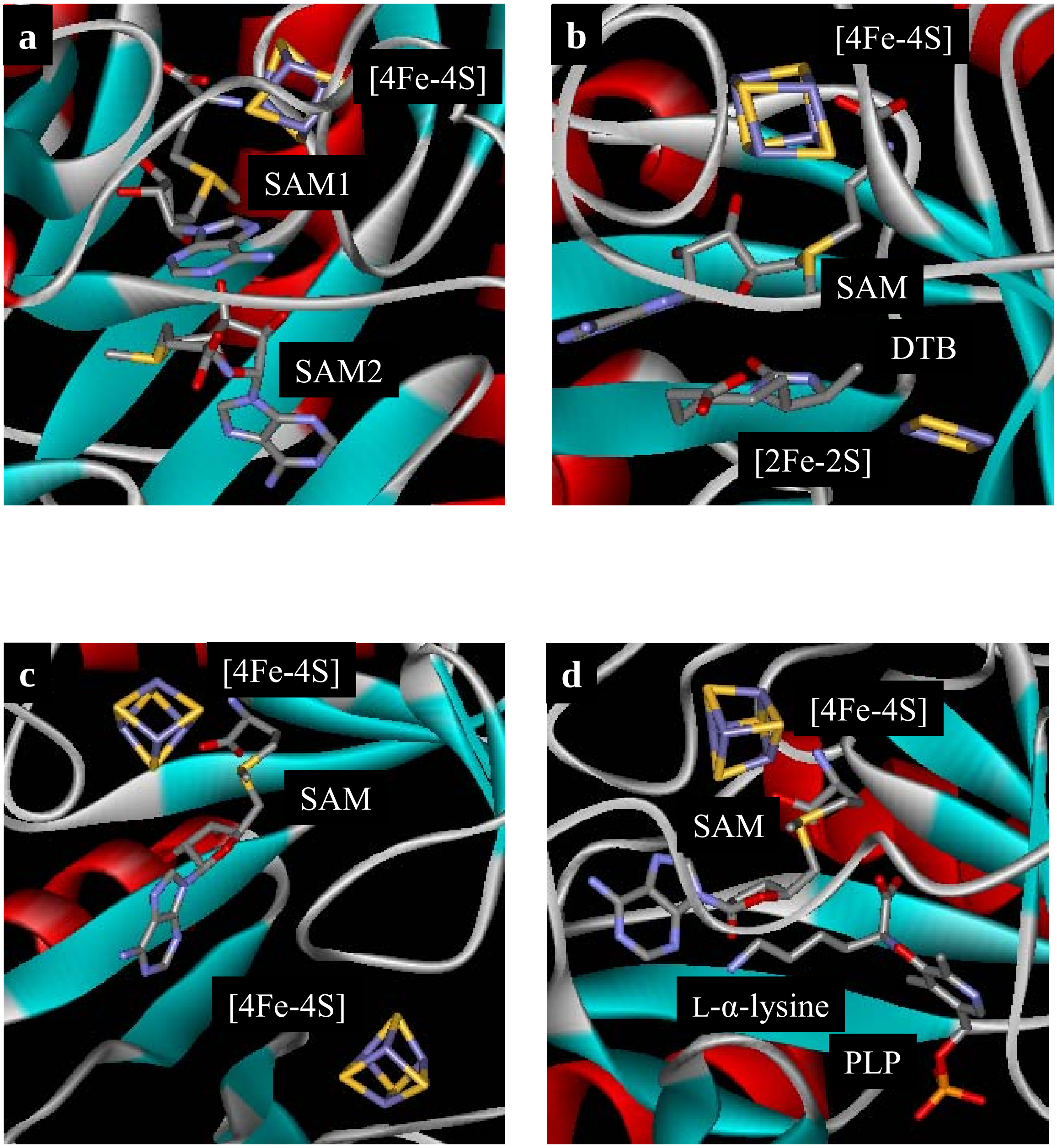
a
[4Fe-4S]
SAM1
SAM2
b
[4Fe-4S]
SAM
DTB
[2Fe-2S]
c
[4Fe-4S]
SAM
[4Fe-4S]
d
[4Fe-4S]
SAM
L-α-lysine
PLP

# CHAPTER 2

# CHARACTERIZATION OF THE COFACTOR COMPOSITION OF ESCHERICHIA COLI BIOTIN SYNTHASE[1]

---

[1] Cosper, Michele Mader[§]; Jameson, Guy N. L.[†]; Hernández, Heather L.[§]; Krebs, Carsten[†]; Huynh, Boi Hanh[†]; Johnson, Michael K.[§]. *Biochemistry*. **2004**, *43*, 2007-2021. Copyright 2004 American Chemical Society. Reprinted here with permission of publisher.

**Abbreviations:** BioB, gene product of *bioB* commonly referred to as biotin synthase; SAM, *S*-adenosyl-L-methionine; DTB, dethiobiotin; DTT, dithiothreitol; DT, dithionite; PLP, pyridoxal 5'-phosphate

## Abstract

The cofactor content of in vivo, as isolated and reconstituted forms of recombinant *Escherichia coli* biotin synthase (BioB) has been investigated using the combination of UV-visible absorption, resonance Raman, and Mössbauer spectroscopies along with parallel analytical and activity assays. In contrast to the recent report that *E. coli* BioB is a pyridoxal phosphate (PLP)-dependent enzyme with intrinsic cysteine desulfurase activity (Ollagnier-deChoudens, S., Mulliez, E., Hewitson, K. S., and Fontecave, M. (2002) *Biochemistry 41*, 9145-9152), no evidence for PLP binding or for PLP-induced cysteine desulfurase or biotin synthase activity was observed with any of the forms of BioB investigated in this work. The results confirm that BioB contains two distinct Fe-S cluster-binding sites. One site accommodates a $[2Fe\text{-}2S]^{2+}$ cluster with partial non-cysteinyl ligation that can only be reconstituted in vitro in the presence of $O_2$. The other site accommodates a $[4Fe\text{-}4S]^{2+,+}$ cluster that binds *S*-adenosylmethionine (SAM) at a unique Fe site of the $[4Fe\text{-}4S]^{2+}$ cluster and undergoes $O_2$-induced degradation via a distinct type of $[2Fe\text{-}2S]^{2+}$ cluster intermediate. In vivo Mössbauer studies show that recombinant BioB in anaerobically grown cells is expressed exclusively in an inactive form containing only the as isolated $[2Fe\text{-}2S]^{2+}$ cluster and demonstrate that the $[2Fe\text{-}2S]^{2+}$ cluster is not a consequence of overexpressing the recombinant enzyme under aerobic growth conditions. Overall the results clarify the confusion in the literature concerning the Fe-S cluster composition and the in vitro reconstitution and $O_2$-induced cluster transformations that are possible for recombinant BioB. In addition, they provide a firm foundation for assessing cluster transformations that occur during turnover and the catalytic competence of the $[2Fe\text{-}2S]^{2+}$ cluster as the immediate S-donor for biotin biosynthesis.

## Introduction

Biotin synthase (BioB)[1] is a homodimeric Fe-S protein found in plants and microorganisms that plays a critical role in catalyzing the final step in the biosynthesis of biotin, namely the activation of two C-H bonds for the stereospecific insertion of sulfur into dethiobiotin (DTB), see scheme 2.1 (for recent reviews see (*1-4*)). Spectroscopic and biochemical studies of *Escherichia coli* BioB (*5-7*) have provided overwhelming evidence that BioB is a member of the "radical-SAM" superfamily of Fe-S enzymes (*8*) which utilize a [4Fe-4S] cluster to generate a 5'-deoxyadenosyl radical via reductive cleavage of *S*-adenosyl-L-methionine (SAM). The 5'-deoxyadenosyl radical then abstracts an H atom from the C-9 position of DTB to yield a DTB radical (*9*). The subsequent steps and the nature of the immediate S donor are less well defined. Incorporation of deuterium at the C-6 position of DTB into the 5'-deoxyadenosine product and the requirement for at least two molecules of SAM for every molecule of biotin produced led Marquet to propose that ring closure involves an additional H-abstraction step involving a 5'-deoxyadenosyl radical generated from a second molecule of SAM (*9*). This model is further supported by the 2:1:1 SAM:DTB:BioB dimer binding stoichiometry that was recently reported by Jarrett and coworkers (*10*). In contrast, Fontecave and coworkers have reported a 1:1 stoichiometry of SAM:biotin using a pyridoxal 5'-phosphate (PLP)-dependent form of BioB (*11*). Likewise the nature of the immediate S donor is still controversial. While there is general agreement that cysteine is the ultimate source of S, both an additional [2Fe-2S] cluster (*12, 13*) and a cysteine pesulfide generated via cysteine desulfurase activity involving an indigenous protein-bound PLP (*14*), have been proposed as the immediate S donor to DTB based on single turnover experiments.

Although major progress has been made over the past decade, three major problems have impeded progress in characterizing the mechanism of *E. coli* BioB. The first is the inability to obtain more than one turnover, i.e. 1 nmol of biotin per 1 nmol of BioB monomer, in a well-defined in vitro assay. However, the possibility that BioB is a reactant rather than an enzyme appears unlikely, since multiple turnovers have been reported using cell-free extracts containing overexpressed recombinant BioB both in *E. coli* (0.5 $hr^{-1}$) (*15*) and in *Arabidopsis thaliana* (2.5-3 $hr^{-1}$) (*16*). Rather the recent studies of Fontecave and coworkers using a PLP-dependent form of BioB indicate that the absence of multiple turnovers in vitro is a consequence of strong product inhibition by 5'-deoxyadenosine (*11*).

The second problem involves variability in the cofactor content. Although there is general agreement that aerobically isolated recombinant BioB contains only $[2Fe\text{-}2S]^{2+}$ clusters, the reported stoichiometries span the range 0.5-1.5 $[2Fe\text{-}2S]^{2+}$ clusters per monomer (*14, 15, 17*), and forms containing ~2 $[2Fe\text{-}2S]^{2+}$ clusters per monomer have been claimed following incubation with $FeCl_3$ under argon (*17*). In accord with the initial discovery of reductive $[2Fe\text{-}2S]^{2+}$ to $[4Fe\text{-}4S]^{2+}$ cluster conversion in BioB (*5*), apo BioB reconstituted with $Fe(NH_4)_2(SO_4)_2$ or $FeCl_3$ and $Na_2S$ under rigorously anaerobic conditions, was subsequently found to contain approximately one $[4Fe\text{-}4S]^{2+,+}$ cluster per monomer (*18*). In contrast, anaerobic reconstitutions of as isolated BioB using $FeCl_3$ and $Na_2S$ in the presence of dithionite and 60% (v/v) ethylene glycol were reported to yield a form of BioB containing approximately two $[4Fe\text{-}4S]^{2+}$ clusters per monomer (*17*) and reconstitution of apo BioB using $FeCl_3$ and $Na_2S$ under an argon atmosphere were found to contain approximately one $[2Fe\text{-}2S]^{2+}$ cluster per monomer (*19*). In addition, anaerobic reconstitution starting with as isolated BioB in the absence of dithionite and ethylene glycol was found to result in a form of BioB containing approximately one $[2Fe\text{-}2S]^{2+}$

and one $[4Fe\text{-}4S]^{2+}$ per monomer that was capable of a single turnover in the absence of added iron and sulfide. This confusing picture has led to the hypothesis that BioB has two distinct cluster binding sites each of which is capable of binding either a $[2Fe\text{-}2S]^{2+}$ or $[4Fe\text{-}4S]^{2+}$ cluster, with the catalytically relevant form corresponding to the form containing one $[2Fe\text{-}2S]^{2+}$ and one $[4Fe\text{-}4S]^{2+}$ cluster per monomer. BioB contains six conserved cysteine residues with the three in the rigorously conserved CxxxCxxC motif (Cys53, Cys57, and Cys60) involved in coordinating the redox active $[4Fe\text{-}4S]^{2+,+}$ cluster that is common to all members of the radical SAM family. The remaining three conserved cysteines (Cys97, Cys128, and Cys188) are good candidates for ligands of the [2Fe-2S] cluster. This hypothesis is supported by cysteine-to-alanine mutagenesis studies (*20, 21*) and by resonance Raman studies which indicate a $[2Fe\text{-}2S]^{2+}$ cluster with partial non-cysteinyl ligation (*5*).

The debate over the cofactor content of the most active form of the enzyme has recently been reopened by the report that *E. coli* BioB is a PLP-dependent enzyme (*14*). PLP binding was reported for as isolated BioB containing approximately 0.5 $[2Fe\text{-}2S]^{2+}$ cluster per monomer (0.3-0.4 PLP/monomer) and for anaerobically reconstituted [4Fe-4S] BioB (0.7-1.0 PLP/monomer). Moreover, the PLP-bound forms exhibited low levels of cysteine desulfurase activity that approximately correlated with the PLP content and PLP-bound [4Fe-4S] form of BioB was found to exhibit enhanced biotin synthase activity corresponding to a single turnover in the absence of added iron and sulfide. This led to the hypothesis that BioB has intrinsic PLP-dependent cysteine desulfurase activity, similar to that found in NifS and IscS (*22, 23*), resulting in the formation of a cysteine persulfide on a conserved cysteine residue, which is subsequently attacked by the DTB radical (*14*). Loss of the PLP-dependent cysteine desulfurase activity in C97A and C128A BioB variants implicated Cys97 or Cys128 as the site for persulfide formation

(*14*). Since the same conserved cysteines are proposed to be ligands to the [2Fe-2S] cluster, the current models for catalytic turnover involving a [2Fe-2S] cluster or a cysteine persulfide as the immediate S-donor appear to be mutually exclusive.

The third problem concerns the catalytic viability of recombinant forms of *E. coli* BioB. Whole cell Mössbauer studies of two BioB overexpressing strains of *E. coli* have recently been reported (*24, 25*). For the strain used in this work (*E. coli* C41[DE3] pT7-7ecbioB-1) , the results showed that recombinant BioB is predominantly, if not exclusively, expressed in an inactive form that contains only the $[2Fe\text{-}2S]^{2+}$ cluster (*24*). In contrast both $[2Fe\text{-}2S]^{2+}$ and $[4Fe\text{-}4S]^{2+}$ clusters in a 3:1 ratio were found in the BioB expressed in the strain used by Marquet and coworkers (*E. coli* TK101 overexpressing BioB), indicating that a significant fraction of recombinant BioB contains a $[4Fe\text{-}4S]^{2+}$ prior to purification and therefore has the potential to be a catalytically competent form. Since both strains were grown aerobically, the partial or complete absence of the $O_2$-sensitive $[4Fe\text{-}4S]^{2+}$ cluster was tentatively attributed to $O_2$ exposure in the cell (*13, 24, 25*). Hence there is clearly a pressing need to characterize recombinant BioB from anaerobically grown cells in order to evaluate the possibility of deleterious effects of $O_2$ exposure during overexpression of BioB.

The objectives of this work were centered on resolving and addressing these three problematic areas of BioB research using the combination of absorption, resonance Raman, Mössbauer and activity studies. Specifically, the objectives were to clarify the Fe-S cluster and PLP composition and activity of as isolated and reconstituted forms of *E. coli* BioB, to investigate the effects of SAM and $O_2$ on the properties of individual Fe-S clusters in purified forms of BioB, and to establish the cofactor composition of recombinant BioB in anaerobically grown cells. The results support the existence of distinct $[4Fe\text{-}4S]^{2+}$ and $[2Fe\text{-}2S]^{2+}$ cluster binding sites in each BioB monomer, provide evidence for SAM binding to the $[4Fe\text{-}4S]^{2+}$ clusters in both the [4Fe-4S] and [2Fe-2S]/[4Fe-4S] forms of BioB, show that the $[4Fe\text{-}4S]^{2+}$ is rapidly degraded by $O_2$ via a distinct $[2Fe\text{-}2S]^{2+}$ intermediate, demonstrate that the as isolated $[2Fe\text{-}2S]^{2+}$ cluster can be reconstituted in apo BioB in the presence of $O_2$, establish that recombinant BioB in anaerobically grown cells is expressed in an inactive form containing only the as isolated $[2Fe\text{-}2S]^{2+}$ cluster, and provide no evidence in support of the proposal that BioB binds PLP or exhibits PLP-dependent cysteine desulfurase activity. Overall the results establish the Fe-S cluster composition and transformations that can occur for various forms of BioB and set the stage for EPR and Mössbauer studies to evaluate the proposal that the [2Fe-2S] cluster in the [2Fe-2S]/[4Fe-4S] form of BioB is the immediate S donor for biotin biosynthesis. The latter studies are presented in the accompanying manuscript.

## Materials and Methods

*Materials.* Chemicals were purchased from Sigma-Aldrich or Fischer, unless otherwise stated. $^{57}$Fe-enriched ferric ammonium citrate and $FeSO_4$ were prepared from $^{57}$Fe metal (>95% isotopic enrichment) as previously described (*24*). Restriction enzymes were purchased from New England Biolabs, and oligonucleotides were ordered from Integrated DNA Technologies. DNA sequencing was carried out by the Molecular Genetics Facility at the University of Georgia. The plasmid pBioBF2 containing the *E. coli bioB* gene was generously supplied by Dr. Katherine Gibson (E. I. du Pont de Nemours and Company, Wilmington), the plasmid pEE1010 containing the gene encoding *E. coli* flavodoxin reductase was a kind gift from Dr. Peter Reichard (Karolinska Institute, Sweden), and the plasmid pBH402 overexpressing polyhistidine-tagged *E. coli* IscS was a generous gift from Dr. Eugene Muller (University of Delaware). The *E.*

*coli* strain DH01 overexpressing *E. coli* flavodoxin was a kind gift from Dr. Rowena Matthews (University of Michigan). The over-expression strain, *E. coli* C41[DE3], was provided by Professor John E. Walker (Medical Research Council, Cambridge, UK). Anaerobic experiments were performed under Ar in a Vacuum Atmospheres glove box at oxygen levels < 5 ppm. Apo BioB was prepared as previously described (*18*) except that sodium dithionite was used as the reductant in place of photochemical reduction mediated by 5-deaza-7,8-dimethyl-10-methyl-isoalloxazine.

*Construction of the E. coli bioB Expression Vector pT7-7ecbioB-1.* The gene encoding BioB was amplified using PCR from pBioBF2 using the primers 5'-GGAATTCCATATGGCTCACCGCC-3' and 5'-ACAACTGCAGTCATAATGCTGCCG-3'. The PCR product was digested with *Nde* I and *Pst* I and ligated into the appropriately digested vector pT7-7 (*26*) to yield pT7-7ecbioB-1.

*Aerobic Overexpression of E. coli BioB.* The *E. coli* C41[DE3] pT7-7ecbioB-1 strain was cultivated at 37 °C in terrific broth containing 100 μg/mL carbenicillin, 40 μg/mL Fe in the form of ferric ammonium citrate or 12 μg/mL $^{57}$Fe in the form of ferric ammonium citrate. When the cultures reached an $OD_{600}$ between 0.9 – 1.2, isopropyl-1-thio-β-D-galactopyranoside (IPTG, Alexis) was added to a final concentration of 1.0 mM, and the bacteria cultures were further cultivated at 29 °C for 20 hours. The cells were harvested by centrifugation at 4,650 × *g* for 5 minutes at 4 °C and stored at –80 °C until further use.

*Anaerobic Overexpression of E. coli BioB.* The *E. coli* BL21-gold[DE3] pT7-7ecbioB-1 or *E. coli* BL21-gold[DE3] pT7-7 (control) strains were cultivated at 37 °C under strictly anaerobic conditions in Spizizen's minimal medium (*27*) with 10 mM $NaNO_3$, 20 μM Fe in the form of ferric ammonium citrate, 0.1 % (w/v) casein hydroxylate, 1.5 μM thiamine, and 100 μg/mL amplicillin. When the cultures reached an $OD_{600}$ between 0.9 – 1.2, IPTG was added to a final concentration of 0.05 mM, and the bacteria cultures were further cultivated at 37 °C for 3 hours and finally stored at 4 °C for 16 hours. The cells were harvested by centrifugation at 4,650 × *g* for 5 minutes at 4 °C and stored at –80 °C until further use.

*Anaerobic and Aerobic Purification of E. coli BioB.* 6.0 g of cell paste were thawed and resuspended in 50 mM Hepes buffer, pH 7.5 (buffer A), with 20 μg/mL chicken egg-white lysozyme, 5 μg/mL DNase I (Roche), and 5 μg/mL RNase A (Roche). Cells were broken by intermittent sonication, and the cell debris was removed by centrifugation at 39,700 × *g* for 1 hour at 4 °C. The cell free extract was applied to a Source Q (Pharmacia) column (26 mm × 10 cm) previously equilibrated with buffer A, and eluted with a 0 – 100% gradient of 50 mM Hepes buffer, pH 7.5, containing 1.0 M NaCl (buffer B). The purest fractions, as judged by SDS-PAGE analysis, were pooled and brought to a final concentration of 0.6 M in ammonium sulfate. This solution was applied to a Phenyl Sepharose High Performance (Pharmacia) column (26 mm × 15 cm) previously equilibrated with 50 mM Hepes buffer, pH 7.5, containing 0.6 M ammonium sulfate (buffer C) and eluted with a 0 – 100 % gradient of buffer A. The purest fractions, as determined by the $A_{453}/A_{280}$ ratio (> 0.215), were pooled and dialyzed into buffer A over a YM30 membrane. *E. coli* C41[DE3] pT7-7ecbioB-1 and BL21-gold[DE3] pT7-7ecbioB-1 cells yielded 2.5 mg BioB/g cell paste and 4.0 mg BioB/g cell paste, respectively. The same procedures were used for anaerobic and aerobic purifications, except that for anaerobic purifications, all manipulations were performed in the glove box and all solutions were degassed prior to use by repeated freeze-pump-thaw cycles under Ar or purging with Ar for one hour.

*Construction of Vector pMCecbbhis-10 for Expression of his$_6$-BioB.* The gene encoding BioB was amplified using PCR from pT7-7ecbioB-1 using the primers 5’-

ATGGCTCACCGCCCACG-3’ and 5’-TAATGCTGCCGCGTTGTAATATTCGTC-3’. Using the TOPO cloning technology (Invitrogen), the PCR product was ligated into pCRT7/NT-TOPO to yield pMCecbbhis-10.

*Overexpression and Purification of His-tagged E. coli BioB.* The *E. coli* BL21-gold[DE3] pMCecbbhis-10 strain was cultivated at 37 °C in LB containing 100 μg/mL amplicillin, 40 μg/mL Fe in the form of ferric ammonium citrate. When the cultures reached an $OD_{600}$ between 0.6 – 0.8, IPTG was added to a final concentration of 0.1 μM, and the bacteria cultures were cultivated further at 37 °C for 3 – 5 hours. Finally, the bacteria cultures were stored at 4 °C for 16 hours under an Ar atmosphere. The cells were harvested by centrifugation at 4,650 × *g* for 5 minutes at 4 °C.

8.0 g of cell paste were thawed and resuspended in 30 mL of 100 mM Tris-HCl buffer, pH 8.0, containing 0.3 M NaCl and 5 mM imidazole (buffer D), with 20 μg/mL chicken egg-white lysozyme, 5 μg/mL DNase I (Roche), and 5 μg/mL RNase A (Roche). Cells were broken by intermittent sonication, and the cell debris was removed by centrifugation at 39,700 × *g* for 1 hour at 4 °C. The cell-free extract was loaded onto a charged and equilibrated 5 mL Ni-chelating column (Pharmacia), and the $his_6$-BioB was eluted with 0 – 100% gradient of 100 mM Tris-HCl buffer, pH 8.0, containing 0.3 M NaCl and 0.5 M imidazole (buffer E). The purest fractions, as determined by SDS-PAGE analysis, were pooled and dialyzed into buffer A over a YM30 membrane. *E. coli* BL21-gold[DE3] pMCecbbhis-10 cells yielded 5.0 mg BioB/g cell paste.

*Reconstitution of $[4Fe\text{-}4S]^{2+}$ centers in BioB.* [4Fe-4S] BioB was prepared under strictly anaerobic conditions according to a previously published procedure (*18*), with the exception of the following modifications. Following incubation of apo BioB (280 μM) in 10 mM DTT for 10 minutes, a 10-fold molar excess of $Fe^{II}(NH_4)_2(SO_4)_2$ was added, followed by the addition of a

10-fold molar excess of $Na_2S$. After 1 hour, the reconstitution mixture was loaded onto a 5 mL HiTrap Q column previously equilibrated with buffer A and eluted with a 0 – 100 % gradient of buffer B. The brown fractions were concentrated over a YM30 (Amicon) membrane.

[2Fe-2S]/[4Fe-4S] BioB was prepared under strictly anaerobic conditions using the method of Jarrett and coworkers (*12*), with the following modifications. Following incubation of as-isolated [2Fe-2S] BioB in 10 mM DTT for 10 minutes, a 10-fold molar excess of $FeCl_3$, ferric ammonium citrate, $Fe^{II}(NH_4)_2(SO_4)_2$, or a 1:1 mixture of $FeCl_3$ and $Fe^{II}(NH_4)_2(SO_4)_2$ was added, followed by the addition of a 10-fold molar excess of $Na_2S$. After 1 hour, the reconstitution mixture was loaded onto a 5-mL HiTrap Q column previously equilibrated with buffer A and eluted with a 0 – 100 % gradient of buffer B. The red-brown fractions were concentrated over a YM30 (Amicon) membrane.

*Reconstitution with Pyridoxal Phosphate (PLP) and Measurement of Cysteine Desulfurase Activity.* Samples of *E. coli* BioB and PLP-depleted IscS-$his_6$ were incubated with a 5-to-10-fold molar excess of PLP at room temperature for time periods between 1– 24 hours, in the presence of 5mM DTT. Excess PLP was removed using a G-25 (Pharmacia) desalting column (26 mm × 15 cm), and the protein was concentrated over a YM30 (Amicon) membrane. The cysteine desulfurase activity of *E. coli* $[4Fe\text{-}4S]^{2+}$ BioB was assessed by analyzing for L-alanine and sulfide after anaerobic incubation with 1xPLP, 5 mM DTT and 500 μM L-cysteine for 2.5 hr at room temperature. The cysteine desulfurase activity of IscS-$his_6$ was assessed in parallel experiments without added PLP. L-alanine was quantified according to the published procedure (*28*) using L-alanine dehydrogenase, which was generously provided by Dr. Robert Phillips (University of Georgia) and sulfide was quantified as previously described (*22, 29*).

*Determination of Protein, Fe and PLP Concentrations.* Protein concentrations were determined by the *DC* protein assay (Bio-Rad), using BSA as a standard. All protein concentrations for wild-type (WT) BioB determined using the *DC* protein assay were multiplied by the correction factor of 1.1, that was assessed based on quantitative amino acid analyses of parallel samples (Commonwealth Biotechnologies). Iron concentrations were determined colorimetrically using bathophenanthroline under reducing conditions, after digestion of the protein in 0.8% $KMnO_4$/0.2 M HCl (*30*), and by inductively coupled plasma atomic emission spectroscopy (University of Georgia Chemical Analysis Laboratory). These two methods agreed to within ± 5% for all samples investigated. All sample concentrations and molar extinction coefficients are expressed per BioB monomer. The concentration of bound PLP in BioB samples was assessed based on absorption and analytical studies of alkaline denatured samples according to the published procedures (*31*).

*Spectroscopic Characterization of Fe-S Centers in BioB.* UV-visible absorption spectra were recorded under anaerobic conditions in screw top 1 mm cuvettes using a Shimadzu UV-3101PC spectrophotometer. Resonance Raman spectra were recorded using an Instruments SA Ramanor U1000 spectrometer fitted with a cooled RCA 31034 photomultiplier tube with a 90º scattering geometry. Spectra were recorded digitally using photon counting electronics, and improvements in signal-to-noise were achieved by signal-averaging multiple scans. Band positions were calibrated using the excitation frequency and are accurate to ±1 $cm^{-1}$. Lines from a Coherent Sabre 10-W Argon Ion Laser, and plasma lines were removed using a Pellin Broca Prism premonochromator. Using a custom-designed sample cell (*32*), samples under an Ar atmosphere were placed on the end of a cold finger of an Air Products Displex Model CSA-202E closed cycle refrigerator. This enables the samples to be cooled down to 17 K, which facilitates improved spectral resolution and prevents laser-induced sample degradation. Scattering was collected from the surface of a frozen 10 μL droplet. The Mössbauer spectra were recorded using the previously described spectrometers (*33*). The zero velocity refers to the centroid of the room temperature spectra of metallic iron foil. Analysis of the Mössbauer data was performed with the program WMOSS (WEB Research).

*Assay of Biotin Synthase Activity.* The BioB assay was performed under strictly anaerobic conditions in a glove box according to the procedure used by Fontecave and coworkers (*14*), except that the assays were performed at 25 ºC rather than 37 ºC. The assays were performed in 100 mM Tris-HCl buffer, pH 8.0, with BioB (35 μM), KCl (50 mM), DTT (5 mM), L-cysteine (2 mM), SAM (200 μM), *E.* coli flavodoxin (20 μM), *E.coli* flavodoxin reductase (5 μM), NADPH (1 mM) , and dethiobiotin (375 μM ). In accord with the results of Jarrett and coworkers (*12*), the omission of L-cysteine did not affect the assay results presented herein. Assays were performed in the absence and presence of 35 μM PLP or 1 mM $Fe^{II}(NH_4)_2(SO_4)_2$. Biotin was assayed using *Lactobacillus plantarum* ATCC 8014 according to published procedures (*34, 35*).

## Results

***Fe-S cluster stoichiometry and conversions***. Three distinct and well defined forms of recombinant E. coli BioB were characterized based on Fe and protein determinations and UV-visible absorption, resonance Raman, and Mössbauer properties: [2Fe-2S] BioB which corresponds to as isolated BioB, [4Fe-4S] BioB, which corresponds to anaerobically reconstituted apo BioB, and [2Fe-2S]/[4Fe-4S] BioB, which corresponds to anaerobically reconstituted as isolated BioB. The properties of each form are summarized in Table 2.1 and compared below with previously published results on the Fe-S cluster stoichiometry of E. coli BioB.

*[2Fe-2S] BioB*: Fourteen different preparations of as isolated recombinant *E. coli* BioB were investigated; twelve purified aerobically from aerobically grown cells, one purified under rigorously anaerobic conditions from aerobically grown cells, and one purified under rigorously anaerobic conditions from anaerobically grown cells. In all cases the results were in remarkably good agreement, with analytical data indicating 1.7 ± 0.2 Fe/monomer, absorption spectra and molar extinction coefficients characteristic of approximately one $[2Fe\text{-}2S]^{2+}$ cluster per monomer ($\varepsilon_{453}$ = 7.2 ± 0.8 $mM^{-1}cm^{-1}$ with $A_{453}/A_{278}$ = 0.22 ± 0.02), see Fig. 2.1(a) and Table 2.1. Moreover, both the resonance Raman and Mössbauer spectra confirm the presence of a homogeneous $[2Fe\text{-}2S]^{2+}$ center as the sole Fe-containing chromophore, see Figs. 2.1(a) and 2.2(a), respectively. Identical resonance Raman spectra were observed for all types of as isolated sample investigated in this work, including His-tagged samples (see below), and the spectrum is characteristic of a unique type of $[2Fe\text{-}2S]^{2+}$ cluster with partial non-cysteinyl ligation (*5*). Tentative vibrational assignments have been made by analogy with well characterized 2Fe ferredoxins (*5*). The 4.2-K Mössbauer spectrum of as-isolated BioB (Fig. 2.2(a)) exhibits a quadrupole doublet with parameters, $\delta$ = 0.29 mm/s and $\Delta E_Q$ = 0.53 mm/s, that are indicative of a $[2Fe\text{-}2S]^{2+}$ cluster. It is, however, inconclusive whether there is partial non-cysteinyl ligation. These data are very similar to those reported in the original characterization of aerobically purified recombinant *E. coli* BioB (*5, 15*) and for samples of *E. coli* BioB purified by other groups (*25, 36*).

In contrast, Jarrett and coworkers reported that as isolated samples of His-tagged *E. coli* BioB contained 1.2-1.5 $[2Fe\text{-}2S]^{2+}$ cluster per monomer based on Fe, $S^{2-}$ and protein analyses and that the Fe stoichiometry increased to 3.7 ± 0.4 Fe/monomer, corresponding to approximately 2 $[2Fe\text{-}2S]^{2+}$ cluster per monomer, following incubation with $FeCl_3$ and removal of excess Fe via anaerobic gel filtration (*17*). The same incubation/repurification procedure used by Jarrett and coworkers resulted in no change in the absorption and resonance Raman characteristics or the Fe/protein ratios for the wild-type recombinant samples of *E. coli* BioB used in this work. The possibility that one $[2Fe\text{-}2S]^{2+}$ cluster is labile and is lost during the more extensive and time-consuming purification protocol that is required for the wild-type protein compared to the His-tagged protein, was investigated by purifying and analyzing samples of N-terminal His-tagged *E. coli* BioB ($his_6$-BioB) under both aerobic and rigorously anaerobic conditions. These samples were purified using a single Ni-chelating column, but were found to be deficient in $[2Fe\text{-}2S]^{2+}$ clusters compared to the wild-type preparations: 1.4 ± 0.2 Fe/monomer and $A_{453}/A_{278} = 0.17 \pm 0.02$. Hence despite extensive analytical and spectroscopic studies of a wide variety of samples, we have failed to find any evidence in support of a stable form of as isolated *E. coli* BioB containing more than one $[2Fe\text{-}2S]^{2+}$ cluster per monomer.

*[4Fe-4S] BioB*: Reconstitution of apo BioB under strictly anaerobic conditions using ferrous ammonium sulfate and sodium sulfide in the presence of DTT followed by anaerobic repurification using a HiTrap Q column resulted in a homogeneous form of BioB containing approximately one $[4Fe\text{-}4S]^{2+}$ cluster/monomer. Seven distinct reconstituted samples of recombinant wild-type apo BioB and two samples of apo $his_6$-BioB were investigated. The analytical data for all nine samples indicated 3.9 ± 0.4 Fe/monomer and the absorption spectra were characteristic of a single $[4Fe\text{-}4S]^{2+}$ center per BioB monomer ($\varepsilon_{410} = 15.6 \pm 1.6\ mM^{-1}cm^{-1}$ with $A_{410}/A_{278} = 0.30 \pm 0.03$), see Fig. 2.1(b) and Table 2.1.

Both the resonance Raman and Mössbauer spectra confirm the presence of a $[4Fe\text{-}4S]^{2+}$ center, see Figs. 2.1(b) and 2.2(b), respectively. Identical resonance Raman spectra were observed for all samples, including His-tagged samples, and the spectra are characteristic of a $[4Fe\text{-}4S]^{2+}$ cluster with the totally symmetric breathing mode at 338 $cm^{-1}$, in a region of overlap between clusters with complete cysteinyl ligation and clusters with one non-cysteinyl-ligated Fe (*5, 7*). Tentative vibrational assignments have been made by analogy with those available for inorganic complexes containing $[4Fe\text{-}4S]^{2+}$ cores and well characterized proteins with $[4Fe\text{-}4S]^{2+}$ clusters (*5*). With 458-nm excitation, the resonant enhancement of $[2Fe\text{-}2S]^{2+}$ centers is approximately 5-fold greater than that of $[4Fe\text{-}4S]^{2+}$ centers (*37-40*). Hence on the basis of the intensity of the weak band at 301 $cm^{-1}$ that could be attributed to $[2Fe\text{-}2S]^{2+}$ clusters, we conclude that less than 5% of the BioB monomers in repurified reconstituted samples contain $[2Fe\text{-}2S]^{2+}$ clusters of the type seen in as isolated samples of BioB. This conclusion was confirmed by Mössbauer studies.

The 4.2-K Mössbauer spectrum of an $^{57}$Fe-reconstituted sample of apo BioB (Fig. 2.2(b)) shows a major quadrupole doublet that is attributable to a $[4Fe\text{-}4S]^{2+}$ cluster and accounts for 90% of the $^{57}$Fe absorption. This major doublet can be simulated as the sum of two overlapping equal intensity doublets, representing two valence-delocalized $Fe^{II}Fe^{III}$ pairs, with parameters ($\delta(1) = 0.45$ mm/s and $\Delta E_Q(1) = 1.28$ mm/s and $\delta(2) = 0.44$ mm/s and $\Delta E_Q(2) = 1.03$ mm/s, see Table 2.1) that are typical for $[4Fe\text{-}4S]^{2+}$ clusters (*41, 42*) and are similar to those reported for the $[4Fe\text{-}4S]^{2+}$ cluster in BioB (*7, 18*). Spectra recorded in the presence of a strong magnetic field (data not shown) show that this major doublet originates from a diamagnetic species, consistent with a $[4Fe\text{-}4S]^{2+}$ cluster assignment. The remaining 10% $^{57}$Fe absorption (small peaks at around

-1 mm/s and 2 mm/s) is attributed to mononuclear ferrous impurities. The presence of $[2Fe\text{-}2S]^{2+}$ cluster is not detected.

Very similar results were reported by Fontecave and coworkers for anaerobically reconstituted and repurified samples of *E. coli* BioB (*18*). The only differences were that the reconstituted samples obtained by these workers contained a mixture of $[4Fe\text{-}4S]^{2+}$ and $[4Fe\text{-}4S]^{+}$ clusters, in addition to slightly larger amounts of mononuclear $Fe^{2+}$ species (10 - 20% of $^{57}Fe$ absorption). Both differences are likely to be a consequence of anaerobic repurification using gel filtration rather than the HiTrap Q column used in this work. In contrast, reconstitution of wild-type apo BioB under semi-anaerobic conditions using ferric chloride and sodium sulfide in the presence of DTT has been reported to yield exclusively $[2Fe\text{-}2S]^{2+}$ clusters (0.85 $[2Fe\text{-}2S]^{2+}$ clusters per monomer) by Marquet and coworkers (*19*) and incubation of dithionite-treated as isolated His-tagged BioB with ferric chloride and sodium sulfide in the presence of DTT and 60% (v/v) ethylene glycol was reported to lead to a derivative containing two $[4Fe\text{-}4S]^{2+}$ clusters per monomer by Jarrett and coworkers (*17*).

In an attempt to reconcile the conflicting reports concerning the products of cluster reconstitution procedures starting with apo BioB, we have duplicated the reconstitution procedures used by both the Marquet and Jarrett groups. In accord with the results of Marquet and coworkers (*19*), analytical, absorption and resonance Raman studies have confirmed that reconstitution with ferric chloride and sodium sulfide in the presence of DTT and oxygen does result in a $[2Fe\text{-}2S]^{2+}$ containing form of BioB almost indistinguishable from as isolated BioB. This is best illustrated by the resonance Raman, which are compared in Figs 2.3(e) and 2.3(a), respectively. Hence the nature of the cluster reconstituted in BioB is critically dependent on the reconstitution conditions. However, using the reconstitution procedure reported by Jarrett and coworkers (*17*), we failed to find any evidence in support of a form of BioB containing two [4Fe-4S]$^{2+}$ clusters per monomer. Although the resulting samples exhibit similar absorption spectra and Fe analyses (~ 8Fe/momer BioB) to those reported by Jarrett and coworkers, the absorption spectrum has a pronounced shoulder centered at ~ 600 nm that is characteristic of non-protein associated soluble polymeric iron sulfides that exhibit broad absorption bands at 420 and 600 nm (*43*). This was confirmed by Mössbauer studies on samples reconstituted with $^{57}$Fe which revealed that approximately half of the Fe was present as [4Fe-4S]$^{2+}$ clusters with the remainder contributing to a broad underlying resonance indicative of polymeric iron sulfides (data not shown). Polymeric iron sulfides are invariably formed during in vitro reconstitution of Fe-S proteins and are often difficult to completely remove using gel filtration repurification protocol used by Jarrett and coworkers (*43*). The presence of this impurity therefore explains the anomalously high Fe determinations and molar extinction coefficients reported by Jarrett and coworkers. Moreover, we have found that this impurity can be removed by anaerobic repurification using a HiTrap Q column to yield a form of BioB containing a single [4Fe-4S]$^{2+}$ cluster on the basis of Fe determinations and absorption properties.

The [4Fe-4S]$^{2+}$ cluster that is assembled in BioB under anaerobic reconstitution conditions is known to be degraded by oxygen to yield a [2Fe-2S]$^{2+}$ cluster (*5, 18, 44*). However, the nature of the degradative process and the relationship of the resultant [2Fe-2S]$^{2+}$ cluster to the [2Fe-2S]$^{2+}$ cluster that is present in as isolated BioB were unresolved questions prior to this study. Hence the time course of air-induced degradation of the [4Fe-4S]$^{2+}$ cluster in the presence of DTT was investigated using resonance Raman and Mössbauer spectroscopies. Resonance Raman proved to be particularly effective for investigating the nature of the [2Fe-2S]$^{2+}$ clusters generated during oxygen-induced degradation, see Fig. 2.3. After 10 minutes of air exposure on the Raman probe, the resonance Raman bands associated with the $[4Fe\text{-}4S]^{2+}$ cluster (Fig. 2.3(b)) have been replaced by a spectrum comprising broad bands centered at 292, 336, 366 and 395 $cm^{-1}$ (Fig. 2.3(c)). The spectrum is characteristic of a $[2Fe\text{-}2S]^{2+}$ cluster and is very similar to those reported for the $[2Fe\text{-}2S]^{2+}$ clusters generated via oxidative degradation of the $[4Fe\text{-}4S]^{2+}$ clusters in the nitrogenase Fe protein (*39*) and in other radical-SAM enzymes, e.g. anaerobic ribonucleotide reductase activating enzyme (*45*), pyruvate formate-lyase activating enzyme (*46*), and the tRNA-methylthiotransferase, MiaB (*47*). However, mixing with aerobic buffer in a syringe for one hour followed by aerobic centricon reconcentration resulted in the appearance of the characteristic resonance Raman spectrum associated with the $[2Fe\text{-}2S]^{2+}$ cluster found in as isolated BioB (Fig. 2.3(d)). The results indicate that oxygen-induced degradation of the $[4Fe\text{-}4S]^{2+}$ cluster proceeds via an unstable $[2Fe\text{-}2S]^{2+}$ cluster in a cluster conversion process that appears to be common to most members of the radical-SAM family. Furthermore, taken together with the results of aerobic reconstitution, see above and Fig. 2.3(e), the data indicate that this cluster degradation process is subsequently followed by aerobic reconstitution of the as-isolated $[2Fe\text{-}2S]^{2+}$ cluster on apo BioB using the ferric ion and sulfide that is generated by the cluster degradation process. Since the latter process is unique to BioB, the most likely explanation for the dramatic difference in the resonance Raman spectra of the $[2Fe\text{-}2S]^{2+}$ centers is that the as-isolated $[2Fe\text{-}2S]^{2+}$ cluster and the transient $[2Fe\text{-}2S]^{2+}$ cluster which results from oxygen-induced damage of the $[4Fe\text{-}4S]^{2+}$ cluster, occupy distinct sites on BioB. Mössbauer studies confirmed rapid oxygen-induced degradation of the $[4Fe\text{-}4S]^{2+}$ cluster and subsequent formation of $[2Fe\text{-}2S]^{2+}$ clusters (data not shown). Unfortunately, Mössbauer spectroscopy does not have the required resolution to distinguish the two distinct types of $[2Fe\text{-}2S]^{2+}$ clusters that are observed in parallel resonance Raman studies.

*[2Fe-2S]/[4Fe-4S] BioB*: Convincing evidence for a form of *E. coli* BioB containing approximately one $[2Fe\text{-}2S]^{2+}$ and $[4Fe\text{-}4S]^{2+}$ cluster per monomer has come from Fe and S analyses, absorption spectra and Mössbauer studies of samples of as isolated [2Fe-2S] BioB that were reconstituted under anaerobic conditions using ferric chloride and sodium sulfide in the presence of DTT (*17, 48*). Using the same reconstitution procedure, we have used the combination of Fe analyses, coupled with UV/visible absorption, resonance Raman and Mössbauer spectroscopy to confirm the existence of separate $[2Fe\text{-}2S]^{2+}$ and $[4Fe\text{-}4S]^{2+}$ cluster binding sites in BioB and to investigate perturbations in each of the clusters that are induced by the presence of the second cluster, see Figs. 2.1 and 2.2 and Table 2.1. In accord with the results of Jarrett and coworkers (*17*), the absorption spectrum of anaerobically reconstituted as-isolated $[2Fe\text{-}2S]^{2+}$ BioB is readily understood in terms of approximately equal contributions from $[2Fe\text{-}2S]^{2+}$ and $[4Fe\text{-}4S]^{2+}$ chromophores, see Fig. 2.1(c). This is best illustrated by the reconstituted minus as-isolated difference spectrum which has a broad shoulder at 410 nm that is characteristic of a $[4Fe\text{-}4S]^{2+}$ cluster. However, in contrast to the results of Jarrett and coworkers which reported stoichiometric $[2Fe\text{-}2S]^{2+}$ and $[4Fe\text{-}4S]^{2+}$ clusters on the basis of analytical data which indicated 5.8 ± 0.3 Fe atoms and 6.2 ± 0.2 $S^{2-}$ ions per monomer, analyses of the eleven distinct preparations investigated in this work indicated only 4.3 ± 0.3 Fe atoms per monomer. In addition, analyses of the absorption spectra using the extinction coefficients determined for $[4Fe\text{-}4S]^{2+}$ and $[2Fe\text{-}2S]^{2+}$ clusters in BioB, see above, consistently indicated 0.72 ± 0.10 $[4Fe\text{-}4S]^{2+}$ and $[2Fe\text{-}2S]^{2+}$ clusters per monomer, see Table 2.1. This discrepancy is likely to be a consequence of using a HiTrap-Q column for repurification of BioB in this work, rather than the gel filtration procedure used by Jarrett and coworkers. Indeed, subsequent Mössbauer studies of

a sample repurified by gel filtration alone showed that 36% of the Fe was not associated with $[2Fe\text{-}2S]^{2+}$ or $[4Fe\text{-}4S]^{2+}$ clusters (*48*).

The vibrational properties of the clusters in [2Fe-2S]/[4Fe-4S] BioB were investigated using resonance Raman with 458-nm excitation, see Fig. 2.1(c). The spectrum is clearly dominated by the vibration modes of the as-isolated $[2Fe\text{-}2S]^{2+}$ cluster, c.f. spectra 1(c) with 1(a). However, subtraction of the resonance Raman spectrum of as isolated [2Fe-2S] BioB, see Fig. 2. 1(d), results in a spectrum characteristic of a $[4Fe\text{-}4S]^{2+}$ cluster and very similar to that of the $[4Fe\text{-}4S]^{2+}$ cluster in [4Fe-4S] BioB, c.f. Figs 2.1(b) and 2.1(d). The small shift in the asymmetric Fe-S(Cys) stretching mode of the $[4Fe\text{-}4S]^{2+}$ center (364 $cm^{-1}$ in [4Fe-4S] BioB compared to 360 $cm^{-1}$ in [2Fe-2S]/[4Fe-4S] BioB) may not be significant may be a consequence of the subtraction procedure. Likewise, subtraction of the resonance Raman spectrum of [4Fe-4S] BioB to minimize the intensity of the 252-$cm^{-1}$ band results in a spectrum very similar to that of the $[2Fe\text{-}2S]^{2+}$ cluster in as isolated BioB (data not shown). Although the resonance Raman can not provide an accurate assessment of the relative amounts of each type of cluster, the spectra support distinct binding sites for $[2Fe\text{-}2S]^{2+}$ and $[4Fe\text{-}4S]^{2+}$ clusters in BioB, with the presence of the additional cluster having only minor effects on the environment of the original cluster.

The most conclusive evidence for distinct $[2Fe\text{-}2S]^{2+}$ and $[4Fe\text{-}4S]^{2+}$ binding sites in [2Fe-2S]/[4Fe-4S] BioB comes from Mössbauer studies. The Mössbauer spectra of four samples of $^{57}$Fe-labeled as-isolated [2Fe-2S] BioB after anaerobic reconstitution using $^{57}$Fe and repurification using a HiTrap-Q column (Fig. 2.2(c)) indicate the presence of approximately equivalent amounts of $[2Fe\text{-}2S]^{2+}$ and $[4Fe\text{-}4S]^{2+}$ clusters ($[4Fe\text{-}4S]^{2+}$:$[2Fe\text{-}2S]^{2+}$ ratio = 0.9 ±0.2). Moreover, the Mössbauer spectrum of a sample of unlabeled [2Fe-2S] BioB reconstituted with $^{57}$Fe (Fig. 2.2(d)) shows that the added Fe is assembled almost exclusively into [4Fe-4S]$^{2+}$ clusters (92% into [4Fe-4S]$^{2+}$ clusters and 8% into [2Fe-2S]$^{2+}$ clusters), while the spectrum of a sample of $^{57}$Fe-labeled [2Fe-2S] BioB reconstituted with $^{56}$Fe (Fig. 2.2(e)) indicated that the indigenous Fe remains largely in the [2Fe-2S]$^{2+}$ form (82% [2Fe-2S]$^{2+}$ and 18% [4Fe-4S]$^{2+}$). In accord with the resonance Raman data, the Mössbauer parameters for the [2Fe-2S]$^{2+}$ and [4Fe-4S]$^{2+}$ clusters are not significantly perturbed by the presence of the second cluster, see Table 2.1. Hence the spectroscopic data point to distinct, well-defined sites for both the [2Fe-2S]$^{2+}$ and [4Fe-4S]$^{2+}$ clusters. The Mössbauer results are in excellent agreement with those reported by Jarrett and coworkers (*48*). The only significant difference lies in the absence of the mononuclear Fe$^{II}$ species in our samples, and this appears to be a consequence of repurification using a HiTrap-Q column rather than gel filtration.

Exposure of [2Fe-2S]/[4Fe-4S] BioB to air for one hour results in complete degradation of the [4Fe-4S]$^{2+}$ cluster as evidenced by absorption, resonance Raman and Mössbauer studies. Moreover, as for [4Fe-4S] BioB, the degradation of the [4Fe-4S]$^{2+}$ cluster was found to proceed via a [2Fe-2S]$^{2+}$ cluster intermediate. This is best demonstrated by resonance Raman studies of air-exposed samples of [2Fe-2S]/[4Fe-4S] BioB, see Fig. 2.4. After 10 min of air exposure, the Raman bands associated with the [4Fe-4S]$^{2+}$ cluster are completely lost (cf. Figs 2.4(a) and 2.1(c)) and subtraction of the resonance Raman spectrum of [2Fe-2S]$^{2+}$ cluster in as isolated [2Fe-2S] BioB (Fig. 2.4(b)) results in a spectrum (Fig. 2.4(c)) that closely resembles the [2Fe-2S]$^{2+}$ cluster produced during $O_2$-induced degradation of the [4Fe-4S]$^{2+}$ cluster in [4Fe-4S] BioB (Fig. 2.4(d)). Hence under these conditions it is possible, at least transiently, to obtain a form of BioB with two distinct types of [2Fe-2S]$^{2+}$ cluster bound in different sites.

***SAM binding to the [4Fe-4S]$^{2+}$ cluster in [2Fe-2S]/[4Fe-4S] BioB.*** Previous resonance Raman and Mössbauer studies of BioB have provided strong evidence for SAM binding to the unique Fe site of the [4Fe-4S]$^{2+}$ cluster in [4Fe-4S] BioB (*7*). Hence we have used the same approach to investigate if SAM binding to the [4Fe-4S]$^{2+}$ cluster is perturbed by the presence of the [2Fe-2S]$^{2+}$ cluster in [2Fe-2S]/[4Fe-4S] BioB. Addition of a 10-fold excess of SAM had no effect on the resonance Raman or Mössbauer properties of the [2Fe-2S]$^{2+}$ cluster in [2Fe-2S] BioB (the resonance Raman spectrum is shown in Fig 2.5(b)). In contrast, both the resonance Raman and Mössbauer studies of [2Fe-2S]/[4Fe-4S] BioB indicate that the SAM-induced changes in the [4Fe-4S]$^{2+}$ cluster that were observed with [4Fe-4S] BioB (*7*) are also observed in [2Fe-2S]/[4Fe-4S] BioB. In the case of resonance Raman, this is best illustrated by comparing the spectrum obtained for [4Fe-4S] BioB + SAM (Fig. 2.5(c)) with the [2Fe-2S]/[4Fe-4S] BioB + SAM minus [2Fe-2S] BioB + SAM difference spectrum (Fig. 2.5(d)). The spectra are very similar, but quite distinct from the equivalent spectra obtained in the absence of SAM, see Fig. 2.1(b) and 2.1(d), respectively. The changes in the resonance Raman spectrum induced by SAM, in particular the increase in the frequency of the symmetric breathing mode of the $Fe_4S_4$ cube from 338 cm$^{-1}$ in the absence of SAM to 342/344 cm$^{-1}$ in the presence of SAM, are consistent with binding a bidentate non-cysteinyl ligand at a unique Fe site of the [4Fe-4S]$^{2+}$ cluster (*7*). The effect of SAM binding on the Mössbauer spectrum of the [4Fe-4S]$^{2+}$ cluster in [2Fe-2S]/[4Fe-4S] BioB are most conveniently assessed using [2$^{56}$Fe-2S]/[4$^{57}$Fe-4S] BioB. As shown in Fig. 2.6, SAM binding induces marked changes in the Mössbauer spectrum of the [4$^{57}$Fe-4S]$^{2+}$ cluster in [2$^{56}$Fe-2S]/[4$^{57}$Fe-4S] BioB, c.f. Figs 2.6(a) and 2.6(b), and the changes are essentially identical to those previously reported for [4$^{57}$Fe-4S] BioB, as judged by the near equivalence of the difference spectra for samples with and without SAM, c.f. Figs 2.6(c) and 2.6(d). The SAM-induced changes in the Mössbauer spectrum have previously been analyzed in detail for [$4^{57}$Fe-4S] BioB and attributed to an increase in coordination number and/or binding of a non-cysteinyl ligand at a unique Fe site (*7*). Hence the presence of the [2Fe-2S]$^{2+}$ does not alter the affinity or mode of binding of SAM to the [4Fe-4S]$^{2+}$ cluster in BioB.

***Cluster composition of recombinant BioB in anaerobically grown E. coli cells***. Our previous whole cell Mössbauer studies of recombinant BioB in aerobically grown cells revealed that the majority, if not all, of the overexpressed BioB was present inside the cells as an inactive form containing only [2Fe-2S]$^{2+}$ clusters (*24*). Hence the as isolated [2Fe-2S]$^{2+}$ cluster was shown not to be an artifact of the purification procedure. However, because the as isolated [2Fe-2S]$^{2+}$ cluster can be assembled in vitro only via an aerobic reconstitution procedure starting with apo BioB and the anaerobically reconstituted [4Fe-4S]$^{2+}$ cluster is rapidly degraded by exposure to oxygen, the whole cell studies raised the possibility that lack of the [4Fe-4S]$^{2+}$ cluster and the presence of the [2Fe-2S]$^{2+}$ might both be artifacts of over-expressing recombinant BioB under aerobic growth conditions (*24*). In order to test this hypothesis, we developed a BioB overproducing strain of *E. coli* suitable for anaerobic growth conditions and investigated the cluster content of cells grown on $^{57}$Fe using whole cell Mössbauer spectroscopy. This strain was particularly effective for over-expression of BioB and gel densitometry indicated that BioB accounted for approximately 20% of the total cellular protein.

The results of the whole cell Mössbauer study of recombinant BioB in anaerobically grown *E. coli* are shown in Fig. 2.7. Control cells grown under identical conditions containing the same plasmid used for over-expressing BioB, but without the BioB insert, exhibited broad quadrupole doublets from ferric (Fig 2.7(a), dashed line) and ferrous (Fig 2.7(a), dotted line) components. In contrast, the dominant feature in the spectrum of cells with over-expressed BioB

(Fig. 2.7(b)) is a quadrupole doublet with parameters ($\delta$ = 0.29 mm/s and $\Delta E_Q$ = 0.53 mm/s) identical to those of the $[2Fe\text{-}2S]^{2+}$ cluster in as isolated [2Fe-2S] BioB (Fig. 2.6(b)). Moreover, removal of the ferrous and ferric contributions from the spectra obtained for whole cells and cell free extract yields spectra (Figs 2.7(c) and 2.7(d), respectively) that are indicative of $[2Fe\text{-}2S]^{2+}$ clusters, revealing that anaerobically overexpressed BioB contains only $[2Fe\text{-}2S]^{2+}$ clusters prior to purification. Hence recombinant BioB is shown to contain only $[2Fe\text{-}2S]^{2+}$ clusters in the over-expressing strains used in this work, irrespective of aerobic or anaerobic growth conditions.

***Is BioB a PLP-dependent enzyme?*** Fontecave and coworkers have reported that BioB as purified contains 0.05 mol of PLP per mol of monomeric BioB and that incubation with a 5-fold excess of PLP in the presence 10 mM DTT, followed by extensive dialysis to remove excess PLP, results in incorporation of up to 0.4 mol of PLP per mol of [2Fe-2S] BioB and up to 1.0 mol of PLP per mole of [4Fe-4S] BioB (*14*). Moreover, PLP was found to induce significant cysteine desulfurase activity in [4Fe-4S] BioB and to enhance the biotin synthase activity of both the [2Fe-2S] and [4Fe-4S] forms of BioB (*14*). As discussed below, we have been unable to confirm any of these results with the samples of *E. coli* BioB used in this work.

As isolated [2Fe-2S] BioB and samples of [4Fe-4S] BioB reconstituted from apo BioB in the presence of a 10-fold stoichiometric excess of PLP, followed by gel-filtration to remove excess PLP, contained < 0.01 mol of bound PLP per mole of monomeric BioB, as judged by absorption and analytical assessment of PLP in alkaline denatured samples. Moreover, incubation of either [2Fe-2S] BioB or [4Fe-4S] BioB with a 5-to-10-fold excess of PLP in the presence of 5 mM DTT for time periods in the range 1-24 hr provided no evidence of PLP binding as judged by absorption studies, see Fig. 2.8. Following removal of excess PLP by gel filtration, the resulting absorption spectra exactly overlaid those of the starting material. The absence of bound PLP was confirmed by absorption and analytical studies of alkaline denatured samples. In contrast, the same procedure using a PLP-depleted sample of his-tagged *E. coli* IscS, a well characterized PLP-dependent cysteine desulfurase (*49*), yielded complete reconstitution of PLP as evidenced by the extinction coefficient of bound PLP ($\varepsilon_{390}$ = 7.5 $mM^{-1}cm^{-1}$), see Fig. 2.8.

Fontecave and coworkers reported maximal (albeit very low) levels of cysteine desulfurase activity for [4Fe-4S] BioB, with ~6 Ala and ~6 $S^{2-}$ produced per BioB monomer after incubating with 1xPLP in the presence of 1 mM L-cysteine and 20 mM DTT for 4 hr at 20 °C (*14*). However, using an assay based on L-alanine dehydrogenase (*28*), we were unable to detect L-alanine above the detection limit (5 μM) after incubating [4Fe-4S] BioB (20 or 40 μM) with 1xPLP in the presence of 500 μM L-cysteine and 5 mM DTT for 2.5 hr at 25 °C, see Table 2.2. Sulfide was generated at the level of ~4 $S^{2-}$/BioB, but this was observed irrespective of the presence of PLP and the sulfide levels were never significantly greater than the amount contained in [4Fe-4S] clusters, see Table 2.2. Moreover, the Ala/$S^{2-}$ ratios (< 0.1) effectively rule out the possibility of cysteine desulfurase activity for these samples of [4Fe-4S] BioB. In order to check the effectiveness of the alanine and sulfide assays used in this work, the same protocol was used to assess cysteine desulfurase activity for his-tagged *E. coli* IscS. The results are in accord with previous assessments of IscS cysteine desulfurase activity (*23, 49*) and indicate Ala/$S^{2-}$ ratios close to 1.0, see Table 2.2.

In accord with previous activity studies of [2Fe-2S], [4Fe-4S] and [2Fe-2S]/[4Fe-4S] forms of *E. coli* BioB (*11, 12, 14*), none of these forms were found to be capable of more than a single turnover per BioB monomer in a well-defined anaerobic assay, see Table 2.1. As reported by Jarrett and coworkers (*12*), the most active form in the absence of added $Fe^{2+}$ is [2Fe-2S]/[4Fe-4S] BioB which undergoes almost a complete turnover based on the cluster content.

[2Fe-2S] BioB exhibits negligible activity if $Fe^{2+}$ is excluded from the reaction mixture, but the activity increases to a level close to one turnover per BioB in the presence of 1 mM $Fe^{II}(NH_4)_2(SO_4)_2$. [4Fe-4S] BioB is only capable of ~10% of turnover in the absence of added $Fe^{2+}$ and this increases to ~30% of a turnover in the presence of 1 mM $Fe^{II}(NH_4)_2(SO_4)_2$. However, in contrast to the results of Fontecave and coworkers which reported a 5-fold increase in biotin formation for [4Fe-4S] BioB on addition of 1×PLP to the reaction mixture (*14*), the addition of 1×PLP to the reaction mixture had no significant effect on the biotin synthase activities of the [2Fe-2S], [4Fe-4S] and [2Fe-2S]/[4Fe-4S] forms of BioB investigated in this work, see Table 2.1.

## Discussion

The cofactor composition of recombinant *E. coli* BioB both in vivo and in purified samples has been the subject of much discussion and controversy since the enzyme was first purified by Sanyal and coworkers in 1994. The results presented herein are an attempt to reconcile the confusion in the literature and to establish the cofactor composition both in vivo and in as isolated and reconstituted forms of purified BioB. Perhaps most surprising is our complete failure to confirm the recent reports that BioB is a PLP-dependent enzyme with intrinsic cysteine desulfurase activity (*11, 14*). Despite extensive assay and analytical studies using conditions similarto those reported by Fontecave and coworkers, we have been unable to find any evidence for PLP binding or for PLP-induced cysteine desulfurase or biotin synthase activity with as isolated or reconstituted samples of purified recombinant BioB. The only significant differences between these two studies lie in our use of gel filtration rather than dialysis to remove excess PLP and in the methods used to analyze for alanine in assaying for cysteine desulfurase activity and for bound PLP. These differences are unlikely to be significant. Gel filtration is the standard method for removing excess PLP from PLP-dependent enzymes after reconstitution and the accuracy of the analytical procedures used in this study were validated by parallel studies of IscS, a well-characterized cysteine desulfurase that binds stoichiometric PLP. Hence we are at a loss to explain the differences between the results presented herein and those of Fontecave and coworkers, but based on our results we see no reason to conclude that BioB is a PLP dependent enzyme with cysteine desulfurase activity.

The combination of absorption, resonance Raman and Mössbauer spectroscopies coupled with analytical studies and enzyme assays has provided a detailed understanding of the cluster composition and the in vitro reconstitution and $O_2$-induced cluster transformations that are possible for recombinant BioB. The results are summarized in Fig. 2.9. In accord with the work of Jarrett and coworkers (*17, 48*), BioB is shown to contain two distinct cluster binding sites. However, the results do not support the conclusion that each binding site can accommodate either a $[4Fe\text{-}4S]^{2+}$ or $[2Fe\text{-}2S]^{2+}$ cluster (*17*). This conclusion was based on the ability to generate stable forms of BioB containing two $[4Fe\text{-}4S]^{2+}$ clusters per monomer or two $[2Fe\text{-}2S]^{2+}$ clusters per monomer (*17*). We have failed to confirm these results and have provided spectroscopic and analytical evidence that both forms are artifacts of analytical studies on incompletely purified reconstituted samples. Rather the results presented herein indicate that one binding site is exclusively associated with the $[2Fe\text{-}2S]^{2+}$ cluster that is present in BioB as isolated and the other accommodates the oxygen-labile $[4Fe\text{-}4S]^{2+}$ cluster that is responsible for binding and reductive cleavage of SAM. In accord with previous results (*5, 15, 18*), the $[4Fe\text{-}4S]^{2+}$ cluster can be reduced to the $[4Fe\text{-}4S]^{+}$ state using dithionite or deazaflavin-mediated photochemical reduction, whereas the $[2Fe\text{-}2S]^{2+}$ cluster is slowly degraded by dithionite to yield apo BioB in the presence of an Fe chelator.

Both the $[4Fe\text{-}4S]^{2+}$ and $[2Fe\text{-}2S]^{2+}$ clusters can be reconstituted in apo BioB by incubation with $Fe^{3+}$ or $Fe^{2+}$ and $S^{2-}$ in the presence of DTT, with the presence of $O_2$ dictating reconstitution of the $[2Fe\text{-}2S]^{2+}$ cluster and rigorously anaerobic conditions being required for reconstitution of the $[4Fe\text{-}4S]^{2+,+}$ cluster, see Fig. 2.9. Hence the apparent discrepancy in the reconstitution products reported in the literature (*18, 19*) can now be readily rationalized in terms of differences in the $O_2$ exposure during the reconstitution procedure. Anaerobic reconstitution starting with $O_2$-stable, as isolated [2Fe-2S] BioB results in the formation of [2Fe-2S]/[4Fe-4S] BioB with $[2Fe\text{-}2S]^{2+}$ and $[4Fe\text{-}4S]^{2+}$ clusters in a 1:1 ratio with approximately 0.7 $[4Fe\text{-}4S]^{2+}$ and $[2Fe\text{-}2S]^{2+}$ clusters per monomer. Analogous results, albeit with near-stoichiometric $[4Fe\text{-}4S]^{2+}$ and $[2Fe\text{-}2S]^{2+}$ clusters, were first reported by Jarrett and coworkers on the basis of absorption and analytical studies (*17*), but the subsequent Mössbauer studies (*48*) would suggest a similar stoichiometry to that observed in this work. The origin of the sub-stoichiometric amounts of each cluster is not fully understood at present. The Mössbauer evidence of substantial formation of $[4^{57}Fe\text{-}4S]^{2+}$ clusters (18% of the total $^{57}Fe$) during reconstitution of $[2^{57}Fe\text{-}2S]$ BioB with natural abundance Fe (Fig. 2.2e), coupled with the inability to reconstitute the $[2Fe\text{-}2S]^{2+}$ cluster under the strict anaerobic conditions of the reconstitution procedure, indicate that the sub-stoichiometric amount of $[2Fe\text{-}2S]^{2+}$ clusters is a consequence of the lability of $[2Fe\text{-}2S]^{2+}$ cluster under reconstitution conditions. However, we currently do not have a good explanation for the observation that only ~0.7 $[4Fe\text{-}4S]^{2+}$ clusters are assembled in reconstitutions starting from [2Fe-2S] BioB, compared to ~1.0 $[4Fe\text{-}4S]^{2+}$ clusters in reconstitutions starting with apo BioB. Nevertheless, the analytical data and Mössbauer results can only be interpreted in terms of at least half of the protein in [2Fe-2S]/[4Fe-4S] BioB containing one $[4Fe\text{-}4S]^{2+}$ and $[2Fe\text{-}2S]^{2+}$ cluster per monomer.

The present study is particularly informative concerning the fate of the $[4Fe\text{-}4S]^{2+}$ cluster in both [4Fe-4S] and [2Fe-2S]/[4Fe-4S] BioB during $O_2$-induced degradation. Resonance Raman studies show that the degradation proceeds via a $[2Fe\text{-}2S]^{2+}$ cluster intermediate that has distinctive properties compared to the $[2Fe\text{-}2S]^{2+}$ cluster in as isolated [2Fe-2S] BioB, see Fig. 2.9. This type of $O_2$-induced $[4Fe\text{-}4S]^{2+}$ cluster degradation appears to be a common to most radical-SAM enzymes (*45-47*), and is complete in BioB after exposure to air for 10 min. However, the $[2Fe\text{-}2S]^{2+}$ cluster in the [4Fe-4S] cluster domain of BioB is less $O_2$ tolerant than in some other radical SAM enzymes, and is further degraded to yield a vacant [4Fe-4S] cluster domain on exposure to air for 1 hr. Hence the ultimate product of exposing [2Fe-2S]/[4Fe-4S] BioB to air is [2Fe-2S] BioB. In contrast, when the [2Fe-2S] domain is vacant as in [4Fe-4S] BioB, the $O_2$-induced breakdown of the $[4Fe\text{-}4S]^{2+}$ cluster is followed by aerobic reconstitution of the $[2Fe\text{-}2S]^{2+}$ cluster in the [2Fe-2S] domain provided DTT is present to prevent disulfide formation, see Fig. 2.9. It is also important to emphasize that the $O_2$-damaged form of [2Fe-2S]/[4Fe-4S] BioB containing two different types of $[2Fe\text{-}2S]^{2+}$ clusters does not appear to be related to the form of BioB containing two $[2Fe\text{-}2S]^{2+}$ clusters that was claimed by Jarrett and coworkers (*17*). For example, we have never observed this species in as isolated samples of BioB or in as isolated samples of BioB that were treated with $FeCl_3$.

The combination of resonance Raman and Mössbauer studies has also shown that SAM binds to the unique site of the $[4Fe\text{-}4S]^{2+}$ cluster in [2Fe-2S]/[4Fe-4S] BioB in the same way as previously demonstrated for [4Fe-4S] BioB (*7*). By analogy with the recent Mössbauer and ENDOR studies of the pyruvate formate-lyase activating enzyme (*50-52*), the mode of binding is likely to involve the amino and carboxylato groups of the methionine fragment. The observation that binding of SAM to the $[4Fe\text{-}4S]^{2+}$ cluster in [2Fe-2S]/[4Fe-4S] BioB has no effect on the spectroscopic properties of the $[2Fe\text{-}2S]^{2+}$ cluster and is unaffected by the presence of the $[2Fe\text{-}2S]^{2+}$ cluster, therefore provides unambiguous proof for distinct [2Fe-2S] and [4Fe-4S] cluster domains with only the latter involved with binding and reductive activation of SAM. Moreover, the $[4Fe\text{-}4S]^{2+}$ cluster in [2Fe-2S]/[4Fe-4S] and [4Fe-4S] BioB was found to be essentially 100% SAM bound using a 10-fold excess of SAM, even in the absence of DTB. This is in stark contrast to the recent results of Jarrett and coworkers (*10*), which reported negligible or weak SAM binding to the $[4Fe\text{-}4S]^{2+}$ clusters in [4Fe-4S] and [2Fe-2S]/[4Fe-4S] BioB, in the absence of DTB, based on equilibrium dialysis experiments. We have no explanation for this discrepancy, but it is difficult to see how the resonance Raman and Mössbauer results can be incorrect, since they facilitate direct observation of SAM binding to the $[4Fe\text{-}4S]^{2+}$ cluster.

Our previous whole cells Mössbauer results raised the possibility that the assembly of the $[2Fe\text{-}2S]^{2+}$ cluster and the lack of assembly of the catalytically essential $[4Fe\text{-}4S]^{2+,+}$ cluster were both artifacts of over-expressing recombinant BioB under aerobic growth conditions (*24*). However, the whole cell Mössbauer studies of an anaerobically grown BioB over-expressing strain of *E. coli* that are presented in this work, unambiguously demonstrate that $O_2$ exposure in the cell is not responsible for overexpression of recombinant BioB in an inactive form containing only the $[2Fe\text{-}2S]^{2+}$ cluster. Rather this appears to an intrinsic property of the over-expressed recombinant enzyme. However, since the recombinant form of the enzyme is expressed in an inactive form, devoid of the catalytically essential $[4Fe\text{-}4S]^{2+,+}$ cluster, under both aerobic and anaerobic growth conditions, it is still possible that the $[2Fe\text{-}2S]^{2+}$ is an artifact that is assembled in error due to absence of specific proteins or conditions that are required for assembly of the

$[4Fe\text{-}4S]^{2+,+}$ cluster. In this connection it may be significant to note that conditions have yet to be found for in vitro reconstitution of the $[2Fe\text{-}2S]^{2+}$ cluster starting with [4Fe-4S] BioB, see Fig. 2.9. Clearly it is now of primary importance to establish the cluster composition of native BioB at the levels expressed under normal growth conditions. Until this is accomplished, it is not possible to reach a definitive conclusion concerning the physiological relevance of the $[2Fe\text{-}2S]^{2+}$ cluster that is invariably present in as isolated samples of recombinant BioB.

In summary, the results presented in this work do not support the proposal advanced by Fontecave and coworkers that BioB is a PLP enzyme with intrinsic cysteine desulfurase activity (*11, 14*). They are, however, consistent with the alternative model, first advanced by Jarrett and workers (*12, 48*), involving a functional [2Fe-2S]/[4Fe-4S] form of BioB with the $[2Fe\text{-}2S]^{2+}$ cluster as the sacrificial S donor and the $[4Fe\text{-}4S]^{2+,+}$ cluster as the site for generating the 5'-deoxyadenosyl radical via reductive cleavage of SAM. In our hands, this is the only form of BioB that is capable of a single turnover in an in vitro assay without the addition of $Fe^{2+}$ and $S^{2-}$. In accord with this model, both absorption (*12*) and more recently Mössbauer (*13*) studies have shown that the $[2Fe\text{-}2S]^{2+}$ cluster is degraded during a single turnover and labeling experiments have shown that cluster-associated S is incorporated into biotin in single turnover experiments (*36, 53*). However, as discussed above, it is too early to speculate if the [2Fe-2S]/[4Fe-4S] form of BioB is the catalytically relevant form that is capable of multiple turnovers in vivo. The possibility that the $[2Fe\text{-}2S]^{2+}$ cluster in [2Fe-2S]/[4Fe-4S] BioB is the immediate S donor to biotin is addressed in the following manuscript which follows the time course of biotin production and $[2Fe\text{-}2S]^{2+}$ degradation in single turnover experiments.

## References

1. Marquet, A. (2001) Enzymology of carbon-sulfur bond formation, *Curr. Opin. Chem. Biol. 5*, 541-549.
2. Fontecave, M., Ollagnier-de-Choudens, S., and Mulliez, E. (2003) Biological radical sulfur insertion reactions, *Chem. Rev. 103*, 2149-2166.
3. Frey, P. A. and Magnusson, O. Th. (2003) *S*-adenosylmethionine: a wolf in sheep's clothing, or a rich man's adenosylcobalamin, *Chem. Rev. 103*, 2129-2148.
4. Jarrett, J. T. (2003) The generation of 5'-deoxyadenosyl radicals by adenosylmethioine-dependent radical enzymes, *Curr. Opin. Chem. Biol. 7*, 174-182.
5. Duin, E. C., Lafferty, M. E., Crouse, B. R., Allen, R. M., Sanyal, I., Flint, D. H., and Johnson, M. K. (1997) [2Fe-2S] to [4Fe-4S] cluster conversion in *Escherichia coli* biotin synthase, *Biochemistry 36*, 11811-11820.
6. Ollagnier-de-Choudens, S., Sanakis, Y., Hewitson, K. S., Roach, P. L., Münck, E., and Fontecave, M. (2002) Reductive cleavage of *S*-adenosylmethionine by biotin synthase from *Escherichia coli*, *J. Biol. Chem. 277*, 13449-13454.
7. Cosper, M. M., Jameson, G. N. L., Davydov, R., Eidsness, M. K., Hoffman, B. M., Huynh, B. H., and Johnson, M. K. (2002) The $[4Fe\text{-}4S]^{2+}$ cluster in reconstituted biotin synthase binds *S*-adenosylmethionine, *J. Am. Chem. Soc. 124*, 14006-14007.
8. Sofia, H. J., Chen, G., Hetzler, B. G., Reyes-Spindola, J. F., and Miller, N. E. (2001) Radical SAM, a novel protein superfamily linking unresolved steps in familiar biosynthetic pathways with radical mechanisms: functional characterization using new analysis and information visualization methods, *Nucleic Acids Res. 29*, 1097-1106.

9. Escalettes, F., Florentin, D., Tse Sum Bui, B., Lesage.D., and Marquet, A. (1999) Biotin synthase mechanism: evidence for hydrogen transfer from the substrate into deoxyadenosine, *J. Am. Chem. Soc. 121*, 3571-3578.

10. Ugulava, N. B., Frederick, K. K., and Jarrett, J. T. (2003) Control of adenosylmethionine-dependent radical generation in biotin synthase: a kinetic and thermodynamic analysis of substrate binding to active and inactive forms of BioB, *Biochemistry 42*, 2708-2719.

11. Ollagnier-de-Choudens, S., Mulliez, E., and Fontecave, M. (2002) The PLP-dependent biotin synthase from *Escherichia coli*: mechanistic studies, *FEBS Lett. 532*, 465-468.

12. Ugulava, N. B., Sacanell, C. J., and Jarrett, J. T. (2001) Spectroscopic changes during a single turnover of biotin synthase: destruction of a [2Fe-2S] cluster accompanies sulfur insertion, *Biochemistry 40*, 8352-8358.

13. Tse Sum Bui, B., Benda, R., Schünemann, V., Florentin, D., Trautwein, A. X., and Marquet, A. (2003) Fate of the $[2Fe\text{-}2S]^{2+}$ cluster of *Escherichia coli* biotin synthase during reaction: a Mössbauer characterization, *Biochemistry 42*, 8791-8798.

14. Ollagnier-de-Choudens, S., Mulliez, E., Hewitson, K. S., and Fontecave, M. (2002) Biotin synthase is a pyridoxal phosphate-dependent cysteine desulfurase, *Biochemistry 41*, 9145-9152.

15. Sanyal, I., Cohen, G., and Flint, D. H. (1994) Biotin synthase: purification, characterization as a [2Fe-2S] cluster protein, and *in vitro* activity of the *Escherichia coli bioB* gene product, *Biochemistry 33*, 3625-3631.

16. Picciocchi, A., Douce, R., and Alban, C. (2001) Biochemical characterization of the Arabidopsis biotin synthase reaction. The importance of mitochondria in biotin synthesis, *Plant Physiol. 127*, 1224-1233.

17. Ugulava, N. B., Gibney, B. R., and Jarrett, J. T. (2001) Biotin synthase contains two distinct iron-sulfur cluster binding sites: chemical and spectroelectrochemical analysis of iron-sulfur cluster interconversions, *Biochemistry 40*, 8343-8351.

18. Ollagnier-de-Choudens, S., Sanakis, Y., Hewitson, K. S., Roach, P., Baldwin, J. E., Münck, E., and Fontecave, M. (2000) Iron-sulfur center of biotin synthase and lipoate synthase, *Biochemistry 39*, 4165-4173.

19. Tse Sum Bui, B., Florentin, D., Marquet, A., Benda, R., and Trautwein, A. X. (1999) Mössbauer studies of *Escherichia coli* biotin synthase: evidence for reversible interconversion between $[2Fe\text{-}2S]^{+}$ and $[4Fe\text{-}4S]^{2+}$ clusters, *FEBS Lett. 459*, 411-414.

20. Hewitson, K. S., Baldwin, J. E., Shaw, N. M., and Roach, P. L. (2000) Mutagenesis of the proposed iron-sulfur cluster binding ligands in *Escherichia coli* biotin synthase, *FEBS Lett. 466*, 372-376.

21. Hewitson, K. S., Ollagnier-de-Choudens, S., Sanakis, Y., Shaw, N. M., Baldwin, J. E., Münck, E., Roach, P. L., and Fontecave, M. (2002) The iron-sulfur center of biotin synthase: site-directed mutants, *J. Biol. Inorg. Chem. 7*, 83-93.

22. Zheng, L., White, R. H., Cash, V. L., Jack, R. F., and Dean, D. R. (1993) Cysteine desulfurase activity indicates a role for NIFS in metallocluster biosynthesis, *Proc. Natl. Acad. Sci. USA 90*, 2754-2758.

23. Mihara, H. and Esaki, N. (2002) Bacterial cysteine desulfurases: their function and mechanisms, *Appl. Microbiol. Biotechnol. 60*, 12-23.

24. Cosper, M. M., Jameson, G. N. L., Eidsness, M. K., Huynh, B. H., and Johnson, M. K. (2002) Recombinant *Escherichia coli* biotin synthase is a $[2Fe\text{-}2S]^{2+}$ protein in whole cells, *FEBS Lett. 529*, 332-336.

25. Benda, R., Tse Sum Bui, B., Schünemann, V., Florentin, D., Marquet, A., and Trautwein, A. X. (2002) Iron-sulfur clusters of biotin synthase in vivo: a Mössbauer study, *Biochemistry 41*, 15000-15006.

26. Tabor, S. (1990) Expression using the T7 RNA polymerase/promotor system, in *Current Protocols in Molecular Biology* (Ausubel, F. A., Brent, R., Kingston, R. E., Moore, D. D., Seidman, J. G., Smith, J. A., and Sthuhl, K., Eds.) pp 16.2.1-16.2.11, Greene Publishing and Wiley Interscience, New York.

27. Harwood, C. R. and Cutting, S. M. (1990) *Modern Microbiological Methods: Molecular Biology Methods for Bacillus*, Wiley and Sons, Chichester, UK.

28. Yoshida, A. and Freese, E. (1970) L-Alanine dehydrogenase (*Bacillus subtilis*), *Meth. Enzymol. 17a*, 176-181.

29. Siegel, L. M. (1965) A direct microdetermination for sulfide, *Anal. Biochem. 11*, 126-132.

30. Fish, W. W. (1988) Rapid colorimetric micromethod for the quantitation of complexed iron in biological samples, *Meth. Enzymol. 158*, 357-364.

31. Bates, C. J., Pentieva, K. D., Matthews, N., and Macdonald, A. (1999) A simple, sensitive and reproducible assay for pyridoxal 5'-phosphate and 4-pyridoxic acid in human plasma, *Clin. Chim. Acta 280*, 101-111.

32. Drozdzewski, P. M. and Johnson, M. K. (1988) A simple anaerobic cell for low temperature Raman spectroscopy, *Appl. Spectrosc. 42*, 1575-1577.

33. Ravi, N., Bollinger, J. M., Huynh, B. H., Edmondson, D. E., and Stubbe, J. (1994) Mechanism of assembly of the tyrosyl radical-diiron(III) cofactor of *E. coli*

ribonucleotide reductase. 1. Mössbauer characterization of the diferric radical precusor, *J. Am. Chem. Soc. 116*, 8007-8014.

34. Tanaka, M., Izumi, Y., and Yamada, H. (1987) Biotin assay using lyophilized and glycerol-suspended cultures, *J. Microbiol. Meth. 6*, 237-246.
35. Tse Sum Bui, B. and Marquet, A. (1997) Biotin synthase of *Bacillus sphaericus*, *Meth. Enzymol. 279*, 357-362.
36. Tse Sum Bui, B., Florentin, D., Fournier, F., Ploux, O., Méjean, A., and Marquet, A. (1998) Biotin synthase mechanism: on the origin of sulphur, *FEBS Lett. 440*, 226-230.
37. Spiro, T. G., Hare, J., Yachandra, V., Gewirth, A., Johnson, M. K., and Remsen, E. (1982) Resonance Raman spectra of iron-sulfur proteins and analogs, in *Iron-sulfur proteins* (Spiro, T. G., Ed.) pp 407-423, Wiley-Interscience, New York.
38. Spiro, T. G., Czernuszewicz, R. S., and Han, S. (1988) Iron-sulfur proteins and analog complexes, in *Resonance Raman spectra of heme and metalloproteins* (Spiro, T. G., Ed.) pp 523-554, John Wiley & Sons, New York.
39. Fu, W., Morgan, T. V., Mortenson, L. E., and Johnson, M. K. (1991) Resonance Raman studies of the [4Fe-4S] to [2Fe-2S] cluster conversion in the iron protein of nitrogenase, *FEBS Lett. 284*, 165-168.
40. Fu, W., Drozdzewski, P. M., Adams, M. W. W., Morgan, T. V., Mortenson, L. E., LeGall, J., Peck, H. D., Jr., DerVartanian, D. V., and Johnson, M. K. (1993) Resonance Raman studies of iron-hydrogenases, *Biochemistry 32*, 4813-4819.
41. Tong, W.-H., Jameson, G. N. L., Huynh, B. H., and Rouault, T. A. (2003) Subcellular compartmentalization of human Nfu, an iron-sulfur cluster scaffold protein and its ability to assemble a [4Fe-4S] cluster, *Proc. Natl. Acad. Sci. USA 100*, 9762-9767.

42. Trautwein, A. X., Bominaar, E. L., and Winkler, H. (1991) Iron-containing proteins and related analogs. Complementary Mössbauer, EPR and magnetic susceptibility studies, *Struct. Bonding 78*, 1-95.

43. Krebs, C., Agar, J. N., Smith, A. D., Frazzon, J., Dean, D. R., Huynh, B. H., and Johnson, M. K. (2001) IscA, an alternative scaffold for Fe-S cluster biosynthesis, *Biochemistry 40*, 14069-14080.

44. Johnson, M. K., Staples, C. R., Duin, E. C., Lafferty, M. E., and Duderstadt, R. E. (1998) Novel roles for Fe-S cluster in stabilizing or generating radical intermediates, *Pure Appl. Chem. 70*, 939-946.

45. Ollagnier, S., Meier, C., Mulliez, E., Gaillard, J., Schuenemann, V., Trautwein, A. X., Mattioli, T., Lutz, M., and Fontecave, M. (1999) Assembly of 2Fe-2S and 4Fe-4S clusters in the anaerobic ribonucleotide reductase from *Escherichia coli*, *J. Am. Chem. Soc. 121*, 6344-6350.

46. Broderick, J. B., Duderstadt, R. E., Fernandez, D. C., Wojtuszewski, K., Henshaw, T. F., and Johnson, M. K. (1997) Pyruvate formate-lyase activating enzyme is an iron-sulfur protein, *J. Am. Chem. Soc. 119*, 7396-7397.

47. Pierrel, F., Hernandez, H., Johnson, M. K., Fontecave, M., and Atta, M. (2003) MiaB protein from *Thermotoga maritime*: characterization of an extremely thermophilic tRNA-methylthiotransferase, *J. Biol. Chem. 278*, 29515-29524.

48. Ugulava, N. B., Surerus, K. K., and Jarrett, J. T. (2003) Evidence from Mössbauer spectroscopy for distinct $[2Fe\text{-}2S]^{2+}$ and $[4Fe\text{-}4S]^{2+}$ cluster binding sites in biotin synthase from *Escherichia coli*, *J. Am. Chem. Soc. 124*, 9050-9051.

49. Flint, D. H. (1996) *Escherichia coli* contains a protein that is homologous in function and N-terminal sequence to the protein encoded by the NIFS gene of *Azotobacter vinelandii* and that can participate in the synthesis of the Fe-S cluster of dihyroxy-acid dehydratase, *J. Biol. Chem. 271*, 16068-16074.

50. Krebs, C., Broderick, W. E., Henshaw, T. F., Broderick, J. B., and Huynh, B. H. (2002) Coordination of adenosylmethionine to a unique iron site of the [4Fe-4S] cluster of pyruvate formate-lyase activating enzyme: a Mössbauer spectroscopic study, *J. Am. Chem. Soc. 124*, 912-913.

51. Walsby, C. J., Hong, W., Broderick, W. E., Cheek, J., Ortillo, D., Broderick, J. B., and Hoffman, B. M. (2002) Electron-nuclear double resonance spectroscopic evidence that *S*-adenosylmethionine binds in contact with the catalytically active $[4Fe\text{-}4S]^+$ cluster in pyruvate formate-lyase activating enzyme, *J. Am. Chem. Soc. 124*, 3143-3151.

52. Walsby, C. J., Ortillo, D., Broderick, W. E., Broderick, J. B., and Hoffman, B. M. (2002) An anchoring role for FeS clusters: chelation of the amino acid moiety of *S*-adenosylmethionine to the unique iron site of the [4Fe-4S] cluster of pyruvate formate-lyase activating enzyme, *J. Am. Chem. Soc. 124*, 11270-11271.

53. Gibson, K. J., Pelletier, D. A., and Turner, I. M., Sr. (1999) Transfer of sulfur to biotin from biotin synthase (bioB protein), *Biochem. Biophys. Res. Commun. 254*, 632-635.

**Table 2.1** Cluster composition, absorption properties, Mössbauer parameters, and activity of [2Fe-2S], [4Fe-4S], and [2Fe-2S]/[4Fe-4S] forms of E. coli BioB

| Form | Cluster composition | | Absorption properties | | Mössbauer parameters (4.2 K) | | | | Activity (Biotin/BioB monomer)[a] | | |
|---|---|---|---|---|---|---|---|---|---|---|---|
| | [2Fe-2S] per BioB | [4Fe-4S] per BioB | ε $mM^{-1}cm^{-1}$(nm) | Ratio ($A_{nm}/A_{nm}$) | $[2Fe\text{-}2S]^{2+}$ | | $[4Fe\text{-}4S]^{2+}$ | | No addition | with $Fe^{2+}$ | with PLP |
| | | | | | δ(mm/s) | $\Delta E_Q$(mm/s) | δ(mm/s) | $\Delta E_Q$(mm/s) | | | |
| [2Fe-2S] | 0.85 ± 0.10 | | 7.2 ± 0.8 (453) | 0.21 ± 0.02<br>($A_{453}/A_{278}$) | 0.29 | 0.53 | | | 0.03 | 0.80 | 0.06 |
| [4Fe-4S] | | 1.00 ± 0.10 | 15.6 ± 1.6 (410) | 0.30 ± 0.03<br>($A_{410}/A_{278}$) | | | 0.45<br>0.44 | 1.28<br>1.03 | 0.11 | 0.30 | 0.12 |
| [2Fe-2S]/[4Fe-4S] | 0.72 ± 0.05[b]<br>0.75 ± 0.09[c] | 0.72 ± 0.05[b]<br>0.66 ± 0.05[c] | 17.1 ± 1.8 (410) | 0.33 ± 0.03<br>($A_{410}/A_{278}$) | 0.28 | 0.5 | 0.45<br>0.43 | 1.32<br>1.08 | 0.62 | 0.70 | 0.62 |

[a] nmoles of biotin produced after 24 hr at 25 ºC per nmoles of BioB monomer (estimated error ± 10%). The assay mixture is as described in the material and methods section without any additional components, with 10x $Fe^{2+}$ added to the reaction mixture, and with 1x PLP added to the reaction mixture.

[b] values derived from absorption data together with Fe and protein determinations.

[c] values derived from Mössbauer data together with Fe and protein determinations.

**Table 2.2** Assays of E. coli [4Fe-4S]$^{2+}$ BioB and his-tagged IscS for cysteine desulfurase activity[a]

| [4Fe-4S]$^{2+}$ BioB | | | | |
|---|---|---|---|---|
| [BioB], μM | [PLP], μM | Ala/BioB[b] | $S^{2-}$/BioB | Ala/$S^{2-}$ |
| 20 | 20 | < 0.25 | 4.4 | < 0.1 |
| 20 | 0 | < 0.25 | 4.1 | < 0.1 |
| 40 | 40 | < 0.13 | 4.1 | < 0.1 |
| 40 | 0 | < 0.13 | 3.6 | < 0.1 |
| His-tagged IscS | | | | |
| [IscS], μM | [PLP], μM | Ala/IscS | $S^{2-}$/IscS | Ala/$S^{2-}$ |
| 0.36 | 0 | 278 | 302 | 0.92 |
| 0.72 | 0 | 234 | 235 | 1.00 |

[a] The cysteine desulfurase activity was assessed by analyzing for L-alanine and sulfide after anaerobic incubation with PLP, 5 mM DTT, and 500 mM L-cysteine for 2.5 hr at 25 °C

[b] The detection limit for the L-alanine assay is 5 μM

**Scheme 2.1**

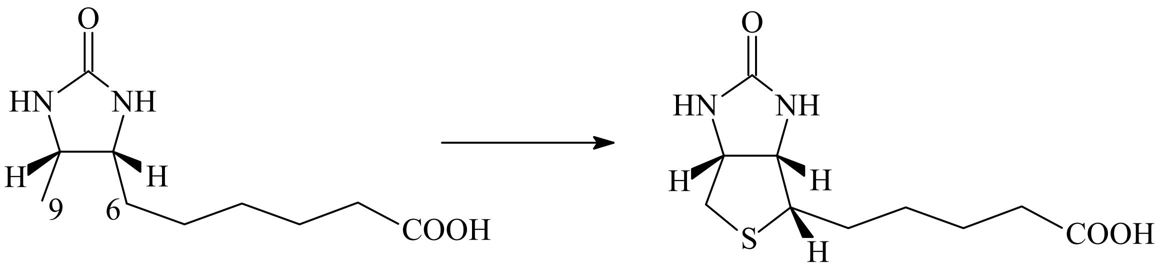
O
HN
NH
H
H
9
6
COOH
O
HN
NH
H
H
S
H
COOH

Dethiobiotin (DTB)

Biotin

**Figure 2.1** UV-visible absorption (left panel) and resonance Raman (right panel) spectra of *E. coli* BioB: (a) $[2Fe\text{-}2S]^{2+}$ BioB; (b) $[4Fe\text{-}4S]^{2+}$ BioB; (c) $[2Fe\text{-}2S]^{2+}/[4Fe\text{-}4S]^{2+}$ BioB. UV-visible absorption and resonance Raman difference spectra, (c) minus (a), are shown in (d). The UV-visible spectra were recorded in 1-mm cuvettes for samples of 290 μM $[2Fe\text{-}2S]^{2+}$ BioB, 170 μM $[4Fe\text{-}4S]^{2+}$ BioB, and 150 μM $[2Fe\text{-}2S]^{2+}/[4Fe\text{-}4S]^{2+}$ BioB in 50 mM Hepes buffer, pH 7.5. The resonance Raman spectra were recorded with 458-nm excitation, using samples that were ~3 mM in BioB frozen at 16 K with 210 mW laser power at the sample. Each scan involved photon counting for 1 s at 0.5 $cm^{-1}$ increments with 8-$cm^{-1}$ spectral resolution, and each spectrum is the sum of ~100 scans. A linear ramp fluorescence background has been subtracted from the resonance Raman spectra.

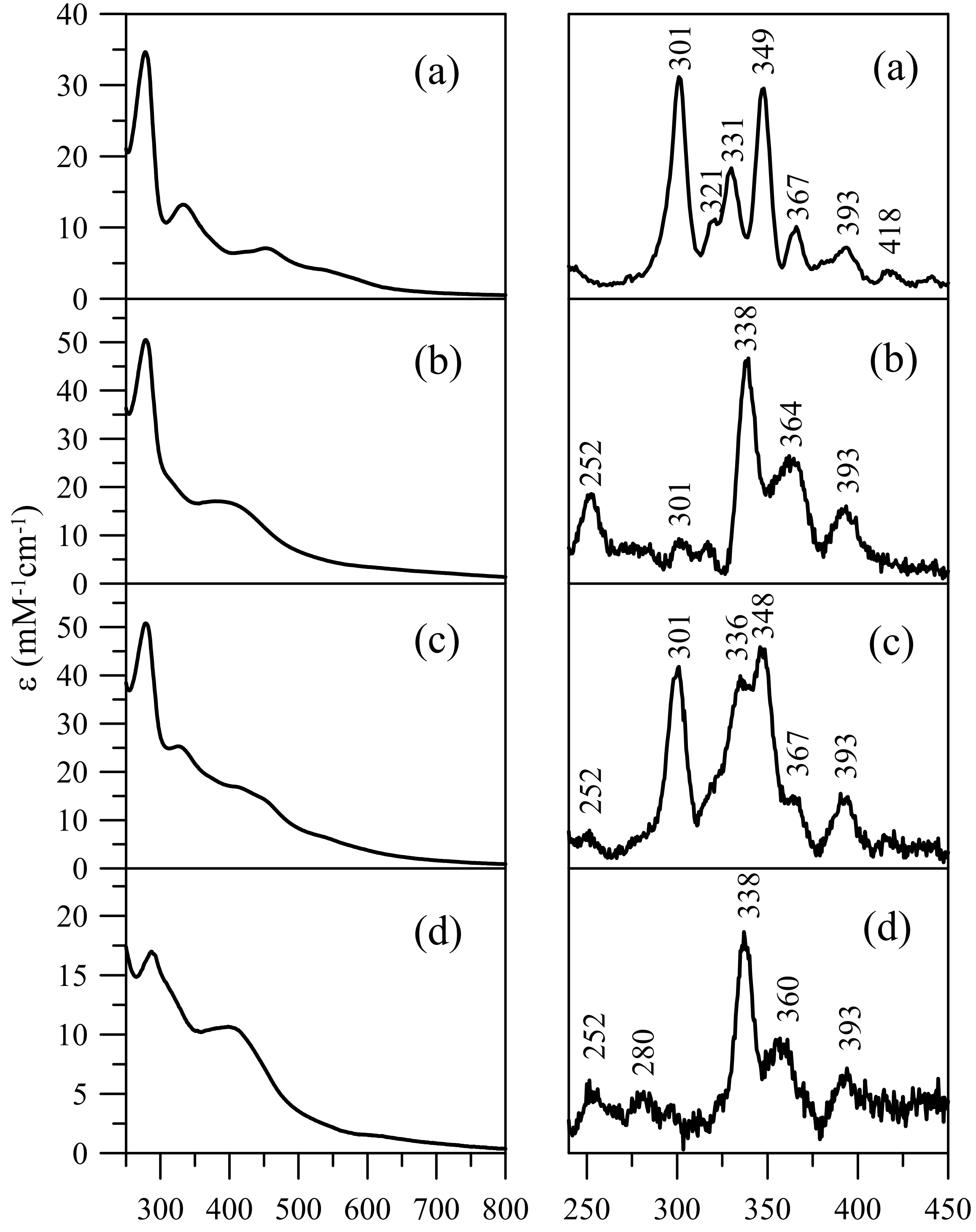
ε (mM⁻¹cm⁻¹)
Wavelength (nm)
Raman Shift (cm⁻¹)
(a)
(b)
(c)
(d)
0
10
20
30
40
50
5
15
300
400
500
600
700
800
250
350
450
301
321
331
349
367
393
418
252
338
364
336
348
280
360

**Figure 2.2** Mössbauer spectra (hatched marks) of [2Fe-2S], [4Fe-4S], and [2Fe-2S]/[4Fe-4S] *E. coli* BioB. (a) [$2^{57}$Fe-2S] BioB, as isolated from cells grown aerobically using $^{57}$Fe in the form of ferric ammonium citrate as the sole source of Fe. The sample was 340 μM in BioB. (b) [$4^{57}$Fe-4S] BioB, prepared by anaerobic reconstitution of apo BioB using $^{57}Fe(NH_4)_2(SO_4)_2$. The sample was 130 μM in BioB. (c) [$2^{57}$Fe-2S]/[$4^{57}$Fe-4S] BioB, prepared by anaerobic reconstitution of as-isolated [$2^{57}$Fe-2S] BioB with $^{57}Fe(NH_4)_2(SO_4)_2$. The sample was 120 μM in BioB. (d) [2Fe-2S]/[$4^{57}$Fe-4S] BioB, prepared by anaerobic reconstitution of unlabeled as-isolated [2Fe-2S] BioB with $^{57}Fe(NH_4)_2(SO_4)_2$. The sample was 140 μM in BioB. (e) [$2^{57}$Fe-2S]/[4Fe-4S] BioB, prepared by anaerobic reconstitution of as-isolated [$2^{57}$Fe-2S] BioB with natural-abundance $Fe(NH_4)_2(SO_4)_2$ (2.2% $^{57}$Fe). The sample was 140 μM in BioB. The solid lines shown in (a) and (b) are theoretical spectra of the $[2Fe\text{-}2S]^{2+}$ and $[4Fe\text{-}4S]^{2+}$ cluster, respectively, simulated with the parameters listed in Table 2.1. In (c) to (e), the dashed and dotted lines are theoretical spectra of the $[2Fe\text{-}2S]^{2+}$ and $[4Fe\text{-}4S]^{2+}$ cluster, respectively, scaled to the absorption percentages listed in Table 2.1. The solid lines plotted over the data are summations of the two respective theoretical spectra. All samples contain 50 mM Hepes buffer, pH 7.5. The spectra were recorded at 4.2 K in a magnetic field of 50 mT oriented parallel to the $\gamma$ beam.

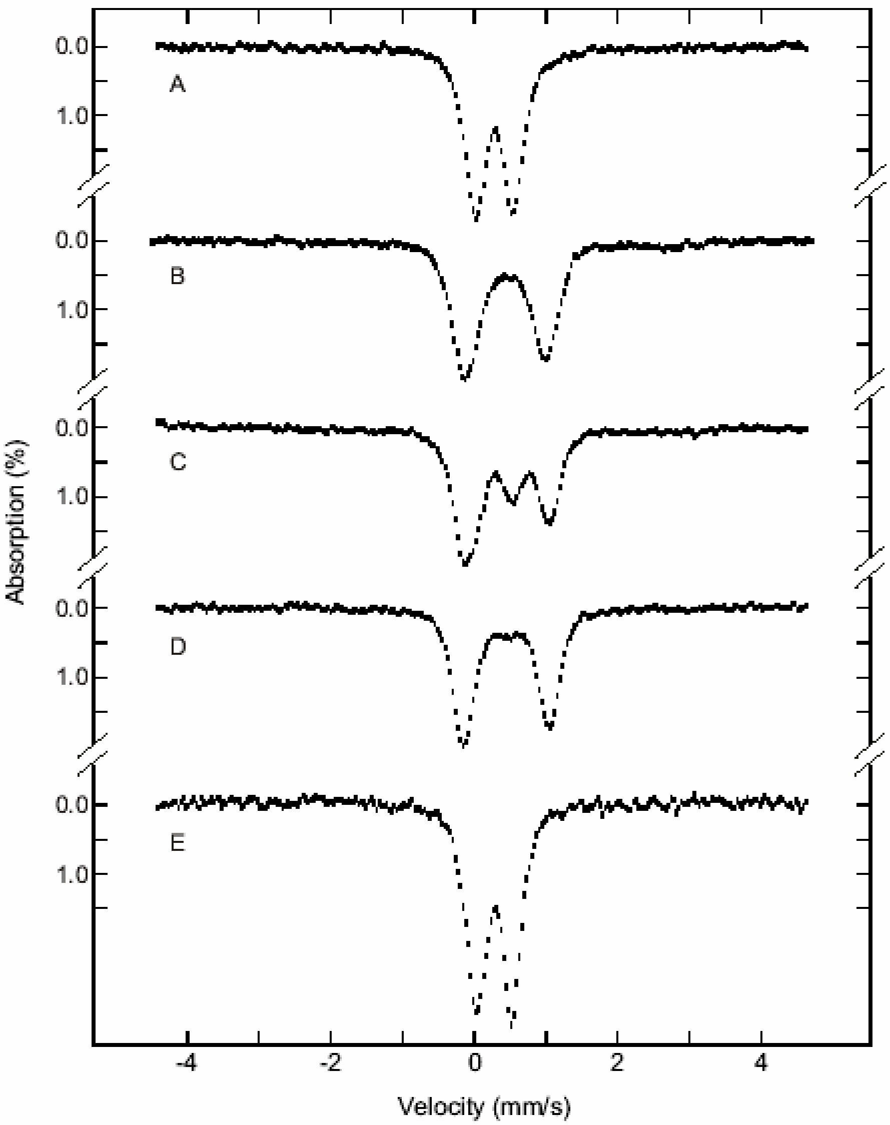
0.0
1.0
A
B
C
D
E
Absorption (%)
-4
-2
0
2
4
Velocity (mm/s)

**Figure 2.3** Resonance Raman spectra of [4Fe-4S] BioB during oxygen-induced cluster degradation and of aerobically reconstituted BioB. (a) As isolated [2Fe-2S] BioB. (b) [4Fe-4S] BioB prepared by anaerobic reconstitution. (c) [4Fe-4S] BioB after exposure to air for 10 min on the Raman probe. (d) [4Fe-4S] BioB after exposure to air for 1 hr. (e) [2Fe-2S] BioB prepared by reconstitution of apo BioB under aerobic conditions in the presence of DTT. The resonance Raman spectra were recorded with 458-nm excitation, using samples that were ~3 mM in BioB frozen at 16 K with 210 mW laser power at the sample. Each scan involved photon counting for 1 s at 0.5 $cm^{-1}$ increments with 8-$cm^{-1}$ spectral resolution, and each spectrum is the sum of ~100 scans. A linear ramp fluorescence background has been subtracted from the resonance Raman spectra.

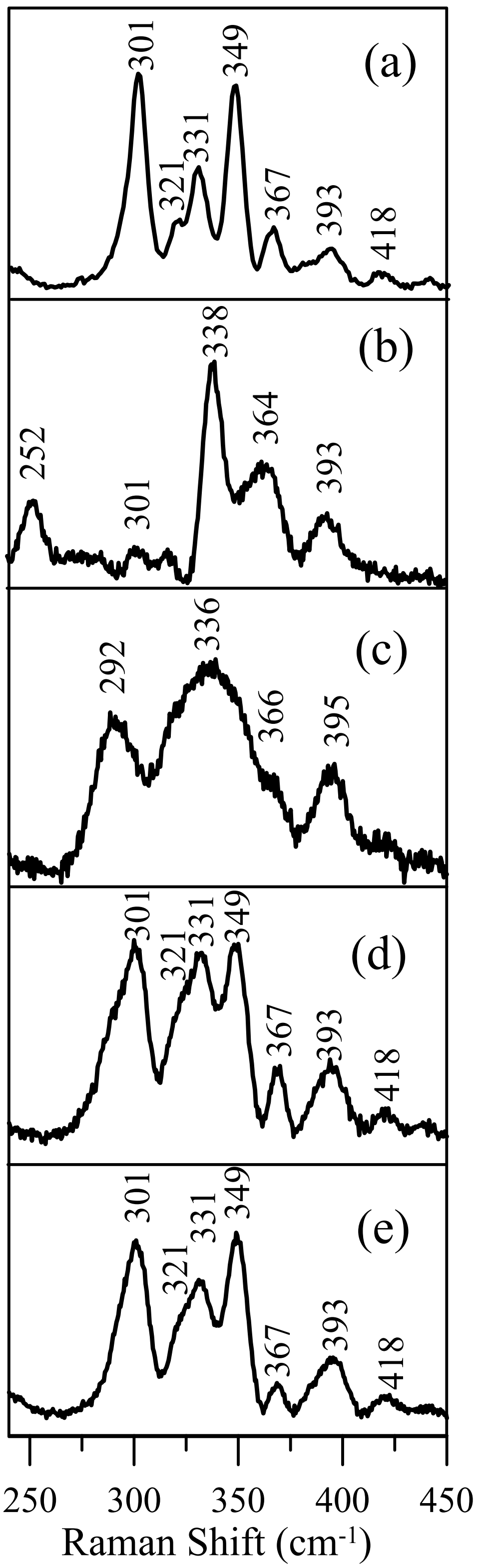
(a)
301
321
331
349
367
393
418
(b)
252
301
338
364
393
(c)
292
336
366
395
(d)
301
321
331
349
367
393
418
(e)
301
321
331
349
367
393
418
250
300
350
400
450
Raman Shift (cm-1)

**Figure 2.4** Resonance Raman spectra of [2Fe-2S]/[4Fe-4S] BioB after exposure to air for 10 mins. (a) [2Fe-2S]/[4Fe-4S] BioB after exposure to air for 10 min on the Raman probe. (b) As isolated [2Fe-2S] BioB. (c) Difference spectrum (a) minus (b). (d) [4Fe-4S] BioB after exposure to air for 10 min on the Raman probe. Measurement and sample conditions are as described in Fig. 2.3.

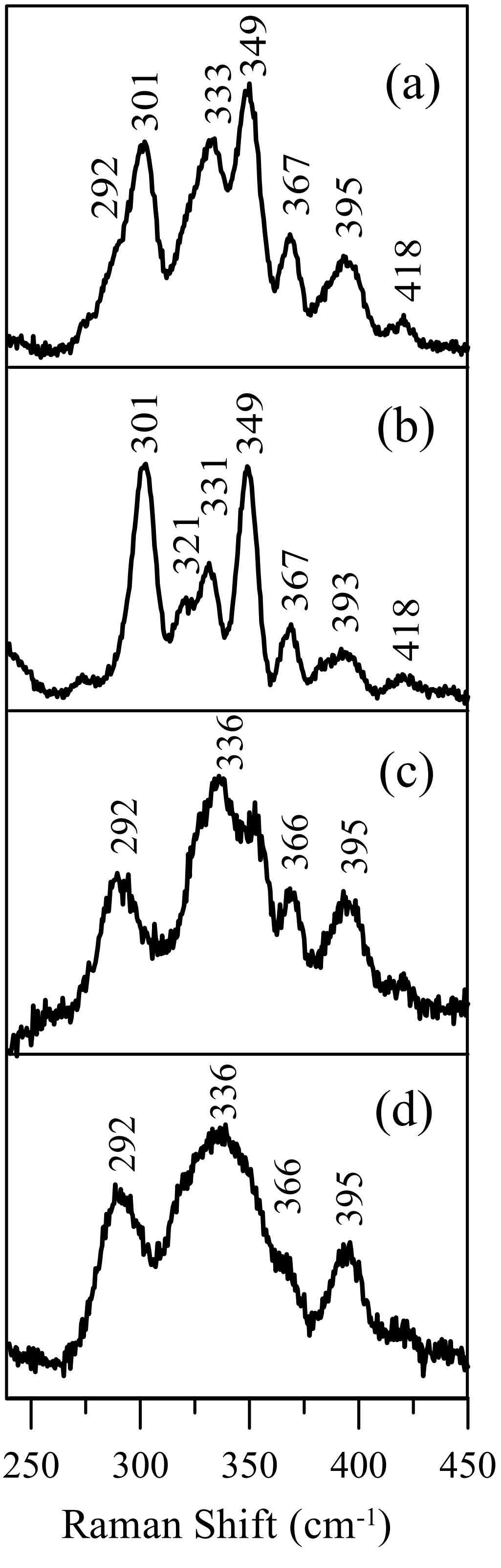
(a)
292
301
333
349
367
395
418
(b)
301
321
331
349
367
393
418
(c)
292
336
366
395
(d)
292
336
366
395
250
300
350
400
450
Raman Shift (cm-1)

**Figure 2.5** Resonance Raman spectra of *E. coli* BioB samples in the presence a 10-fold stoichiometric excess of SAM: (a) [2Fe-2S]/[4Fe-4S] BioB; (b) [2Fe-2S] BioB; (c) [4Fe-4S] BioB. The difference spectrum corresponding to (a) minus (b) is shown in (d). Samples were prepared in 50 mM Tris-HCl buffer, pH 8.5, with 1 mM DTT and 0.2 M NaCl. The resonance Raman spectra were recorded with 458-nm excitation, using samples that were ~3 mM in BioB frozen at 16 K, with 210 mW laser power at the sample. Each scan involved photon counting for 1 s at 0.5 $cm^{-1}$ increments with 8-$cm^{-1}$ spectral resolution, and each spectrum is the sum of ~100 scans. A linear ramp fluorescence background has been subtracted from the resonance Raman spectra. Bands resulting from residual $[2Fe\text{-}2S]^{2+}$ clusters and a lattice mode of ice are indicted by # and *, respectively.

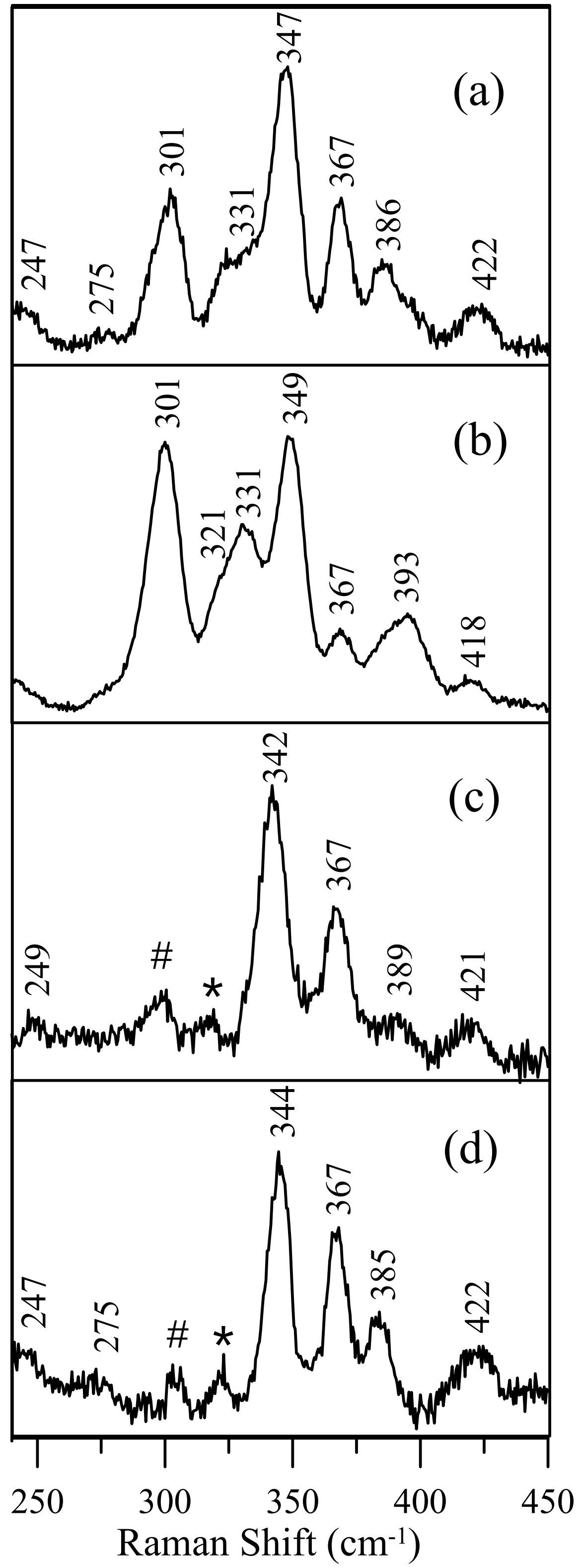
(a)
247
275
301
331
347
367
386
422
(b)
301
321
331
349
367
393
418
(c)
249
#
*
342
367
389
421
(d)
247
275
#
*
344
367
385
422
250
300
350
400
450
Raman Shift (cm-1)

**Figure 2.6** The effect of SAM on the Mössbauer spectrum of [2Fe-2S]/[4$^{57}$Fe-4S] BioB. (a) Without SAM. (b) In the presence of a 10-fold stoichiometric excess of SAM. The spectra were recorded at 4.2 K in a magnetic field of 50 mT oriented parallel to the γ beam. The sample of [2Fe-2S]/[4$^{57}$Fe-4S] BioB was in 50 mM Tris-HCl buffer, pH 8.5, with 1 mM DTT and 0.2 M NaCl and was 275 μM in BioB. The difference spectrum corresponding to (a) minus (b) is shown in (c). The previously published difference spectrum corresponding to [4$^{57}$Fe-4S] BioB minus [4$^{57}$Fe-4S] BioB plus 10 × SAM is shown in (d) (*24*).

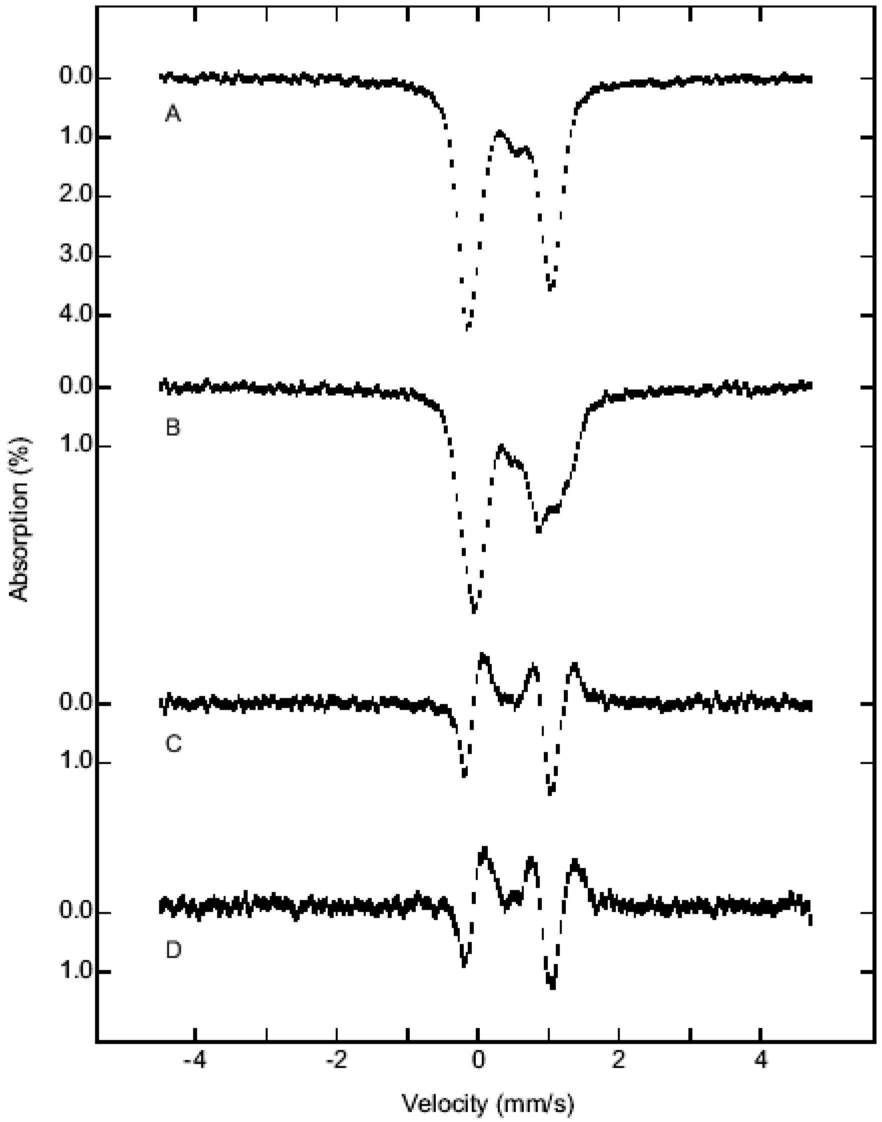
0.0
1.0
2.0
3.0
4.0
A
0.0
1.0
B
0.0
1.0
C
0.0
1.0
D
Absorption (%)
-4
-2
0
2
4
Velocity (mm/s)

**Figure 2.7** Mössbauer spectra (hatched marks) of anaerobically grown $^{57}$Fe-enriched whole cells of *E. coli* with and without overexpression of BioB: (a) *E. coli* BL21-gold[DE3] pT7-7 control whole cells, which contain the same plasmid used for expression of BioB but without the *bioB* insert; (b) *E. coli* BL21-gold[DE3] pT7-7ecbioB-1 whole cells with over-expression of BioB. The spectra were recorded at 4.2 K in a magnetic field of 50 mT, oriented parallel to the $\gamma$ beam. The dotted and dashed lines in (a) are theoretical simulations of the ferrous (55%) and ferric (45%) components, respectively. Each component is simulated using two equal-intensity quadrupole doublets with the following parameters: $\delta(1) = 1.34$ mm/s, $\Delta E_Q(1) = 3.25$ mm/s, $\Gamma(1) = 0.48$ mm/s, $\delta(2) = 1.26$ mm/s, $\Delta E_Q(2) = 2.74$ mm/s, and $\Gamma(2) = 0.65$ mm/s for the ferrous component, and $\delta(1) = 0.45$ mm/s, $\Delta E_Q(1) = 0.57$ mm/s, $\Gamma(1) = 0.76$ mm/s, $\delta(2) = 0.45$ mm/s, $\Delta E_Q(2) = 1.15$ mm/s, $\Gamma(2) = 0.43$ mm/s for the ferric component. The solid line in (a) is the addition of these two components. Removal of the contributions of the ferrous (17%) and ferric (24%) component from spectrum (b) yields the spectrum shown in (c). The spectrum shown in (d) is the cell-free extract corresponding to the whole cell sample shown in spectrum (b) with the contributions of the ferrous (10%) and ferric (22%) components removed.

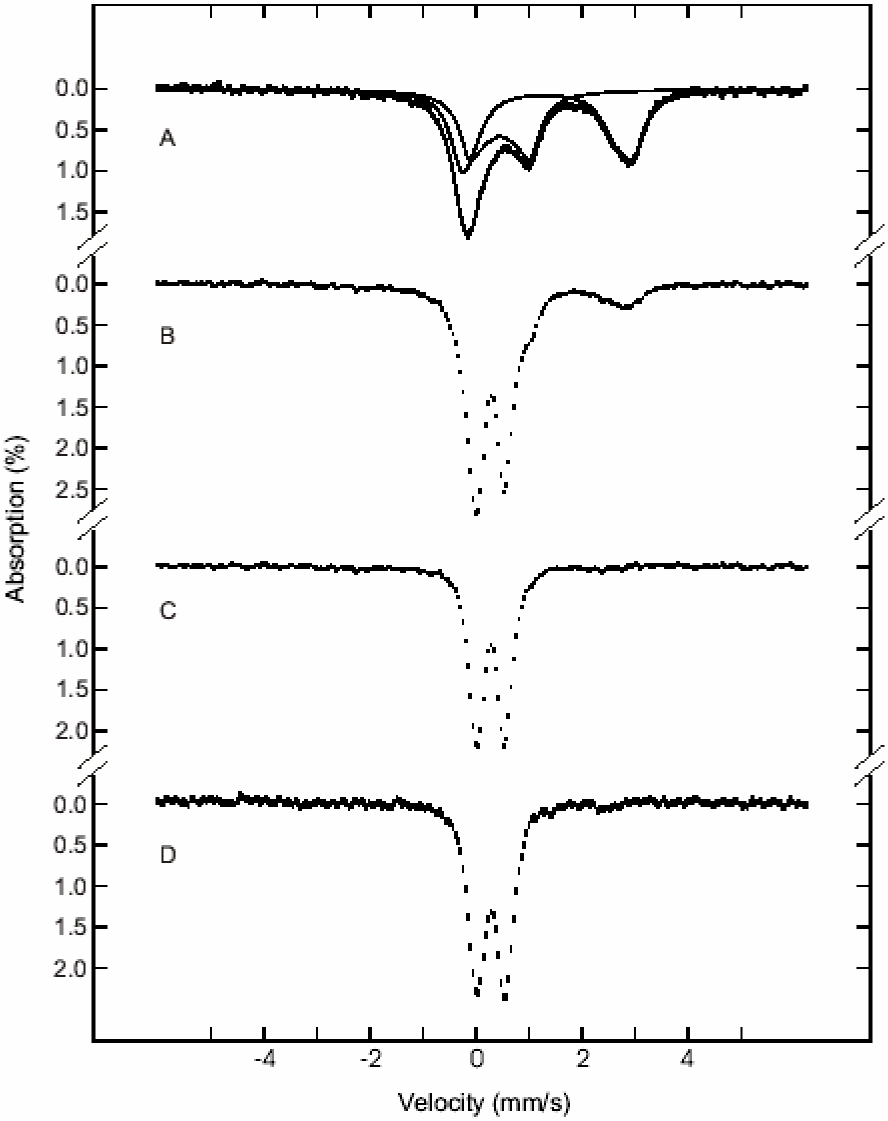
0.0
0.5
1.0
1.5
A
0.0
0.5
1.0
1.5
2.0
2.5
B
0.0
0.5
1.0
1.5
2.0
C
0.0
0.5
1.0
1.5
2.0
D
Absorption (%)
-4
-2
0
2
4
Velocity (mm/s)

**Figure 2.8** UV-visible absorption spectra of *E. coli* [4Fe-4S] BioB (left panel), *E. coli* [2Fe-2S] BioB (middle panel), and *E. coli* IscS-his$_6$ (right panel): (a) before the addition of PLP; (b) in the presence of a 5-10-fold molar excess of PLP; (c) after removal of excess PLP using a desalting column. The spectra were recorded in 1-mm cuvettes using 170 µM [2Fe-2S] BioB and 240 µM [4Fe-4S] BioB , both in 50 mM Hepes buffer, pH 7.5, with 5 mM DTT, and 350 µM IscS-his$_6$ in 50 mM potassium phosphate buffer, pH 7.5, with 5 mM $MgCl_2$, 100 mM KCl, and 0.1 mM EDTA.

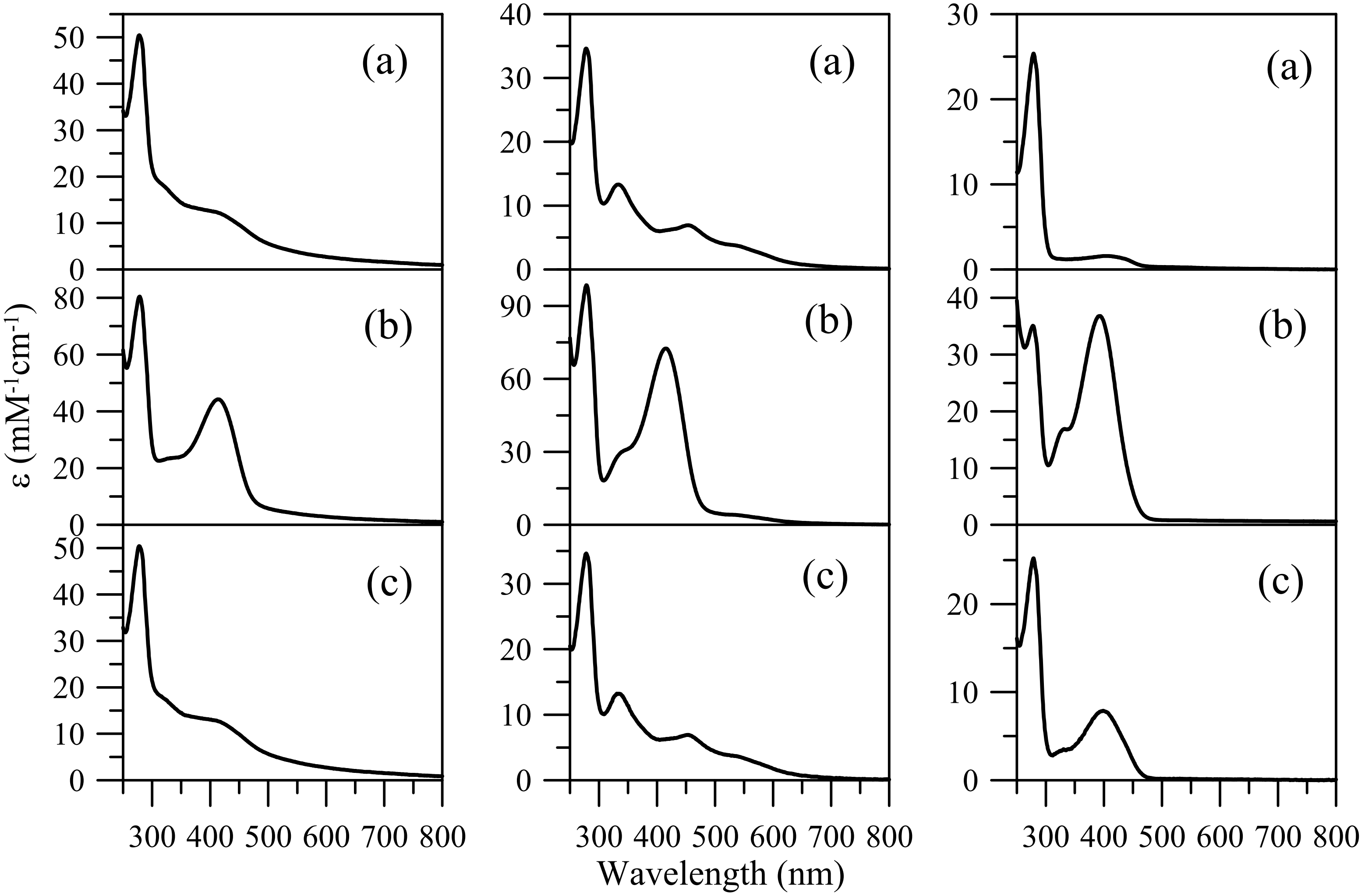
ε (mM⁻¹cm⁻¹)
Wavelength (nm)
(a)
(b)
(c)
(a)
(b)
(c)
(a)
(b)
(c)
0
10
20
30
40
50
60
80
90
300
400
500
600
700
800

**Figure 2.9** Summary of cluster-bound forms, cluster reconstitutions, and $O_2$-induced cluster conversions in *E. coli* BioB. An asymmetric shape is used for BioB to depict distinct cluster binding sites and the additional parenthesis indicate an intermediate $[2Fe\text{-}2S]^{2+}$ cluster that is form during $O_2$-induced degradation of the $[4Fe\text{-}4S]^{2+}$ cluster.

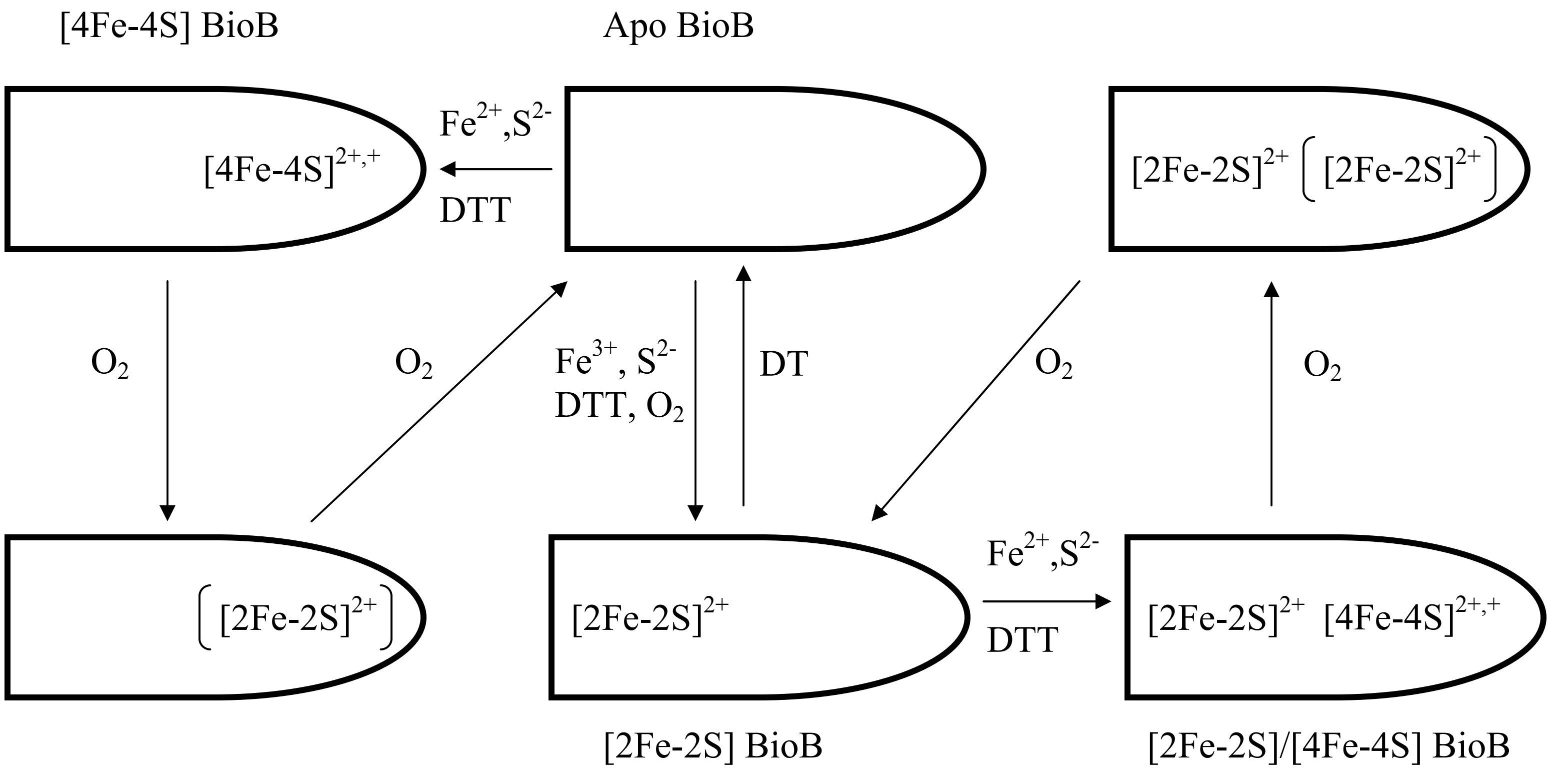
[4Fe-4S] BioB
Apo BioB
[4Fe-4S]$^{2+,+}$
Fe$^{2+}$,S$^{2-}$
DTT
[2Fe-2S]$^{2+}$ ([2Fe-2S]$^{2+}$)
O$_2$
O$_2$
Fe$^{3+}$, S$^{2-}$
DTT, O$_2$
DT
O$_2$
O$_2$
([2Fe-2S]$^{2+}$)
[2Fe-2S]$^{2+}$
Fe$^{2+}$,S$^{2-}$
DTT
[2Fe-2S]$^{2+}$ [4Fe-4S]$^{2+,+}$
[2Fe-2S] BioB
[2Fe-2S]/[4Fe-4S] BioB

# CHAPTER 3

# ROLE OF THE [2FE-2S] CLUSTER IN RECOMBINANT ESCHERICHIA COLI BIOTIN SYNTHASE[1]

---

[1] Jameson, Guy N. L.[†]; Cosper, Michele Mader[§]; Hernández, Heather L.[§]; Johnson, Michael K.[§]; Huynh, Boi Hanh[†]. *Biochemistry*. **2004**, *43*, 2022-2031. Copyright 2004 American Chemical Society.
Reprinted here with permission of publisher.

**Abbreviations**: BioB, gene product of *bioB* commonly referred to as biotin synthase; DTB, dethiobiotin; PLP, pyridoxal 5'-phosphate; SAM, *S*-adenosyl-L-methionine; DTT, dithiothreitol

## Abstract

Biotin synthase (BioB) converts dethiobiotin into biotin by inserting a sulfur atom between C6 and C9 of dethiobiotin in an *S*-adenosylmethionine (SAM)-dependent reaction. The as-purified recombinant BioB from *Escherichia coli* is a homodimeric molecule containing one $[2Fe\text{-}2S]^{2+}$ cluster per monomer. It is inactive in vitro without the addition of exogenous Fe. Anaerobic reconstitution of the as-purified [2Fe-2S]-containing BioB with $Fe^{2+}$ and $S^{2-}$ produces a form of BioB that contains approximately one $[2Fe\text{-}2S]^{2+}$ and one $[4Fe\text{-}4S]^{2+}$ cluster per monomer ([2Fe-2S]/[4Fe-4S] BioB). In the absence of added Fe, the [2Fe-2S]/[4Fe-4S] BioB is active and can produce up to approximately 0.7 equivalents of biotin per monomer. To better define the roles of the Fe-S clusters in the BioB reaction, Mössbauer and EPR spectroscopy have been used to monitor the states of the Fe-S clusters during the conversion of dethiobiotin to biotin. The results show that the $[4Fe\text{-}4S]^{2+}$ cluster is stable during the reaction and present in the SAM-bound form, supporting the current consensus that the functional role of the [4Fe-4S] cluster is to bind SAM and facilitate the reductive cleavage of SAM to generate the catalytically essential 5′-deoxyadenosyl radical. The results also demonstrate that approximately 2/3 of the [2Fe-2S] clusters are degraded by the end of the turnover experiment (24 hr at 25 ºC). A transient species with spectroscopic properties consistent with a $[2Fe\text{-}2S]^{+}$ cluster is observed during turnover, suggesting that the degradation of the $[2Fe\text{-}2S]^{2+}$ cluster is initiated by reduction of the cluster. This observed degradation of the [2Fe-2S] cluster during biotin formation is consistent with the proposed sacrificial S-donating function of the [2Fe-2S] cluster put forth by Jarrett and coworkers (Ugulava et al. (2001) *Biochemistry*, *40*, 8352-8358). Interestingly, degradation of the $[2Fe\text{-}2S]^{2+}$ cluster was found not to parallel biotin formation. The initial decay rate of the $[2Fe\text{-}2S]^{2+}$ cluster is about one order of magnitude faster than the initial formation rate of biotin,

indicating that if the [2Fe-2S] cluster is the immediate S donor for biotin synthesis, insertion of S into dethiobiotin would not be the rate-limiting step. Alternatively, the [2Fe-2S] cluster may not be the immediate S donor. Instead, degradation of the [2Fe-2S] cluster may generate a protein bound polysulfide or persulfide that serves as the immediate S donor for biotin production.

## Introduction

The ultimate step in the biosynthetic pathway of biotin involves the insertion of sulfur into dethiobiotin (DTB)[1] at the C6 and C9 positions with the loss of two hydrogen atoms. This reaction is catalyzed by the *bioB* gene product, termed biotin synthase or BioB, in a *S*-adenosyl-L-methionine (SAM)-dependent reaction (Scheme 3.1). The as-purified recombinant BioB from *Escherichia coli* is a homodimeric molecule of 78 kDa containing one $[2Fe\text{-}2S]^{2+}$ cluster per monomer (*1-4*). The presence of $[2Fe\text{-}2S]^{2+}$ clusters has also been reported in the as-purified recombinant BioBs from *Bacillus sphaericus* and *Arabidopsis thaliana* (*5*, *6*). However, the physiological relevance and functional roles of the [2Fe-2S] cluster have been the subjects of controversy ever since its identification, because spectroscopic and biochemical evidence accumulated so far (see preceding paper (*4*) and below) strongly implicate that BioB belongs to the “radical SAM” family of Fe-S enzymes (*7*), which utilize a [4Fe-4S] cluster (not a [2Fe-2S] cluster) to mediate reductive cleavage of SAM to generate a 5’-deoxyadenosyl radical as the catalytically essential oxidant.

Direct evidence for the involvement of adenosyl radicals in the activation and breaking of the two C-H bonds at the 6 and 9 positions of DTB has come from mass spectrometry studies of the BioB reaction which showed transfer of deuterium from the deuterated substrate DTB, labeled at the C6 and/or C9 positions, to the product deoxyadenosine (*8*). The obligatory SAM dependence of the biotin synthase reaction and the initial discovery that the $[2Fe\text{-}2S]^{2+}$ cluster in the as-purified enzyme can be converted quantitatively to $[4Fe\text{-}4S]^{2+}$ clusters using dithionite in the presence of 60% ethylene glycol or glycerol (*2*) led to the suggestion of a [4Fe-4S]-containing functional form of BioB. However, questions concerning the composition and type of Fe-S cluster in wild-type functional BioB were complicated by subsequent reports which showed that various forms of BioB, containing either exclusively [2Fe-2S] or [4Fe-4S] or a 1:1 mixture of [2Fe-2S] and [4Fe-4S] clusters, can be obtained under different reconstitution and experimental conditions (*3, 9-11*). These observations have led to the proposal that BioB contains two distinct Fe-S cluster-binding sites, with each site capable of binding either a [2Fe-2S] or a [4Fe-4S] cluster (*11*). Subsequently, it was shown by Mössbauer spectroscopy that the two clusters can be selectively labeled with $^{57}Fe$, indicating the presence of distinct [2Fe-2S] and [4Fe-4S] binding sites in BioB (*12*). Taking into account the electrochemical properties obtained for these various forms of BioB and the expected redox potential in cells, Jarrett and coworkers (*11*) have proposed that the BioB form containing a 1:1 mixture of [2Fe-2S] and [4Fe-4S] clusters is the functional form of BioB in vivo. This form of BioB was also found to have maximal activity in vitro producing approximately 0.9 equivalents of biotin per monomer in the absence of added Fe (*13*).

Single turnover experiments involving [2Fe-2S]/[4Fe-4S] BioB, which indicated the loss of the [2Fe-2S] cluster based on Fe and S analyses and UV/visible absorption changes, led Jarrett and coworkers to propose a mechanism in which the [4Fe-4S] cluster mediates the reductive cleavage of SAM and a bridging S of the [2Fe-2S] cluster serves as the immediate S donor for biotin (*13*). The [2Fe-2S] cluster is therefore destroyed by the end of the reaction. Degradation of the $[2Fe\text{-}2S]^{2+}$ cluster during turnover was demonstrated recently by a Mössbauer investigation of partially purified BioB (*14*). In contrast, BioB preparations containing mostly the [4Fe-4S] form of BioB were reported to have the capability of binding pyridoxal 5’-phosphate (PLP) and catalyzing desulfuration of cysteine by a mechanism similar to that used by the NifS and IscS enzymes (*15*). An alternative mechanism was therefore proposed, in which BioB possesses an intrinsic PLP-dependent cysteine desulfurase activity and the immediate S donor is a protein-bound persulfide generated via the intrinsic desulfurase reaction. Desulfurase-activity investigations of site-specific variants further suggest that the conserved cysteine residues Cys97 and Cys128 are the likely candidates for the persulfide binding site (*15*).

In the preceding paper, we have used a combination of UV/visible absorption, resonance Raman and Mössbauer spectroscopies, coupled with analytical and activity measurements to characterize the various Fe-S cluster-containing forms of recombinant *E. coli* BioB, and to establish the transformations that can occur among these various forms of BioB (*4*). The results support the existence of distinct [4Fe-4S] and [2Fe-2S] binding sites in each BioB monomer. BioB contains six conserved cysteine residues, three of which are arranged in the CXXXCXXC (Cys53, Cys57 and Cys60) motif that is shared by all members of the radical SAM family to coordinate the catalytically active [4Fe-4S] cluster. Spectroscopic and reactivity studies of site-specific Cys to Ala variants of BioB support coordination of these three cysteines to the [4Fe-4S] cluster (*16, 17*). The remaining three conserved cysteine residues (Cys97, Cys128 and Cys188) were thus likely to be the ligands for the [2Fe-2S] cluster. Our results also showed that the BioB form containing a 1:1 ratio of [2Fe-2S] to [4Fe-4S] ([2Fe-2S]/[4Fe-4S] BioB) is the most active form in vitro without added Fe, in agreement with the finding of Ugulava et al. (*11*). Our data, however, provide no evidence to support PLP binding or PLP-dependent cysteine desulfurase activity for BioB.

In this manuscript, Mössbauer and EPR spectroscopy have been used to monitor the Fe-S clusters in [2Fe-2S]/[4Fe-4S] BioB during catalytic turnover. The objectives were to obtain information to enhance our understanding of the BioB mechanism and to evaluate the proposed sacrificial S-donating function of the [2Fe-2S] cluster. The results show that during turnover the [4Fe-4S] cluster is stable and present in the SAM-bound $[4Fe\text{-}4S]^{2+}$ state, while the majority of the [2Fe-2S] cluster is destroyed, in general agreement with the conclusion made by Jarrett and coworkers (*13*) and with the Mössbauer results obtained for the partially purified BioB (*14*). However, in contrast to the UV/visible absorption studies, our data demonstrate that not all of the $[2Fe\text{-}2S]^{2+}$ clusters are destroyed and that degradation of the $[2Fe\text{-}2S]^{2+}$ cluster proceeds via a $[2Fe\text{-}2S]^{+}$ intermediate and does not parallel the production of biotin during turnover. Implications of these observations on the possible functional roles of the [2Fe-2S] cluster and on the BioB mechanism are presented.

## Materials and Methods

*Materials.* Chemicals were purchased from Sigma-Aldrich or Fisher, unless otherwise stated. $^{57}$Fe-enriched metal nuggets (95.4% enrichment) were purchased from WEB Research. $^{57}$Fe-enriched ferric ammonium citrate and $Fe^{II}SO_4$ was prepared by a literature method (*18*). The plasmid pEE1010 containing the gene encoding *E. coli* flavodoxin reductase was a kind gift from Peter Reichard at the Karolinska Institute, and the *E. coli* strain DH01 overexpressing *E. coli* flavodoxin was a kind gift from Rowena Matthews at the University of Michigan. Anaerobic experiments were performed under an argon atmosphere in a Vacuum Atmospheres glove box at oxygen levels < 5 ppm. *E. coli* BL21-gold[DE3] pT7-7ecbioB-1 was anaerobically cultivated, and *E. coli* wild-type (WT) [2Fe-2S] BioB was aerobically purified as previously described (*4*).

*E. coli* WT [2Fe-2S]/[4Fe-4S] BioB was prepared by reconstitution of the as-purified [2Fe-2S] BioB by a previously published method (*4*, *13*). For Mössbauer studies, $^{57}$Fe-enriched [2Fe-2S] BioB was purified from *E. coli* cells grown in $^{57}$Fe-enriched medium and subsequently reconstituted with either natural Fe (2.2% $^{57}$Fe) or $^{57}$Fe (95.4% enrichment) to produce [2Fe-2S]/[4Fe-4S] BioB with either only the [2Fe-2S] cluster or both clusters labeled with $^{57}$Fe.

*Assay of biotin synthase activity.* The BioB assay was performed under strictly anaerobic conditions according to a procedure specified by Gibson and colleagues (*19*, *20*), with the following modifications. In 100 mM Tris-HCl (pH 8.0) buffer with 10 mM KCl, 200 µM *E. coli* WT [2Fe-2S]/[4Fe-4S] BioB was combined with 10 mM DTT, 2 mM cysteine, 10 mM fructose-1,6-biphosphate, 2 mM NADPH, 80 µM flavodoxin, 40 µM flavodoxin reductase, and 2 mM SAM. The reaction was commenced by the addition of 400 µM DTB, and the BioB reaction was allowed to proceed at 25 ºC. At various time points, from 5 minutes to 24 hours, samples were removed, placed in a Mössbauer cup or EPR tube, and immediately frozen in liquid $N_2$. EPR spectra of Mössbauer samples were recorded after the collection of the Mössbauer data was completed. In addition, a 50 µL aliquot was removed and added to 5 µL of saturated sodium acetate (pH 4.0), which resulted in the precipitation of protein. The protein was removed by centrifugation at 13,000×*g* for 10 minutes, and the supernatant was analyzed for biotin using the *Lactobacillus plantarum* ATCC 8014 microbiological assay (*21*, *22*). The BioB assay was also performed using the conditions specified by Jarrett and coworkers (*13*).

*Determination of protein and Fe concentrations.* Protein concentrations were determined by the *DC* protein assay (Bio-Rad), using BSA as a standard. All protein concentrations for wild-type BioB were multiplied by the correction factor of 1.1 (*4*). Iron concentrations were determined using bathophenanthroline under reductive conditions after digestion of the protein in

0.8% $KMnO_4$/0.2 M HCl (*13*) as described by Fish (*23*). All sample concentrations are expressed per BioB monomer.

*Spectroscopic studies*. UV-visible absorption spectra were recorded under anaerobic conditions in screw top 1 mm cuvettes using a Shimadzu UV-3101PC spectrophotometer. X-band (~ 9.5 GHz) EPR spectra were recorded on a Bruker ESP-300E EPR spectrometer equipped with an ER-4116 dual-mode cavity and an Oxford Instrument ESR-9 flow cryostat. Resonances were quantified under non-saturating conditions using a 1 mM CuEDTA standard. EPR spectra were simulated using the Bruker Simphonia and WinEPR software packages. Mössbauer spectra were recorded in a weak-field and a strong-field spectrometer described elsewhere (*24*). The zero velocity of the spectra refers to the centroid of the room temperature spectrum of a metallic iron foil. Analysis of the Mössbauer data was performed with the program WMOSS (Web Research).

## Results

*Mössbauer results.* [2Fe-2S]/[4Fe-4S] BioB with the [2Fe-2S] cluster selectively labeled with $^{57}$Fe ([2$^{57}$Fe-2S]/[4Fe-4S] BioB) was prepared for single turnover experiments (see Materials and Methods). At reaction time points of 5 min, 45 min, and 24 hr, samples were removed and frozen for Mössbauer investigations. Since Mössbauer spectroscopy can detect only $^{57}$Fe, these measurements allowed us to selectively monitor changes to the [2Fe-2S] clusters during enzymatic turnover. To monitor changes occurring at both [2Fe-2S] and [4Fe-4S] clusters during turnover, proteins of [2Fe-2S]/[4Fe-4S] BioB with both clusters labeled with $^{57}$Fe were also prepared and samples were taken at reaction time points of 5 min, 45 min, 90 min, 3 hr, 5 hr, and 24 hr for Mössbauer investigations. In an effort to correlate the Mössbauer observations, which provide information on the time evolution of the Fe-S clusters, with the production of biotin, samples were also removed at the same time points for biotin assay. The results are presented below.

*[$2^{57}$Fe-2S]/[4Fe-4S] BioB.* Figure 3.1A shows the Mössbauer spectrum (hatched marks) of the as-prepared [$2^{57}$Fe-2S]/[4Fe-4S] BioB recorded at 4.2 K in a magnetic field of 50 mT oriented parallel to the γ-beam. As expected, the spectrum is very similar to that of the [$2^{57}$Fe-2S]/[4Fe-4S] BioB reported in the preceding paper (*4*). It consists of a major quadrupole doublet representing the [2Fe-2S]$^{2+}$ cluster accounting for approximately 90% of the total Fe absorption and a minor doublet (~10%) that may be assigned to a [4Fe-4S]$^{2+}$ cluster. The solid line overlaid with the experimental spectrum is a superposition of the two corresponding doublets reported in the preceding paper (*4*) with the percent absorptions mentioned above. In all of our [2Fe-2S]/[4Fe-4S] BioB preparations, we have consistently obtained an Fe stoichiometry of 4.3 to 4.4 Fe per BioB monomer, suggesting a constant cluster composition in our preparations. For the BioB preparation of this turnover experiment, protein and Fe determination also yield 4.4 Fe/BioB monomer. On the basis of this observation and the approximate 0.75:0.66 [2Fe-2S]:[4Fe-4S] cluster content obtained for our [2Fe-2S]/[4Fe-4S] BioB preparations (*4*), it is assumed that this preparation of BioB also contains approximately 0.75 [2Fe-2S] cluster per BioB monomer. In other words, it is assumed that 90% Fe absorption (percent absorption found for the [2Fe-2S] cluster) of these turnover samples corresponds to 0.75 [2Fe-2S] cluster/monomer (or 1.5 Fe/monomer).

*Mössbauer time course for the single turnover of [$2^{57}$Fe-2S]/[4Fe-4S] BioB.* Also shown in Figure 3.1 are the Mössbauer spectra (hatched marks) of samples taken at 5 min (B), 45 min (C), and 24 hr (D) reaction time points during the single turnover reaction of [$2^{57}$Fe-2S]/[4Fe-4S] BioB. These spectra were recorded at 4.2 K in a parallel field of 50 mT. Detailed analysis of the data indicates that these spectra can be decomposed into four spectral components, details of which are presented in the following. The major spectral component observed in the spectrum of the 5-min sample (Figure 3.1B) is the central quadrupole doublet originating from the $[2Fe\text{-}2S]^{2+}$ cluster. Under turnover conditions, the parameters obtained for the $[2Fe\text{-}2S]^{2+}$ cluster ($\Delta E_Q$ = 0.51 ± 0.03 mm/s, $\delta$ = 0.29 ± 0.02 mm/s, halfwidth (left) = 0.29 mm/s, and halfwidth (right) = 0.27 mm/s) are within statistical errors similar to those obtained for the $[2Fe\text{-}2S]^{2+}$ cluster in the as-prepared [2Fe-2S]/[4Fe-4S] BioB (*4*). The dotted line displayed in Figure 3.1B is a quadrupole doublet simulated with the above parameters and scaled to 58% of the Fe absorption. In addition to this central doublet, the spectrum of the 5-min sample exhibits at least two more spectral components, one of which is a broad paramagnetic spectrum with absorption ranging from −3 mm/s to +3 mm/s. In accordance with the EPR measurement (see below), which shows the appearance of paramagnetic species after 5 minutes, this broad spectrum must be associated with the paramagnetic species detected in the EPR measurements. As presented below, the EPR data suggest two possible assignments, $S$ = 1/2 $[2Fe\text{-}2S]^{+}$ or $[4Fe\text{-}4S]^{+}$ clusters, with the relaxation properties strongly favoring the $[2Fe\text{-}2S]^{+}$ cluster assignment. The total hyperfine splitting of this paramagnetic Mössbauer spectral component (~ 6 mm/s) is too large for that of a typical $[4Fe\text{-}4S]^{+}$ cluster (~ 4 mm/s) but is consistent with that of a $[2Fe\text{-}2S]^{+}$ cluster. To illustrate this point, a theoretical spectrum of the reduced parsley ferredoxin (*25*), a [2Fe-2S]-containing ferredoxin, is plotted on top of the experimental data as a dashed line (Figure 3.1B). In order to match the amplitude of the paramagnetic spectral component, the theoretical spectrum is scaled to 20 % of the total Fe absorption, indicating that it represents approximately 0.2 $[2Fe\text{-}2S]^{+}$ cluster per monomer of BioB. This value is in good agreement with the spin quantitation of the corresponding EPR signal. Taken together, the EPR and Mössbauer evidence support the appearance of $[2Fe\text{-}2S]^+$ clusters at the beginning of the turnover reaction. Unfortunately, due to the sub-stoichiometric accumulation of this species, the broad features of this paramagnetic component and the limit on protein concentration that can be used for the turnover experiments (less than 200 μM in BioB monomer), it is impractical to obtain spectra with sufficient statistics that would allow us to determine the hyperfine parameters of this paramagnetic component.

The third spectral component is a broad quadrupole doublet, the positions of which are indicated by the two arrows shown in the 5-min spectrum (Figure 3.1B). The intensity of this component increases substantially and becomes more visible in the spectrum of the 45-min sample (Figure 3.1C), which can thus be used for the characterization of this component. In our analysis, we have used two equal-intensity overlapping quadrupole doublets to simulate the line shape of this broad quadrupole doublet, and the parameters obtained are: $\Delta E_Q(1) = 3.36$ mm/s , $\delta(1) = 0.73$ mm/s, $\Delta E_Q(2) = 3.65$ mm/s and $\delta(2) = 0.86$ mm/s. These parameters are typical for high-spin $Fe^{II}$ compounds and the parameters for doublet 1 are characteristic of tetrahedral, sulfur-coordinated $Fe^{II}$ compounds. The broad line shape suggests a distribution in the Fe coordination environment. This component is thus assigned to possible degradation products of the $[2Fe\text{-}2S]^{2+}$ cluster and is labeled as $Fe^{II}S_4/N/O$. For illustration, a theoretical simulation of this component is plotted as a dashed line in Figure 3.2C and is scaled to 25% of the total Fe absorption. Similar $Fe^{II}S_4/N/O$ species have also been observed as minor components in reconstituted BioB, and have been assigned as impurities (*10*, *12*).

The fourth spectral component detected in this turnover study is another quadrupole doublet that can be assigned to a SAM-bound $[4Fe\text{-}4S]^{2+}$ cluster. The presence of this component is most obvious in the spectrum of the 24-hr sample (Figure 3.1D). To illustrate the presence of such a component, a theoretical spectrum of the SAM-bound [4Fe-4S] cluster in BioB (*26*) is plotted in Figure 3.1D as a dotted line and scaled to 38% of the total Fe absorption. Using these four spectral components, namely, the $[2Fe\text{-}2S]^{2+}$, $[2Fe\text{-}2S]^{+}$, $Fe^{II}S_4$/N/O and SAM-bound $[4Fe\text{-}4S]^{2+}$ components, it is possible to reproduce the three reaction-time dependent spectra shown in Figure 3.1B-D. The solid lines overlaid with the experimental data are superpositions of these four spectral components with the absorption percentages listed in Table 3.1. With the above mentioned assumption that 90% of the Fe absorption corresponds to 1.5 Fe/BioB monomer, it is possible to convert the observed time-dependent percentages of these four components into equivalents/monomer (listed in Table 3.1), and thus provide information about the time evolution of these four Fe species. The results indicate that under the turnover conditions, within the first 5 minutes, the $[2Fe\text{-}2S]^{2+}$ cluster is partially reduced to the $[2Fe\text{-}2S]^{+}$ state and partially degraded to the mononuclear $Fe^{II}S_4$/N/O species. Degradation of the $[2Fe\text{-}2S]^{2+}$ cluster most likely occurs via the reduced $[2Fe\text{-}2S]^{+}$ state, since the reduced cluster appears to be a transient state based on both Mössbauer and EPR studies (see below). At 45 minutes, a substantial number of the $[2Fe\text{-}2S]^{2+}$ clusters have disintegrated and more $Fe^{II}S_4$/N/O species are observed. However, the increased amount of $Fe^{II}S_4$/N/O can not account for all the Fe released from the degraded $[2Fe\text{-}2S]^{2+}$ clusters, and interestingly, additional $[4Fe\text{-}4S]^{2+}$ clusters (SAM-bound) are formed. The degradation of the $[2Fe\text{-}2S]^{2+}$ cluster and formation of the $[4Fe\text{-}4S]^{2+}$ cluster were observed to continue with reaction time, and by 24 hr, approximately 50% of the Fe released through the degradation of the [2Fe-2S] cluster is reassembled as [4Fe-4S] clusters. Conversion of [2Fe-2S] clusters to [4Fe-4S] clusters in BioB under anaerobic conditions has been observed previously (*2, 9*), but has not been reported under turnover conditions. Our inability to assemble a $[4Fe\text{-}4S]^{2+}$ cluster at the [2Fe-2S] binding site (*4*), coupled with the fact that the assembled [4Fe-4S] cluster appears in the SAM-bound form, indicates that the [4Fe-4S] cluster is assembled at the

[4Fe-4S] binding site. With the limited number of available time points, it is not possible to formulate a mechanistic model to describe this cluster disintegration and reassembly process observed here. A possible scenario would be for the Fe to be released into solution through degradation of the [2Fe-2S] cluster and then reassembled at unoccupied [4Fe-4S] binding sites. The appearance of the $Fe^{II}S_4$/N/O species prior to the assembly of the [4Fe-4S] cluster supports such a scenario.

*Mössbauer time course for the single turnover of $^{57}$Fe-enriched [2Fe-2S]/[4Fe-4S] BioB.* Figure 3.2 shows the Mössbauer spectra (hatched marks) of the as-prepared $^{57}$Fe-enriched [2Fe-2S]/[4Fe-4S] BioB (A) and of samples taken at various time points (B-E) during a single turnover reaction of the $^{57}$Fe-enriched enzyme. The data were recorded at 4.2 K in a parallel field of 50 mT. Similar to the spectrum of the [2Fe-2S]/[4Fe-4S] BioB reported in the preceding paper (*4*), the as-prepared [2Fe-2S]/[4Fe-4S] BioB for the turnover experiment also exhibits two quadrupole doublets representing the $[2Fe\text{-}2S]^{2+}$ and the $[4Fe\text{-}4S]^{2+}$ clusters. The parameters of these two doublets are identical to those reported previously (*4*), but the absorption ratio of these two doublets of the turnover preparation, 18:82 [2Fe-2S]:[4Fe-4S], is different from that of the preceding paper (36:64 [2Fe-2S]:[4Fe-4S]) (*4*). This observation could be rationalized by a lower than normal population of [2Fe-2S] cluster in the turnover preparation. However, this preparation of BioB has a metal content (4.4 Fe/BioB monomer), UV-visible absorption properties, EPR properties (see below), and biotin synthase activity (see below) that are comparable to those of our other [2Fe-2S]/[4Fe-4S] BioB preparations. It is therefore likely that this preparation of BioB contains a cluster composition that is similar to the other preparations (i.e. ~0.72 to 0.75 [2Fe-2S] and ~0.66 to 0.72 [4Fe-4S] clusters per monomer). Since the $^{57}$Fe-enriched [2Fe-2S]/[4Fe-4S] BioB was prepared by reconstituting a [4Fe-4S] cluster onto the [2Fe-2S] BioB isolated from cells grown in $^{57}$Fe-enriched medium, the lower than expected Mössbauer absorption for the [2Fe-2S]$^{2+}$ cluster may reflect an inefficient $^{57}$Fe enrichment of the [2Fe-2S] cluster during cell growth. Unfortunately, it is not possible to distinguish between these two possibilities and this ambiguity does introduce an uncertainty into our interpretation of the time-dependent Mössbauer data presented next. On the basis of the above mentioned chemical, spectroscopic and biochemical evidence, we have assumed the latter possibility for the interpretation of the Mössbauer time course data. Despite the above noted ambiguity, the data do provide definitive information on the state of the [4Fe-4S] cluster during turnover, which cannot be obtained with the [2$^{57}$Fe-2S]/[4Fe-4S] BioB, and the assumed [2Fe-2S] content does yield time-dependent information about the [2Fe-2S] cluster that is in good agreement with results obtained from the [2$^{57}$Fe-2S]/[4Fe-4S] BioB turnover study.

At first glance, the time-dependent Mössbauer spectra (hatched marks) taken during the single turnover of the $^{57}$Fe-enriched [2Fe-2S]/[4Fe-4S] BioB (Figure 3.2, B-E) appear to show little time variation. Since the major Fe absorption in these samples arises from the [4Fe-4S] cluster (~ 80%), the lack of major changes in these spectra indicates that the state of the [4Fe-4S] cluster remains constant throughout these time points. Furthermore, a comparison of the turnover spectra with a previously reported theoretical spectrum of a SAM-bound [4Fe-4S]$^{2+}$ cluster in BioB (*26*) indicates that under turnover conditions, the majority of the [4Fe-4S] clusters is present in the SAM-bound [4Fe-4S]$^{2+}$ form; the SAM-bound [4Fe-4S]$^{2+}$ spectrum is plotted as solid lines in Figure 3.2, B-E, and scaled to 76% of the total Fe absorption of each experimental spectrum. Consequently, the time variation observed for these spectra are mainly due to changes occurring at the [2Fe-2S]$^{2+}$ cluster. The main features that can be seen to change with time are (1) a decrease in intensity of the high energy line of the [2Fe-2S]$^{2+}$ doublet (marked by a central arrow) and (2) an increase in intensity of the $Fe^{II}S_4$/N/O doublet (marked by two arrows at the sides). These changes are consistent with those observed for the turnover of the [$2^{57}$Fe-2S]/[4Fe-4S] BioB and indicate degradation of the [2Fe-2S] cluster during turnover. To demonstrate that quantitative information about the time evolution of the [2Fe-2S] cluster can be obtained from these spectra, despite the fact that the major contribution to these spectra is from the SAM-bound $[4Fe\text{-}4S]^{2+}$ cluster, we have removed the [4Fe-4S] contribution from the 5-min turnover spectrum and plotted the resulting spectrum in Figure 3.3 (hatched marks) and compared it with the 5-min turnover spectrum of the [$2^{57}$Fe-2S]/[4Fe-4S] BioB (solid line). It can be seen that the central quadrupole doublets representing the [2Fe-2S] cluster in these two spectra are very similar and the high-energy line is practically identical. Consequently, it is possible to use the $[2Fe\text{-}2S]^{2+}$ doublet (described in the preceding section) to estimate the percent absorption of the $[2Fe\text{-}2S]^{2+}$ cluster in the $^{57}$Fe-enriched $[2Fe\text{-}2S]^{2+}/[4Fe\text{-}4S]^{2+}$ BioB samples during turnover. The results obtained are 13, 10, 9, 9, 7 and 6 percent for the 5-min, 45-min, 90-min, 3-hr, 5-hr and 24-hr sample, respectively. Assuming the starting material contains 0.75 $[2Fe\text{-}2S]^{2+}$ cluster per BioB monomer (see above), these estimated percent absorptions can be converted into equivalents of clusters and the results are plotted in Figure 3.4 (opened circles).

*Degradation of the $[2Fe\text{-}2S]^{2+}$ cluster does not parallel the production of biotin during turnover*. As presented above, the Mössbauer data provide a quantitative measure of the time evolution of the $[2Fe\text{-}2S]^{2+}$ cluster in BioB during turnover. Figure 3.4 displays the data obtained from both turnover experiments with the [$2^{57}$Fe-2S]/[4Fe-4S] BioB (filled circles) and the $^{57}$Fe-enriched $[2Fe\text{-}2S]^{2+}/[4Fe\text{-}4S]^{2+}$ BioB (opened circles). Within experimental uncertainty, both sets of data are in very good agreement and show a rapid disappearance of the $[2Fe\text{-}2S]^{2+}$ clusters within the first 45 minutes followed by a much slower decay of the cluster. After 24 hr, approximately one third of the clusters (~0.25 $[2Fe\text{-}2S]^{2+}$/monomer) remain intact. This biphasic behavior cannot be described by a simple single exponential decay, and probably reflects a complex degradation process. With the limited time points available, it is neither possible nor desirable to attempt to deduce a mechanistic model for this apparently complex decay of the $[2Fe\text{-}2S]^{2+}$ cluster. However, the data are sufficient, both in number and accuracy, for examining whether the decay of the $[2Fe\text{-}2S]^{2+}$ cluster during turnover can be correlated with the production of biotin. For such a purpose, we have simulated the time evolution of the $[2Fe\text{-}2S]^{2+}$ cluster, $A(t)$, as an addition of two exponential decays (Equation 1).

$$A(t) = A_1\exp(-k_1t) + A_2\exp(-k_2t)\ , \qquad (1)$$

The solid line plotted in Figure 3.4 is a theoretical curve of Equation 1 with $A_1$ = 0.37 clusters/monomer, $A_2$ = 0.38 clusters/monomer, $k_1$ = 0.13 $\text{min}^{-1}$, and $k_2$ = 0.0003 $\text{min}^{-1}$. In this simulation, we have assumed that the sum of $A_1$ and $A_2$ is 0.75 clusters/monomer. It should be emphasized that this approach is only to provide a quantitative simulation of the time course of the decay of the $[2Fe\text{-}2S]^{2+}$ cluster for the purpose of comparison with the production of biotin, to be presented below, and should not be taken literally that the degradation of the $[2Fe\text{-}2S]^{2+}$ cluster involves two independent exponential decays.

To correlate the degradation of the [2Fe-2S] cluster with the formation of biotin, we have performed the biotin assay on samples taken at the same time points during turnover (Materials and Methods). The results are plotted in Figure 3.4 as squares. These data also cannot be simulated with a single exponential function, and thus, Equation 2 was used.

$$B(t) = B_1\,[1 - \exp(-k_1 t)] + B_2\,[1 - \exp(-k_2 t)]\,, \qquad (2)$$

The dashed line displayed in Figure 3.4 is a simulation of Equation 2 with $B_1$ = 0.22 biotin/monomer, $A_2$ = 0.63 biotin/monomer, $k_1$ = 0.012 $\mathrm{min}^{-1}$, and $k_2$ = 0.001 $\mathrm{min}^{-1}$. Comparing these parameters with those obtained for the decay of the $[2Fe\text{-}2S]^{2+}$ cluster indicates clearly that the production of biotin does not parallel the degradation of the $[2Fe\text{-}2S]^{2+}$ cluster. Particularly, the initial decay rate of the [2Fe-2S] cluster is about one order of magnitude faster than the initial formation rate of biotin.

*Effects of DTB on the stability of the [2Fe-2S] cluster*. To examine whether the stability of the [2Fe-2S] cluster is affected by the presence of DTB, we have performed a control experiment, in which $[2^{57}Fe\text{-}2S]^{2+}/[4Fe\text{-}4S]^{2+}$ BioB was incubated anaerobically at 25 °C for 3.5 hr in a solution identical to that of the turnover experiments except that DTB was not present. Figure 3.5 shows the Mössbauer spectrum of such a sample recorded at 4.2 K in a parallel field of 50 mT. The spectrum is very similar to that of the as-prepared $[2^{57}Fe\text{-}2S]/[4Fe\text{-}4S]$ BioB (Figure 3.1A) and can be similarly decomposed into two components: a major quadrupole doublet accounting for ~90% of the Fe absorption arising from the $[2Fe\text{-}2S]^{2+}$ cluster and a minor doublet (~10 %) that resembles the spectrum of a SAM-bound $[4Fe\text{-}4S]^{2+}$ cluster. The percent absorptions determined for the two clusters in the as-prepared and control $[2^{57}Fe\text{-}2S]/[4Fe\text{-}4S]$ BioB samples are practically identical, indicating that the $[2Fe\text{-}2S]^{2+}$ cluster is stable in the absence of DTB. This observation, together with the results obtained from the turnover experiments, establishes that DTB is definitely involved in the degradation of the $[2Fe\text{-}2S]^{2+}$ cluster during turnover.

*EPR signals observed during single turnover of [2Fe-2S]/[4Fe-4S] BioB.* To further characterize the paramagnetic species generated during turnover, parallel EPR experiments were carried out using natural abundance [2Fe-2S]/[4Fe-4S] BioB (4.4 Fe/monomer) prepared with conditions identical to those used in the Mössbauer studies reported above. A transient EPR resonance was observed with maximum intensity in samples frozen after 15 minutes, see Figure 3.6A. This spectrum was simulated as a superposition of three EPR signals in Figure 3.6B: an isotropic radical signal at $g$ = 2.002 (Figure 3.6C) which accounts for 7.5% of the total EPR absorption; an anisotropic $S$ = 1/2 resonance with $g$ = 2.01, 1.96 and 1.88 corresponding to 28.5% of the total EPR absorption (Figure 3.6D); and an anisotropic $S$ = 1/2 resonance with $g$ = 2.00, 1.94 and 1.85 corresponding to 64% of the total EPR absorption. The radical signal is attributed to the reducing system (NADPH/flavodoxin/flavodoxin reductase), since it was observed with similar intensity in all turnover samples (0 min to 24 hr) and in control samples that did not contain BioB. The $g$-values of the two anisotropic resonances are indicative of $S$ = 1/2 Fe-S clusters but unambiguous simulation of the two is difficult because the low field components are obscured by the radical signal. However, the assignment of the low-field components is in part based on the similarity to the EPR resonance reported by Jarrett and coworkers in samples of [2Fe-2S]/[4Fe-4S] BioB frozen under turnover conditions in the presence of $FeCl_3$, $Na_2S$, and DTT (*13*). These workers observed a broad, anisotropic, rhombic resonance, $g$ ~ 2.00, 1.95, and 1.85, without contributions from a radical species, that progressively increased during turnover in the presence of exogenous ferric iron, at a rate comparable with biotin formation. This resonance was erroneously assigned to a $[3Fe\text{-}4S]^+$ cluster based on partial loss of intensity on addition of dithionite and the two low-field $g$-values (*13*). However, a temperature dependent investigation indicates that these Fe-S cluster signals can be observed up to 70 K without significant broadening. Such temperature dependence behavior is typical for $S = 1/2$ $[2Fe\text{-}2S]^+$ clusters and is inconsistent with assignment to either $S = 1/2$ $[3Fe\text{-}4S]^+$ or $[4Fe\text{-}4S]^+$ clusters. Also, as presented above, the $[2Fe\text{-}2S]^+$ assignment is consistent with the overall magnetic hyperfine splitting of the paramagnetic species detected in the Mössbauer spectra.

The transient nature of the $[2Fe\text{-}2S]^+$ EPR signals observed during a single turnover of BioB is illustrated by the EPR spectra of samples taken at 5 min, 15 min, 3 hr and 24 hr shown in Figure 3.7. After subtraction of the radical signal, spin quantitation of the two anisotropic resonances attributed to $[2Fe\text{-}2S]^+$ clusters under non-saturating conditions (50 K and 1 mW), together account for 0.20, 0.31, 0.08, and 0.03 spins/BioB monomer in the 5-min, 15-min, 3-hr and 24-hr samples, respectively. The relative contributions of the two distinct resonances do not change significantly, suggesting they correspond to conformational substates of the same $[2Fe\text{-}2S]^+$ cluster intermediate, rather than sequential $[2Fe\text{-}2S]^+$ cluster intermediates in the $[2Fe\text{-}2S]^{2+}$ cluster degradation pathway. Quantitatively, analogous EPR results at equivalent reaction times were obtained for the turnover samples of the $[2^{57}Fe\text{-}2S]/[4Fe\text{-}4S]$ and $[2^{57}Fe\text{-}2S]/[4^{57}Fe\text{-}4S]$ BioB samples that were used in the Mössbauer turnover experiments discussed above. Hence the EPR and Mössbauer quantitations concur in finding ~ 0.2 $[2Fe\text{-}2S]^+$ clusters per BioB monomer in the 5-min sample of $[2^{57}Fe\text{-}2S]/[4Fe\text{-}4S]$ BioB. Further, the EPR data support the assumption that the lower than expected Mössbauer absorption of the $[2^{57}Fe\text{-}2S]^{2+}$ signal in the $[2^{57}Fe\text{-}2S]/[4^{57}Fe\text{-}4S]$ BioB samples is a consequence of inefficient $^{57}Fe$ enrichment during growth. In summary, the EPR data clearly demonstrate that a $[2Fe\text{-}2S]^+$ cluster is formed as a transient intermediate in the rapid initial stage of $[2Fe\text{-}2S]^{2+}$ cluster degradation during turnover of $[2Fe\text{-}2S]/[4Fe\text{-}4S]$ BioB.

## Discussion

We have used Mössbauer and EPR spectroscopy to monitor the time evolution of the Fe-S clusters in [2Fe-2S]/[4Fe-4S] BioB during turnover. The results indicate that under turnover conditions the [4Fe-4S] cluster is stable and present in a form that is similar to the SAM-bound $[4Fe\text{-}4S]^{2+}$ state reported previously for BioB containing only the [4Fe-4S] cluster (*26*). Spectroscopic evidence presented in our earlier study indicates that SAM binds to the $[4Fe\text{-}4S]^{2+}$ cluster at a unique Fe site (*26*). Binding of SAM to a unique Fe site of a $[4Fe\text{-}4S]^{2+}$ cluster has also been observed previously in a radical SAM enzyme, pyruvate formate-lyase activating enzyme (*27-29*), and is considered to be a common and functionally important property shared by radical SAM enzymes. Our observation thus supports the current consensus that BioB belongs to the family of radical SAM enzymes and suggests that the functional role of the [4Fe-4S] cluster in BioB is to bind SAM and facilitate the reductive cleavage that generates the catalytically important adenosyl radical. The fact that the $[4Fe\text{-}4S]^{2+}$ cluster is present in the SAM-bound form under turnover conditions suggests further that the immediate step following SAM binding, that is, the injection of an electron to the [4Fe-4S] cluster, must be the rate limiting step in the reaction pathway involving the [4Fe-4S] cluster.

The changes occurring to the [2Fe-2S] cluster during turnover were also observed by our Mössbauer and EPR measurements, which show clearly that approximately 2/3 of the [2Fe-2S] clusters were degraded by the end of the turnover experiment (24 hr) with about half of the $[2Fe\text{-}2S]^{2+}$ clusters degraded within the first hour. Transient paramagnetic species, which exhibit spectroscopic properties that are indicative of $[2Fe\text{-}2S]^{+}$ clusters, were detected by both EPR and

Mössbauer measurements, strongly suggesting that degradation of the $[2Fe\text{-}2S]^{2+}$ cluster is initiated by reduction of the cluster.

Degradation of the $[2Fe\text{-}2S]^{2+}$ cluster during [2Fe-2S]/[4Fe-4S] BioB turnover was initially reported by Jarrett and coworkers, who used UV/visible absorption spectroscopy to investigate changes occurring at/to the Fe-S clusters during catalysis (*13*). The decrease in absorbance at 460 nm was used as a quantitative measure of $[2Fe\text{-}2S]^{2+}$ degradation and was found to parallel the production of biotin, both in rate and in stoichiometry. On the basis of this UV/visible absorption data, together with Fe and S analysis, which showed a decrease in Fe and S contents consistent with loss of one [2Fe-2S] cluster per BioB, it was concluded that during catalysis the [4Fe-4S] cluster is preserved while the [2Fe-2S] cluster is destroyed. A mechanistic scheme consistent with such a conclusion was therefore proposed, in which the [4Fe-4S] cluster mediates the cleavage of SAM to generate an adenosyl radical that abstracts the C9 hydrogen atom of DTB to form a DTB radical, which, in turn, attacks a bridging sulfide of the $[2Fe\text{-}2S]^{2+}$ cluster initiating the destruction of the $[2Fe\text{-}2S]^{2+}$ cluster. A second adenosyl radical generated via the [4Fe-4S] cluster then abstracts the C6 hydrogen atom followed by ring closure and formation of biotin. For the formation of biotin to parallel the destruction of the $[2Fe\text{-}2S]^{2+}$ cluster, the rate limiting step in the proposed mechanism must correspond to [2Fe-2S] cluster degradation or a step preceding initiation of [2Fe-2S] cluster degradation. The Mössbauer and EPR data presented here are in general agreement with the conclusion made by Ugulava et al. (*13*) and provide direct evidence establishing that the [4Fe-4S] cluster is indeed preserved and that the $[2Fe\text{-}2S]^{2+}$ cluster is degraded during catalysis. However, the degradation of the $[2Fe\text{-}2S]^{2+}$ cluster was found not to parallel the formation of biotin, neither in rate nor in stoichiometry. Approximately half of the $[2Fe\text{-}2S]^{2+}$ clusters decay initially with a rate that is about one order of magnitude faster than that of the initial production of biotin. After 24 hr, 0.7 biotin per BioB monomer were produced while only 0.5 $[2Fe\text{-}2S]^{2+}$ clusters per BioB monomer were destroyed, leaving approximately 0.25 $[2Fe\text{-}2S]^{2+}$ clusters per BioB monomer still intact. However, taking into consideration the estimated error in the biotin bioassay (0.7 ± 0.1 biotin per BioB monomer), and the possibility that some $[2Fe\text{-}2S]^{2+}$ clusters are reassembled under turnover conditions, the small difference in stoichiometry between biotin production and cluster destruction is unlikely to be significant.

Marquet and coworkers (*14*) have recently applied Mössbauer spectroscopy to investigate the states of the Fe-S clusters after catalysis in a partially purified fraction of BioB presumably having a 1:1 $[2Fe\text{-}2S]^{2+}$:$[4Fe\text{-}4S]^{2+}$ ratio. Since the protein fractions were partially purified, Fe content, and thus cluster content, per BioB monomer could not be obtained. Only the Mössbauer absorption ratio for the $[2Fe\text{-}2S]^{2+}$ and $[4Fe\text{-}4S]^{2+}$ could be determined. Their data also indicate that not all the $[2Fe\text{-}2S]^{2+}$ clusters are destroyed after turnover (37 °C for 3 hr). Assuming that the $[4Fe\text{-}4S]^{2+}$ cluster is preserved after catalysis, the cluster absorption ratio determined by Marquet and coworkers indicates that approximately half of the [2Fe-2S] clusters remain intact, in good agreement with the results reported here.

In the scheme proposed by Ugulava et al. (*13*), the [2Fe-2S] cluster functions as the immediate sulfur donor for biotin production and the destruction of the $[2Fe\text{-}2S]^{2+}$ cluster begins with an attack of the bridging sulfide by a DTB radical. To investigate the involvement of DTB in the destruction of the [2Fe-2S] cluster, we have performed a control experiment in which DTB is left out of the turnover solution. In the absence of DTB, we found that the [2Fe-2S] cluster is stable for at least 3 hr, by which time more than half of the $[2Fe\text{-}2S]^{2+}$ clusters had been degraded under turnover conditions. Consequently, DTB must be involved in the destruction of the cluster. Taken together, the involvement of DTB in the destruction of the [2Fe-2S] cluster and the observed decay of the $[2Fe\text{-}2S]^{2+}$ cluster during biotin production support the scheme proposed by Ugulava et al. (*13*). Since putative catalytic intermediates (the 6- or 9-thio derivatives of DTB) are not significantly active in the biotin bioassay (*30*), the observation that the initial rate of $[2Fe\text{-}2S]^{2+}$ cluster degradation is an order of magnitude faster than that of biotin formation, can be explained by invoking a subsequent step in biotin synthesis, e.g. the ring closure, to be the rate limiting step. Alternatively, it is possible that a cluster degradation product, rather than the [2Fe-2S] cluster itself, is the immediate S donor. The degradation of the [2Fe-2S] cluster may generate protein-bound polysulfide or persulfide groups, which, in turn, serve as the immediate sulfur source for biotin production. Generation of protein-bound polysulfide groups following Fe-S cluster degradation is well established in at least one Fe-S enzyme, aconitase (*31*). This alternative explanation, which suggests a protein bound persulfide or polysulfide group to be the S donor for biotin production, raises a rather interesting possibility concerning the active form of BioB. That is, the catalytically functional form of BioB may contain only a [4Fe-4S] cluster in addition to an active polysulfide or persulfide entity (i.e., the presence of a [2Fe-2S] cluster may not be required.). Reactivation of such an active form of BioB after each single turnover would then involve regeneration of the active polysulfide or persulfide group rather than the reassembly of a [2Fe-2S] cluster as proposed for the [4Fe-4S]/[2Fe-2S] BioB. In the preceding paper (*4*), we have shown that, in our hands, BioB does not exhibit an intrinsic cysteine desulfurase activity. Therefore, regeneration of the active polysulfide or persulfide group in BioB would require an additional enzyme, such as a cysteine desulfurase possibly coupled with a specific sulfurtransferase as in the thiamin and 4-thiouridine biosynthetic pathways (*32*-*34*). Experiments are planned to investigate the validity of this rather intriguing possibility.

## References

1. Sanyal, I., Cohen, G., and Flint, D. H. (1994) Biotin synthase: purification, characterization as a [2Fe-2S] cluster protein, and *in vitro* activity of the *Escherichia coli bioB* gene product, *Biochemistry 33,* 3625-31.

2. Duin, E. C., Lafferty, M. E., Crouse, B. R., Allen, R. M., Sanyal, I., Flint, D. H., and Johnson, M. K. (1997) [2Fe-2S] to [4Fe-4S] cluster conversion in *Escherichia coli* biotin synthase, *Biochemistry 36*, 11811-11820.

3. Tse Sum Bui, B., Florentin, D., Marquet, A., Benda, R., and Trautwein, A. X. (1999) Mössbauer studies of *Escherichia coli* biotin synthase: evidence for reversible interconversion between $[2Fe\text{-}2S]^{2+}$ and $[4Fe\text{-}4S]^{2+}$ clusters, *FEBS Lett. 459*, 411-414.

4. Cosper, M. M., Jameson, G. N. L., Hernández, H. L., Krebs, C., Huynh, B. H., and Johnson, M. K. (2003) Characterization of the cofactor composition of *Escherichia coli* biotin synthase, *Biochemistry*, submitted with this paper.

5. Mejean, A., Tse Sum Bui, B., Florentin, D., Ploux, O., Izumi, Y., and Marquet, A. (1995) Highly purified biotin synthase can transform dethiobiotin into biotin in the absence of any other protein, in the presence of photoreduced deazaflavin, *Biochem. Biophys. Res. Commun. 217*, 1231-1237.

6. Baldet, P., Alban, C., and Douce, R. (1997) Biotin synthesis in higher plants: purification and characterization of *bioB* gene product equivalent from Arabidopsis thaliana overexpressed in *Escherichia coli* and its subcellular localization in pea leaf cells, *FEBS Lett. 419*, 206-210.

7. Sofia, H. J., Chen, G., Hetzler, B. G., Reyes-Spindola, J. F., and Miller, N. E. (2001) Radical SAM, a novel protein superfamily linking unresolved steps in familiar biosynthetic pathways

with radical mechanisms: functional characterization using new analysis and information visualization methods, *Nucleic Acids Research 29*, 1097-1106.

8. Escalettes, F., Florentin, D., Tse Sum Bui, B., Lesage, D., and Marquet, A. (1999) Biotin synthase mechanism: evidence for hydrogen transfer from the substrate into deoxyadenosine, *J. Am. Chem. Soc. 121*, 3571-3578.

9. Ugulava, N. B., Gibney, B. R., and Jarrett, J. T. (2000) Iron-sulfur cluster interconversions in biotin synthase: dissociation and reassociation of iron during conversion of [2Fe-2S] to [4Fe-4S] clusters, *Biochemistry 39*, 5206-5214.

10. Ollagnier-de Choudens, S., Sanakis, Y., Hewitson, K. S., Roach, P., Baldwin, J. E., Münck, E., and Fontecave, M. (2000) Iron-sulfur center of biotin synthase and lipoate synthase, *Biochemistry 39*, 4165-4173.

11. Ugulava, N. B., Gibney, B. R., and Jarrett, J. T. (2001) Biotin synthase contains two distinct iron-sulfur cluster binding sites: chemical and spectroelectrochemical analysis of iron-sulfur cluster interconversions, *Biochemistry 40*, 8343-8351.

12. Ugulava, N. B., Surerus, K. K., and Jarrett, J. T. (2002) Evidence from Mössbauer spectroscopy for distinct $[2Fe\text{-}2S]^{2+}$ and $[4Fe\text{-}4S]^{2+}$ cluster binding sites in biotin synthase from *Escherichia coli, J. Am. Chem. Soc. 124*, 9050-9051.

13. Ugulava, N. B., Sacanell, C. J., and Jarrett, J. T. (2001) Spectroscopic changes during a single turnover of biotin synthase: destruction of a [2Fe-2S] cluster accompanies sulfur insertion, *Biochemistry 40*, 8352-8358.

14. Tse Sum Biu, B., Brenda, R., Schünemann, Florentin, D., Trautwein, A. X., and Marquet, A. (2003) Fate of the $[2Fe\text{-}2S]^{2+}$ cluster of *Escherichia coli* biotin synthase during reaction: a Mössbauer characterization, *Biochemistry 42*, 8791-8798.

15. Ollagnier-de-Choudens, S., Mullier, E., Hewitson, K. S., and Fontecave, M. (2002) Biotin synthase is a pyridoxal phosphate-dependent cysteine desulfurase, *Biochemistry 41*, 9145-9152.

16. Hewitson, K. S., Ollagnier-de-Choudens, S., Sanakis, Y., Shaw, N. M., Baldwin, J. E., Münck, E., Roach, P. L., and Fontecave, M. (2002) The iron-sulfur center of biotin synthase: site-directed mutants, *J. Biol. Inorg. Chem. 7*, 83-93.

17. Ollagnier-de-Choudens, S., Sanakis, Y., Hewitson, K. S., Roach, P., Münck, E., and Fontecave, M. (2002) Reductive cleavage of *S*-adenosylmethionine by biotin synthase from *Escherichia coli*, *J. Biol. Chem. 277*, 13449-13454.

18. Cosper, M. M., Jameson, G. N. L., Eidsness, M. K., Huynh, B. H., and Johnson, M. K. (2002) Recombinant *Escherichia coli* biotin synthase is a $[2Fe\text{-}2S]^{2+}$ protein in whole cells, *FEBS Letters 529*, 332-336.

19. Sanyal, I., Gibson, K. J., and Flint, D. H. (1996) *Escherichia coli* biotin synthase: an investigation into the factors required for its activity and its sulfur donor, *Arch. Biochem. Biophys. 326*, 48-56.

20. Gibson, K. J., Pelletier, D. A., and Turner, I. M. (1999) Transfer of sulfur to biotin from biotin synthase (BioB protein), *Biochem. Biophys. Res. Commun. 254*, 632-635.

21. Tse Sum Bui, B., and Marquet, A. (1997) Biotin synthase of *Bacillus sphaericus*, *Meth. Enzymol. 279*, 356-362.

22. Tanaka, M., Izumi, Y., and Yamada, H. (1987) Biotin assay using lyophilized and glycerol-suspended cultures, *J. Microbiol. Meth. 6*, 237-246.

23. Fish, W. W. (1998) Rapid colorimetric micromethod for the quantitation of complexed iron in biological samples, *Meth. Enzym. 158*, 357-364.

24. Ravi, N., Bollinger, J. M., Jr., Huynh, B. H., Stubbe, J., and Edmondson, D. E. (1994) Mechanism of assembly of the tyrosyl radical-diiron(III) cofactor of *E. coli* ribonucleotide reductase: 1. Mössbauer characterization of the diferric radical precursor, *J. Am. Chem. Soc. 116*, 8007-8014.

25. Dunham, W. R., Bearden, A. J., Salmeen, I. T., Palmer, G., Sands, R. H., Orme-Johnson, W. H., and Beinert, H. (1971) Electronic properties of two-iron, two-sulfur proteins. II. Two-iron ferredoxins in spinach, parsley, pig adrenal cortex, *Azotobacter vinelandii,* and *Clostridium pasteurianum*. Magnetic field Mössbauer spectroscopy, *Biochim. Biophys. Acta 253,* 134-152.

26. Cosper, M. M., Jameson, G. N. L., Davydov, R., Eidsness, M. K., Hoffman, B. M., Huynh, B. H., and Johnson, M. K. (2002) The $[4Fe\text{-}4S]^{2+}$ cluster in reconstituted biotin synthase binds *S*-adenosyl-L-methionine*, J. Am. Chem. Soc. 124*, 14006-14007.

27. Krebs, C., Broderick, W. E., Henshaw, T. F., Broderick, J. B., and Huynh, B. H. (2002) Coordination of adenosylmethionine to a unique iron site of the [4Fe-4S] of pyruvate formate-lyase activating enzyme: a Mössbauer spectroscopic study, *J. Am. Chem. Soc. 124*, 912-913.

28. Walsby, C. J., Ortillo, D., Broderick, W. E., Broderick, J. B., and Hoffman, B. M. (2002) An anchoring role for FeS clusters: Chelation of the amino acid moiety of *S*-adenosylmethionine to the unique iron site of the [4Fe-4S] cluster of pyruvate formate-lyase activating enzyme, *J. Am. Chem. Soc. 124*, 11270-11271.

29. Walsby, C. J., Hong, W., Broderick, W. E., Cheek, J., Ortillo, D., Broderick, J. B., and Hoffman, B. M. (2002) Electron-nuclear double resonance spectroscopic evidence that *S*-adenosylmethionine binds in contact with the catalytically active $[4Fe\text{-}4S]^{+}$ cluster of pyruvate formate-lyase activating enzyme, *J. Am. Chem. Soc. 124*, 3143-3151.

30. Marquet, A., Frappier, F., Guillerm, G., Azoulay, M., Florentin, D., and Tabet, J.-C. (1993) Biotin biosynthesis: synthesis and biological evaluation of the putative intermediate thiols, *J. Am. Chem. Soc*. 115, 2139-2145

31. Kennedy, M. C., and Beinert, H. (1988) The state of cluster sulfhydryl and sulfide of aconitase during cluster interconversions and removal. A convenient preparation of apoenzyme, *J. Biol. Chem. 263*, 8194-8198.

32. Palenchar, P. M., Buck, C., J., Cheng, H., Larson, T. J., and Mueller, E. G. (2000) Evidence that ThiI, an enzyme shared between thiamin and 4-thiouridine biosynthesis, may be a sulfurtransferase that proceeds through a persulfide intermediate, *J. Biol. Chem. 275*, 8283-8286.

33. Kambampati, R., and Lauhon, C. T. (2000) Evidence for the transfer of sulfane sulfur from IscS to ThiI during in vitro biosynthesis of 4-thiouridine in *Escherichia coli* tRNA, *J. Biol. Chem. 275*, 10727-10730.

34. Mueller, E. G., Palenchar, P. M., and Buck, C., J. (2001) The role of the cysteine residues of ThiI in the generation of 4-thiouridine in tRNA, *J. Biol. Chem. 276*, 33588-33595.

**Table 3.1** Mössbauer percent absorption and quantification of $^{57}$Fe species detected in [2$^{57}$Fe-2S]/[4Fe-4S] BioB during single turnover.

| Reaction time | Fe species<br>Percent absorption (clusters/monomer) | | | | |
|---|---|---|---|---|---|
| | $[2Fe\text{-}2S]^{2+}$ | $[2Fe\text{-}2S]^{+}$ | $[4Fe\text{-}4S]^{2+}$ | SAM-$[4Fe\text{-}4S]^{2+}$ | $Fe^{II}S_4$/N/O |
| 0 | 90 ± 3 (0.75 ± 0.03) | | 10 ± 2 (0.04 ± 0.01) | | |
| 5 min | 58 ± 3 (0.48 ± 0.03) | ~ 20 (~ 0.17) | | 7 ± 2 (0.03 ± 0.01) | 6 ± 2 |
| 45 min | 53 ± 3 (0.44 ± 0.03) | ~ 10 (~ 0.08) | | 16 ± 3 (0.07 ± 0.01) | 25 ± 3 |
| 24 hr | 25 ± 3 (0.21 ± 0.03) | | | 38 ± 3 (0.16 ± 0.01) | 36 ± 3 |

**Scheme 3.1**

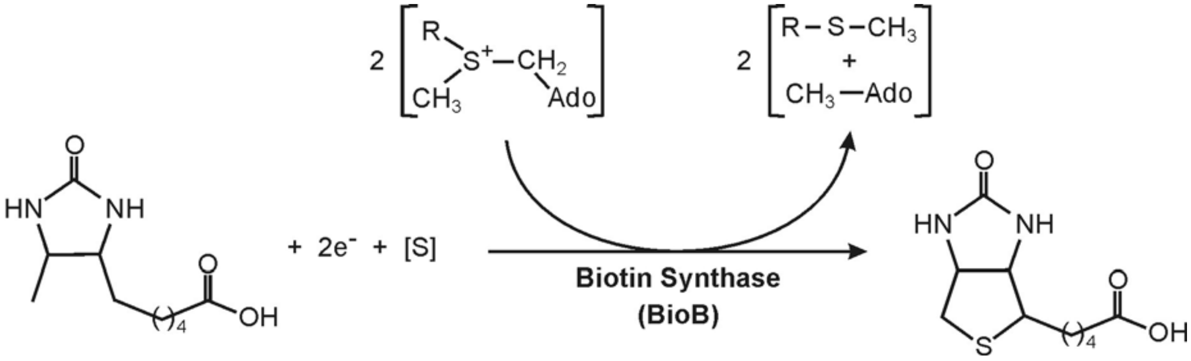
2
R
S+
CH2
CH3
Ado
2
R – S – CH3
+
CH3 – Ado
HN
NH
O
OH
()4
+ 2e- + [S]
Biotin Synthase
(BioB)
S

**Figure 3.1** Mössbauer spectra (hatched marks) of as-prepared [$2^{57}$Fe-2S]/[4Fe-4S] BioB (A) and samples taken at 5 min (B), 45 min (C) and 24 hr (D) reaction time points during the single turnover reaction of the enzyme. The data were recorded at 4.2 K in a field of 50 mT oriented parallel to the $\gamma$-beam. The solid lines overlaid with the experimental spectra are superpositions of theoretical spectra of the spectral components described in text and using the absorption percentages listed in Table 3.1. Also shown are some of the individual spectral components: $[2Fe\text{-}2S]^{2+}$, dotted line in B and dashed line in D; $[2Fe\text{-}2S]^{+}$, dashed line in B; SAM bound $[4Fe\text{-}4S]^{2+}$, dotted line in D; $Fe^{II}S_4$/N/O, dashed line in C. These spectral components are scaled to the percent absorption listed in Table 3.1. The two arrows in B indicate the positions of the doublet arising from the $Fe^{II}S_4$/N/O species.

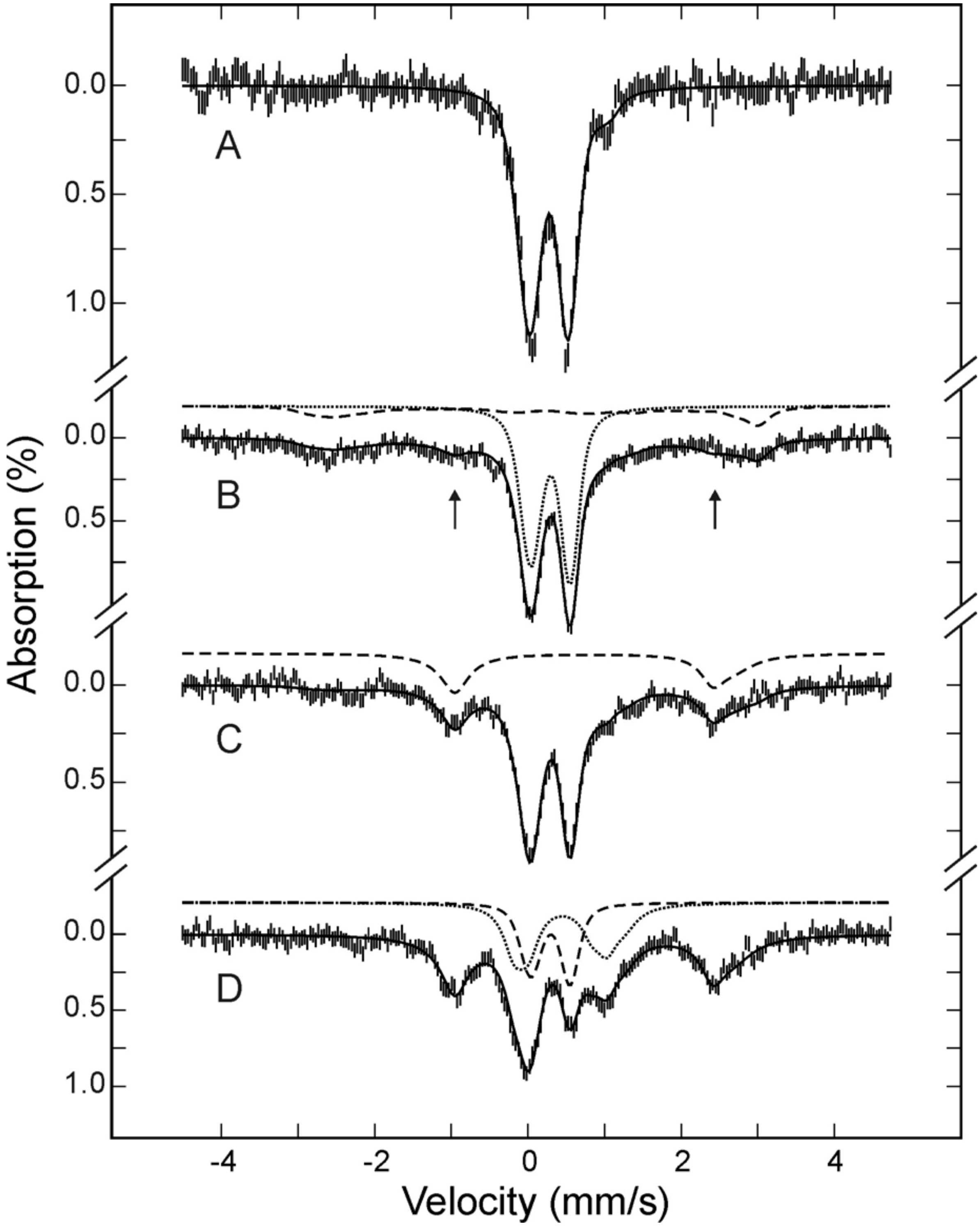
A
B
C
D
0.0
0.5
1.0
0.0
0.5
0.0
0.5
0.0
0.5
1.0
Absorption (%)
-4
-2
0
2
4
Velocity (mm/s)

**Figure 3.2** Time-dependent Mössbauer spectra (hatched marks) of $^{57}$Fe-enriched [2Fe-2S]/[4Fe-4S] BioB during single turnover. Samples were taken at 0 (A), 5 min (B), 45 min (C), 3 hr (D), and 24 hr (E) reaction time points during turnover and the spectra were recorded at 4.2 K in a field of 50 mT oriented parallel to the $\gamma$-beam. The solid line in A is the superposition of theoretical spectra of the $[2Fe\text{-}2S]^{2+}$ and $[4Fe\text{-}4S]^{2+}$ cluster simulated with parameters reported in the preceding paper (*4*) and percent absorptions mentioned in text. The solid lines shown in B-E are simulated theoretical spectra of the SAM-bound $[4Fe\text{-}4S]^{2+}$ cluster (*26*) and are scaled to 76% of the total absorptions. The central arrow in E indicates the position of the high energy line of the quadrupole doublet of the $[2Fe\text{-}2S]^{2+}$ cluster and the other two arrows indicate the positions of the broad quadrupole doublet of the $Fe^{II}S_4$/N/O species.

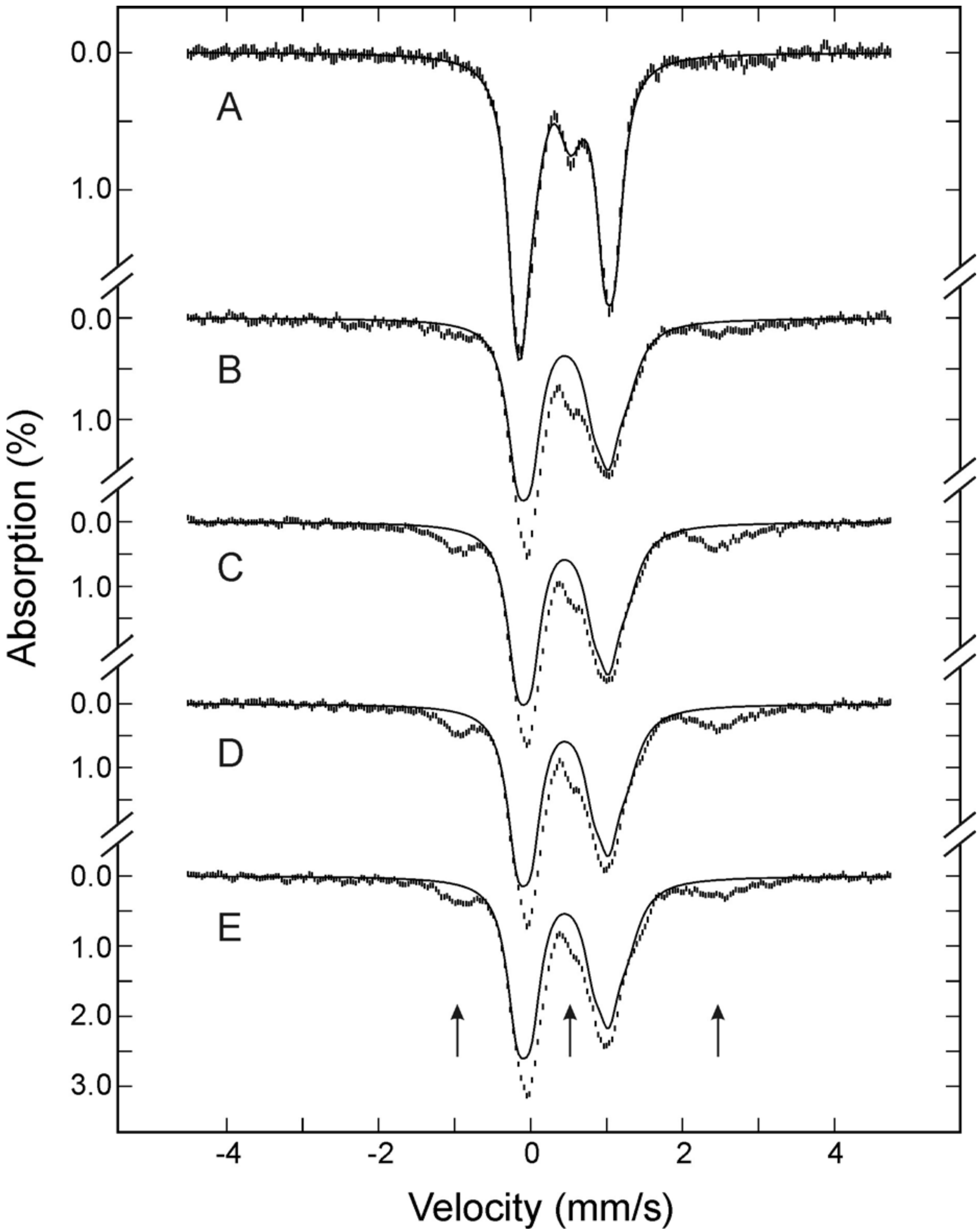
A
B
C
D
E
0.0
1.0
2.0
3.0
Absorption (%)
-4
-2
0
2
4
Velocity (mm/s)

**Figure 3.3** Mössbauer spectrum (hatched marks) prepared from the spectrum shown in Figure 3.2A by removing the contribution of the SAM-bound [4Fe-4S]$^{2+}$ cluster. This prepared spectrum compares well with that of the 5-min sample (solid line) during turnover of the [2$^{57}$Fe-2S]/[4Fe-4S] BioB shown in Figure 3.1B.

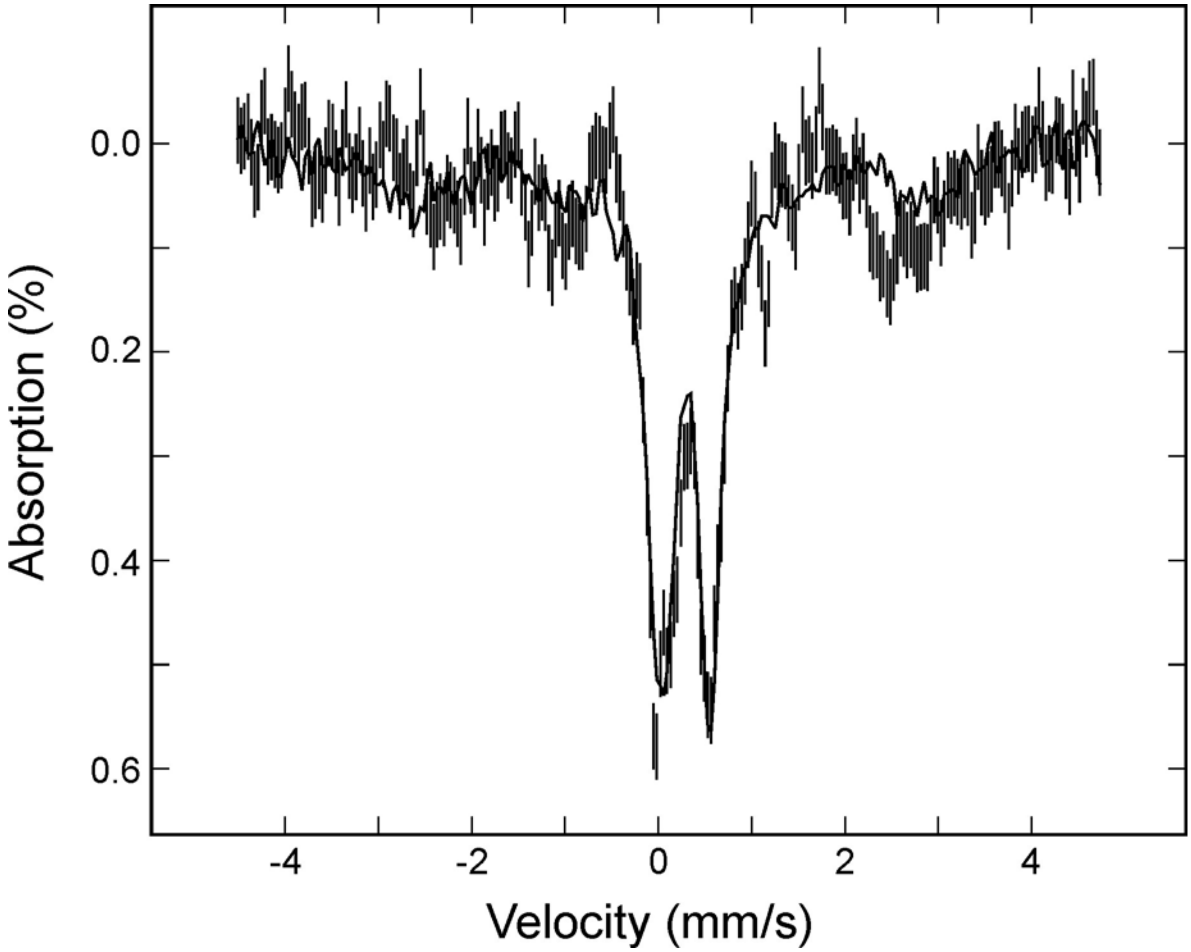
Absorption (%)
0.0
0.2
0.4
0.6
-4
-2
0
2
4
Velocity (mm/s)

**Figure 3.4** $[2Fe\text{-}2S]^{2+}$ cluster degradation (circles) and biotin production (squares) during BioB single turnover. The filled circles are data obtained from the $[2^{57}Fe\text{-}2S]/[4Fe\text{-}4S]$ BioB turnover, and the empty circles are from the $^{57}Fe$-enriched $[2Fe\text{-}2S]/[4Fe\text{-}4S]$ BioB turnover. The solid and dashed lines are simulations of the $[2Fe\text{-}2S]^{2+}$ decay and biotin production, respectively, as described in text.

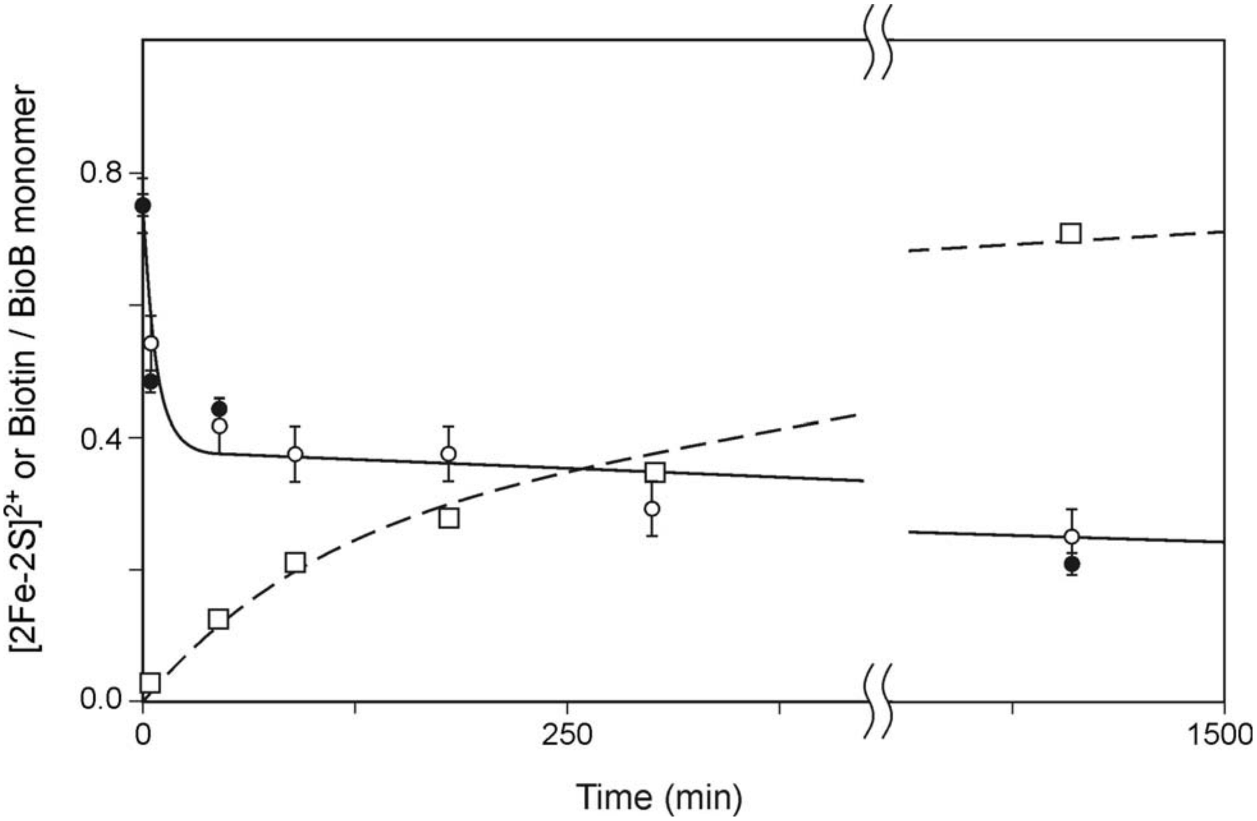

[2Fe-2S]$^{2+}$ or Biotin / BioB monomer
0.8
0.4
0.0
0
250
1500
Time (min)

**Figure 3.5** Mössbauer spectrum of a control sample of [$2^{57}$Fe-2S]/[4Fe-4S] BioB, which was incubated anearobically for 3.5 hr in a solution identical to that used in the turnover experiment but without the presence of DTB. The spectrum was recorded at 4.2 K in a field of 50 mT oriented parallel to the γ-beam.

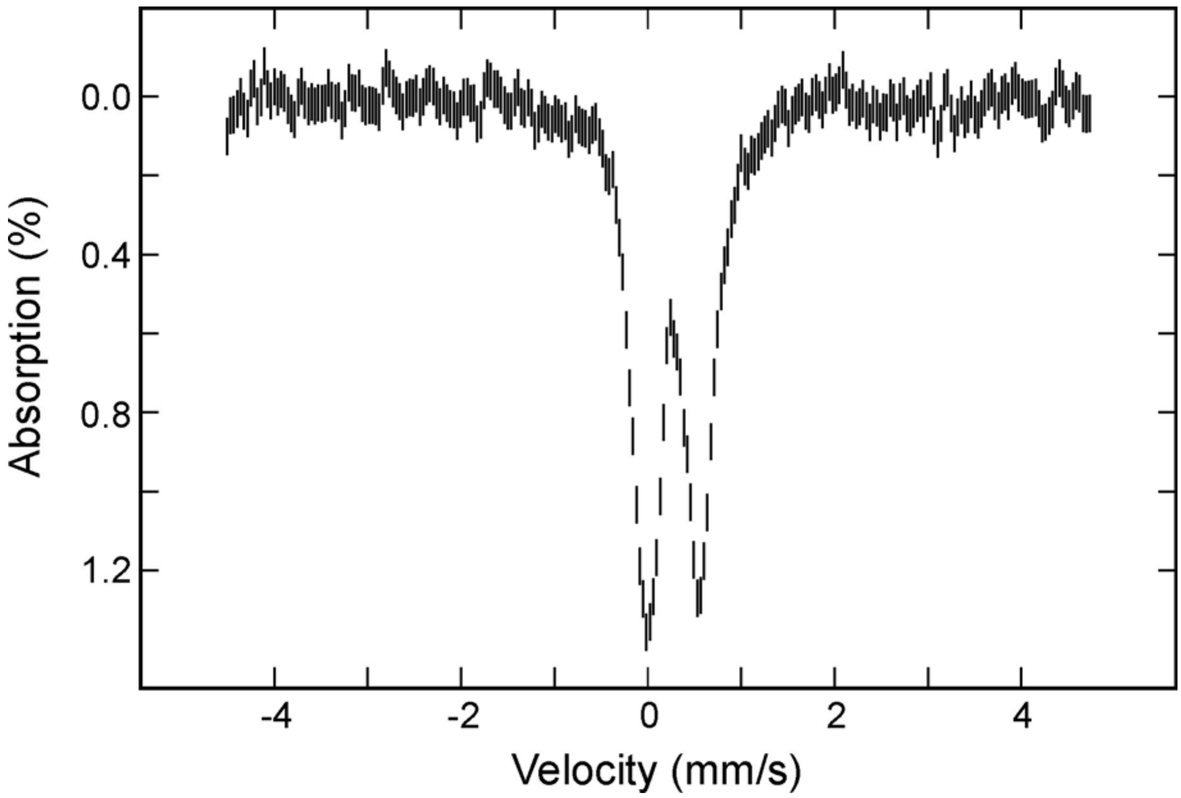
Absorption (%)
0.0
0.4
0.8
1.2
-4
-2
0
2
4
Velocity (mm/s)

**Figure 3.6** EPR spectrum of a natural abundance [2Fe-2S]/[4Fe-4S] BioB sample (200 μM) taken at 15 min reaction time, during the single turnover reaction of the enzyme (A). Conditions of measurement: microwave frequency, 9.603 GHz; modulation amplitude, 0.63 mT; microwave power, 1 mW; temperature, 12 K. B is a simulation of the spectrum in A as the sum of the three components: 7.6% of $g_{x,y,z}$ = 2.0015, 2.0015, 2.0018 and $\Gamma_{x,y,z}$ = 2.0, 2.0, 2.0 mT (C); 28.7 % of $g_{x,y,z}$ = 1.880, 1.955, 2.010 and $\Gamma_{x,y,z}$ = 5.0, 4.0, 4.5 mT (D); 63.7% of $g_{x,y,z}$ = 1.845, 1.940, 2.000 and $\Gamma_{x,y,z}$ = 5.0, 4.0, 5.0 mT (E).

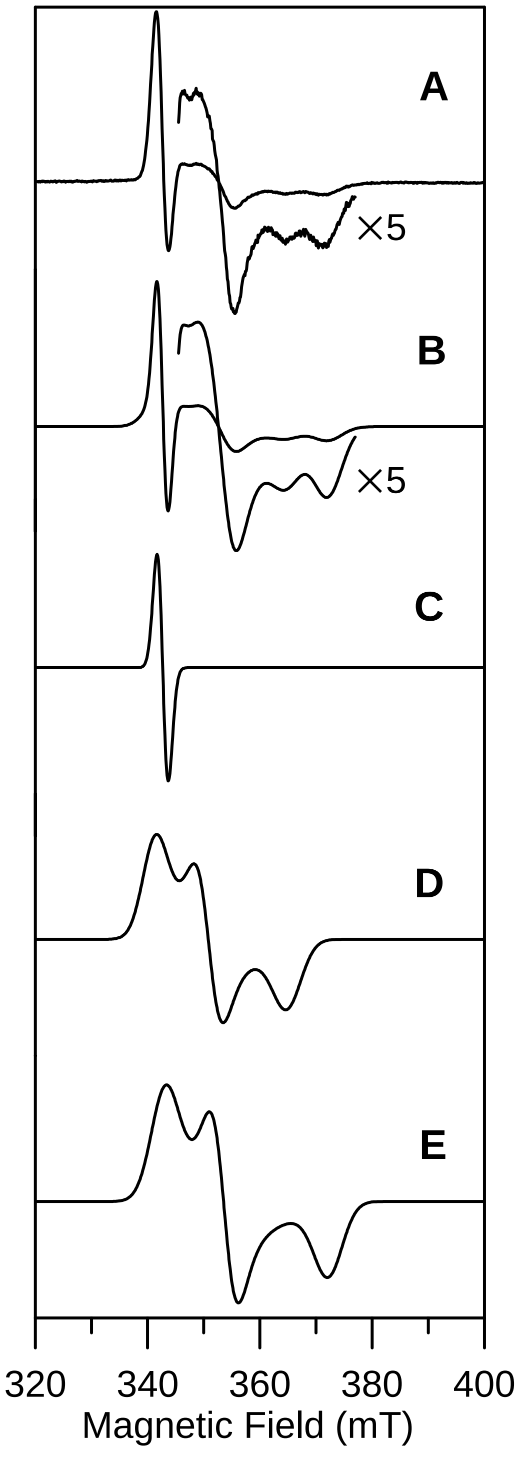
A
×5
B
×5
C
D
E
320
340
360
380
400
Magnetic Field (mT)

**Figure 3.7** EPR spectra of a natural abundance [2Fe-2S]/[4Fe-4S] BioB sample (200 μM) taken at the indicated time periods during the single turnover reaction of the enzyme. Conditions of measurement: microwave frequency, 9.603 GHz; modulation amplitude, 0.63 mT; microwave power, 2 mW; temperature, 35 K.

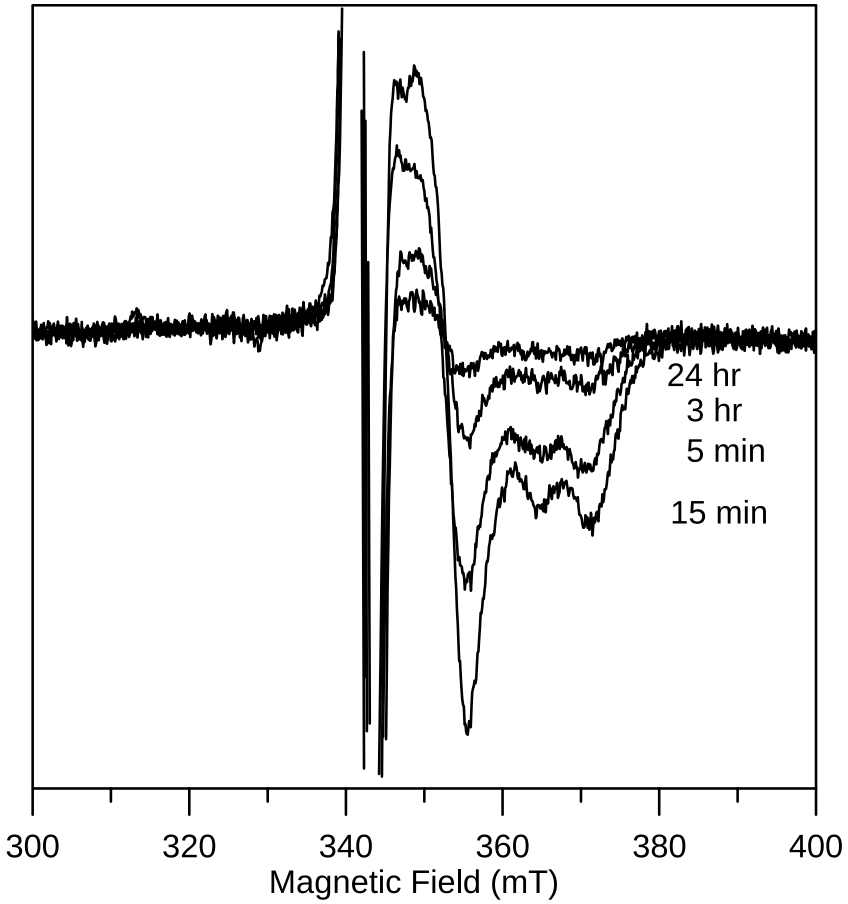
24 hr
3 hr
5 min
15 min
300
320
340
360
380
400
Magnetic Field (mT)

# CHAPTER 4

# COFACTOR COMPOSITION, SPECTROSCOPIC PROPERTIES AND ACTIVITY STUDIES OF BACILLUS SUBTILIS BIOTIN SYNTHASE[1]

---

[1] Hernández, H. L., García-Serres, R., Cosper, M. M., Agar, N. Y. R., Jameson, G. N. L., Huynh, B. H., Johnson, M. K. To be submitted to *Biochemistry*.

**Abbreviations:** BioB, gene product of *bioB* commonly referred to as biotin synthase; SAM, *S*-adenosyl-L-methionine; DTB, dethiobiotin; DTT, dithiothreitol; DT, dithionite; PLP, pyridoxal 5'-phosphate; CD, circular dichroism

## Abstract

The Fe-S cluster composition of *in vivo*, as-purified, and reconstituted forms of *Bacillus subtilis* biotin synthase (BioB) have been characterized using analytical studies together with UV/visible absorption/CD, resonance Raman, EPR, and Mössbauer spectroscopies, and correlated with parallel activity assays. The results indicate that like *E. coli* BioB, *B. subtilis* BioB has two distinct Fe-S cluster binding sites. One site contains an oxidatively labile $[4Fe\text{-}4S]^{2+}$ cluster that is responsible for binding and reductively cleaving *S*-adenosyl-L-methionine, but readily degrades during purification. The other site contains an oxidatively inert $[2Fe\text{-}2S]^{2+}$ cluster with spectroscopic properties similar to but distinct from those of the $[2Fe\text{-}2S]^{2+}$ cluster found in *E. coli* BioB. Moreover, unlike the $[2Fe\text{-}2S]^{2+}$ cluster in *E. coli* BioB, the $[2Fe\text{-}2S]^{2+}$ cluster in *B. subtilis* BioB degrades during anaerobic reconstitution of the $[4Fe\text{-}4S]^{2+}$ cluster in the as-purified enzyme. The resulting samples of reconstituted *B. subtilis* BioB still retain activity comparable to the most active form of *E. coli* BioB, despite having a [2Fe-2S]/[4Fe-4S] cluster ratio <0.1, compared to 1.0 for the most active preparations of *E. coli* BioB. This observation suggests that the $[2Fe\text{-}2S]^{2+}$ cluster is not essential for *B. subtilis* BioB activity and that a sulfur-containing [2Fe-2S] cluster degradation product is a competent S-donor for biotin biosynthesis.

## Introduction

The final step in the biosynthetic formation of biotin is catalyzed by the *bioB* gene product, biotin synthase (BioB), a homodimer which is responsible for catalyzing the insertion of a sulfur atom into the substrate, dethiobiotin (DTB), between two unactivated carbons, C-6 and C-9, see Scheme 4.1. The detailed mechanism of this complex reaction has remained elusive despite over a decade of research, for a recent review see (*1*).

It has become overwhelmingly evident that BioB is a member of the superfamily of *S*-adenosyl-L-methionine (SAM) dependent iron-sulfur enzymes in which a $[4Fe\text{-}4S]^+$ center, coordinated by the CxxxCxxC motif common to all radical-SAM proteins, generates a 5'-deoxyadenosyl radical via reductive cleavage of SAM (*2-6*). Crystallographic and spectroscopic data have shown that the $[4Fe\text{-}4S]^{2+}$ cluster of BioB binds SAM at the unique iron (*7;8*) and once reduced to a $[4Fe\text{-}4S]^+$ cluster, an electron is transferred from the cluster to the sulfonium ion of SAM causing reductive cleavage and the formation of methionine and the 5'-deoxyadenosyl radical (*3;9*). This radical then abstracts a hydrogen at the C-9 carbon of DTB, forming the intermediate 9-mercaptodethiobiotin by attaching to a proximal sulfur (*10*). It has been speculated that the reaction is completed in one of two ways. The process can be repeated with a 5'-deoxyadenosyl radical from a second molecule of SAM, activating the C-6 carbon enabling sulfur insertion and ring closure (*10*). This model is supported by a study showing that BioB has a 2:1:1 SAM/DTB/BioB binding stoichiometry (*11*). In contrast, Fontecave and coworkers published evidence for a pyridoxal 5'-phosphate (PLP)-bound form of BioB that requires only one molecule of SAM for the formation of one molecule of biotin and hypothesized that a thiyl radical is responsible for H-abstraction from the C-6 position enabling ring closure of the substrate (*12*).

Spectroscopic evidence has established that *E. coli* BioB has two separate and distinct cluster binding sites and can be obtained in one of three different cluster containing forms (*13-15*), with each cluster ligated by three rigorously conserved cysteines. The as-purified form contains one air-stable $[2Fe\text{-}2S]^{2+}$ cluster per monomer in the second cluster binding site and no cluster in the radical-SAM active site, resulting in an inactive protein (*15;16*). This inactive form of BioB is not a purification artifact as it is the dominant form of BioB in anaerobically grown whole cells, and this observation has raised questions concerning the physiological relevance of the over-expressed recombinant enzyme (*15*). Under reducing conditions, the $[2Fe\text{-}2S]^{2+}$ cluster completely degrades leaving the site devoid of cluster (*5*). There has been one report that this second site can also house a $[4Fe\text{-}4S]^{+}$ cluster upon reconstituting the protein in the presence of ethylene glycol followed by reduction with dithionite (*13*), but this result could not be reproduced in other laboratories (*15*). Fe-S cluster reconstitution under anaerobic conditions starting with the apo protein form of BioB leads to a form containing only a $[4Fe\text{-}4S]^{2+}$ cluster in the radical-SAM active site (*15*). When exposed to air, the radical-SAM $[4Fe\text{-}4S]^{2+}$ cluster breaks down via a transient $[2Fe\text{-}2S]^{2+}$ cluster ultimately yielding the apo protein (*15*). Fe-S cluster reconstitution of as-purified BioB under anaerobic conditions results in the assembly of a $[4Fe\text{-}4S]^{2+}$ cluster in the radical-SAM cluster binding site, while maintaining the $[2Fe\text{-}2S]^{2+}$ cluster in the second cluster binding site (*13;15*). The [4Fe-4S]/[2Fe-2S] cluster-bound form of BioB has proven to be the most active of the three forms in *in vitro* experiments. However, in common with all preparations of BioB reported thus far, it is only capable of forming 1 biotin per BioB monomer. Hence BioB may be a substrate rather than an enzyme, although it does appear to undergo multiple turnovers *in vivo* (*17*).

In 2004, Drennan and coworkers published a crystal structure of [4Fe-4S]/[2Fe-2S] *E. coli* BioB at 3.4-Å resolution that confirmed the presence of two clusters with SAM bound to the unique Fe of the $[4Fe\text{-}4S]^{2+}$ cluster and dethiobiotin positioned midway between the SAM and the $[2Fe\text{-}2S]^{2+}$ cluster (*8*). The crystal structure also revealed that the [2Fe-2S] cluster is coordinated by the three conserved cysteines and one conserved arginine, thus providing the first example of arginine as an Fe-S cluster ligand.

The most ardently debated topics in the BioB literature to date are the source of the sulfur inserted into DTB and the role of the [2Fe-2S] cluster. While there is general agreement that cysteine is the ultimate S-donor, the nature of the immediate S-donor to DTB is still controversial. Sulfur isotope and Se labeling studies have shown that the [2Fe-2S] cluster can act as sacrificial S-donor during a single turnover (*18;19*). In accord with this proposal, the [2Fe-2S] cluster was found to degrade during turnover (*20-22*). However, recent Mössbauer studies showed that [2Fe-2S] cluster degradation is at least an order of magnitude faster than the initial rate of biotin formation (*21*), which leaves open the question of whether the cluster itself or a cluster degradation product is the immediate S-donor. In contrast, Fontecave and coworkers reported that BioB is a PLP dependent enzyme that possesses intrinsic cysteine desulfurase activity (*12;23*). On the basis of mutagenesis studies, cysteine persulfides formed on two of the second group of conserved cysteines were proposed to be the immediate S-donors, with the [2Fe-2S] cluster as an artifact of recombinant overexpression (*12;23*). However, we have been unable to confirm evidence for PLP or indigenous cysteine desulfurase activity in *E. coli* BioB (*15*).

The goal of this study was purification and characterization of the cofactor content and activity of BioB from *Bacillus subtilis*, in order to gain further insight into the role of the $[2Fe\text{-}2S]^{2+}$ cluster and the nature of the immediate S-donor. While preliminary reports of purification of BioB from *Bacillus sphaericus* (*24*), *B. subtilis* (*25*), and *Arabidopsis thaliana* (*26*) have been published, only *E. coli* BioB has been fully characterized. The results demonstrate that recombinant *B. subtilis* BioB contains an oxygen-inert $[2Fe\text{-}2S]^{2+}$ cluster, with properties that are similar but not identical to those of the $[2Fe\text{-}2S]^{2+}$ in *E. coli* BioB, in addition to an oxygen-labile radical-SAM $[4Fe\text{-}4S]^{2+}$ cluster. However, the ability to obtain activity comparable to that of [2Fe-2S]/[4Fe-4S] forms of *E. coli* BioB, with *B. subtilis* BioB samples depleted in the [2Fe-2S] cluster, suggests that a sulfur-containing cluster degradation product is a competent S-donor for biotin biosynthesis.

## Materials and Methods

*Materials.* Chemicals were purchased from Sigma-Aldrich or Fischer, unless otherwise stated. $^{57}$Fe-enriched ferric ammonium citrate and $FeSO_4$ were prepared from $^{57}$Fe metal (>95% isotopic enrichment) as previously described (*27*). The plasmids pYK2001 containing the wild-type *B. subtilis bioB* gene and pXHisBioB containing the polyhistidine-tagged *B. subtilis bioB* gene were generously supplied by Dr. John Perkins and Dr. Abel Ferrández (Roche Pharmaceuticals, Basel, Switzerland). The over-expression strain, *E. coli* C41[DE3], was provided by Professor John E. Walker (Medical Research Council, Cambridge, UK), the plasmid pEE1010 containing the gene encoding *E. coli* flavodoxin reductase was a kind gift from Dr. Peter Reichard (Karolinska Institute, Sweden), and the plasmid pBH402 overexpressing polyhistidine-tagged *E. coli* IscS was a generous gift from Dr. Eugene Muller (University of Delaware). The *E. coli* strain DH01 overexpressing *E. coli* flavodoxin was a kind gift from Dr. Rowena Matthews (University of Michigan). Anaerobic experiments were performed under Ar in a Vacuum Atmospheres glove box at oxygen levels < 5 ppm.

*Construction of the wild type B. subtilis bioB Expression Vector pT7-7BsbioB-1.* The gene encoding BioB was amplified using PCR from pYK2001 using the primers 5'-GGAATTCCATATGAATCAATGGATGG-3' and 5'-ACAACTGCAGTCAGCTTTTCGACT-3'. The PCR product was digested with *Nde* I and *Pst* I and ligated into the appropriately digested vector pT7-7 (*28*) to yield pT7-7 BsbioB-1.

*Anaerobic overexpression of wild-type B. subtilis BioB. E. coli* BL21[DE3] gold pT7-7 BsbioB-1 and the *E. coli* BL21-gold[DE3] pT7-7 control strain were cultivated at 37 °C under strictly anaerobic conditions in Spizizen's minimal medium (*29*) with 10 mM $NaNO_3$, 20 μM $^{57}$Fe in the form of ferric ammonium citrate, 0.1 % (w/v) casein hydroxylate, 1.5 μM thiamine, and 100 μg/mL amplicillin. When the cultures reached an $OD_{600}$ between 0.9 – 1.2, IPTG was added to a final concentration of 0.05 mM, and the bacteria cultures were further cultivated at 37 °C for 3 hours and finally stored at 4 °C for 16 hours. The cells were harvested by centrifugation at 4,650 × *g* for 5 minutes at 4 °C and stored at –80 °C until further use.

*Aerobic Overexpression of wild-type B. subtilis BioB.* The *E. coli* C41[DE3] pT7-7bioB-1 strain was cultivated at 37 °C in terrific broth containing 100 μg/mL carbenicillin and 40 μg/mL Fe in the form of ferric ammonium citrate. When the cultures reached an $OD_{600}$ between 0.9 – 1.2, isopropyl-1-thio-β-D-galactopyranoside (IPTG, Alexis) was added to a final concentration of 1.0 mM, and the bacteria cultures were further cultivated at 29 °C for 20 hours. The cells were harvested by centrifugation at 4,650 × *g* for 5 minutes at 4 °C and stored at –80 °C until further use.

*Purification of wild-type B. subtilis BioB.* 6.0 g of cell paste were thawed and resuspended in 50 mM Tris buffer, pH 8.0, 5% glycerol and 2 mM DTT (buffer A), with 20 μg/mL chicken egg-white lysozyme, 5 μg/mL DNase I (Roche), and 5 μg/mL RNase A (Roche).

Cells were broken by intermittent sonication, and the cell debris was removed by centrifugation at 39,700 × *g* for 1 hour at 4 °C. The cell free extract was applied to a Source Q (Pharmacia) column (26 mm × 10 cm) previously equilibrated with buffer A, and eluted with a 0 – 100% gradient of 100 mM Tris buffer, pH 8.0, 5% glycerol, 2 mM DTT and 1.0 M NaCl (buffer B). The purest fractions, as judged by SDS-PAGE analysis, were pooled and brought to a final concentration of 0.6 M in ammonium sulfate. This solution was applied to a Phenyl Sepharose High Performance (Pharmacia) column (26 mm × 15 cm) previously equilibrated with 100 mM Tris buffer, pH 8.0, containing 0.6 M ammonium sulfate (buffer C) and eluted with a 0 – 100 % gradient of buffer A. The purest fractions, as determined by the $A_{453}/A_{280}$ ratio (> 0.18), were pooled and dialyzed into buffer A over a YM30 membrane. *E. coli* C41[DE3] pT7-7 BsbioB-1 cells yielded 0.1 mg BioB/g cell paste.

*Overexpression and Purification of His-tagged B. subtilis BioB.* The *E. coli* BL21-gold[DE3] pXHisBioB strain was cultivated at 37 °C in LB containing 100 μg/mL amplicillin, 40 μg/mL Fe or 5 μg/mL $^{57}$Fe in the form of ferric ammonium citrate. When the cultures reached an $OD_{600}$ between 0.6 – 0.8, the temperature was decreased to 28 °C and the cells were cultivated overnight. The cells were harvested by centrifugation at 4,650 × *g* for 5 minutes at 4 °C.

8.0 g of cell paste were thawed and resuspended in 30 mL of 100 mM Tris-HCl buffer, pH 8.0, containing 0.3 M NaCl and 5 mM imidazole (buffer D), with 20 μg/mL chicken egg-white lysozyme, 5 μg/mL DNase I (Roche), and 5 μg/mL RNase A (Roche). Cells were broken by intermittent sonication, and the cell debris was removed by centrifugation at 39,700 × *g* for 1 hour at 4 °C. The cell-free extract was loaded onto a charged and equilibrated 5 mL Ni-chelating column (Pharmacia), and the $his_6$-BioB was eluted with 0 – 100% gradient of 100 mM Tris-HCl buffer, pH 8.0, containing 0.3 M NaCl and 0.5 M imidazole (buffer E). The purest fractions, as determined by SDS-PAGE analysis, were pooled and dialyzed into buffer A over a YM30 membrane. *E. coli* BL21-gold[DE3] pXHisBioB yielded 4.0 mg BioB/g cell paste.

*Reconstitution of [4Fe-4S]$^{2+}$ centers in as-purified B. subtilis BioB.* Reconstitution of the [4Fe-4S]$^{2+}$ cluster in as-purified *B. subtilis* BioB was carried out under strictly anaerobic conditions using the method of Jarrett and coworkers (*20*), with the following modifications. Following incubation of as-isolated BioB in 10 mM DTT for 10 minutes, a 10-fold molar excess of $FeCl_3$, $Fe(NH_4)_2(SO_4)_2$ or $^{57}Fe(NH_4)_2(SO_4)_2$ was added, followed by the addition of a 10-fold molar excess of $Na_2S$. The use of $Fe(NH_4)_2(SO_4)_2$ or $FeCl_3$ in the reaction mixture made no difference to the outcome of the reconstitution experiments reported in this work. After 1-6 hours, the reconstitution mixture was loaded onto a 5-mL HiTrap Q column previously equilibrated with buffer A and eluted with a 0 – 100 % gradient of buffer B. The red-brown fractions were concentrated over a YM30 (Amicon) membrane. The IscS-mediated reconstitution was prepared as stated above except in lieu of $Na_2S$ a 1:50 ratio of IscS to BioB and a 10-fold excess of L-cysteine was added.

*Growth, Overexpression, purification and reconstitution of E. coli BioB*. The growth, overexpression, purification and reconstitution of *E. coli* BioB were reported elsewhere (*15*).

*Determination of Protein and Fe Concentrations.* Protein concentrations were determined by the *DC* protein assay (Bio-Rad), using BSA as a standard. Iron concentrations were determined colorimetrically using bathophenanthroline under reducing conditions, after digestion of the protein in 0.8% $KMnO_4$/0.2 M HCl (*30*). All sample concentrations and molar extinction coefficients are expressed per BioB monomer.

*Assay of Biotin Synthase Activity.* The BioB assay of *B. subtilis* BioB and *E. coli* BioB was performed in parallel under strictly anaerobic conditions in a glove box according to the procedure used by Fontecave and coworkers (*23*), except that the assays were performed at 25 ºC rather than 37 ºC. The assays were performed in 100 mM Tris-HCl buffer, pH 8.0, with BioB (100 μM), KCl (10 mM), DTT (10 mM), L-cysteine (1 mM), fructose bisphosphate (5 mM), SAM (1 mM), *E.* coli flavodoxin (40 μM), *E. coli* flavodoxin reductase (20 μM), NADPH (1 mM), and dethiobiotin (400 μM ). In accord with the results of Jarrett and coworkers (*20*), the omission of L-cysteine did not affect the assay results presented herein. Biotin was assayed using *Lactobacillus plantarum* ATCC 8014 according to published procedures (*31;32*).

*Spectroscopic Characterization of the Fe-S Centers in BioB.* UV-visible absorption spectra were recorded under aerobic or anaerobic conditions in screw top 1 mm cuvettes using a Shimadzu UV-3101PC spectrophotometer. Resonance Raman spectra were recorded using an Instruments SA Ramanor U1000 spectrometer fitted with a cooled RCA 31034 photomultiplier tube with a 90º scattering geometry. Spectra were recorded digitally using photon counting electronics, and improvements in signal-to-noise were achieved by signal-averaging multiple scans. Band positions were calibrated using the excitation frequency and are accurate to ±1 $\text{cm}^{-1}$. Lines from a Coherent Sabre 10-W Argon Ion Laser were use for Raman studies, and plasma lines were removed using a Pellin Broca Prism premonochromator. Using a custom-designed sample cell (*33*), Raman scattering was collected from the surface of 20 μL frozen droplets at 18 K using an Air Products Displex Model CSA-202E closed cycle refrigerator. Mössbauer spectra were recorded using the previously described spectrometers (*34*). The zero velocity refers to the centroid of the room temperature spectra of metallic iron foil. Analysis of the Mössbauer data was performed with the program WMOSS (WEB Research). Circular dichroism measurements were made under anaerobic conditions in screw top 1-mm cuvettes using a Jasco J-715 spectropolarimeter.

## Results

*Whole cell Mössbauer studies*. Mössbauer spectroscopy was used to investigate the Fe-S cluster content of heterologously expressed recombinant *B. subtilis* BioB in whole cells of an overproducing strain of *E. coli* that was grown on an $^{57}$Fe-enriched medium under anaerobic conditions. Gel densitometry indicated that *B. subtilis* BioB was approximately 20% of the total cellular protein with a concentration of ~120 μM. The results of the whole cell Mössbauer study are shown in Figure 4.1. Control cells lacking the gene for overexpressing BioB, and grown under identical conditions, exhibited broad quadrupole doublets from ferric and ferrous components, see Figure 4.1A, solid line. In contrast, the dominate features in the spectrum of cells with overexpressed BioB are overlapping quadrupole doublets indicative of $[4Fe\text{-}4S]^{2+}$ and $[2Fe\text{-}2S]^{2+}$ clusters in *B. subtilis* BioB, see Figure 4.1A, hatched line. After subtracting the extraneous ferrous and ferric components, the spectrum was fit as the composite of two quadrupole doublets: one corresponding to 66% of the total intensity with isomer shift and quadrupole splitting indicative of a $[2Fe\text{-}2S]^{2+}$ cluster ($\delta = 0.28$ mm/s and $\Delta E_Q = 0.58$ mm/s), and one corresponding to 34% of the total intensity with $\delta = 0.42$ mm/s and $\Delta E_Q = 1.22$ mm/s indicative of $[4Fe\text{-}4S]^{2+}$ cluster, see Figure 4.1C. Hence, in contrast to previously published recombinant *E. coli* BioB whole cell results where only $[2Fe\text{-}2S]^{2+}$ clusters were observed in both aerobically and anaerobically grown cells (*15;27*), recombinant *B. subtilis* BioB in anaerobically grown cells contains both $[2Fe\text{-}2S]^{2+}$ and $[4Fe\text{-}4S]^{2+}$ clusters in an approximate 4:1 ratio, prior to purification.

*As-purified B. subtilis BioB*. Samples of WT and his-tagged *B. subtilis* BioB were purified from aerobically grown cells under both aerobic and anaerobic conditions. Within experimental error, the preparations were essentially identical and indicative of samples with approximately near stoichiometric amounts of $[2Fe\text{-}2S]^{2+}$ clusters and trace amounts of $[4Fe\text{-}4S]^{2+}$ clusters, based on Fe analyses, UV-visible absorption and CD, resonance Raman and Mössbauer spectroscopies, see Table 4.1. Hence the his-tag does not perturb the properties of the $[2Fe\text{-}2S]^{2+}$ center and any $[4Fe\text{-}4S]^{2+}$ clusters that are present prior to purification are significantly degraded during purification. The preparations were found to contain 1.9 ± 0.2 Fe/monomer and exhibited UV/visible absorption spectra and molar extinction coefficients characteristic of approximately one $[2Fe\text{-}2S]^{2+}$ cluster per monomer ($\varepsilon_{453} = 6.9 \pm 1.1$ mM$^{-1}$ cm$^{-1}$ with $A_{453}/A_{278} = 0.20 \pm 0.04$), see Table 4.1 and Figure 4.2a. These properties are very similar to as-purified *E. coli* BioB, see Table 4.1 and Figure 4.2a, ($\varepsilon_{453} = 7.2 \pm 0.8$ mM$^{-1}$ cm$^{-1}$ with $A_{453}/A_{278} = 0.21 \pm 0.02$ and 1.7 ± 0.2 Fe/monomer). However, there are significant differences in the excited state electronic properties of the $[2Fe\text{-}2S]^{2+}$ centers as revealed by both UV-visible absorption and CD, see Figure 4.2. In particular, the band at 417 nm in the as-purified *B. subtilis* BioB spectrum is more intense and blue-shifted compared to the equivalent band in the as-purified *E. coli* BioB spectrum, see Figure 4.2. The differences in absorption and CD properties suggest subtle differences in the local environments of the $[2Fe\text{-}2S]^{2+}$ clusters in the BioBs from *B. subtilis* and *E. coli*.

As is the case with *E. coli* BioB, the $[2Fe\text{-}2S]^{2+}$ cluster of as-purified *B. subtilis* BioB is not reducible to yield a stable $[2Fe\text{-}2S]^{+}$ state and gradually degrades under strongly reducing conditions (5). In the presence of dithionite, the absorption features of the $[2Fe\text{-}2S]^{2+}$ center gradually and irreversibly disappear over a period of several hours (data not shown). Irreversible reductive degradation of the $[2Fe\text{-}2S]^{2+}$ cluster was confirmed by EPR spectroscopy. As-purified *B. subtilis* BioB has no discernible EPR signals as expected for a $S = 0$ $[2Fe\text{-}2S]^{2+}$ cluster. Dithionite reduced samples exhibit a very weak $S = 1/2$ EPR signal accounting for < 0.02 spins per BioB monomer at temperatures below 20 K with g-values and relaxation properties analogous to those of the $[4Fe\text{-}4S]^{+}$ clusters in dithionite-reduced reconstituted samples, see below. Such behavior is similar to that observed for *E. coli* BioB (*5;15*) and is interpreted in terms of reductive degradation of $[2Fe\text{-}2S]^{2+}$ clusters and reconstitution of $[4Fe\text{-}4S]^{2+,+}$ clusters in the radical-SAM active site, under anaerobic reducing conditions.

Mössbauer spectra of aerobically purified BioB are indicative of a homogenous $[2Fe\text{-}2S]^{2+}$ center. A single quadrupole doublet is observed with parameters $\delta = 0.28$ mm/s and $\Delta E_Q = 0.54$ mm/s, see Table 4.1 and Figure 4.3A. These parameters are very similar to the ones observed for the $[2Fe\text{-}2S]^{2+}$ cluster in as-purified *E. coli* BioB. However, aerobically purified samples of *B. subtilis* BioB were found to contain approximately 8% of the total iron in the form of $[4Fe\text{-}4S]^{2+}$ clusters and this increased to approximately 13% of the total iron in anaerobically purified samples, compare Figure 4.3A and 4.3B. Hence the combination of the Mössbauer and Fe analyses indicate that all as-purified samples of *B. subtilis* BioB contain 0.85 ± 0.10 $[2Fe\text{-}2S]^{2+}$ cluster and 0.05 ± 0.20 $[4Fe\text{-}4S]^{2+}$ cluster per BioB monomer, see Table 4.1. This is in contrast to *E. coli* BioB where no $[4Fe\text{-}4S]^{2+}$ clusters were observed in the as-purified form whether purified aerobically or anaerobically (*15*), and presumably reflects the presence of $[4Fe\text{-}4S]^{2+}$ clusters in recombinant *B. subtilis* BioB *in vivo*.

The most striking difference in the spectroscopic properties of the $[2Fe\text{-}2S]^{2+}$ centers in as-purified samples of *B. subtilis* and *E. coli* BioB was apparent in the resonance Raman spectra. A comparison of the resonance Raman spectra obtained using 458-, 488-, and 514-nm excitation is presented in Figure 4.4. In light of the marked differences in the spectra, particularly with 458-nm excitation, and the much broader bands for *B. subtilis* BioB, we explicitly considered the possibility that as-purified *B. subtilis* BioB contains two distinct types of $[2Fe\text{-}2S]^{2+}$; one with a resonance Raman spectrum similar to the $[2Fe\text{-}2S]^{2+}$ cluster in as-purified *E. coli* BioB and one resulting from $O_2$-induced degradation of the $[4Fe\text{-}4S]^{2+}$ cluster in the radical-SAM site during purification. However, several pieces of evidence argue for a homogeneous $[2Fe\text{-}2S]^{2+}$ cluster in as-purified *B. subtilis* BioB. First, the relative intensities of bands in the resonance Raman spectrum were invariant for six distinct preparations, including WT and his-tagged samples purified both aerobically and anaerobically. Likewise, the consistency of UV-visible absorption and CD spectra and Mössbauer parameters for different as-purified samples provides no indication of heterogeneity. Second, resonance Raman spectra, as well as UV-visible absorption and CD spectra, are unchanged on prolonged exposure to $O_2$. In contrast, the $[2Fe\text{-}2S]^{2+}$ cluster that is formed during $O_2$-induced degradation of the radical-SAM $[4Fe\text{-}4S]^{2+}$ cluster in *E. coli* BioB is an intermediate on the degradation pathway and gradually degrades on prolonged exposure to $O_2$ (*15*).

By characterizing the resonance Raman of the $[2Fe\text{-}2S]^{2+}$ centers in *B. subtilis* and *E. coli* BioB at several wavelengths, see Figure 4.4, it becomes apparent that the differences relate primarily to excitation profiles of discrete bands and increased bandwidths as a result of greater heterogeneity in the cluster environment, rather than major frequency shifts in Fe-S stretching modes. Indeed the spectra are in reasonable agreement with 514-nm excitation, a region in which UV-visible absorption and CD studies indicate congruent excited state electronic properties, see Figure 4.2. The close correspondence in vibrational frequencies enables individual bands to be assigned by direct analogy with the assignments made for *E. coli* BioB (*5*). The only major frequency shift is a 7-$cm^{-1}$ downshift for the totally symmetric Fe-S(Cys) ($A_g^t$) mode which is assigned to bands at 349 and 342 $cm^{-1}$ in *E. coli* and *B. subtilis* BioB, respectively. The other major difference is the appearance of a pronounced band at 288 $cm^{-1}$ in the *B. subtilis* BioB spectra. It would appear that two bands overlap to give the intense 301 cm$^{-1}$ band in *E. coli* BioB and that one of them shifts to lower frequency in *B. subtilis* BioB. These two modes are likely to be the Fe-S-C bending mode and out-of-phase symmetric Fe-S(Cys) ($B_{3u}^{t}$) stretching modes (*35*). Since studies with mutant [2Fe-2S] ferredoxins indicate that the $A_g^t$ and $B_{3u}^t$ Fe-S(Cys) stretching modes are very sensitive to anomalous coordination at one Fe site (*5*), and both shift in the same direction in response to a change from S to O ligation, it is tempting to assign the 288 cm$^{-1}$ band to the $B_{3u}^t$ Fe-S(Cys) stretching mode and attribute the downshifts in both the $A_g^t$ and $B_{3u}^t$ Fe-S(Cys) stretching modes to a change in the nature of the non-cysteinyl ligand in *B. subtilis* BioB. Indeed the high frequencies of the $A_g^t$ and $B_{3u}^t$ Fe-S(Cys) stretching modes in *E. coli* BioB provided the initial evidence for a [2Fe-2S] cluster ligated with three cysteinyl and one O or N (non-histidine) ligand (*5*), which was subsequently identified as arginine based on the low resolution crystal structure (*8*). Although the arginine is conserved in *B. subtilis* BioB, the resonance Raman results raise the possibility that it may not be a cluster ligand in this case. However, we cannot rule out the possibility that the frequency shifts in the $A_g^t$ and $B_{3u}^t$ Fe-S(Cys) stretching modes in *B. subtilis* BioB arise from changes in the Fe-S-C-C dihedral angles of one or more of the coordinated cysteines (*35*).

*Reconstituted forms of B. subtilis BioB.* Since as-purified forms of *B. subtilis* BioB were largely devoid of the catalytically essential [4Fe-4S]$^{2+}$ cluster in the radical-SAM cluster binding site, attempts were made to reconstitute the cluster using the same procedures that have proven successful with *E. coli* BioB (*13;15*). Two forms of reconstituted *E. coli* BioB have been prepared. Anaerobic reconstitution of apo BioB resulted in [4Fe-4S] BioB with stoichiometric [4Fe-4S]$^{2+}$ clusters in the radical-SAM cluster binding site, whereas anaerobic reconstitution of as-purified BioB resulted in [2Fe-2S]/[4Fe-4S] BioB with near stoichiometric amounts of both

$[2Fe\text{-}2S]^{2+}$ and $[4Fe\text{-}4S]^{2+}$ clusters. Since apo forms of *B. subtilis* BioB were unstable and readily precipitated in solution, only the latter type of reconstitution was attempted. The results are consistent with separate [2Fe-2S] and [4Fe-4S] cluster binding sites, but in contrast to *E. coli* BioB, they indicate that degradation of the $[2Fe\text{-}2S]^{2+}$ cluster occurs concomitant with assembly of a $[4Fe\text{-}4S]^{2+}$ cluster in the radical-SAM cluster binding site.

Initial reconstitution attempts mimicked those used for formation of [2Fe-2S]/[4Fe-4S] *E. coli* BioB, i.e., anaerobic addition of a 10-fold excess of $FeCl_3$ or $Fe(NH_4)_2(SO_4)_2$ and $Na_2S$ and incubation for 1 hour before repurification using anion exchange chromatography. The resulting samples contained 3.5 ± 0.3 Fe/BioB (average of three experiments) compared to 4.3 ± 0.3 Fe/BioB for *E. coli* BioB (*15*) and representative Mössbauer, UV-visible absorption, and resonance Raman spectra are compared to those obtained for *E. coli* BioB in Figures 4.3, 4.5, and 4.6. Mössbauer gives the most reliable estimate of cluster content, and analysis of the Mössbauer spectrum in terms of the Fe content indicates 0.63 ± 0.06 $[2Fe\text{-}2S]^{2+}$ and 0.35 ± 0.04 $[4Fe\text{-}4S]^{2+}$ cluster per BioB monomer. This analysis is in quantitative agreement with the absorption data, using the $[2Fe\text{-}2S]^{2+}$ cluster spectrum and molar extinction coefficients for *B. subtilis* BioB and the $[4Fe\text{-}4S]^{2+}$ cluster spectrum and molar extinction coefficient established for *E. coli* [4Fe-4S] BioB (*15*). The presence of $[4Fe\text{-}4S]^{2+}$ clusters is not readily apparent in the resonance Raman because $[2Fe\text{-}2S]^{2+}$ cluster typically have 5-10-fold greater resonance enhancement than $[4Fe\text{-}4S]^{2+}$ clusters using 458-nm excitation. The only indication is the increased intensity at 338 $cm^{-1}$, corresponding to the totally symmetric breathing mode of the $[4Fe\text{-}4S]^{2+}$ cluster, which is by far the most intense band in the resonance Raman spectrum of *E. coli* [4Fe-4S] BioB, see Figure 4.6. Overall the results indicate a lower level of $[4Fe\text{-}4S]^{2+}$ reconstitution (0.35 $[4Fe\text{-}4S]^{2+}$ clusters/BioB) than for *E. coli* BioB (0.66 [4Fe-

4S]$^{2+}$clusters/BioB) and suggest that a larger decrease in [2Fe-2S]$^{2+}$ cluster degradation accompanies [4Fe-4S]$^{2+}$ cluster reconstitution (from 0.85 to 0.63 [2Fe-2S]$^{2+}$ clusters/BioB for *B. subtilis* BioB and from 0.85 to 0.75 [2Fe-2S]$^{2+}$ clusters/BioB for *E. coli* BioB), see Table 4.1.

Longer incubation periods were used in reconstitution experiments in an attempt to effect more complete [4Fe-4S]$^{2+}$ cluster reconstitution. Samples reconstituted for between 4 and 6 hours were found to have between 4.5 and 6.5 Fe/BioB following repurification and the Fe content correlated with the reconstitution time within experimental error. UV-visible absorption, Mössbauer and resonance Raman studies of these samples indicate near stoichiometric amounts of [4Fe-4S]$^{2+}$ clusters and low or negligible amounts of [2Fe-2S]$^{2+}$ clusters. The Mössbauer spectrum of a sample that was reconstituted for 4 hours and contained 4.5 Fe/BioB is shown in Figure 4.3D. The spectrum is dominated by the quadrupole doublet from [4Fe-4S]$^{2+}$ cluster which accounts for 60% of the total Fe and therefore corresponds to approximately 0.68 [4Fe-4S]$^{2+}$ clusters/BioB, see Table 4.1 and Figure 4.3D. It is difficult to assess the contribution from [2Fe-2S]$^{2+}$ because of the underlying signal from adventitiously bound Fe species. The maximal amount that can be accommodated is shown in Figure 4.3D, and corresponds to 13% of the Fe which translates to 0.30 [2Fe-2S]$^{2+}$ clusters/BioB. However, as the Mössbauer data can be fit to a good approximation without a contribution from a [2Fe-2S]$^{2+}$ cluster, the actual stoichiometry is likely to be substantially < 0.30 [2Fe-2S]$^{2+}$ clusters/BioB.

The UV-visible absorption spectra of samples of *B. subtilis* BioB that have been reconstituted for 4-6 hours before repurification are characterized by a broad shoulder centered at 410 nm, see Figure 4.5 left panel, which is characteristic of a [4Fe-4S]$^{2+}$ cluster. Moreover, the $\varepsilon_{410}$ values and $A_{410}/A_{280}$ ratios correlate with the incubation time indicating increasing assembly of [4Fe-4S]$^{2+}$ clusters in the radical-SAM site. Likewise resonance Raman spectra show a progressive increase in bands associated with $[4Fe\text{-}4S]^{2+}$ clusters, relative to the bands associated with the $[2Fe\text{-}2S]^{2+}$ cluster, with increasing incubation time. Figure 4.6c compares the resonance Raman spectrum of *B. subtilis* BioB repurified after 6 hours of reconstitution with that of the *E. coli* [4Fe-4S] BioB which has the $[4Fe\text{-}4S]^{2+}$ cluster in the radical-SAM cluster binding site as the sole prosthetic group (*15*). The Fe-S stretching modes of the $[4Fe\text{-}4S]^{2+}$ in *E. coli* BioB have been assigned by analogy with other well-characterized biological $[4Fe\text{-}4S]^{2+}$ centers (*15*) and the same bands clearly dominate the spectrum of the reconstituted BioB sample, albeit overlapped with those originating from the $[2Fe\text{-}2S]^{2+}$ cluster. In light of 5-10-fold greater resonance enhancement of the $[2Fe\text{-}2S]^{2+}$ center, the resonance Raman data indicates that the ratio of $[4Fe\text{-}4S]^{2+}$ to $[2Fe\text{-}2S]^{2+}$ clusters in the reconstituted *B. subtilis* BioB sample is greater than 10:1.

Direct confirmation and quantitation of the degradation of $[2Fe\text{-}2S]^{2+}$ cluster during reconstitution of the $[4Fe\text{-}4S]^{2+}$ cluster on *B. subtilis* BioB was provided by CD spectroscopy and additional Mössbauer studies. The negligible UV-visible CD intensity for $[4Fe\text{-}4S]^{2+}$ centers compared to $[2Fe\text{-}2S]^{2+}$ centers in proteins (*36*) makes CD a convenient method for monitoring the fate of the $[2Fe\text{-}2S]^{2+}$ cluster during reconstitution of *B. subtilis* BioB. In these experiments IscS and cysteine were used to slow down sulfide production and thereby minimize light scattering problems resulting from the formation of colloidal precipitates of iron sulfide. A time course of the changes in the UV-visible absorption and CD spectra for a reconstitution reaction mixture containing 500 μM as-purified *B. subtilis* BioB, with 10 mM DTT, a 10-fold excess of ferrous ammonium sulfate and L-cysteine, and IscS in a 1:50 ratio to BioB, is shown in Figure 4.7. The degradation of the $[2Fe\text{-}2S]^{2+}$ cluster is clearly evident in the CD data and is shown to be approximately linear in time over an 8-hour period to yield a sample with only 25% of the original $[2Fe\text{-}2S]^{2+}$ cluster content. The absorption changes over the first 6 hours indicate the concomitant assembly of $[4Fe\text{-}4S]^{2+}$ clusters, with further incubation resulting in the production of colloidal iron sulfides.

The ability of Mössbauer to selectively monitor $^{57}$Fe also provides a method for monitoring the fate of the $[2Fe\text{-}2S]^{2+}$ cluster during reconstitution. The experiment involves using as-purified *B. subtilis* BioB purified from cells grown on $^{57}$Fe-enriched media and recording the Mössbauer spectrum of the reaction mixture before and after reconstitution with a 10-fold excess of $^{56}FeCl_3$ and $Na_2S$. The results are shown in Figure 4.8A and 4.8B, respectively. Before reconstitution, 96% of the $^{57}$Fe in the sample is in the form of $[2Fe\text{-}2S]^{2+}$ clusters. After 6 hours of reconstitution, ~15% of the $^{57}$Fe is in the form $[4Fe\text{-}4S]^{2+}$ clusters with the remainder almost exclusively present as extraneous $Fe^{II}$ or $Fe^{III}$ species. The implication is that almost all the $[2^{57}Fe\text{-}2S]^{2+}$ clusters have degraded and that some of the resulting $^{57}$Fe has been used in the assembly of $[4Fe\text{-}4S]^{2+}$ clusters. To obtain a more quantitative assessment of the extent $[2Fe\text{-}2S]^{2+}$ cluster degradation, the Mössbauer spectrum was also recorded after repurification to remove extraneous Fe species, see Figure 4.8C. The resulting spectrum has $^{57}$Fe in $[4Fe\text{-}4S]^{2+}$ and $[2Fe\text{-}2S]^{2+}$ clusters in a 3:1 ratio, indicating that only 5% of the original $[2Fe\text{-}2S]^{2+}$ clusters remain after reconstituting for 6 hours.

The spectroscopic and analytical results for *B. subtilis* BioB clearly point to concomitant degradation of the $[2Fe\text{-}2S]^{2+}$ cluster and assembly of the $[4Fe\text{-}4S]^{2+}$ cluster during prolonged reconstitution of the as-purified sample. This result is in direct contrast to *E. coli* BioB where parallel studies indicated no significant degradation of the $[2Fe\text{-}2S]^{2+}$ cluster during reconstitution of the $[4Fe\text{-}4S]^{2+}$ cluster in the radical-SAM cluster binding site. The $[4Fe\text{-}4S]^{2+}$ cluster-containing form of *B. subtilis* BioB that was generated via reconstitution was used in activity assays and in experiments to assess the redox and SAM-binding properties of the [4Fe-4S]$^{2+}$ cluster.

*Redox and SAM binding properties of the [4Fe-4S] cluster*. The presence of a redox active [4Fe-4S]$^{2+,+}$ cluster in reconstituted samples of *B. subtilis* BioB was demonstrated using X-band EPR spectroscopy. EPR spectra were recorded for repurified samples that had been reconstituted for 6 hours, both before and after anaerobic reduction with a 10-fold excess of sodium dithionite. In accord with the absorption, Mössbauer and resonance Raman evidence for a $S = 0$ [4Fe-4S]$^{2+}$ cluster, the non-reduced sample did not have any EPR signals indicative of paramagnetic Fe-S cluster and exhibited only a slow relaxing isotropic $g = 2.00$ feature, that remained visible at temperatures greater than 70 K, indicative of minor organic radical species (data not shown). Parallel UV-visible absorption studies indicated that the [4Fe-4S]$^{2+}$ cluster was ~50% reduced on addition of dithionite and EPR studies revealed a mixed spin [4Fe-4S]$^{+}$ cluster with a near-axial, fast-relaxing $S = 1/2$ resonance ($g_{\|} = 2.04$ and $g_{\perp} = 1.94$) accounting for 0.3 spins/BioB, see Figure 4.9, and a weak $S = 3/2$ ($E/D \sim 0.15$) resonance with low-field components at $g = 5.7$ and 4.8 (data not shown). Similar EPR characteristics have previously been reported for [4Fe-4S]$^{+}$ clusters in the radical-SAM cluster binding site of *E. coli* BioB (*5;37*). The results indicate a [4Fe-4S]$^{2+,+}$ cluster in the radical-SAM cluster binding site of *B. subtilis* BioB with a redox potential close to that of sodium dithionite at pH 8, i.e. ~ –430 mV (vs NHE).

The $O_2$ sensitivity and SAM-binding ability of the [4Fe-4S]$^{2+}$ cluster in reconstituted *B. subtilis* BioB were investigated using resonance Raman spectroscopy. Figure 4.6d demonstrates that the [4Fe-4S]$^{2+}$ cluster in reconstituted *B. subtilis* BioB mirrors the behavior of the [4Fe-4S]$^{2+}$ cluster in *E. coli* [4Fe-4S] BioB on exposure to $O_2$. Both are rapidly degraded via a semi-stable

$[2Fe\text{-}2S]^{2+}$ cluster intermediate that exhibits a characteristic resonance Raman spectrum comprising broad bands centered at ~290, 336, 366 and 395 $cm^{-1}$. Similar resonance Raman spectra have been observed during $O_2$-induced degradation of active-site $[4Fe\text{-}4S]^{2+}$ clusters in numerous radical-SAM enzymes (*15*) and this $O_2$-induced cluster conversion appears to be a unifying attribute of $[4Fe\text{-}4S]^{2+}$ clusters in a radical-SAM cluster binding motif. Figure 4.10 shows that the changes in the resonance Raman properties of the $[4Fe\text{-}4S]^{2+}$ cluster in reconstituted *B. subtilis* BioB on addition of excess SAM also mirror those of the $[4Fe\text{-}4S]^{2+}$ cluster in *E. coli* [4Fe-4S] BioB. While some of the $[4Fe\text{-}4S]^{2+}$ Raman bands in *B. subtilis* BioB are obscured by overlap with bands from the $[2Fe\text{-}2S]^{2+}$, the 3-4 $cm^{-1}$ downshift in the band at 253 $cm^{-1}$, the 3-4 $cm^{-1}$ upshift in the band at 338 $cm^{-1}$, and the appearance of a band at ~420 $cm^{-1}$, were all shown to be hallmarks of SAM binding to the active-site $[4Fe\text{-}4S]^{2+}$ cluster in *E. coli* [4Fe-4S] BioB (*7*). These spectroscopic studies leave no doubt that the $[4Fe\text{-}4S]^{2+}$ cluster reconstituted in *B. subtilis* BioB is assembled in the radical-SAM cluster binding site and is competent for binding and reductive cleavage of SAM.

*Activity of B. subtilis BioB*. The activity of as-purified and 6-hour-reconstituted *B. subtilis* BioB was assessed as a function of time and compared to that of *E. coli* BioB prepared under the same conditions, see Figure 4.11. The cluster content of the samples used for activity assays as assessed by spectroscopic and analytical data were as follows: as-purified *B. subtilis* BioB, 0.85 $[2Fe\text{-}2S]^{2+}$ and 0.07 $[4Fe\text{-}4S]^{2+}$; as-purified *E. coli* BioB, 0.85 $[2Fe\text{-}2S]^{2+}$; reconstituted *B. subtilis* BioB, < 0.1 $[2Fe\text{-}2S]^{2+}$ and 0.8 $[4Fe\text{-}4S]^{2+}$; reconstituted *E. coli* BioB, 0.7 $[2Fe\text{-}2S]^{2+}$ and 0.7 $[4Fe\text{-}4S]^{2+}$. In agreement with previously published data for *E. coli* BioB (*12;15;20;21;23*), neither form of *B. subtilis* BioB was capable of more than a single turnover per BioB monomer after 24 hours at 25 ºC. In contrast to as-purified *E. coli* BioB which had negligible activity, as-purified *B. subtilis* BioB exhibited significant activity corresponding to 0.20 ± 0.03 nmol biotin per nmol BioB monomer. This activity is tentatively attributed to the presence of some catalytically competent $[4Fe\text{-}4S]^{2+}$ clusters in as-purified *B. subtilis* BioB. The reconstituted samples of both *B. subtilis* and *E. coli* BioB were both competent for one complete turnover in 24 hours at 25 ºC based on $[4Fe\text{-}4S]^{2+}$ cluster content (0.77 ± 0.12 verses 0.84 ± 0.12 nmol biotin per nmol BioB monomer, respectively). These activity data were surprising in light of the proposed role of the $[2Fe\text{-}2S]^{2+}$ cluster as the immediate S-donor to DTB, and indicate that a sulfur-containing [2Fe-2S] cluster degradation product is a competent S-donor for biotin biosynthesis.

## Discussion

Recombinant *E. coli* BioB has been extensively characterized over the past decade and shown to be a member of the radical-SAM family of enzymes with two distinct cluster binding sites (*1;5;8;14;15*). One is shared with all other radical-SAM enzymes and accommodates a redox-active and oxidatively labile $[4Fe\text{-}4S]^{2+,+}$ cluster ligated by three conserved cysteines that is responsible for anchoring SAM at the unique Fe site in order to effect reductive cleavage of SAM and generation of the transient 5'-deoxyadenosyl radical (*4;7;8*). The other accommodates an oxidatively inert and reductively labile $[2Fe\text{-}2S]^{2+}$ cluster (*5;14;15*) ligated by three conserved cysteines and one conserved arginine (*8*), that is competent to act as a sacrificial S-donor during a single enzyme turnover (*18-22*). However, there are many puzzling aspects and unresolved questions concerning the proposed role of the $[2Fe\text{-}2S]^{2+}$ cluster as a sacrificial S-donor. First, despite intensive efforts in many research groups it has not been possible to facilitate turnover *in vitro* via reassembly of the $[2Fe\text{-}2S]^{2+}$ cluster using components of ISC machinery. Moreover, the crystal structure shows the $[2Fe\text{-}2S]^{2+}$ cluster is buried and likely to be very difficult to reassemble without removal of the [4Fe-4S] cluster (*8*). However, the available evidence indicates that BioB is capable of multiple turnovers *in vivo* (*17*). Second, the recombinant enzyme is expressed in the cell as an inactive enzyme containing only the $[2Fe\text{-}2S]^{2+}$ cluster (*27*). This has raised the possibility that the $[2Fe\text{-}2S]^{2+}$ cluster may be an artifact of recombinant overexpression and that the immediate S-donor to DTB may be a degradation product of the $[2Fe\text{-}2S]^{2+}$ cluster, rather than the cluster itself (*21;27*). In order to address these questions, it was clearly important to characterize the cluster composition and activity of a BioB other than *E. coli* BioB. This has now been accomplished with heterologously expressed *B. subtilis* BioB which has only 28% sequence homology with *E. coli* BioB, but has the conserved residues (six cysteines and one arginine) that serve as cluster ligands in *E. coli* BioB. As discussed below, the results reveal similarities and differences compared to *E. coli* BioB and show that the presence of an intact $[2Fe\text{-}2S]^{2+}$ cluster is not required for biotin production in a single turnover reaction.

Mössbauer studies of anaerobically grown whole cells indicate that heterologously expressed wild-type *B. subtilis* BioB contains both $[4Fe\text{-}4S]^{2+}$ and $[2Fe\text{-}2S]^{2+}$ clusters in a 1:4 ratio, whereas parallel studies of homologously expressed wild-type *E. coli* BioB revealed only $[2Fe\text{-}2S]^{2+}$ clusters (*27*). The reason for this difference is unclear but may be a consequence of much lower levels of expression for *B. subtilis* BioB. Moreover, it is unclear if the *in vivo* results should be interpreted in terms of recombinant *B. subtilis* BioB being present in the cell as a mixture of forms containing solely $[2Fe\text{-}2S]^{2+}$ or $[4Fe\text{-}4S]^{2+}$ clusters or one form containing only $[2Fe\text{-}2S]^{2+}$ clusters and another containing both $[2Fe\text{-}2S]^{2+}$ and $[4Fe\text{-}4S]^{2+}$ clusters. Both scenarios can be rationalized based on the available *in vitro* studies. For example, the *in vitro* reconstitution studies presented in this work indicate that *B. subtilis* BioB is either unable to accommodate both types of cluster simultaneously or that the $[2Fe\text{-}2S]^{2+}$ cluster is unstable under *in vitro* reconstitution conditions. As yet there is no direct evidence in support of the proposal that the *E. coli* Fe-S cluster assembly machinery is capable of assembling both $[4Fe\text{-}4S]^{2+}$ and [2Fe-2S] clusters in BioB

Although both enzymes are purified in a form almost completely devoid of the catalytically essential $[4Fe\text{-}4S]^{2+}$ cluster in the radical-SAM binding site, $[4Fe\text{-}4S]^{2+}$ clusters with very similar properties are readily assembled in both enzymes under standard *in vitro* Fe-S cluster reconstitution conditions. The $S = 0$ $[4Fe\text{-}4S]^{2+}$ clusters assembled in both enzymes exhibit analogous UV-visible absorption, Mössbauer and resonance Raman spectra. EPR studies indicate that both are partially reduced to mixed spin ($S = 1/2$ and $3/2$) $[4Fe\text{-}4S]^{+}$ clusters on addition of dithionite. Resonance Raman studies also demonstrate that the $[4Fe\text{-}4S]^{2+}$ clusters in both enzymes bind SAM in the same way and are rapidly degraded in air via an analogous $[2Fe\text{-}2S]^{2+}$ cluster intermediate.

The as-purified samples of recombinant *B. subtilis* and *E. coli* BioB both contain near stoichiometric amounts of $[2Fe\text{-}2S]^{2+}$ clusters that are oxidatively inert and reductively labile. However, they show some interesting differences in excited state electronic structure as revealed by UV-visible absorption and CD, and resonance Raman excitation profiles, and in cluster ligation or environment as revealed by significant changes in the frequencies of resonance Raman bands associated primarily with Fe-S(Cys) stretching modes. These differences most likely relate to the nature of the non-cysteinyl ligand, which appears to be arginine in *E. coli* based on the 3.4-Å resolution crystal structure, or to changes in the dihedral angles of one or more of the ligated cysteine residues. Most dramatically, the $[2Fe\text{-}2S]^{2+}$ clusters in as prepared samples of *B. subtilis* and *E. coli* BioB, differ in their behavior under the conditions required to reconstitute the catalytically essential $[4Fe\text{-}4S]^{2+}$ cluster in the radical-SAM cluster binding site. In contrast to *E. coli* BioB, where the $[2Fe\text{-}2S]^{2+}$ cluster remains essentially intact during reconstitution of the $[4Fe\text{-}4S]^{2+}$ cluster (*14;15*), the $[2Fe\text{-}2S]^{2+}$ cluster in *B. subtilis* BioB degrades concomitant with the assembly of the $[4Fe\text{-}4S]^{2+}$ cluster. The implication is that *B. subtilis* BioB can only accommodate a cluster in one or the other of the two binding sites or that the $[2Fe\text{-}2S]^{2+}$ clusters in *B. subtilis* and *E. coli* BioB differ substantially in their stability under *in vitro* Fe-S cluster reconstitution conditions.

The most intriguing result in relation to understanding the mechanism of BioB is that degradation of the $[2Fe\text{-}2S]^{2+}$ cluster during reconstitution of the $[4Fe\text{-}4S]^{2+}$ cluster on *B. subtilis* BioB has no significant effect on biotin production in single turnover experiments, when compared to reconstituted *E. coli* BioB samples in which the $[2Fe\text{-}2S]^{2+}$ cluster is intact. Since sulfur isotope and Se labeling studies have shown that the $[2Fe\text{-}2S]^{2+}$ cluster can act as S-donor during a single turnover (*18;19*) and spectroscopic studies concur in finding $[2Fe\text{-}2S]^{2+}$ cluster degradation during biotin formation (*20-22*), the implication is that a S-containing degradation product of the $[2Fe\text{-}2S]^{2+}$ cluster is competent for insertion into DTB. This conclusion is further supported by the low activity observed for *E. coli* [4Fe-4S] BioB which is formed by reconstitution of the apo protein (*14;15*), and is consistent with Mössbauer studies which revealed that $[2Fe\text{-}2S]^{2+}$ cluster degradation during a single turnover of *E. coli* BioB occurs at least an order of magnitude faster than the initial rate of biotin production (*21*). It is important to emphasize that these new results do not rule out the possibility that $[2Fe\text{-}2S]^{2+}$ cluster degradation and reassembly is intrinsic to enzymatic biotin biosynthesis. Under such a scenario, the results reported would merely dictate that cluster breakdown precedes the S-insertion step into DTB. However, the *B. subtilis* BioB results do show that the $[2Fe\text{-}2S]^{2+}$ cluster is not required for biotin production in a single turnover reaction. Consequently they add support to the alternative proposal in which the $[2Fe\text{-}2S]^{2+}$ cluster is an artifact of recombinant expression that occupies the site of the physiological S-donor and can form the physiological S-donor species on degradation (*21;27*). Catalytic turnover would then require the biochemical machinery for reformation of the S species rather than reassembly of the $[2Fe\text{-}2S]^{2+}$ cluster.

The nature of the functional S-donor species in purified samples of reconstituted *B. subtilis* BioB has yet to be determined. The most obvious candidates would be a cysteine persulfide or polysulfide which would require formal two-electron oxidation of one of the bridging sulfides. The origin of the oxidizing equivalents is unclear although the ferric ions of the $[2Fe\text{-}2S]^{2+}$ cluster are the most obvious candidates. A sulfide species seems unlikely in light of the low activity observed for the *E. coli* [4Fe-4S] BioB which is formed by reconstitution of the apo protein in the presence of excess sulfide (*14;15*). Clearly there is a pressing need to purify and characterize a native, non-recombinant form of BioB in order to directly address the physiological relevance of the $[2Fe\text{-}2S]^{2+}$ cluster and to investigate the nature of the S-donor species in reconstituted forms of *B. subtilis* BioB. Such experiments are ongoing in our laboratories.

## References

1. Jarrett, J. T. (2005) The novel structure and chemistry of iron-sulfur clusters in the adenosylmethionine-dependent radical enzyme biotin synthase, *Arch. Biochem. Biophys. 433*, 312-321.

2. Birch, O. M., Fuhrmann, M., and Shaw, N. M. (1995) Biotin synthase from *Escherichia coli*, and investigation of the low molecular weight and protein components required for activity *in vitro*., *J. Biol. Chem. 270*, 19158-19165.

3. Guianvarc'h, D., Florentin, D., Tse Sum Bui, B., Nunzi, F., and Marquet, A. (1997) Biotin synthase, a new member of the family of enzymes which uses S-adenosylmethionine as a source of deoxyadenosyl radical, *Biochem. Biophys. Res. Com. 236*, 402-406.

4. Sofia, H. J., Chen, G., Hetzler, B. G., Reyes-Spindola, J. F., and Miller, N. E. (2001) Radical SAM, a novel protein superfamily linking unresolved steps in familiar biosynthetic pathways with radical mechanisms: Functional characterization using new analysis and information visualization methods, *Nucleic Acids Res. 29*, 1097-1106.

5. Duin, E. C., Lafferty, M. E., Crouse, B. R., Allen, R. M., Sanyal, I., Flint, D. H., and Johnson, M. K. (1997) [2Fe-2S] to [4Fe-4S] cluster conversion in *Escherichia coli* biotin synthase, *Biochemistry 36*, 11811-11820.

6. Ollagnier-de-Choudens, S., Sanakis, Y., Hewitson, K. S., Roach, P. L., Münck, E., and Fontecave, M. (2002) Reductive cleavage of *S*-adenosylmethionine by biotin synthase from *Escherichia coli*, *J. Biol. Chem. 277*, 13449-13454.

7. Cosper, M. M., Jameson, G. N. L., Davydov, R., Eidsness, M. K., Hoffman, B. M., Huynh, B. H., and Johnson, M. K. (2002) The $[4Fe\text{-}4S]^{2+}$ cluster in reconstituted biotin synthase binds *S*-adenosylmethionine, *J. Am. Chem. Soc. 124*, 14006-14007.

8. Berkovitch, F., Nicolet, Y., Wan, J. T., Jarrett, J. T., and Drennan, C. L. (2004) Crystal structure of biotin synthase, an *S*-adenosylmethionine-dependent radical enzyme, *Science 303*, 76-79.

9. Shaw, N. M., Birch, O. M., Tinschert, A., Venetz, V., Dietrich, R., and Savoy, L.-A. (1998) Biotin synthase from *Escherichia coli*: Isolation of an enzyme-generated intermediate and stoichiometry of *S*-adenosylmethionine use, *Biochem. J. 330*, 1079-1085.

10. Escalettes, F., Florentin, D., Tse Sum Bui, B., Lesage.D., and Marquet, A. (1999) Biotin synthase mechanism: Evidence for hydrogen transfer from the substrate into deoxyadenosine, *J. Am. Chem. Soc. 121*, 3571-3578.

11. Ugulava, N. B., Frederick, K. K., and Jarrett, J. T. (2003) Control of adenosylmethionine-dependent radical generation in biotin synthase: A kinetic and thermodynamic analysis of substrate binding to active and inactive forms of BioB, *Biochemistry 42*, 2708-2719.

12. Ollagnier-de-Choudens, S., Mulliez, E., and Fontecave, M. (2002) The PLP-dependent biotin synthase from *Escherichia coli*: mechanistic studies, *FEBS Lett. 532*, 465-468.

13. Ugulava, N. B., Gibney, B. R., and Jarrett, J. T. (2001) Biotin synthase contains two distinct iron-sulfur cluster binding sites: Chemical and spectroelectrochemical analysis of iron-sulfur cluster interconversions, *Biochemistry 40*, 8343-8351.

14. Ugulava, N. B., Surerus, K. K., and Jarrett, J. T. (2003) Evidence from Mössbauer spectroscopy for distinct $[2Fe\text{-}2S]^{2+}$ and $[4Fe\text{-}4S]^{2+}$ cluster binding sites in biotin synthase from *Escherichia coli*, *J. Am. Chem. Soc. 124*, 9050-9051.

15. Cosper, M. M., Krebs, B., Hernandez, H., Jameson, G., Eidsness, M. K., Huynh, B. H., and Johnson, M. K. (2004) Characterization of the cofactor content of *Escherichia coli* biotin synthase, *Biochemistry 43*, 2007-2021.

16. Sanyal, I., Cohen, G., and Flint, D. H. (1994) Biotin synthase: Purification, characterization as a [2Fe-2S] cluster protein, and *in vitro* activity of the *Escherichia coli bioB* gene product, *Biochemistry 33*, 3625-3631.

17. Choi-Rhee, E. and Cronan, J. E. (2005) Biotin synthase is catalytic in vivo, but catalysis endangers destruction of the protein, *Chemistry and Biology 12*, 461-468.

18. Tse Sum Bui, B., Florentin, D., Fournier, F., Ploux, O., Méjean, A., and Marquet, A. (1998) Biotin synthase mechanism: On the origin of sulfur, *FEBS Lett. 440*, 226-230.

19. Tse Sum Bui, B., Mattioli, T., Florentin, D., Bolbach, G., and Marquet, A. (2006) *Escherichia coli* biotin synthase produces selenobiotin. Further evidence of the involvement of the $[2Fe\text{-}2S]^{2+}$ cluster in the sulfur insertion step, *Biochemistry 45*, 3824-3834.

20. Ugulava, N. B., Sacanell, C. J., and Jarrett, J. T. (2001) Spectroscopic changes during a single turnover of biotin synthase: Destruction of a [2Fe-2S] cluster accompanies sulfur insertion, *Biochemistry 40*, 8352-8358.

21. Jameson, G. N. L., Cosper, M. M., Hernández, H. L., Johnson, M. K., and Huynh, B. H. (2004) Role of the [2Fe-2S] cluster in recombinant *Escherichia coli* biotin synthase, *Biochemistry 43*, 2022-2031.

22. Tse Sum Bui, B., Benda, R., Schünemann, V., Florentin, D., Trautwein, A. X., and Marquet, A. (2003) Fate of the $[2Fe\text{-}2S]^{2+}$ cluster of *Escherichia coli* biotin synthase during reaction" A Mössbauer characterization., *Biochemistry 42*, 8791-8798.

23. Ollagnier-de-Choudens, S., Mulliez, E., Hewitson, K. S., and Fontecave, M. (2002) Biotin synthase is a pyridoxal phosphate-dependent cysteine desulfurase, *Biochemistry 41*, 9145-9152.

24. Méjean, A., Tse Sum Bui, B., Florentin, D., Ploux, O., Izumi, Y., and Marquet, A. (1995) Highly purified biotin synthase can transform dethiobiotin into biotin in the absence of

any other protein in the presence of photoreduced deazaflavin, *Biochem. Biophys. Res. Commun. 217*, 1231-1237.

25. Kiyasu, T., Asakura, A., Nagahashi, Y., and Hoshino, T. (2002) Biotin synthase of *Bacillus subtilis* shows less reactivity than that of *Escherichia coli* in in vitro reaction systems, *Arch. Microbiol. 179*, 26-32.

26. Baldet, P., Alban, C., and Douce, R. (1997) Biotin synthesis in higher plants: purification and characterization of the *bioB* gene product equivalent from *Arabidopsis thaliana* overexpressed in *Escherichia coli* and its subcellular location in pea leaf cells, *FEBS Lett. 419*, 206-210.

27. Cosper, M. M., Jameson, G. N. L., Eidsness, M. K., Huynh, B. H., and Johnson, M. K. (2002) Recombinant *Escherichia coli* biotin synthase is a $[2Fe\text{-}2S]^{2+}$ protein in whole cells, *FEBS Lett. 529*, 332-336.

28. Tabor, S. (1990) Expression using the T7 RNA polymerase/promotor system, in *Current Protocols in Molecular Biology* (Ausubel, F. A., Brent, R., Kingston, R. E., Moore, D. D., Seidman, J. G., Smith, J. A., and Sthuhl, K., Eds.) pp 16.2.1-16.2.11, Greene Publishing and Wiley Interscience, New York.

29. Harwood, C. R. and Cutting, S. M. (1990) *Modern Microbiological Methods: Molecular Biology Methods for Bacillus* Wiley and Sons, Chichester, UK.

30. Fish, W. W. (1988) Rapid colorimetric micromethod for the quantitation of complexed iron in biological samples, *Meth. Enzymol. 158*, 357-364.

31. Tanaka, M., Izumi, Y., and Yamada, H. (1987) Biotin assay using lyophilized and glycerol-suspended cultures, *J. Microbiol. Meth. 6*, 237-246.

32. Tse Sum Bui, B. and Marquet, A. (1997) Biotin synthase of *Bacillus sphaericus*, *Meth. Enzymol. 279*, 357-362.

33. Drozdzewski, P. M. and Johnson, M. K. (1988) A simple anaerobic cell for low temperature Raman spectroscopy, *Appl. Spectrosc. 42*, 1575-1577.

34. Ravi, N., Bollinger, J. M., Huynh, B. H., Edmondson, D. E., and Stubbe, J. (1994) Mechanism of assembly of the tyrosyl radical-diiron(III) cofactor of *E. coli* ribonucleotide reductase. 1. Mössbauer characterization of the diferric radical precusor, *J. Am. Chem. Soc. 116*, 8007-8014.

35. Han, S., Czernuszewicz, R. S., and Spiro, T. G. (1989) Vibrational spectra and normal mode analysis for [2Fe-2S] protein analogues using $^{34}S$, $^{54}Fe$, and $^{2}H$ substitution: Coupling of Fe-S stretching and S-C-C bending modes, *J. Am. Chem. Soc. 111*, 3496-3504.

36. Stephens, P. J., Thomson, A. J., Dunn, J. B. R., Keiderling, T. A., Rawlings, J., Rao, K. K., and Hall, D. O. (1978) Circular dichroism and magnetic circular dichroism of iron-sulfur proteins, *Biochemistry 17*, 4770-4778.

37. Ollagnier-de-Choudens, S., Sanakis, Y., Hewitson, K. S., Roach, P., Baldwin, J. E., Münck, E., and Fontecave, M. (2000) Iron-sulfur center of biotin synthase and lipoate synthase, *Biochemistry 39*, 4165-4173.

**Table 4.1:** Cluster content, UV-visible absorption properties, and Mössbauer parameters of as-purified and reconstituted forms of *B. subtilis* and *E. coli* BioB

| | | | | | Mössbauer parameters (mm/s) | | | |
|---|---|---|---|---|---|---|---|---|
| | Cluster composition/BioB[a] | | Absorption properties | | $[2Fe\text{-}2S]^{2+}$ | | $[4Fe\text{-}4S]^{2+}$ | |
| **As-purified** | **$[2Fe\text{-}2S]^{2+}$** | **$[4Fe\text{-}4S]^{2+}$** | **$\varepsilon_{453}$ ($mM^{-1}$ $cm^{-1}$)** | **$A_{453}/A_{278}$** | **$\Delta E_Q$** | **$\delta$** | **$\Delta E_Q$** | **$\delta$** |
| *B. subtilis* BioB | 0.85 ± 0.10 | 0.05 ± 0.02 | 6.9 ± 1.1 | 0.20 ± 0.04 | 0.54 | 0.28 | 1.17 | 0.43 |
| *E. coli* BioB | 0.85 ± 0.10 | N/A | 7.2 ± 0.8 | 0.21 ± 0.02 | 0.53 | 0.29 | N/A | N/A |
| **Reconstituted[b]** | **$[2Fe\text{-}2S]^{2+}$** | **$[4Fe\text{-}4S]^{2+}$** | **$\varepsilon_{410}$ ($mM^{-1}$ $cm^{-1}$)** | **$A_{410}A_{278}$** | **$\Delta E_Q$** | **$\delta$** | **$\Delta E_Q$** | **$\delta$** |
| *B. subtilis* BioB1 | 0.63 ± 0.06 | 0.35 ± 0.04 | 12.4 ± 1.4 | 0.35 ± 0.03 | 0.57 | 0.28 | 1.17 | 0.43 |
| *B. subtilis* BioB2 | < 0.30 | 0.68 ± 0.05 | 17.0 ± 1.3 | 0.40 ± 0.03 | 0.57 | 0.26 | 1.17 | 0.43 |
| *E. coli* BioB | 0.75 ± 0.09 | 0.66 ± 0.05 | 17.1 ± 1.8 | 0.33 ± 0.03 | 0.50 | 0.28 | 1.32 | 0.45 |
| | | | | | | | 1.08 | 0.43 |

[a] Based on Fe and protein determinations, and analysis of Mössbauer data

[b] As-purified samples reconstituted with $FeCl_3$ or $Fe^{II}(NH_4)_2(SO_4)_2$ and $Na_2S$ and repurified as described in Materials and Methods. *B. subtilis* BioB1 and *E. coli* BioB samples were reconstituted for 1 hour and *B. subtilis* BioB2 samples was reconstituted for 4 hours

**Scheme 4.1**

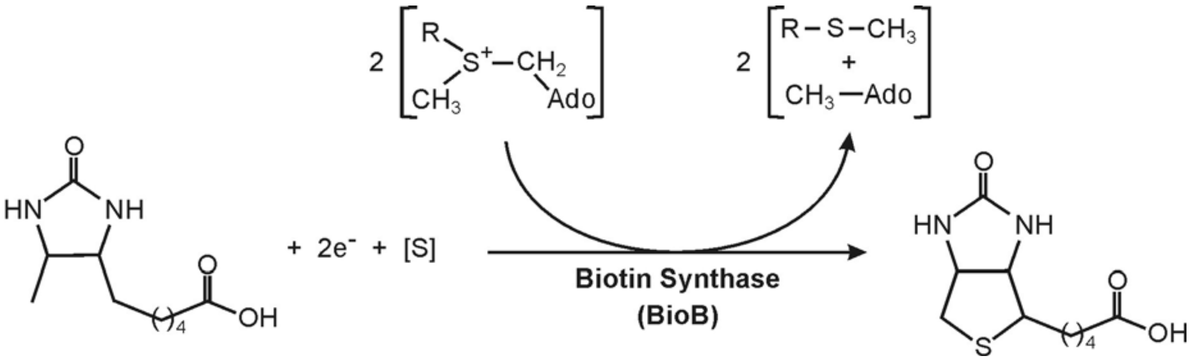
2
R
S+
CH2
CH3
Ado
2
R – S – CH3
+
CH3 — Ado
HN
NH
O
OH
( )4
+ 2e- + [S]
Biotin Synthase
(BioB)
HN
NH
O
S
( )4
OH

**Figure 4.1**: Mössbauer spectra of anaerobically grown $^{57}$Fe-enriched whole cells of *E. coli* with and without overexpression of *B. subtilis* BioB. (A) The *E. coli* overexpressing strain of wild-type *B. subtilis* BioB, *E. coli* BL21-gold[DE3] pT7-7 BsbioB-1 (hatched marks) and control whole cells, *E. coli* BL21-gold[DE3] pT7-7, which contains the same plasmid used for expression of BioB but without the BioB insert (solid line). The latter was simulated as two ferric and two ferrous doublets. The ferrous simulation was kept as a reference and the absorption scale is relative to the *B. subtilis* BioB containing spectrum. (B) Spectrum (A) after removing the ferrous component (hatched marks). The reference spectrum is scaled to 21% of the area of the remaining *B. subtilis* BioB containing spectrum. (C) Difference between the two spectra in (B) (hatched marks). Solid black line is a composite simulation of $[2Fe\text{-}2S]^{2+}$ clusters with $\delta = 0.28$ mm/s, $\Delta E_Q = 0.58$ mm/s, $\Gamma = 0.38, 0.39$ mm/s (light blue, 66% of total Fe) and $[4Fe\text{-}4S]^{2+}$ clusters with $\delta = 0.42$ mm/s, $\Delta E_Q = 1.22$ mm/s, $\Gamma = 0.44$ mm/s (dark blue, 34% of total Fe). The spectra were recorded at 4.2 K in a magnetic field of 50 mT, oriented parallel to the $\gamma$-ray beam

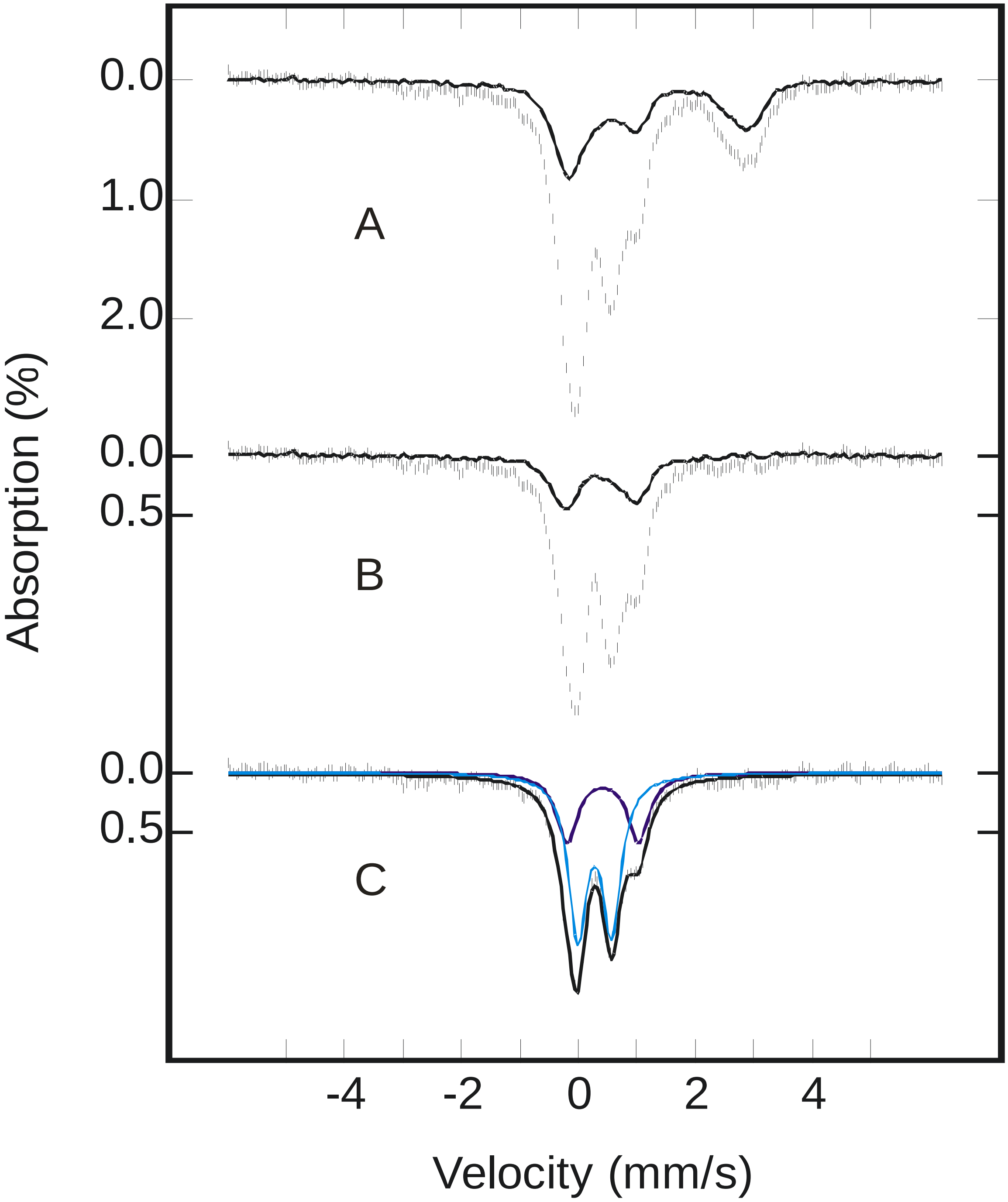
0.0
1.0
2.0
A
0.0
0.5
B
0.0
0.5
C
Absorption (%)
-4
-2
0
2
4
Velocity (mm/s)

**Figure 4.2:** Comparison of the UV-visible absorption (upper panel) and CD (lower panel) spectra of his-tagged as-purified *B. subtilis* BioB (black) and his-tagged as-purified *E. coli* BioB (red). The spectra were recorded in 1-mm cuvettes. The sample of *B. subtilis* BioB was in 100 mM Tris-HCl buffer, pH 8.0, with 100 mM NaCl and the sample of *E. coli* BioB was in 50 mM Hepes buffer, pH 7.5.

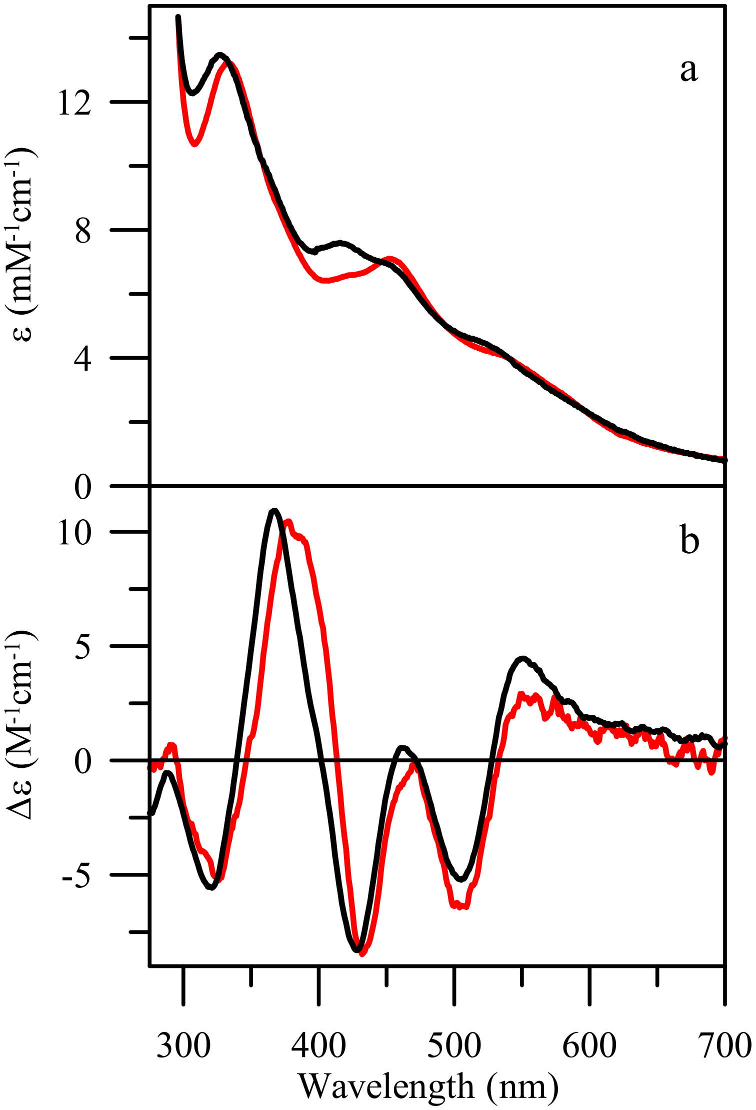
a
b
ε (mM⁻¹cm⁻¹)
Δε (M⁻¹cm⁻¹)
12
8
4
0
10
5
0
-5
300
400
500
600
700
Wavelength (nm)

**Figure 4.3**: Mössbauer spectra (hatched marks) of as-purified and reconstituted forms of his-tagged *B. subtilis* BioB. In each spectrum, the solid black line is a composite simulation of quadrupole doublets from $[2Fe\text{-}2S]^{2+}$ clusters (light blue) and $[4Fe\text{-}4S]^{2+}$ clusters (dark blue). (A) His-tagged *B. subtilis* BioB (187 µM in BioB) as purified aerobically from cells grown aerobically in $^{57}$Fe-enriched media. $[2Fe\text{-}2S]^{2+}$ clusters with $\delta = 0.28$ mm/s, $\Delta E_Q = 0.54$ mm/s, $\Gamma = -0.25$ mm/s account for 92% of the total Fe and $[4Fe\text{-}4S]^{2+}$ with $\delta = 0.43$ mm/s, $\Delta E_Q = 1.17$ mm/s, $\Gamma = -0.35$ mm/s account for 8% of the total Fe. (B) His-tagged *B. subtilis* BioB (263 µM in BioB) as purified anaerobically from cells grown aerobically in $^{57}$Fe-enriched media. $[2Fe\text{-}2S]^{2+}$ clusters account for 87% of the total Fe and $[4Fe\text{-}4S]^{2+}$ clusters account for 13% of the total Fe. The Mössbauer parameters for both clusters are the same as in (A). (C) Sample (B) anaerobically repurified after reconstitution with $^{57}Fe(NH_4)_2(SO_4)_2$ and $Na_2S$ for 1 hour (170 µM in BioB). $[4Fe\text{-}4S]^{2+}$ clusters with the same parameters as in (A) account for 44% of the total Fe and $[2Fe\text{-}2S]^{2+}$ clusters with $\delta = 0.28$ mm/s, $\Delta E_Q = 0.59$ mm/s, $\Gamma = -0.33$ mm/s account for 36% of the total Fe. (D) Sample (A) anaerobically repurified after reconstitution with $^{57}Fe(NH_4)_2(SO_4)_2$ and $Na_2S$ for 4 hours (151 µM in BioB). $[4Fe\text{-}4S]^{2+}$ clusters with the same parameters as in (A) account for 60% of total Fe and $[2Fe\text{-}2S]^{2+}$ clusters with $\delta = 0.26$ mm/s, $\Delta E_Q = 0.57$ mm/s, $\Gamma = -0.35$ mm/s that maximally account for 13% of the total Fe. Unaccounted for Fe is in the form of extraneous ferric and ferrous species. All samples were in 100 mM Tris-HCl buffer, pH 8.0, with 100 mM NaCl. The spectra were recorded at 4.2 K in a magnetic field of 50 mT oriented parallel to the γ-ray beam.

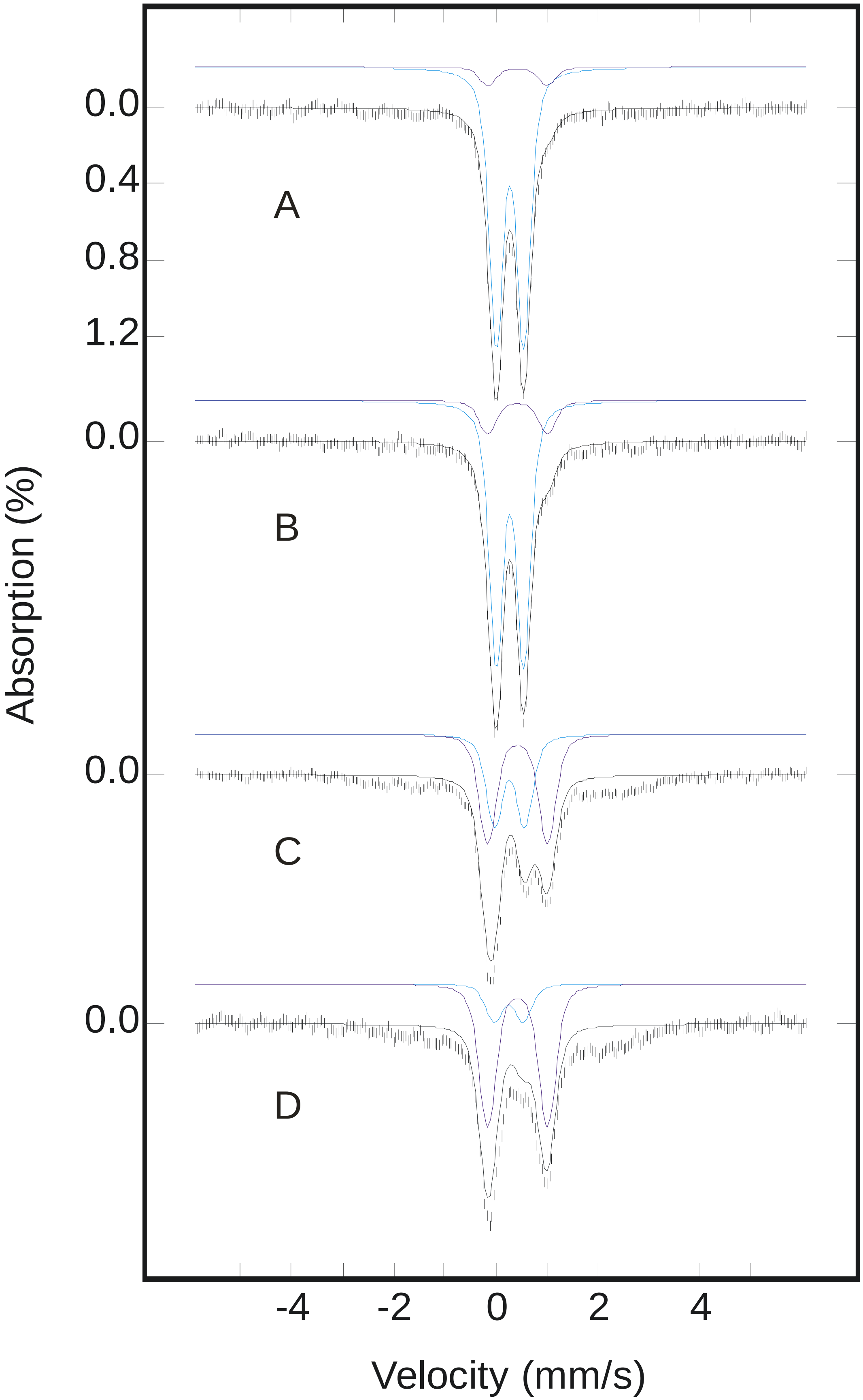
0.0
0.4
0.8
1.2
0.0
0.0
0.0
A
B
C
D
Absorption (%)
-4
-2
0
2
4
Velocity (mm/s)

**Figure 4.4**: Comparison of the low-temperature resonance Raman spectra of as-purified *B. subtilis* BioB (left panel) and as-purified *E. coli* BioB (right panel) using 458-, 488-, and 514-nm excitation. The samples were ~3 mM in BioB and were in the form a frozen droplet at 18 K. Each scan involved photon counting for 1 s at 0.5 $cm^{-1}$ increments with 8 $cm^{-1}$ spectral resolution, and each spectrum is the sum of ~100 scans. A linear ramp fluorescence background and bands arising from the frozen buffer solution have been subtracted from each spectrum.

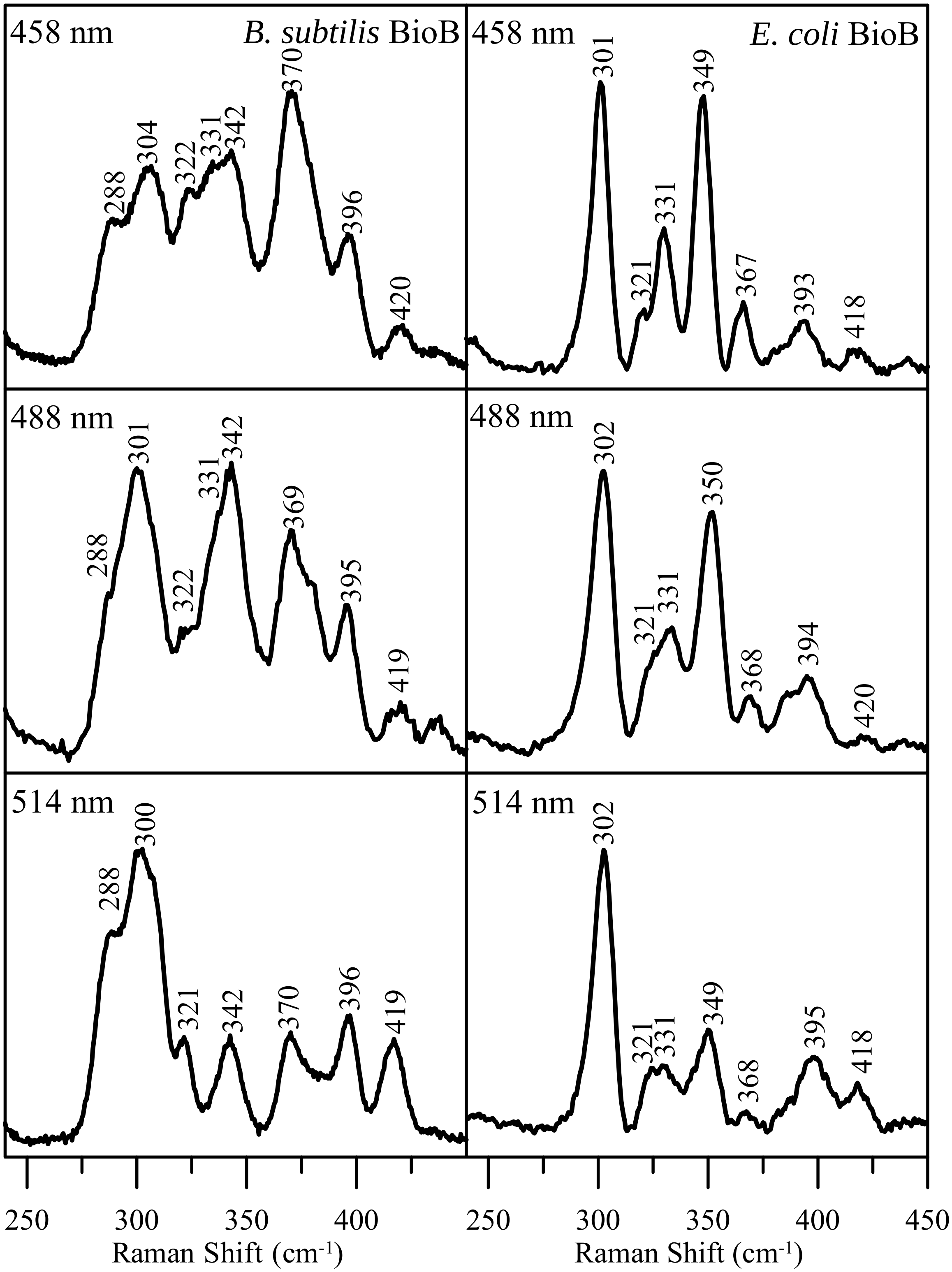
458 nm
B. subtilis BioB
288
304
322
331
342
370
396
420
458 nm
E. coli BioB
301
321
331
349
367
393
418
488 nm
288
301
322
331
342
369
395
419
488 nm
302
321
331
350
368
394
420
514 nm
288
300
321
342
370
396
419
514 nm
302
321
331
349
368
395
418
250
300
350
400
250
300
350
400
450
Raman Shift (cm-1)
Raman Shift (cm-1)

**Figure 4.5**: UV-visible absorption spectra of as-purified and reconstituted forms of his-tagged *B. subtilis* BioB (left panel) and wild-type *E. coli* BioB (right panel). Left panel: as-purified his-tagged *B. subtilis* BioB (black); as purified his-tagged *B. subtilis* BioB after anaerobic reconstitution for 1 hour and repurification (red); as purified his-tagged *B. subtilis* BioB after anaerobic reconstitution for 6 hours and repurification (blue). Right panel: as-purified wild-type *E. coli* BioB (black); as purified wild-type *E. coli* BioB after anaerobic reconstitution for 1 hour and repurification (red). The extinction coefficients are based on BioB concentration. Samples of *B. subtilis* BioB were in 100 mM Tris-HCl buffer, pH 8.0, with 100 mM NaCl and samples of *E. coli* BioB in 50 mM Hepes buffer, pH 7.5.

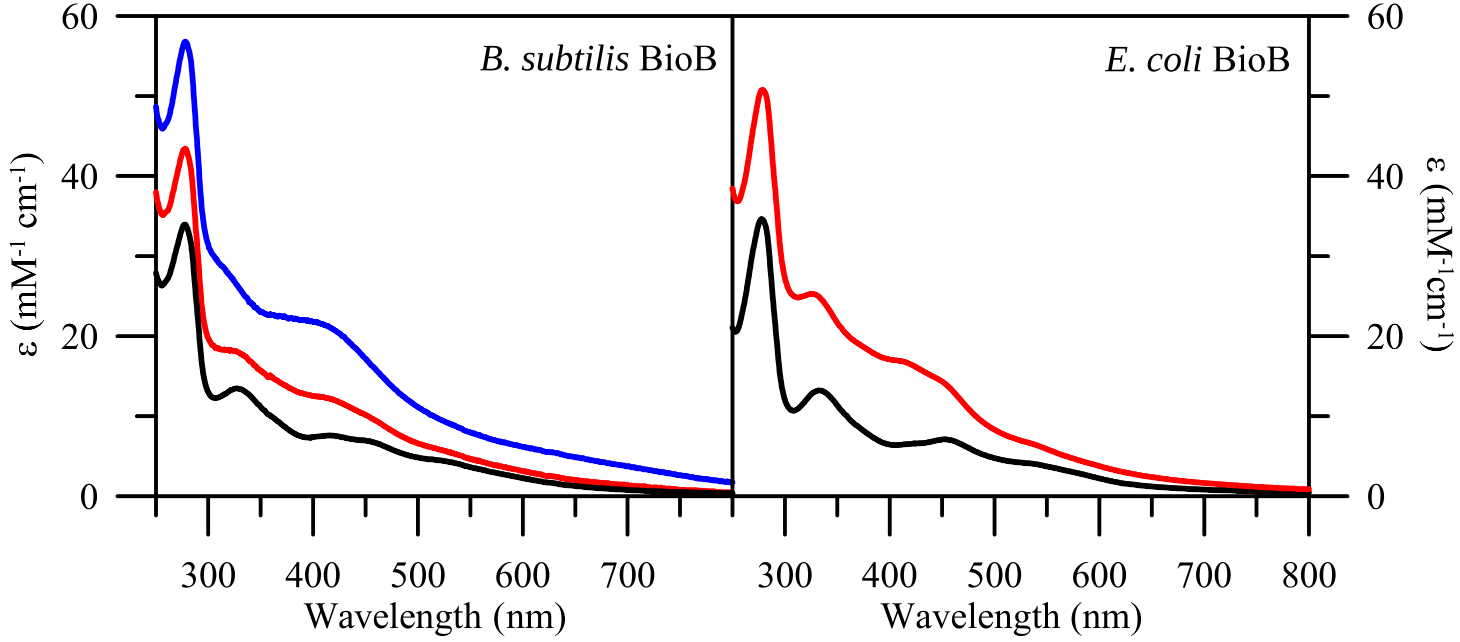
B. subtilis BioB
E. coli BioB
ε (mM-1 cm-1)
ε (mM-1cm-1)
0
20
40
60
300
400
500
600
700
800
Wavelength (nm)
Wavelength (nm)

**Figure 4.6**: Comparison of low-temperature resonance Raman spectra for equivalent forms of *B. subtilis* BioB (left panel) and *E. coli* BioB (right panel). Left panel: (a) as-purified wild-type *B. subtilis* BioB; (b) as-purified his-tagged *B. subtilis* BioB reconstituted for 1 hour; (c) as-purified his-tagged *B. subtilis* BioB reconstituted for 6 hours; (d) sample (c) exposed to air for 10 minutes. Right panel: (a) as-purified wild-type *E. coli* BioB; (b) as-purified his-tagged *E. coli* BioB reconstituted for 1 hour; (c) wild-type *E. coli* [4Fe-4S] BioB; (d) sample (c) exposed to air for 10 minutes. The spectra were recorded with 458-nm excitation, using samples that were ~3 mM in BioB in the form of frozen droplets at 18 K. Each scan involved photon counting for 1 s at 0.5 $cm^{-1}$ increments with 8 $cm^{-1}$ spectral resolution, and each spectrum in the sum of ~100 scans. A linear ramp fluorescence background and bands arising from the frozen buffer solution have been subtracted from each spectrum.

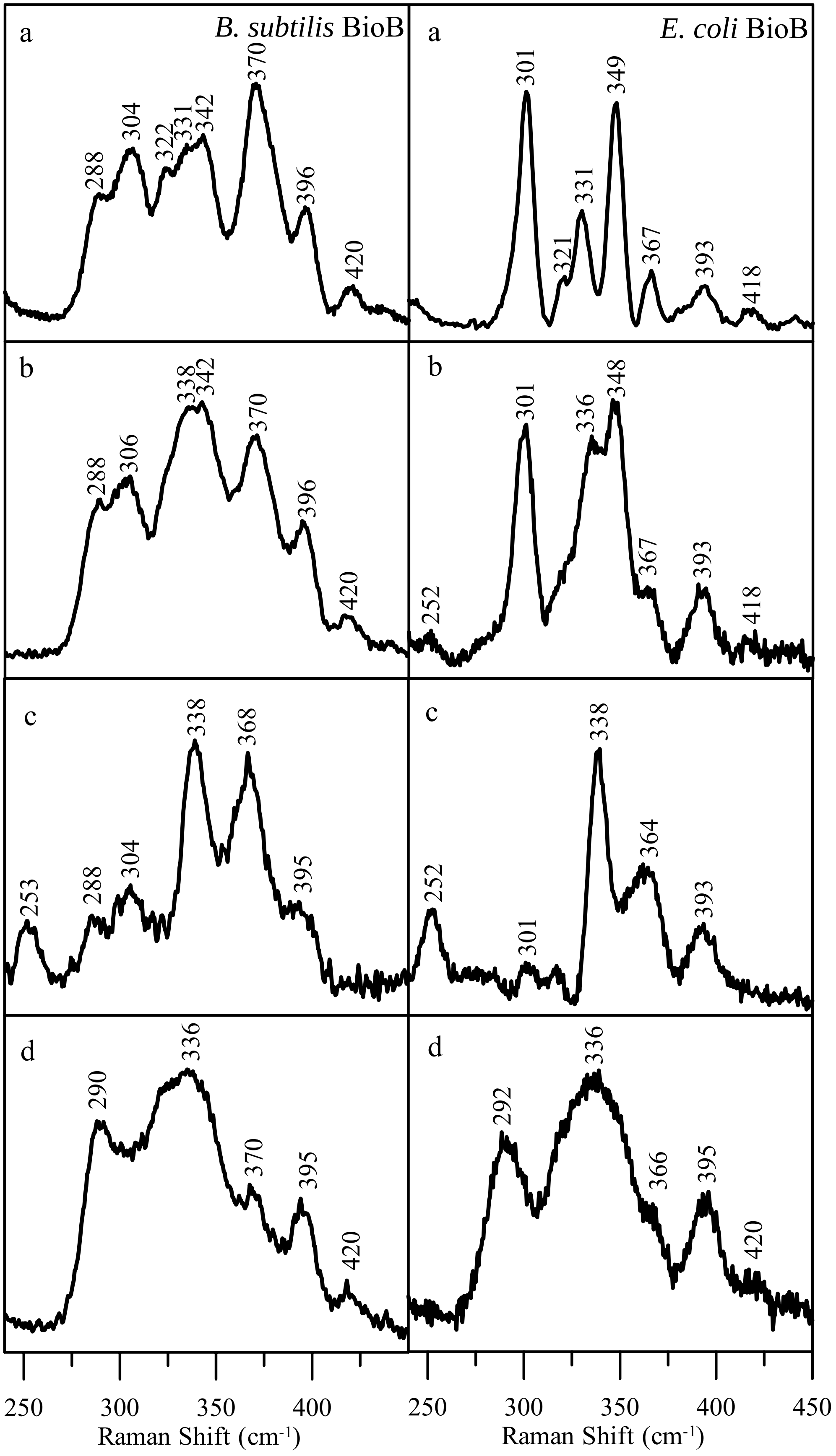
a
B. subtilis BioB
288
304
322
331
342
370
396
420
a
E. coli BioB
301
321
331
349
367
393
418
b
288
306
338
342
370
396
420
b
252
301
336
348
367
393
418
c
253
288
304
338
368
395
c
252
301
338
364
393
d
290
336
370
395
420
d
292
336
366
395
420
250
300
350
400
250
300
350
400
450
Raman Shift (cm-1)
Raman Shift (cm-1)

**Figure 4.7**: Time dependent CD and UV/visible absorption spectra of an IscS mediated reconstitution of as-purified *B. subtilis* BioB. (a) Absorption spectra collected at 1 hour intervals for a period of 8 hours. (b) CD spectra collected at 1 hour intervals for a period of 8 hours. The spectra were recorded in 1-mm cuvettes and the anaerobic reaction mixture contained 500 μM as-purified *B. subtilis* BioB, with 10 mM DTT, a 10-fold excess of ferrous ammonium sulfate and L-cysteine, and IscS in a 1:50 ratio to BioB. The reaction was initiated by the addition of cysteine. The arrows indicate the direct of change with increasing time.

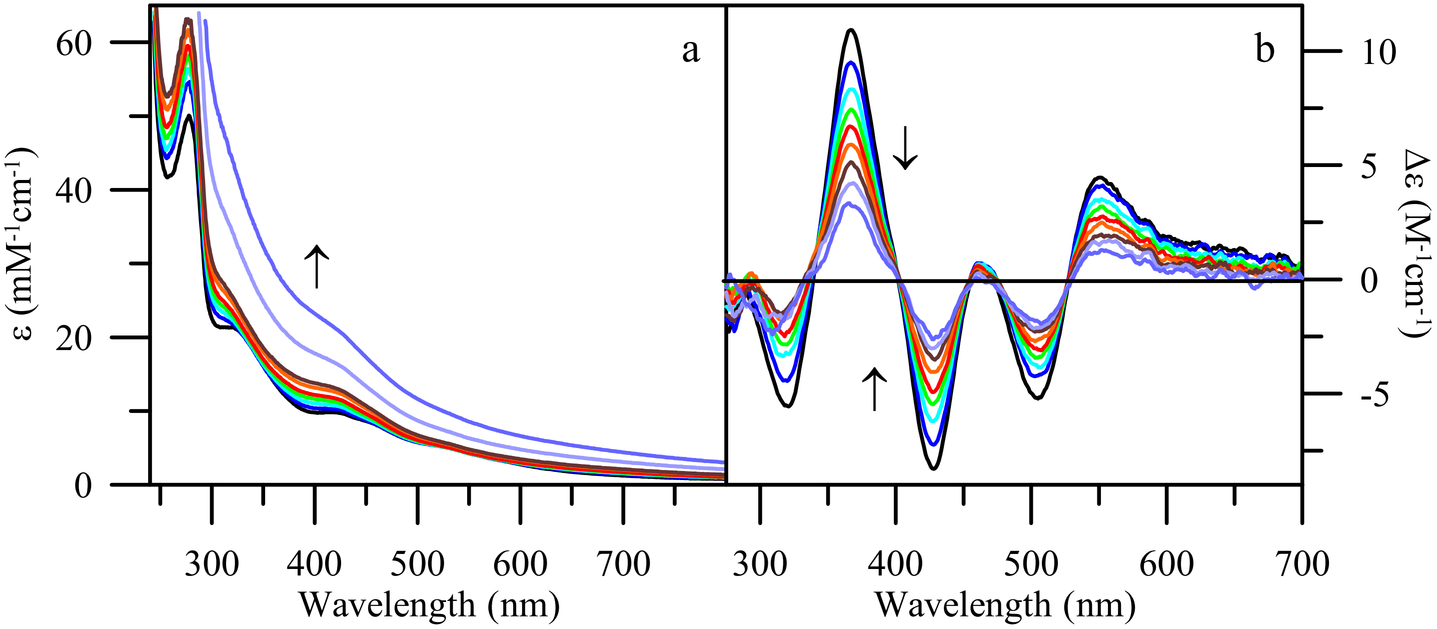
a
b
ε (mM-1cm-1)
Δε (M-1cm-1)
60
40
20
0
10
5
0
-5
300
400
500
600
700
Wavelength (nm)
300
400
500
600
700
Wavelength (nm)
↑
↓
↑

**Figure 4.8**: Mössbauer spectra of $^{57}$Fe-enriched as-purified *B. subtilis* BioB before and after reconstitution for 6 hours with a 10-fold excess of $^{56}$FeCl$_3$ and Na$_2$S. In each spectrum, a solid black line is a composite simulation of quadrupole doublets from [2Fe-2S]$^{2+}$ clusters (light blue) and [4Fe-4S]$^{2+}$ clusters (dark blue). (A) His-tagged *B. subtilis* BioB (300 μM in BioB) as purified aerobically from cells grown aerobically in $^{57}$Fe-enriched media. [2Fe-2S]$^{2+}$ clusters with $\delta$ = 0.28 mm/s, $\Delta E_Q$ = 0.54 mm/s, $\Gamma$ = -0.24 mm/s account for 96% of the total Fe and [4Fe-4S]$^{2+}$ with $\delta$ = 0.43 mm/s, $\Delta E_Q$ = 1.17 mm/s, $\Gamma$ = -0.35 mm/s account for 4% of the total Fe. (B) Sample (A) anaerobically reconstituted with a 10-fold excess of $^{56}$FeCl$_3$ for 6 hours and frozen without purification (288 μM in BioB). The [4Fe-4S]$^{2+}$ cluster (dark blue) corresponds to ~15% of the total $^{57}$Fe concentration and has the same parameters as in (A). The remaining $^{57}$Fe is predominantly present as a broad resonance from ill-defied Fe(II) and Fe(III) species. (C) Sample (A) anaerobically reconstituted with a 10-fold excess of $^{56}$FeCl$_3$ for 6 hours and repurified (162 μM in BioB). The parameters used to simulate the spectrum are the same as those used in (A) and the simulation corresponds to 15% of the $^{57}$Fe in [2Fe-2S]$^{2+}$ clusters and 44% of the $^{57}$Fe in [4Fe-4S]$^{2+}$ clusters. All samples were in 100 mM Tris-HCl buffer, pH 8.0, with 100 mM NaCl. The spectra were recorded at 4.2 K in a magnetic field of 50 mT oriented parallel to the $\gamma$-ray beam.

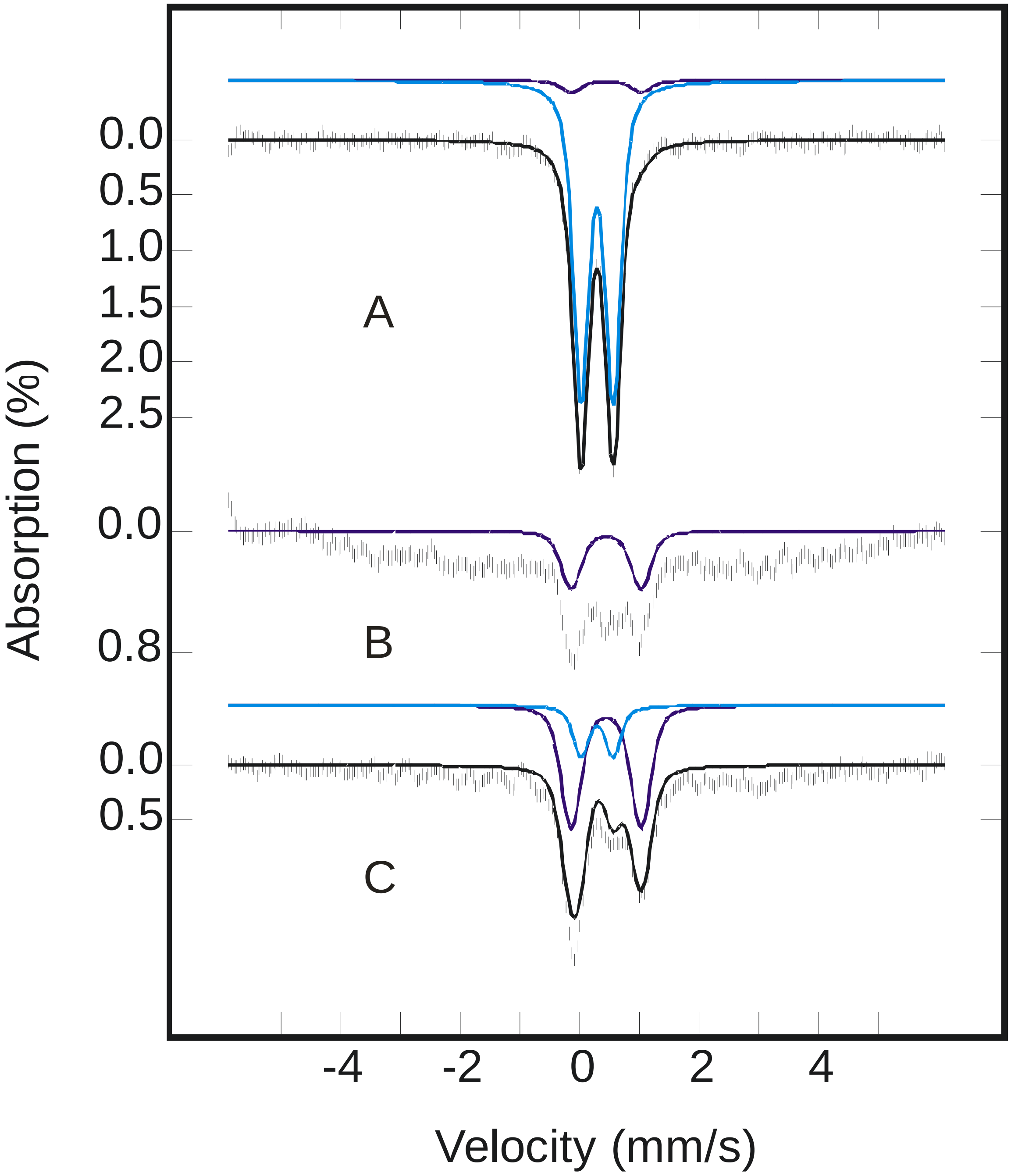
Absorption (%)
0.0
0.5
1.0
1.5
2.0
2.5
A
0.0
0.8
B
0.0
0.5
C
-4
-2
0
2
4
Velocity (mm/s)

**Figure 4.9**: X-band EPR spectrum of his-tagged *B. subtilis* BioB reconstituted for 6 hours using a 10-fold excess of $FeCl_3$ and $Na_2S$, repurified and reduced with a 10-fold excess dithionite. The sample was 0.23 mM in BioB Conditions of measurement: temperature, 20 K; microwave power, 50 mW; microwave frequency, 9.62 GHz; modulation amplitude, 0.63 mT.

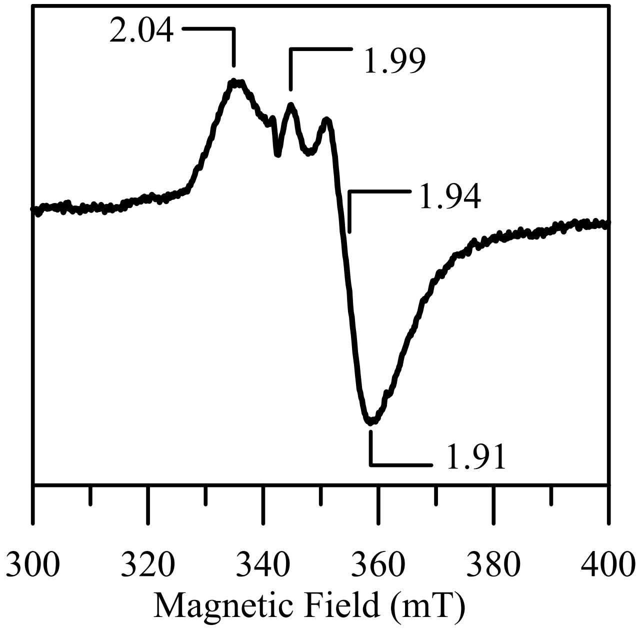
2.04
1.99
1.94
1.91
300
320
340
360
380
400
Magnetic Field (mT)

**Figure 4.10**: Effect of SAM on the low-temperature resonance Raman spectra of the $[4Fe\text{-}4S]^{2+}$ clusters in reconstituted *B. subtilis* BioB (left panel) and *E. coli* [4Fe-4S] BioB (right panel). Left panel: (a) As-purified his-tagged *B. subtilis* BioB reconstituted for 6 hours and repurified; (b) As (a) except for the addition of a 20-fold excess of SAM. Right panel (data taken from (*7*)): (a) *E. coli* [4Fe-4S] BioB; (b) As (a) except for the addition of a 10-fold excess of SAM. The spectra were recorded with 458-nm excitation, using samples that were ~3 mM in BioB in the form of frozen droplets at 18 K. Each scan involved photon counting for 1 s at 0.5 $cm^{-1}$ increments with 8 $cm^{-1}$ spectral resolution, and each spectrum in the sum of ~100 scans. A linear ramp fluorescence background and bands arising from the frozen buffer solution have been subtracted from each spectrum.

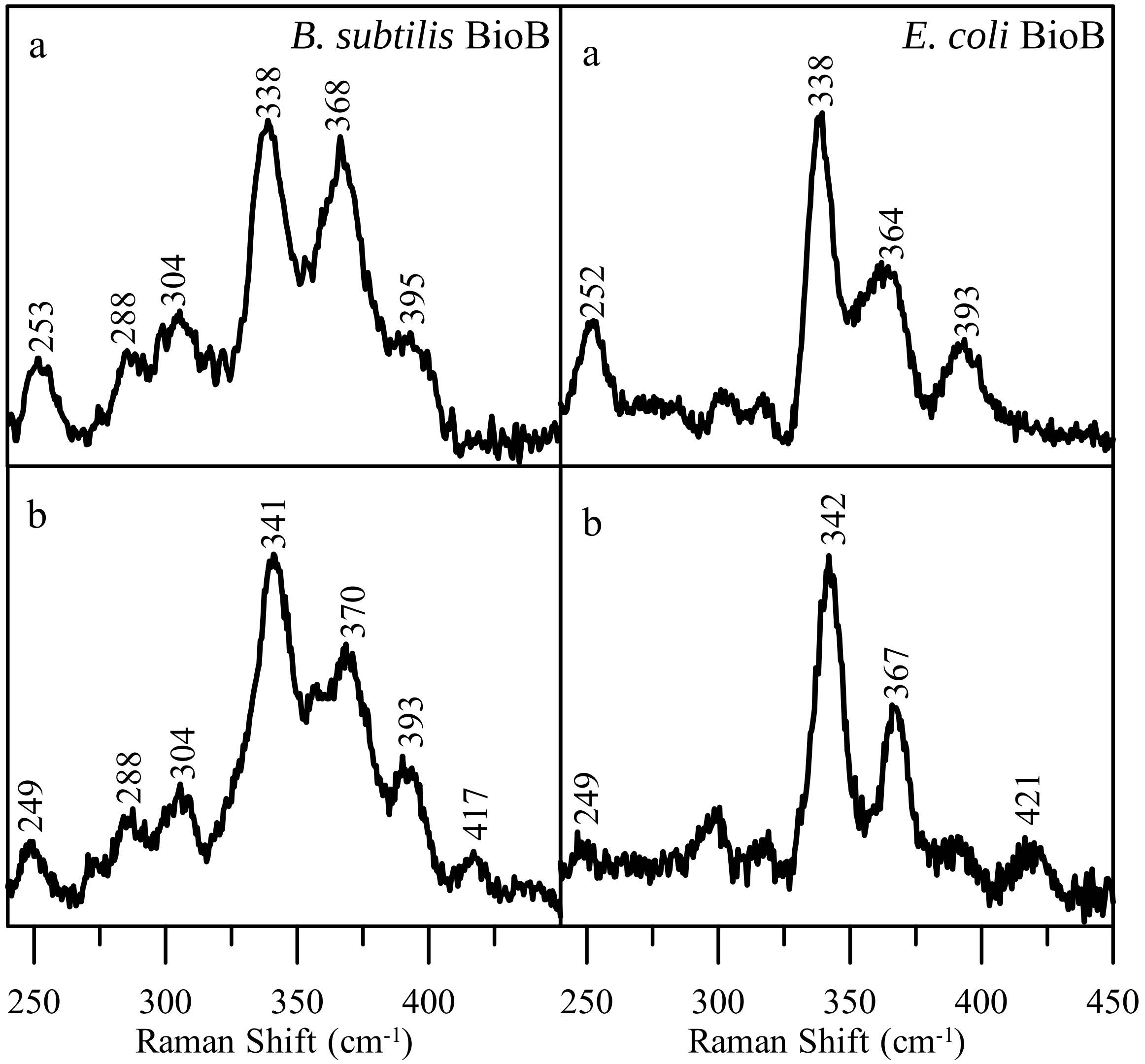
a
B. subtilis BioB
253
288
304
338
368
395
a
E. coli BioB
252
338
364
393
b
249
288
304
341
370
393
417
b
249
342
367
421
250
300
350
400
250
300
350
400
450
Raman Shift (cm-1)
Raman Shift (cm-1)

**Figure 4.11:** Activity assays comparing biotin production as a function of time by samples of *B. subtilis* and *E. coli* BioB. Biotin formation per BioB monomer is shown for as-purified his-tagged *B. subtilis* BioB (cyan triangles), as-purified his-tagged *B. subtilis* BioB reconstituted for 6 hours and repurified (blue triangles), as-purified his-tagged *E. coli* BioB (magenta circles), and as-purified his-tagged *E. coli* BioB reconstituted for 1 hour and repurified (red circles). Each data point is the average of 3 assays. The assays were performed under anaerobic conditions in 100 mM Tris-HCl buffer, pH 8.0, at 25 °C, with BioB (100 μM), KCl (10 mM), DTT (10 mM), L-cysteine (1 mM), fructose bisphosphate (5 mM), SAM (1 mM), *E. coli* flavodoxin (40 μM), *E. coli* flavodoxin reductase (20 μM), NADPH (1 mM). Turnover was initiated by addition of dethiobiotin (400 μM). Reactions were quenched at various time intervals by the addition of saturated sodium acetate, pH 4, and biotin was assayed using *Lactobacillus plantarum* ATCC 8014 as previously described (*31;32*).

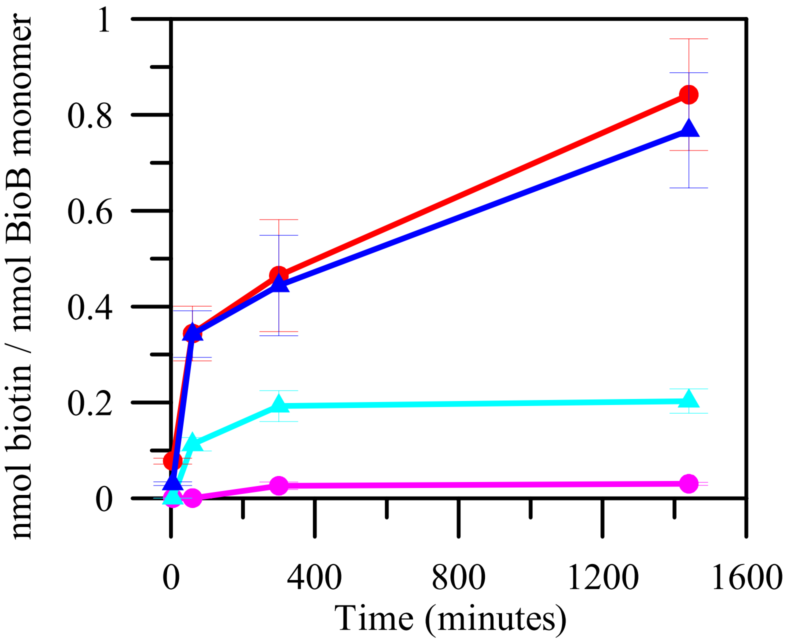
nmol biotin / nmol BioB monomer
1
0.8
0.6
0.4
0.2
0
0
400
800
1200
1600
Time (minutes)

# CHAPTER 5

# CHARACTERIZATION OF MOCS1A, AN OXYGEN-SENSITIVE IRON-SULFUR PROTEIN INVOLVED IN HUMAN MOLYBDENUM COFACTOR BIOSYNTHESIS[1]

---

[1] Hänzelmann, Petra; Hernández, Heather L.; Menzel, Christian; García-Serres, Ricardo; Huynh, Boi Hanh; Johnson, Michael K.; Mendel, Ralf R.; Schindelin, Hermann. *J. Biol. Chem*. **2004**, *279*, 34721-34732.
Reprinted here with permission of publisher.

**Abbreviations:** AdoMet, *S*-adenosylmethionine; ARR-AE, anaerobic ribonucleotide reductase activating enzyme; FeS, iron-sulfur; GTP cyclohydrolase, GTP-CH; MOCS, molybdenum cofactor synthesis; MPT, molybdopterin; PFL-AE, pyruvate formate lyase activating enzyme; RR, resonance Raman; VTVH, variable-temperature and variable-field; VTMCD, variable-temperature magnetic circular dichroism

## Abstract

The human proteins MOCS1A and MOCS1B catalyze the conversion of a guanosine derivative to precursor Z during molybdenum cofactor biosynthesis. MOCS1A shares homology with *S*-adenosylmethionine (AdoMet)-dependent radical enzymes, which catalyze the formation of protein and/or substrate radicals by reductive cleavage of AdoMet through a [4Fe-4S] cluster. Sequence analysis of MOCS1A shows two highly conserved cysteine motifs, one near the N-terminus and one near the C-terminus. MOCS1A has been heterologously expressed in *Escherichia coli* and purified under aerobic and anaerobic conditions. Individual mutations of the conserved cysteines to serine revealed that all are essential for synthesis of precursor Z *in vivo*. The type and properties of the iron-sulfur (FeS) clusters have been investigated using a combination of UV-visible absorption, variable-temperature magnetic circular dichroism, resonance Raman, Mössbauer and EPR spectroscopies, coupled with iron and acid-labile sulfide analyses. The results indicate that anaerobically purified MOCS1A is a monomeric protein containing two oxygen-sensitive FeS clusters each coordinated by only three cysteine residues. A redox-active $[4Fe\text{-}4S]^{2+,+}$ cluster is ligated by an N-terminal $CX_3CX_2C$ motif, as is the case with all other AdoMet-dependent radical enzymes investigated thus far. A C-terminal $CX_2CX_{13}C$ motif that is unique to MOCS1A and its orthologs, primarily ligates a $[3Fe\text{-}4S]^0$ cluster. However, MOCS1A can be reconstituted *in vitro* under anaerobic conditions to yield a form containing two $[4Fe\text{-}4S]^{2+}$ clusters. The N-terminal $[4Fe\text{-}4S]^{2+}$ cluster was rapidly degraded by oxygen via a semistable $[2Fe\text{-}2S]^{2+}$ cluster intermediate, and the C-terminal $[4Fe\text{-}4S]^{2+}$ cluster was rapidly degraded by oxygen to yield a semistable $[3Fe\text{-}4S]^0$ cluster intermediate.

## Introduction

The molybdenum cofactor in eukaryotic molybdoenzymes consists of a mononuclear molybdenum coordinated by the dithiolene moiety of a tricyclic pyranopterin, termed molybdopterin (MPT) (1). In humans, defects in molybdenum cofactor biosynthesis lead to the pleiotropic loss of the molybdoenzymes sulfite oxidase, aldehyde oxidase and xanthine dehydrogenase (2,3). Affected patients usually die shortly after birth and show neurological abnormalities, such as attenuated growth of the brain, untreatable seizures and dislocated ocular lenses (4). The first step during human molybdenum cofactor biosynthesis is catalyzed by MOCS1A and MOCS1B, leading to the synthesis of precursor Z, an oxygen-sensitive 6-alkyl pterin with a cyclic phosphate, from a guanosine derivative, most likely 5*'*-GTP (5-7).

Analogous to other pteridine biosynthetic pathways, synthesis of precursor Z has been proposed to occur via a GTP cyclohydrolase (GTP-CH) like reaction mechanism (5,6). In contrast to these pathways, the C8 atom of 5*'*-GTP is not released as formate, but is retained and incorporated in a rearrangement reaction as the first carbon atom of the precursor Z side chain. In the second step of molybdenum cofactor biosynthesis catalyzed by MOCS3 (8) and MPT synthase (*MOCS2*) precursor Z is converted into MPT (9-11). Finally, molybdenum is incorporated into MPT by the multifunctional protein gephyrin (12,13).

MOCS1A contains two highly conserved cysteine motifs (Fig. 5.1) proposed to be involved in iron-sulfur (FeS) cluster binding (14,15), one is located near the N-terminus (consensus sequence: $CX_3CX_2C$, where *X* denotes any amino acid) and one near the C-terminus (consensus sequence: $CX_2CX_{13}C$). Several mutations identified in molybdenum cofactor deficiency patients are located in these conserved cysteine motifs indicating their functional importance for protein activity (2,3). Based on sequence similarities to proteins such as biotin synthase, pyruvate formate lyase activating enzyme (PFL-AE) and anaerobic ribonucleotide reductase activating enzyme (ARR-AE), MOCS1A has been classified as a member of the superfamily of *S*-adenosylmethionine (AdoMet)-dependent radical enzymes (16). In this class of enzymes, AdoMet serves as the free radical initiator and undergoes cleavage to methionine and a 5′-deoxyadenosyl radical, which in turn propagates radical formation by abstracting hydrogen atoms, either from substrate molecules to form radical intermediates, or from glycyl residues of enzymes to activate them for radical-based biochemistry (17-20). The source of the electron required for the cleavage of AdoMet is a reduced form of a FeS cluster. In MOCS1A the N-terminal cysteine motif is highly homologous to a motif in AdoMet-dependent radical enzymes, which ligates a [4Fe-4S] cluster, whereas the C-terminal motif is unique to MOCS1A and its orthologs.

Here, we describe the purification of MOCS1A, the spectroscopic characterization of its FeS clusters and site-directed mutagenesis investigations of the role of the N- and the C-terminal cysteines. Single and triple Cys → Ser mutants were generated and analyzed in terms of catalytic activity and spectroscopic properties. The results show that all six cysteines are essential for activity. The results also indicate that anaerobically purified MOCS1A is a monomeric protein containing two oxygen-sensitive FeS clusters each ligated by only three cysteine residues. A redox-active $[4Fe\text{-}4S]^{2+,+}$ cluster is ligated by the N-terminal $CX_3CX_2C$ motif, as is the case with all other AdoMet-dependent radical enzymes investigated thus far, whereas a $[3Fe\text{-}4S]^0$ cluster is ligated by the C-terminal $CX_2CX_{13}C$ motif. However, MOCS1A can be reconstituted *in vitro* to yield a form containing two $[4Fe\text{-}4S]^{2+}$ clusters and both clusters appear to degrade via $[3Fe\text{-}4S]^0$ and/or $[2Fe\text{-}2S]^{2+}$ cluster intermediates on exposure to oxygen.

## Experimental Procedures

*Expression and Purification of MOCS1A and Mutated Proteins*—All expressions were conducted in LB medium at 30 °C in the *E. coli* strains BL21(DE3) or CL100 (*iscS*<sup>-</sup>)(DE3). Cultures were induced by the addition of 0.1 mM IPTG at an optical density $OD_{600}$ of 0.1. After 8 h of growth, cells were harvested and stored at –80 °C. For cells grown for Mössbauer measurements, 5 mg/l of $^{57}$Fe, as ferric ammonium citrate, was added to the growth media at induction. All purification steps were carried out either under anaerobic conditions inside a glove box (Coy Laboratories) in an Ar atmosphere containing less than 2 ppm $O_2$ at 4 °C or under aerobic conditions. Cells were thawed and resuspended in buffer A (50 mM Tris/HCl, pH 9.0, 300 mM NaCl, 10% (v/v) glycerol) containing 20 mM imidazole and 1% (v/v) Triton X-100. Hen egg white lysozyme (2 mg/ml) and a few crystals of bovine pancreas DNase were added, the mixture stirred for 30 min and sonicated. After centrifugation (60 min, 4 °C, 48,000 x g) MOCS1A was purified by Ni-NTA affinity chromatography (Qiagen, 1.5 ml matrix per liter culture volume) equilibrated with the same buffer. The column was washed with 10 bed volumes of buffer A containing 20 mM imidazole and 1% (v/v) Triton X-100, followed by 10 bed volumes of buffer A containing 20 mM imidazole and proteins were eluted with buffer A containing 500 mM imidazole. Brown colored fractions were pooled, desalted by size exclusion chromatography on Sephadex G-25 equilibrated with buffer B (100 mM Tris/HCl, pH 9.0, 300 mM NaCl), concentrated to 10-15 mg/ml by ultrafiltration (Centriprep-30, Millipore) and stored at –80 °C.

*Oligomeric state of MOCS1A*—FPLC size exclusion chromatography with a Superdex 200 (Amersham Biosciences) column (1.0 x 30 cm) equilibrated with buffer B was used for size determination. The column was calibrated using aldolase ($M_r$ = 158 kDa), bovine serum albumin

($M_r$ = 67 kDa), ovalbumin ($M_r$ = 43 kDa), chymotrypsinogen A ($M_r$ = 25 kDa) and, ribonuclease A ($M_r$ = 13.7 kDa) as marker proteins.

*Reconstitution of the FeS cluster*—Expression and purification of *E. coli* IscS was as described by Leimkühler and Rajagopalan (21). All steps of the reconstitution procedure were made anaerobically as described above. Anaerobically purified MOCS1A (250 µM) in buffer B was incubated with 5 mM DTT for 30 min. Then a 10-fold molar excess of $FeCl_3$ and L-cysteine and 200 µM pyridoxal phosphate (PLP) in buffer B containing 5 mM DTT was added. After addition of 2.5-5 µM of IscS the mixture was incubated for 4 h at 4°C. Reconstituted proteins were desalted over Sephadex G-25, equilibrated with buffer B to remove PLP and adventitiously bound Fe and sulfide.

*Electrophoresis and Immunoblot Analysis*—Protein samples were analyzed by 12% SDS-PAGE and gels were stained with Coomassie Brilliant Blue G-250. Immunoblotting on PVDF membranes was carried out with primary polyclonal antibodies generated against recombinant MOCS1A (1:5000 diluted serum). The membranes were probed with alkaline phosphatase-conjugated secondary antibody and bands were visualized with the BCIP/NBT detection system (Promega).

*Nitrate Reductase Overlay Assay*—For functional complementation the *E. coli moaA* mutant strain KB2037 (*moaA*940delT) was transformed with the corresponding expression plasmids. Qualitative analysis of nitrate reductase activity was performed by a colony overlay assay (22).

*In Vivo Assay for Precursor Z Synthesizing Activity*—The *E. coli moaD* mutant strain MJ7*chlM* (DE3) was transformed with the corresponding expression plasmids and grown anaerobically in 50 ml LB medium containing 0.4% (w/v) nitrate and 0.1 mM IPTG. Precursor Z was detected as compound Z in crude cell extracts by HPLC as described (7).

*Analytic Procedures*—Protein concentrations were determined by the method of Bradford (23) standardized against bovine serum albumin. Protein-bound Fe and acid labile sulfide were determined by the methods of Fish (24) and Fogo and Popowsky (25), respectively, standardized against either iron(II) ethylenediammonium sulfate or ammonium sulfide.

*Spectroscopic Methods*— UV-visible absorption spectra were recorded using a Hewlett Packard 8453 diode array spectrophotometer. X-band (~9.6 GHz) EPR spectra were recorded on a Bruker ESP-300E EPR spectrometer equipped with an ER-4116 dual-mode cavity and an Oxford Instruments ESR-9 flow cryostat. Resonances were quantified under non-saturating conditions using a 1 mM Cu-EDTA standard. Resonance Raman (RR) spectra were recorded using an Instruments SA U1000 spectrometer fitted with a cooled RCA 31034 photomultiplier tube with 90° scattering geometry. Spectra were recorded digitally using photon-counting electronics, and improvements in signal-to-noise were achieved by averaging multiple scans. Band positions were calibrated using the excitation frequency and are accurate to ± 1 $cm^{-1}$. Lines from a Coherent Sabre 10-W Argon Ion Laser were used for excitation, and plasma lines were removed using a Pellin Broca prism premonochromator. Scattering was collected from the surface of a frozen droplet of sample at 17 K using a custom designed anaerobic sample cell (26) attached to the cold finger of an Air Products Displex model CSA-202E closed cycle refrigerator. Bands originating form lattice modes of ice and a linear ramp fluorescent background have been subtracted from each spectrum shown in this work.

Variable-temperature magnetic circular dichroism (VTMCD) measurements were carried out with an Oxford Instruments Spectromag 4000 split-coil superconducting magnet mated to either a Jasco J715 or a Jasco J730 spectropolarimeter using published protocols (27,28). Variable-field and variable-temperature (VTVH) MCD saturation magnetization data were collected by monitoring MCD intensity at fixed temperatures as a function of the applied magnetic field. The data were corrected for temperature-independent contributions by extrapolating plots of MCD intensity versus inverse temperature to infinite temperature and subtracting a proportional correction at each field. Data are plotted as percent magnetization against $\beta B/2kT$, where percent magnetization is the percentage of the MCD intensity relative to magnetic saturation, $\beta$ is the Bohr magneton, B is the magnetic field strength, k is the Boltzmann constant, and T is the absolute temperature. Theoretical VTVH MCD saturation magnetization data were constructed as published (29). Mössbauer spectra were recorded using described spectrometers (30). The zero velocity refers to the centroid of the room temperature spectra of metallic Fe foil. Analysis of the Mössbauer data was performed with the program WMOSS (WEB Research).

## Results

*Effect of ISC and SUF proteins as well as the GroES/EL chaperonine system on the expression of MOCS1A*—MOCS1A contains an N-terminal extension of ~56 amino acids not found in any of its bacterial orthologs. Due to an increased stability in comparison to the full-length protein, MOCS1A without its N-terminal extension (MOCS1A-Δ1-56, 39 kDa) was expressed with an N-terminal His-tag. Deletion of the additional amino acids at the N-terminus increased the *in vivo* precursor Z synthesizing activity by about a factor of 1.5 (data not shown).

MOCS1A and orthologous MoaA proteins in eukaryotes and prokaryotes were characterized as FeS cluster containing proteins (15,31). The *de novo* synthesis and assembly of

FeS clusters in *E. coli* is mediated by the ISC (iron-sulfur cluster) system *(iscRSUA-hscBA-fd*x) (32), while the SUF (sulfur) system (*sufABCDS*E) (33) has been proposed to be involved in the repair of oxidatively damaged FeS clusters and/or play a role in FeS biosynthesis under conditions of Fe-limitation (34). Expression of MOCS1A in the *E. coli iscS* mutant strain CL100 (35) resulted in an inactive Fe-free insoluble MOCS1A protein showing that MOCS1A is only stable in its holoform (data not shown). Apo-MOCS1A is improperly folded due to the absence of the FeS clusters and tends to aggregate in inclusion bodies. Coexpression of MOCS1A with *iscSUA-hscBA-fdx* or *sufABCDSE* and the *E. coli* chaperonine system *groES/EL* in the *E. coli* strain BL21(DE3) increased the amount of soluble MOCS1A by a factor of 1.7-2.2 and MOCS1A could be purified by Ni-NTA chromatography with a yield of about 10 mg/l cell culture. However, coexpression of MOCS1A with the ISC or SUF proteins revealed no changes in the FeS cluster composition of purified proteins (data not shown). These studies show that under overexpression conditions MOCS1A requires (i) the assistance of chaperones (GroES/EL) and/or (ii) proteins for efficient *de novo* biosynthesis of FeS clusters (ISC, SUF) for proper folding and/or insertion of the FeS cluster.

*Spectroscopic characterization of the FeS cluster composition of MOSC1A*—MOSC1A was purified under aerobic conditions and under anaerobic conditions in an argon atmosphere. Both samples were brown, indicating the presence of FeS clusters, and the nature and properties of the FeS clusters in aerobic and anaerobic preparations were investigated using UV-visible absorption, RR, EPR, VTMCD and Mössbauer spectroscopies coupled with Fe, acid-labile sulfide and protein analyses.

Aerobically purified samples of MOCS1A contained 3.6 ± 0.2 mol Fe and 3.9 ± 0.3 mol acid labile sulfide per mol of MOCS1A, and the absorption spectrum exhibited peaks/shoulders around 320-330 nm, 415 nm and in the region between 500 and 600 nm (Fig. 5.2A). The spectrum is more typical of a $[2Fe\text{-}2S]^{2+}$ cluster than a $[4Fe\text{-}4S]^{2+}$ cluster (36-39), however, the Fe content of almost 4 mol per mol of protein, as well as an estimated $\varepsilon_{410}$ of about 13 500 $M^{-1}$ $cm^{-1}$, is more typical of $[4Fe\text{-}4S]^{2+}$ clusters ($\varepsilon_{410}$ ~15 000 $M^{-1}$ $cm^{-1}$) than $[2Fe\text{-}2S]^{2+}$ clusters (8000-10000 $M^{-1}$ $cm^{-1}$) (36,38). More definitive assessment of the FeS cluster content was provided by RR, EPR and VTMCD, which indicate that aerobically purified MOCS1A primarily contains a mixture of $[3Fe\text{-}4S]^0$ and $[2Fe\text{-}2S]^{2+}$ clusters. The RR spectrum (Fig. 5.3A) of the protein as purified comprises broad bands centered at 290, 338, 369 and 392 $cm^{-1}$ and is very similar to those reported for the $[2Fe\text{-}2S]^{2+}$ clusters that are observed during oxygen-induced degradation of the $[4Fe\text{-}4S]^{2+}$ clusters in other members of the AdoMet-dependent radical enzymes, e.g. ARR-AE (40), PFL-AE (41), biotin synthase (42) and the tRNA-methylthiotransferase, MiaB (39). EPR studies only show a near-isotropic $S = 1/2$ resonance centered near $g = 2.01$ (Fig. 5.4) with relaxation properties (observable only below 30 K) indicative of a $[3Fe\text{-}4S]^+$ cluster (43), in addition to a large $g = 4.3$ resonance from adventitiously bound ferric ions. However, spin quantitation indicates that the $g = 2.01$ resonance is a very minor component accounting for only 0.01 $[3Fe\text{-}4S]^+$ clusters per MOCS1A monomer.

Parallel-mode X-band EPR and VTMCD studies of aerobically purified MOCS1A revealed the presence of $S = 2$ $[3Fe\text{-}4S]^0$ clusters in addition to $S = 0$ $[2Fe\text{-}2S]^{2+}$ clusters. A broad low-field resonance centered near $g = 9.4$ is observed in the conventional perpendicular mode X-band EPR spectrum, and the resonance sharpens and intensifies in parallel mode (Fig. 5.5). Similar integer spin EPR signals have been reported for a range of $S = 2$ $[3Fe\text{-}4S]^0$ clusters (43). Moreover, parallel VTMCD studies (Fig. 5.6A, data not shown) show a pattern of intense, temperature-dependent MCD bands that are uniquely characteristic of the excited state properties of cubane-type $S = 2$ $[3Fe\text{-}4S]^0$ clusters (43). On the basis of the intensity of the VTMCD spectrum, $[3Fe\text{-}4S]^0$ clusters are the major component of aerobically purified MOCS1A with between 0.5 and 1.0 $[3Fe\text{-}4S]^0$ clusters per monomer. $[3Fe\text{-}4S]^0$ clusters give rise to very weak RR spectra compared to $[2Fe\text{-}2S]^{2+}$ clusters using 457.9 nm laser (at least 20x weaker (43)) and this presumably explains the absence of bands attributable to $[3Fe\text{-}4S]^0$ clusters in the RR spectrum shown in Fig. 5.3A.

Reduction of aerobically isolated MOCS1A with dithionite resulted in partial bleaching of the visible absorption (data not shown), loss of the $g = 2.01$ resonance and the appearance of a near-axial $S = 1/2$ resonance, $g = 2.03, 1.92, 1.88$ ($g = 2.03$ resonance), with relaxation properties (observable without substantial broadening only below 35 K) consistent with assignment to a $S = 1/2$ $[4Fe\text{-}4S]^+$ cluster (Fig. 5.4). Spin quantitation of the $g = 2.03$ resonance indicated 0.14 $[4Fe\text{-}4S]^+$ clusters per MOCS1A monomer. Parallel RR studies indicated the complete degradation of the $[2Fe\text{-}2S]^{2+}$ center, as evidenced by the loss of the characteristic RR bands shown in Fig. 5.3A, and showed only very weak bands that are best interpreted in terms of a $[4Fe\text{-}4S]^{2+}$ cluster (data not shown). In accord with the EPR results, VTMCD studies show the characteristic temperature-dependent MCD bands of a $[4Fe\text{-}4S]^+$ cluster (44-46) (Fig. 5.6B) and the intensity of the MCD indicates between 0.5 and 1.0 $[4Fe\text{-}4S]^+$ clusters per monomer. Moreover, the complete absence of MCD bands that can be attributed to $S = 2$ $[3Fe\text{-}4S]^0$ clusters, coupled with the loss of the $g = 9.4$ parallel mode EPR signal, indicates that these clusters have been degraded or converted to $[4Fe\text{-}4S]^{2+,+}$ clusters. The pattern of VTMCD bands is indicative of significant contributions from a $S > 1/2$ $[4Fe\text{-}4S]^+$ cluster (46), and this is further supported by VHVT MCD saturation magnetization data, which cannot be fit based solely on an $S = 1/2$ ground state and indicate the presence of Kramers $S > 1/2$ component (Fig. 5.7). This is not particularly surprising as mixed spin $[4Fe\text{-}4S]^+$ clusters appear to be the norm rather than the exception for $[4Fe\text{-}4S]^+$ centers with one oxygenic ligand (45,47). EPR and Mössbauer studies are currently in progress to identify the $S > 1/2$ spin state. Taken together with the RR data, we conclude that the low $S = 1/2$ spin quantitation (0.14 spin/monomer) is likely to be the consequence of incomplete reduction to the $[4Fe\text{-}4S]^+$ state and a mixed spin ground state, coupled with partial oxidative cluster degradation during purification. In summary, the spectroscopic results indicate that aerobically purified samples of MOCS1A contain a mixture of $[3Fe\text{-}4S]^0$ and $[2Fe\text{-}2S]^{2+}$ clusters as purified. However, both the $[3Fe\text{-}4S]^0$ and $[2Fe\text{-}2S]^{2+}$ clusters are degraded or converted to a $[4Fe\text{-}4S]^{2+,+}$ cluster following anaerobic reduction with excess sodium dithionite.

Anaerobically purified samples of MOCS1A had increased Fe and acid-labile sulfide contents of 5.0 ± 0.4 and 5.3 ± 0.3 mol per mol of protein, respectively, and an absorption spectrum that is more indicative of a $[4Fe\text{-}4S]^{2+}$ cluster as the dominant cluster type (Fig. 5.2A). In particular, the broad shoulder between 500 and 600 nm had decreased and the shoulder at 400 nm was more pronounced. Moreover, the extinction coefficient at 410 nm ($\varepsilon_{410}$ ~16 000 $M^{-1}$ $cm^{-1}$) is indicative of approximately one $[4Fe\text{-}4S]^{2+}$ cluster per MOCS1A molecule. Addition of dithionite resulted in a decrease of the absorbance in the visible region, demonstrating that the $[4Fe\text{-}4S]^{2+,+}$ cluster is redox-active (Fig. 5.2A, inset). Evidence for the presence of $[4Fe\text{-}4S]^{2+}$ clusters in anaerobically purified MOCS1A is also obvious in the RR spectrum (Fig. 5.3B) which comprises weak bands at 255, 365, and 390 $cm^{-1}$ and an intense band at 338 $cm^{-1}$. The latter band is attributed to the symmetric breathing mode of the $Fe_4S_4$ cubane and the spectrum is very similar to those reported for $[4Fe\text{-}4S]^{2+}$ clusters in AdoMet-dependent radical enzymes (39,41,42). The bands from the $[4Fe\text{-}4S]^{2+}$ cluster are superimposed on bands originating from the $[2Fe\text{-}2S]^{2+}$ cluster that is present in the aerobically purified protein, as evidenced by the band at 290 $cm^{-1}$. However, the contribution from $[2Fe\text{-}2S]^{2+}$ clusters is greatly overemphasized by RR due to the ~5-10-fold greater resonance enhancement for $[2Fe\text{-}2S]^{2+}$ clusters compared to $[4Fe\text{-}4S]^{2+}$ clusters with 457.9 nm excitation (48). The observation of $[2Fe\text{-}2S]^{2+}$ clusters in the RR spectrum of the anaerobically prepared sample is likely to be a consequence, in whole or in part, of freezing and thawing of samples. Although frozen samples were transported for spectroscopic measurements, and thawed under anaerobic conditions, UV-visible absorption and RR studies (data not shown) indicate that partial degradation of the $[4Fe\text{-}4S]^{2+}$ clusters accompanies freeze/thaw cycles.

Mössbauer studies of anaerobically prepared MOCS1A revealed the presence of $[3Fe\text{-}4S]^0$ and $[4Fe\text{-}4S]^{2+}$ clusters in distinct FeS cluster-binding sites. Fig. 5.8C shows the 4.2 K spectrum (hatched marks) of anaerobically purified MOCS1A in a weak parallel, applied field of 50 mT. A central quadrupole doublet superposed with a broad paramagnetic spectrum is observed. The paramagnetic spectrum, which accounts for 60% of the total Fe absorption, is identical to the spectrum of the $[3Fe\text{-}4S]^0$ cluster characterized in the N-terminal triple Cys → Ser variant (see below) shown in Fig. 5.8B. Removal of the $[3Fe\text{-}4S]^0$ contribution results in a quadrupole doublet (Fig. 5.8D) that is consistent with that of a $[4Fe\text{-}4S]^{2+}$ cluster (38,49,50). Since the N-terminal triple Cys → Ser variant contains a $[3Fe\text{-}4S]^0$ cluster (see below), which therefore must be coordinated by the three conserved C-terminal cysteine residues, the observation of a $[4Fe\text{-}4S]^{2+}$ cluster in addition to a $[3Fe\text{-}4S]^0$ cluster in MOCS1A suggests that the $[4Fe\text{-}4S]^{2+}$ cluster is coordinated by the conserved $CX_3CX_2C$ N-terminal cysteine residues that are known to coordinate a $[4Fe\text{-}4S]^{2+,+}$ cluster in AdoMet-dependent radical enzymes. Taken together, the Fe content of the Mössbauer sample (4.8 Fe per monomer), the observation that the $[3Fe\text{-}4S]^0$ cluster is close to full occupancy in the N-terminal triple Cys → Ser variant (see below), and the analysis of the Mössbauer absorption which indicates 60% of the Fe in $[3Fe\text{-}4S]^0$ clusters and 40% of the Fe in $[4Fe\text{-}4S]^{2+}$ clusters, indicate that the $[3Fe\text{-}4S]^0$ cluster is present at full occupancy in the C-terminal domain and that the $[4Fe\text{-}4S]^{2+}$ cluster is present with approximately 50% occupancy in the N-terminal domain.

The presence of a $S = 2$ $[3Fe\text{-}4S]^0$ cluster in as prepared samples of anaerobically purified MOCS1A was confirmed by EPR and VTMCD studies. EPR studies revealed a fast-relaxing, near-isotropic $S = 1/2$ resonance centered near $g = 2.01$ accounting for 0.05 spins per monomer, indicative of a minor contribution from $[3Fe\text{-}4S]^+$ clusters (Fig. 5.4). In addition, parallel and perpendicular mode EPR studies in the low-field region revealed the $g = 9.4$ resonance that is the hallmark of $S = 2$ $[3Fe\text{-}4S]^0$ cluster (Fig. 5.5) (43). The VTMCD spectrum comprises an intense pattern of temperature-dependent MCD bands that are very similar to those observed in the aerobically purified sample and are uniquely indicative of a $[3Fe\text{-}4S]^0$ cluster (43). Moreover, the $S = 2$ ground state for the temperature-dependent MCD bands is confirmed by VHVT MCD saturation magnetization data collected at 720 nm (Fig. 5.7).

EPR studies of dithionite-reduced anaerobically purified MOCS1A (Fig. 5.4) revealed an $S = 1/2$ resonance ($g = 2.03$, 1.92, and 1.89) very similar to that observed for dithionite-reduced samples of aerobically prepared MOCS1A, but with greater spin concentration (0.29 spins per monomer). As for the aerobically purified enzyme, VTMCD studies (Fig. 5.6B) indicate that the $[3Fe\text{-}4S]^0$ cluster is completely lost on dithionite reduction and the pattern of bands, coupled with VHVT MCD saturation magnetization data, which are very similar to that observed for the dithionite-reduced aerobically purified enzyme (Fig. 5.7) are indicative of a mixed-spin $[4Fe\text{-}4S]^+$ cluster. In common with other AdoMet-dependent radical enzymes such as PFL-AE and ARR-AE, in which $[2Fe\text{-}2S]^{2+}$ clusters are degraded or converted to $[4Fe\text{-}4S]^{2+,+}$ clusters under reducing conditions (41,51), the RR spectrum of dithionite-reduced anaerobically purified MOCS1A indicates degradation of $[2Fe\text{-}2S]^{2+}$ clusters, as evidenced by the loss of the 290 $cm^{-1}$ band (Fig. 5.3C). Since $[4Fe\text{-}4S]^{+}$ clusters have negligible resonance enhancements with 457.9 nm excitation (48), the dithionite-reduced sample therefore affords the opportunity to investigate the RR spectrum of the $[4Fe\text{-}4S]^{2+}$ cluster in isolation, albeit with poorer signal-to-noise as a result of partial reduction. Hence the $S = 1/2$ spin quantitation is likely to be a substantial under-estimate of the [4Fe-4S] cluster stoichiometry due to incomplete reduction and a mixed-spin ground state. In summary, spectroscopic studies indicate that MOCS1A purified anaerobically contains predominantly sub-stoichiometric amounts of $[4Fe\text{-}4S]^{2+}$ clusters coordinated by the conserved cysteines in the N-terminal domain and near-stoichiometric amounts of a $[3Fe\text{-}4S]^{0}$ cluster coordinated by the conserved cysteines in the C-terminal domain. Reduction with dithionite results in degradation or conversion of the $[3Fe\text{-}4S]^{0}$ and the trace amounts of $[2Fe\text{-}2S]^{2+}$ clusters, to yield partially reduced $[4Fe\text{-}4S]^{2+,+}$ clusters as the sole type of cluster present in the protein.

*Stability of FeS clusters in MOCS1A*—Oxygen-induced $[4Fe\text{-}4S]^{2+}$ cluster degradation via a semi-stable $[2Fe\text{-}2S]^{2+}$ cluster intermediate has emerged as a common property of almost all of the AdoMet-dependent radical enzymes investigated thus far (37,39-41). Hence the effects of oxygen on the FeS clusters in MOCS1A were investigated using RR and UV-visible absorption spectroscopies. The $[4Fe\text{-}4S]^{2+}$ cluster in the anaerobically purified protein was almost completely degraded after exposure to air for 10 min at room temperature, as evidenced by the loss or decrease in the intensity of the bands at 255 and 338 $cm^{-1}$ in the RR spectrum (cf. Figs. 5.3B and 5.3D). The resulting spectrum is almost identical to that of the aerobically purified enzyme within experimental error. Hence the $[4Fe\text{-}4S]^{2+}$ in the N-terminal domain is shown to be rapidly degraded by oxygen via a semi-stable $[2Fe\text{-}2S]^{2+}$ cluster intermediate.

In contrast, absorption studies indicate that the $[2Fe\text{-}2S]^{2+}$ and $[3Fe\text{-}4S]^{0}$ clusters in aerobically purified MOCS1A undergo a much slower oxygen-induced degradation with a half-life of 21 h after air exposure (Fig. 5.2B, upper panel) that does not occur under anaerobic conditions. This effect can be significantly delayed in the presence of 5′-GTP and the half-life increased to 34 h (Fig. 5.2B, lower panel). The stabilizing effect of 5′-GTP occurs already with a 1:1 protein to 5′-GTP stoichiometry. Furthermore, the effect of 5’-GTP, 5’-GDP, 5’-GMP and 5′-ATP was analyzed. The half-life of the FeS cluster increases with an increase in phosphate groups (5’-GTP 34 h, 5’-GDP 27 h, 5’-GMP 24 h), perhaps indicating a stronger interaction. In contrast, 5′-ATP had no effect on MOCS1A stability as documented by a half-life of 18 h.

*Oligomeric state of MOCS1A*—Size exclusion chromatography of aerobically purified MOCS1A shows two major peaks corresponding to the monomer with an apparent molecular mass of 40 kDa and dimer (~80 kDa) (supplemental Fig. 5.S1). Addition of up to 5 mM DTT to prevent oxidation of sulfhydryl groups or to reduce already existing disulfide bonds did not significantly alter the aggregation behavior. The MOCS1A monomer and dimer show different Fe contents and UV-visible absorption spectra (supplemental Fig. 5.S1, inset). The monomeric form has a higher cluster content based on Fe analysis and absorption intensity (4.2 ± 0.2 mol Fe per mol of monomeric MOCS1A, $\varepsilon_{410}$ ~15 500 $M^{-1}$ $cm^{-1}$), while the dimeric form has a decreased cluster content (2.8 ± 0.5 mol Fe per mol of monomeric MOCS1A, $\varepsilon_{452}$ ~10 500 $M^{-1}$ $cm^{-1}$ per monomer). Purification of MOCS1A under anaerobic conditions led to the monomeric state (data not shown), indicating loss of Fe during aerobic purification and subsequent dimerization possibly as a result of oxidative modification of free sulfhydryl groups.

*In vitro FeS cluster assembly in MOCS1A*—As isolated, most AdoMet-dependent radical enzymes contain low amounts of Fe as well as catalytically inactive $[2Fe\text{-}2S]^{2+}$ clusters and in some cases $[3Fe\text{-}4S]^{+}$ clusters (17-20). However, reconstitution of apo-proteins under anaerobic conditions with Fe and sulfide creates a $[4Fe\text{-}4S]^{2+}$ cluster in these proteins. In order to obtain MOCS1A with homogenous [4Fe-4S] clusters, MOCS1A was treated with EDTA under anaerobic reducing conditions, to obtain the apo-protein. In agreement with the observed aggregation of MOCS1A in the *iscS* mutant strain, complete removal of the FeS cluster was accompanied by precipitation of the protein. However, after an IscS catalyzed reconstitution of the anaerobically purified protein with a 6-fold molar excess of L-cysteine and $FeCl_3$ in the presence of DTT, MOCS1A shows a broad absorption band centered at 410 nm, typical of $[4Fe\text{-}4S]^{2+}$ clusters (Fig. 5.2C). The reconstituted FeS clusters are extremely oxygen-sensitive and are rapidly degraded yielding polymeric Fe-sulfides, as demonstrated by the appearance of absorption maxima at 420 and 610 nm (Fig. 5.2C, inset). The Fe content of anaerobically reconstituted MOCS1A, 8.1 ± 1.2 mol Fe per mol of monomeric MOCS1A and the extinction coefficient at 410 nm of ~30 000 $M^{-1}$ $cm^{-1}$, are both indicative of two $[4Fe\text{-}4S]^{2+}$ clusters in reconstituted MOCS1A.

The conclusion that anaerobically reconstituted MOCS1A contains [4Fe-4S] clusters in both the C-terminal and N-terminal cluster-binding domains is supported by RR, VTMCD and EPR studies. The RR spectrum (Fig. 5.3E) is characteristic of $[4Fe\text{-}4S]^{2+}$ clusters (48), albeit with greater linewidths that presumably reflect the overlap of the spectra from two similar, but not identical, $[4Fe\text{-}4S]^{2+}$ clusters. The reconstituted samples show no evidence for the 290 $cm^{-1}$ band that is the hallmark of the $[2Fe\text{-}2S]^{2+}$ cluster produced via oxygen-induced degradation of $[4Fe\text{-}4S]^{2+}$ clusters. VTMCD studies showed only weak predominantly temperature-independent bands (data not shown) consistent with the presence of only $S = 0$ $[4Fe\text{-}4S]^{2+}$ clusters, with no significant contribution from the intense transitions from the $S = 2$ $[3Fe\text{-}4S]^0$ clusters that dominate the spectrum of the aerobically and anaerobically purified samples (Fig. 5.6A). EPR studies revealed a weak, slow-relaxing radical signal centered around $g = 2.005$ (Fig. 5.4). Dithionite reduction leads to the formation of $[4Fe\text{-}4S]^+$ clusters with EPR and VTMCD properties (Figs. 5.4, 5.6B and 5.7) quantitatively similar to those seen for anaerobically purified samples. The $S = 1/2$ EPR resonance ($g = 2.03, 1.92, 1.89$) accounts for 0.28 spins per monomer and the VTMCD spectra and VHVT MCD magnetization data indicate the presence of a mixed spin $[4Fe\text{-}4S]^+$ cluster. Hence the low $S = 1/2$ spin quantitation is likely to be a consequence of the presence of $S > 1/2$ $[4Fe\text{-}4S]^+$ clusters and incomplete reduction using dithionite.

*Characterization of single* Cys → Ser *mutants*—MOCS1A is characterized by two highly conserved cysteine motifs (Fig. 5.1), and to analyze the involvement of the six MOCS1A conserved cysteine residues in formation/stabilization of two FeS clusters and their importance for catalytic activity, all six cysteine residues of full-length MOCS1A (Cys80, Cys84, Cys87, Cys312, Cys315, and Cys329) were individually changed to serine. The choice of cysteine substitution by serine was made to preserve as much as possible H-bonding character and side chain geometry of the original cysteine residues. For functional characterization, the *E. coli moaA* mutant strain KB2037 was reconstituted with wild type or mutant MOCS1A, and reconstitution of molybdenum cofactor biosynthesis was determined by a nitrate reductase overlay assay (Fig. 5.9A). All six Cys → Ser mutants showed no complementation. Immunoblot analysis of wild type MOCS1A and Cys → Ser variants, revealed similar expression levels for the wild type protein and the mutants of the N-terminal cysteine motif (Fig. 5.9A). However, replacements of the cysteines of the C-terminal motif destabilize MOCS1A so much that only low amounts of protein could be detected in extracts (Fig. 5.9A). All six single Cys → Ser variants were purified as described for the wild type protein under aerobic conditions and characterized by UV-visible absorption spectroscopy and Fe content analysis. While the mutants of the N-terminal cysteine motif could be purified in amounts comparable to wild type MOCS1A (Fig. 5.9B, upper panel), the yield of the mutants of the C-terminal cysteine motif was only about 20% (Fig. 5.9B, lower panel).

Mutants affecting the N-terminal cysteine motif (Fig. 5.9B, upper panel) as well as the C-terminal cysteine motif (Fig. 5.9B, lower panel) show a decreased absorption in the whole visible region in comparison to wild type MOCS1A. Accordingly, the Fe contents of the N-terminal cysteines decreased by 30-50% of wild type levels: 3.4 mol Fe/mol wild type MOCS1A, 2.0 mol Fe/mol C80S, 2.4 mol Fe/mol C84S, 1.7 mol Fe/mol C87S. The Fe contents of the C-terminal cysteine variants range from 80 to 90% of wild type MOCS1A: 3.4 mol Fe/mol wild type MOCS1A, 2.9 mol Fe/mol C312S, 2.7 mol Fe/mol C315S, 3.1 mol Fe/mol C327S. Although, mutants of the C-terminal cysteine motif did not show such a significant effect as mutants of the N-terminal cysteine motif, these data are indicative for an involvement of all six cysteine residues in FeS cluster binding, suggesting two different FeS binding sites.

*Characterization of triple* Cys → Ser *mutants*—In order to obtain further evidence for two different FeS cluster binding sites, one ligated by the N-terminal $CX_3CX_2C$ motif and one by the C-terminal $CX_2CX_{13}C$ motif, triple mutants (C80S/C84S/C87S, C312S/C315S/C329S) of MOCS1A-Δ1-56 were generated, purified under anaerobic conditions and analyzed by UV-visible absorption spectroscopy as well as Fe analysis. MOCS1A-Δ1-56-C80/84/87S, reflecting the proposed C-terminal FeS cluster, has an Fe content of 2.9 mol per mol protein and shows an UV-visible absorption spectrum with a shoulder at 390 nm and a broad weak absorption centered near 700 nm (Fig. 5.2D). The spectrum is readily reconciled in terms of a mixture of $[3Fe\text{-}4S]^0$ and $[4Fe\text{-}4S]^{2+}$ clusters. $[3Fe\text{-}4S]^0$ generally exhibit a broad ill-defined shoulder centered near 400 nm and a weak broad band centered near 700 nm (43), whereas $[4Fe\text{-}4S]^{2+}$ clusters have a well resolved shoulder centered near 400 nm as their major UV-visible absorption feature (38). In light of the overwhelming spectroscopic evidence for $[3Fe\text{-}4S]^0$ clusters in this variant, see below, the sensitivity to oxygen shown in the inset is likely to reflect oxidative conversion of $[4Fe\text{-}4S]^{2+}$ clusters to $[3Fe\text{-}4S]^0$ clusters. It is not unusual for FeS proteins to assemble a FeS cluster, with the correct nuclearity, when one of the cysteine ligands is mutated to the nearly isosteric serine (47,52). To rule out the possibility of serinate ligation, a triple Cys → Ala mutant (C80A/C84A/C87A) of the N-terminal cysteine motif was also generated. In comparison to the serine variant, this variant shows greatly reduced expression indicative of major structural changes. However, the assembly of a FeS cluster in the C80A/C84A/C87A variant, as evidenced by broad monotonically increasing absorption throughout the visible region (data not shown), suggests ligation of the observed FeS cluster by the C-terminal $CX_2CX_{13}C$ motif.

The nature of the FeS cluster present in the anaerobically prepared MOCS1A N-terminal triple Cys → Ser variant was assessed using Mössbauer, RR, EPR and VTMCD spectroscopies. In accord with the Fe analysis (2.7 Fe per monomer), Mössbauer provided unambiguous evidence for $[3Fe\text{-}4S]^0$ clusters as the sole or dominant FeS cluster in the $^{57}$Fe enriched sample prepared specifically for Mössbauer studies. The 4.2 K zero-field Mössbauer spectrum (Fig. 5.8A, hatched marks) exhibits two quadrupole doublets with an intensity ratio of 2:1. A least-squares fit (*solid line* in Fig. 5.8A) of the spectrum yields parameters ($\Delta E_Q = 1.44$ mm/s and $\delta = 0.47$ mm/s for the more intense doublet and $\Delta E_Q = 0.56$ mm/s and $\delta = 0.28$ mm/s for the less intense doublet) that are essentially identical to those observed for $[3Fe\text{-}4S]^0$ clusters (53-56).

The sample contains a minor impurity, ~ 10% of total Fe, in the form of high-spin $Fe^{2+}$ that shows weak absorptions at ~ 0.8 mm/s and +2.2 mm/s. Most significantly, in a weak applied field of 50 mT, the two doublets are broadened beyond recognition (Fig. 5.8B), indicating that both doublets are associated with the same paramagnetic electronic state. This sensitive field-dependent behavior, together with the 2 to 1 intensity ratio and the characteristic parameters observed for the two doublets, are trade marks of a reduced $[3Fe\text{-}4S]^0$ cluster. Subsequent high-field Mössbauer studies (data not shown) indicate that ~10% of the absorption may originate from quadrupole doublets associated with diamagnetic $[4Fe\text{-}4S]^{2+}$ and/or $[2Fe\text{-}2S]^{2+}$ clusters, and this result is consistent with the RR spectrum shown in Fig. 5.3F. $[3Fe\text{-}4S]^0$ clusters exhibit very weak RR spectra with dominant bands centered near 270 and 370 $cm^{-1}$ with 457.9 nm excitation (43). Hence weak bands at 270 and 369 $cm^{-1}$ are attributed to the dominant $[3Fe\text{-}4S]^0$ cluster. The RR spectrum also provides evidence for the presence of $[4Fe\text{-}4S]^{2+}$ clusters (bands at 253 and 338 $cm^{-1}$) and $[2Fe\text{-}2S]^{2+}$ clusters (290 $cm^{-1}$ band). However, the stoichiometry of the $[4Fe\text{-}4S]^{2+}$ and especially $[2Fe\text{-}2S]^{2+}$ clusters relative to the $[3Fe\text{-}4S]^0$ clusters is greatly overemphasized in the RR spectrum due to much greater resonance enhancement.

Additional evidence for the dominant presence of $[3Fe\text{-}4S]^0$ clusters was provided by VTMCD and EPR studies. EPR samples showed only a very weak slow-relaxing radical signal centered at $g = 2.004$ (Fig. 5.4) and the characteristic low-field resonance of the $[3Fe\text{-}4S]^0$ cluster centered at $g = 9.4$ that is enhanced in parallel mode (Fig. 5.5). The pattern, intensity and saturation magnetization behavior of the bands in the VTMCD spectrum (Figs. 5.6A and 5.7) can only be interpreted in terms of $S = 2$ $[3Fe\text{-}4S]^0$ as the dominant type of cluster in the anaerobically prepared MOCS1A N-terminal Cys → Ser variant. EPR studies have not provided evidence for ferricyanide oxidation of the $[3Fe\text{-}4S]^0$ cluster to yield a $S = 1/2$ $[3Fe\text{-}4S]^+$ cluster, indicating that the midpoint potential is likely to be greater than +420 mV (vs NHE). However, reduction with dithionite results in the formation of a $[4Fe\text{-}4S]^{+}$ cluster as evidenced by the appearance of a $S = 1/2$ resonance ($g = 2.03, 1.92, 1.89$) accounting for 0.21 spins per monomer that is very similar to those observed in dithionite-reduced aerobically and anaerobically purified MOCS1A samples (Fig. 5.4).

In accord with the results for the single mutants involving the C-terminal cysteines, MOCS1A-Δ1-56-C312/315/327S, reflecting the proposed N-terminal FeS cluster, shows low expression (~10% of wild type) consistent with a function of the C-terminal FeS cluster in maintaining the structural integrity of MOCS1A. This variant has an Fe content of 2.6 mol per mol of protein and shows an UV-visible absorption spectrum with a distinct maximum between 410-420 nm and a broad feature in the region of 500-700 nm more typical for $[2Fe\text{-}2S]^{2+}$ clusters (Fig. 5.2D). A remarkable decrease in protein solubility (~2-3 mg/ml) and the tendency to aggregate reflects the low soluble expression yields of this variant and prevented further spectroscopic characterization.

In summary, the results for the triple mutants of the N-terminal and the C-terminal cysteine motif provide clear evidence for two cluster binding regions. Each variant has approximately half the Fe content of anaerobically purified wild type MOCS1A and each shows different absorption characteristics indicative of different types of FeS clusters. The N-terminal triple Cys → Ser variant can accommodate a $[4Fe\text{-}4S]^{2+,+}$ cluster, but this cluster is clearly rapidly degraded to yield a more stable $[3Fe\text{-}4S]^{0}$ cluster during purification. While more spectroscopic studies are required to fully characterize the cluster content of the C-terminal triple Cys → Ser variant, the absorption data are best interpreted in terms of $[2Fe\text{-}2S]^{2+}$ clusters which are likely to be breakdown products of the $[4Fe\text{-}4S]^{2+,+}$ cluster required for reductive cleavage of AdoMet.

## Discussion

In the present study, human MOCS1A has been heterologously expressed in *E. coli* and purified as a soluble His-tagged protein under aerobic and anaerobic conditions. In accord with the studies of the homologous MoaA protein from *Arthrobacter nicotinovorans* (14,15), MOCS1A is shown to be an FeS protein that requires two highly conserved cysteine motifs, one near the N-terminus ($CX_3CX_2C$) and one near the C-terminus ($CX_2CX_{13}C$). The mutagenesis results presented herein demonstrate that all six of the conserved cysteines in MOCS1A are required for catalytic activity and that the N-terminal and C-terminal cysteine-binding motifs ligate distinct FeS clusters. The type and properties of the FeS clusters in aerobically purified, anaerobically purified and anaerobically reconstituted MOCS1A and the anaerobically purified N-terminal triple Cys → Ser variant have been investigated using UV-visible absorption, RR, EPR, VTMCD and Mössbauer spectroscopies, coupled with Fe and acid-labile sulfide analyses. Overall, the results indicate that MOCS1A is a monomeric protein containing two very oxygen-sensitive FeS clusters, each ligated by only three cysteine residues.

A redox-active $[4Fe\text{-}4S]^{2+,+}$ cluster that is readily degraded by exposure to oxygen and/or freeze thaw cycles via a transient $[3Fe\text{-}4S]^{+}$ cluster and a semi-stable $[2Fe\text{-}2S]^{2+}$ cluster intermediate, is ligated by the N-terminal cysteine motif. Such cluster-conversion behavior is characteristic of $[4Fe\text{-}4S]^{2+,+}$ clusters in AdoMet-dependent radical enzymes and both the electronic and vibrational properties of the $[4Fe\text{-}4S]^{2+,+}$ and $[2Fe\text{-}2S]^{2+}$ clusters are very similar to those previously reported for the equivalent clusters in enzymes of this protein family

(17,19,20,42). Hence, we conclude that analogous to AdoMet-dependent radical enzymes, the $[4Fe\text{-}4S]^{2+,+}$, $[3Fe\text{-}4S]^{+}$, and $[2Fe\text{-}2S]^{2+}$ clusters are all ligated by the three cysteines in the N-terminal motif and that the non-cysteinyl-ligated unique Fe site of the $[4Fe\text{-}4S]^{2+}$ cluster is essential for anchoring AdoMet (57-61), in order to induce reductive cleavage. Experiments designed to assess the ability of the $[4Fe\text{-}4S]^{2+,+}$ cluster in MOCS1A to bind and reductively cleave AdoMet are currently in progress.

The functional form of the cluster ligated by the C-terminal cysteine motif is also likely to be a redox-active $[4Fe\text{-}4S]^{2+,+}$ cluster based on spectroscopic studies of anaerobically reconstituted MOCS1A. However, the $[4Fe\text{-}4S]^{2+}$ cluster is readily degraded by oxygen to yield a semi-stable $[3Fe\text{-}4S]^{0}$ cluster, and the spectroscopic results clearly demonstrate that the $[3Fe\text{-}4S]^{0}$ cluster is the dominant type of cluster present in this C-terminal cluster binding site in both aerobically and anaerobically purified samples of MOCS1A and the anaerobically purified N-terminal triple Cys → Ser variant. Hence we conclude that the C-terminal cysteine-binding motif ligates a $[4Fe\text{-}4S]^{2+,+}$ cluster with only three cysteine ligands and that the non-cysteinyl-ligated Fe is readily removed under mild oxidative conditions to yield a $[3Fe\text{-}4S]^{0}$ cluster. Indeed our inability to purify MOCS1A in a form corresponding to the anaerobically reconstituted form that contains two $[4Fe\text{-}4S]^{2+}$ clusters, even under anaerobic conditions, may be a consequence of overexpression under aerobic conditions.

This study of MOCS1A constitutes the first successful attempt to characterize the type and properties of FeS clusters in a purified MoaA-type protein. In previous work, MoaA from *A. nicotinovorans* was heterologously expressed in *E. coli* and purified as an N-terminal fusion protein with either a glutathione-S-transferase or a hexa-histidine tag. Both proteins were reported to be brown, albeit with “no significant features” in their UV-visible absorption spectra, and evidence for the presence of a $[3Fe\text{-}4S]^+$ cluster was based on Fe and acid-labile sulfide determinations (approximately four irons and three acid-labile sulfides per MoaA monomer) and the observation of a weak isotropic $g = 2.01$ EPR signal that was present in the as isolated, but not the dithionite-reduced sample (15). However, these EPR signals were observed at 70 K and hence are likely to correspond to radical species, since $[3Fe\text{-}4S]^+$ clusters exhibit fast-relaxing $S = 1/2$ resonances that are not observable at 70 K (43). Indeed, we observed weak (< 0.01 spins per MOCS1A monomer), isotropic $g = 2.01$ resonances at 70 K with relaxation properties indicative of a radical species in both the aerobically and anaerobically purified samples of MOCS1A investigated in this work (data not shown). His-tagged *Rhodobacter capsulatus* MoaA was heterologously expressed as inclusion bodies in *E. coli* and evidence for the presence of a $[3Fe\text{-}4S]^+$ cluster was based on the presence of a fast-relaxing $S = 1/2$ resonance ($g = 2.023, 2.015, 2.004$) of unknown concentration in the 2 K EPR spectrum of the washed insoluble pellet (31).

The important question that results from these studies is why MOCS1A requires two $[4Fe\text{-}4S]^{2+,+}$ clusters. By analogy to other members of the AdoMet-dependent family of radical enzymes, the N-terminal [4Fe-4S] cluster is clearly implicated in reductive cleavage of AdoMet to generate the 5′-deoxyadenosyl radical. A purely structural or electron transfer role for the C-terminal [4Fe-4S] cluster is considered unlikely, as the cluster is easily degraded and has incomplete cysteinyl ligation. Thus far two members of the AdoMet-dependent family of FeS containing radical enzymes have been structurally characterized by x-ray crystallography, biotin synthase (BioB) and coproporphyrinogen III oxidase (HemN) (60,61), and both confirm the mode of binding of AdoMet to the unique Fe site of the [4Fe-4S] cluster proposed based on spectroscopic studies (57,58). In the case of biotin synthase, the assembly of two FeS clusters at different binding sites has been demonstrated: an oxygen-sensitive $[4Fe\text{-}4S]^{2+,+}$ cluster ligated by a $CX_3CX_2C$ motif that binds AdoMet and an air-stable [2Fe-2S] cluster ligated by three conserved cysteines and an arginine residue in a $CX_{30}CX_{59}CX_{71}R$ arrangement (42,59,61-63). While the physiological relevance of the [2Fe-2S] cluster in recombinant biotin synthase is still a subject of debate, it has been shown to be capable of providing the S for biotin formation in a single turnover experiment (64-66). Since the formation of MPT involves the attachment of two S atoms, one possibility is that the C-terminal [4Fe-4S] cluster in MOCS1A functions as a sacrificial S donor. However, *in vitro*, the addition of both sulfurs to precursor Z to form the MPT dithiolene group has been shown to be catalyzed by MPT synthase $[(MoaD\text{-}MoaE)_2]$ (67,68). Analogous to ThiI in thiamine biosynthesis, the S used for dithiolene formation is carried in the form of a thiocarboxylate at the MoaD C-terminus (69). In addition, the structure of the oxygen sensitive precursor Z revealed no S atoms (70,71). Although the loss of a terminally bound labile S during purification of precursor Z cannot be excluded, it seems very unlikely that the cluster bound by the C-terminal cysteine motif in MOCS1A functions as a sacrificial S donor in MPT synthesis. However, we cannot completely exclude the possibility that MOCS1A is capable in providing one S via its C-terminal FeS cluster analogous to biotin synthase and that the second S is attached by MoaD, via a mechanism analogous to ThiI in thiamine biosynthesis, in order to form the dithiolene group of molybdopterin.

Another more likely function is to invoke a role of the C-terminal FeS cluster in facilitating catalysis by binding and activating the substrate. The paradigm here is aconitase, in which the active site comprises a [4Fe-4S] cluster ligated by only three cysteines, with the non-cysteinyl-ligated unique Fe site involved in the binding and activation of the substrate (72,73). The formation of precursor Z involves a rearrangement reaction of the carbon atom at the eight position of 5′-GTP (5,6). The unique Fe site of the C-terminal FeS cluster could be involved in temporary release of this carbon atom as formate. This would be analogous to a proposed GTP-CH like reaction mechanism (5,6). GTP-CHs require Zn for their catalytic activity (74-76), and the Zn is proposed to generate a hydroxide nucleophile which attacks the carbon atom at the eight position of 5′-GTP. Hence the unique Fe site on the C-terminal [4Fe-4S] cluster of MOCS1A may play a similar role in the hydrolytic release of formate. A third possibility is that both the N-terminal and C-terminal [4Fe-4S] clusters in MOCS1A are involved in the reductive cleavage of AdoMet, which would imply that the three C-terminal cysteines constitute a new motif for the assembly of a [4Fe-4S] cluster capable for reductive cleavage of AdoMet. This hypothesis implies that the catalytic reaction requires radical generation at two distinct sites on the substrate. Although it is not yet possible to identify a specific role for the C-terminal FeS cluster, the spectroscopic characterization of the N-terminal and C-terminal clusters of MOCS1A reported in this work set the stage for experiments to assess the ability of the C-terminal cluster to bind 5′-GTP or AdoMet. In particular, the potential to selectively label the unique Fe site of the C-terminal [4Fe-4S] with $^{57}$Fe should facilitate the use of Mössbauer spectroscopy to address the ability of the unique Fe site to bind exogenous molecules.

The results presented herein show that the C-terminal FeS cluster is essential for the structural integrity of MOCS1A. Replacement of one cysteine by serine destabilizes the protein so much that only low amounts of protein can be detected in extracts, suggesting improper folding of the protein in the absence of the FeS cluster and increased susceptibility to degradation by cellular proteases.

MOCS1A with most likely two [4Fe-4S] clusters in the catalytically competent form is clearly a novel member of the AdoMet-dependent family of FeS radical enzymes, and there is a pressing need for additional spectroscopic and structural studies to clarify the role of the C-terminal cluster and to define the defects caused by mutations leading to molybdenum cofactor deficiency. The determination of the three-dimensional structure of MOCS1A should provide valuable insights into the molecular mechanism of MOCS1A and is a major goal of our current studies.

## Acknowledgements

We thank Dr. Silke Leimkühler (Technical University Braunschweig) for providing plasmid pSL219 and *E. coli* strain MJ7*chlM* (*moaD*$^-$)(DE3). This work was supported by grants from the National Institutes of Health (DK54835 to H. S., GM62542 to M. K. J., and GM47295 to B. H. H.) and the Deutsche Forschungsgemeinschaft (ME1266/12-3 to R. R. M.).

## References

1. Rajagopalan, K. V., and Johnson, J. L. (1992) *J. Biol. Chem.* **267**, 10199-10202
2. Reiss, J. (2000) *Hum. Genet.* **106**, 157-163
3. Reiss, J., and Johnson, J. L. (2003) *Hum. Mutat.* **21**, 569-576
4. Johnson, J. L., Rajagopalan, K. V., and Wadman, S. K. (1993) *Adv. Exp. Med. Biol.* **338**, 373-378
5. Wuebbens, M. M., and Rajagopalan, K. V. (1995) *J. Biol. Chem.* **270**, 1082-1087
6. Rieder, C., Eisenreich, W., O'Brien, J., Richter, G., Gotze, E., Boyle, P., Blanchard, S., Bacher, A., and Simon, H. (1998) *Eur. J. Biochem.* **255**, 24-36
7. Hänzelmann, P., Schwarz, G., and Mendel, R. R. (2002) *J. Biol. Chem.* **277**, 18303-18312
8. Matthies, A., Rajagopalan, K. V., Mendel, R. R., and Leimkühler, S. (2004) *Proc. Natl. Acad. Sci. U S A* **101**, 5946-5951
9. Stallmeyer, B., Drugeon, G., Reiss, J., Haenni, A. L., and Mendel, R. R. (1999) *Am. J. Hum. Genet.* **64**, 698-705
10. Sloan, J., Kinghorn, J. R., and Unkles, S. E. (1999) *Nucleic. Acids Res.* **27**, 854-858
11. Leimkühler, S., Freuer, A., Araujo, J. A., Rajagopalan, K. V., and Mendel, R. R. (2003) *J. Biol. Chem.* **278**, 26127-26134
12. Stallmeyer, B., Schwarz, G., Schulze, J., Nerlich, A., Reiss, J., Kirsch, J., and Mendel, R. R. (1999) *Proc. Natl. Acad. Sci. U S A* **96**, 1333-1338
13. Feng, G., Tintrup, H., Kirsch, J., Nichol, M. C., Kuhse, J., Betz, H., and Sanes, J. R. (1998) *Science* **282**, 1321-1324
14. Menendez, C., Igloi, G., Henninger, H., and Brandsch, R. (1995) *Arch. Microbiol.* **164**, 142-151
15. Menendez, C., Siebert, D., and Brandsch, R. (1996) *FEBS Lett.* **391**, 101-103
16. Sofia, H. J., Chen, G., Hetzler, B. G., Reyes-Spindola, J. F., and Miller, N. E. (2001) *Nucleic. Acids Res.* **29**, 1097-1106
17. Cheek, J., and Broderick, J. B. (2001) *J. Biol. Inorg. Chem.* **6**, 209-226
18. Frey, P. A. (2001) *Annu. Rev. Biochem.* **70**, 121-148
19. Jarrett, J. T. (2003) *Curr. Opin. Chem. Biol.* **7**, 174-182
20. Frey, P. A., and Magnusson, O. T. (2003) *Chem. Rev.* **103**, 2129-2148
21. Leimkühler, S., and Rajagopalan, K. V. (2001) *J. Biol. Chem.* **276**, 22024-22031

22. Glaser, J. H., and DeMoss, J. A. (1972) *Mol. Gen. Genet.* **116**, 1-10
23. Bradford, M. M. (1976) *Anal. Biochem.* **72**, 248-254
24. Fish, W. W. (1988) *Methods Enzymol.* **158**, 357-364
25. Fogo, J. K., and Popowsky, M. (1949) *Anal. Biochem.* **21**, 732-734
26. Drozdzewski, P. M., and Johnson, M. K. (1988) *Appl. Spectrosc.* **42**, 1575-1577
27. Johnson, M. K. (1988) in *Metal clusters in proteins* (Que, L., ed), American Chemical Society, Washington, D.C.
28. Thomson, A. J., Cheesman, M. R., and George, S. J. (1993) *Meth. Enzymol.* **226**, 199-232
29. Bennett, D. E., and Johnson, M. K. (1987) *Biochim. Biophys. Acta* **911**, 71-80
30. Ravi, N., Bollinger, J. M., Huynh, B. H., Edmondson, D. E., and Stubbe, J. (1994) *J. Am. Chem. Soc.* **116**, 8007-8014
31. Solomon, P. S., Shaw, A. L., Lane, I., Hanson, G. R., Palmer, T., and McEwan, A. G. (1999) *Microbiology* **145**, 1421-1429
32. Zheng, L., Cash, V. L., Flint, D. H., and Dean, D. R. (1998) *J. Biol. Chem.* **273**, 13264-13272
33. Takahashi, Y., and Tokumoto, U. (2002) *J. Biol. Chem.* **277**, 28380-28383
34. Nachin, L., Loiseau, L., Expert, D., and Barras, F. (2003) *Embo J.* **22**, 427-437
35. Lauhon, C. T., and Kambampati, R. (2000) *J. Biol. Chem.* **275**, 20096-20103
36. Dailey, H. A., Finnegan, M. G., and Johnson, M. K. (1994) *Biochemistry* **33**, 403-407
37. Duin, E. C., Lafferty, M. E., Crouse, B. R., Allen, R. M., Sanyal, I., Flint, D. H., and Johnson, M. K. (1997) *Biochemistry* **36**, 11811-11820
38. Agar, J. N., Krebs, C., Frazzon, J., Huynh, B. H., Dean, D. R., and Johnson, M. K. (2000) *Biochemistry* **39**, 7856-7862
39. Pierrel, F., Hernandez, H. L., Johnson, M. K., Fontecave, M., and Atta, M. (2003) *J. Biol. Chem.* **278**, 29515-29524
40. Ollagnier, S., Meier, C., Mulliez, E., Gaillard, J., Schuenemann, V., Trautwein, A. X., Mattioli, T., Lutz, M., and Fontecave, M. (1999) *J. Am. Chem. Soc.* **121**, 6344-6350
41. Broderick, J. B., Duderstadt, R. E., Fernandez, D. C., Wojtuszewski, K., Henshaw, T. F., and Johnson, M. K. (1997) *J. Am. Chem. Soc.* **119**, 7396-7397
42. Cosper, M. M., Jameson, G. N., Hernandez, H. L., Krebs, C., Huynh, B. H., and Johnson, M. K. (2004) *Biochemistry* **43**, 2007-2021
43. Johnson, M. K., Duderstadt, R. E., and Duin, E. C. (1999) *Adv. Inorg. Chem.* **47**, 1-82

44. Johnson, M. K., Robinson, A. E., and Thomson, A. J. (1982) in *Iron-sulfur proteins* (Spiro, T. G., ed), Wiley-Interscience, New York

45. Conover, R. C., Kowal, A. T., Fu, W. G., Park, J. B., Aono, S., Adams, M. W., and Johnson, M. K. (1990) *J. Biol. Chem.* **265**, 8533-8541

46. Onate, Y. A., Finnegan, M. G., Hales, B. J., and Johnson, M. K. (1993) *Biochim. Biophys. Acta* **1164**, 113-123

47. Brereton, P. S., Duderstadt, R. E., Staples, C. R., Johnson, M. K., and Adams, M. W. (1999) *Biochemistry* **38**, 10594-10605

48. Spiro, T. G., Czernuszewicz, R. S., and Han, S. (1988) in *Iron-sulfur proteins and analog complexes* (Spiro, T. G., ed), John Wiley & Sons, New York

49. Middleton, P., Dickson, D. P. E., Johnson, C. E., and Rush, J. D. (1978) *Eur. J. Biochem.* **88**, 135-141

50. Tong, W.-H., Jameson, G. N. L., Huynh, B. H., and Rouault, T. A. (2003) *Proc. Natl. Acad. Sci. USA* **100**, 9762-9767

51. Mulliez, E., Ollagnier-de Choudens, S., Meier, C., Cremonini, M., Luchinat, C., Trautwein, A. X., and Fontecave, M. (1999) *J. Biol. Inorg. Chem.* **4**, 614-620

52. Moulis, J., Davasse, V., Golinelli, M., Meyer, J., and Quinkal, I. (1996) *J. Biol. Inorg. Chem.* **1**, 2-14

53. Emptage, M. H., Kent, T. A., Huynh, B. H., Rawlings, J., Orme-Johnson, W. H., and Münck, E. (1980) *J. Biol. Chem.* **255**, 1793-1796

54. Huynh, B. H., Moura, J. J. G., Moura, I., Kent, T. A., LeGall, J., Xavier, A. V., and Münck, E. (1980) *J. Biol. Chem.* **255**, 3242-3244

55. Kent, T. A., Dreyer, J.-C., Kennedy, M. C., Huynh, B. H., Emptage, M. H., Beinert, H., and Münck, E. (1982) *Proc. Natl. Acad. Sci. USA* **79**, 1096-1100

56. Papaefthymiou, V., Girerd, J.-J., Moura, I., Moura, J. J. G., and Münck, E. (1987) *J. Am. Chem. Soc.* **109**, 4703-4710

57. Walsby, C. J., Ortillo, D., Broderick, W. E., Broderick, J. B., and Hoffman, B. M. (2002) *J. Am. Chem. Soc.* **124**, 11270-11271

58. Walsby, C. J., Hong, W., Broderick, W. E., Cheek, J., Ortillo, D., Broderick, J. B., and Hoffman, B. M. (2002) *J. Am. Chem. Soc.* **124**, 3143-3151

59. Cosper, M. M., Jameson, G. N., Davydov, R., Eidsness, M. K., Hoffman, B. M., Huynh, B. H., and Johnson, M. K. (2002) *J. Am. Chem. Soc.* **124**, 14006-14007

60. Layer, G., Moser, J., Heinz, D. W., Jahn, D., and Schubert, W. D. (2003) *Embo J.* **22**, 6214-6224

61. Berkovitch, F., Nicolet, Y., Wan, J. T., Jarrett, J. T., and Drennan, C. L. (2004) *Science* **303**, 76-79

62. Ugulava, N. B., Gibney, B. R., and Jarrett, J. T. (2001) *Biochemistry* **40**, 8343-8351

63. Ugulava, N. B., Surerus, K. K., and Jarrett, J. T. (2002) *J. Am. Chem. Soc.* **124**, 9050-9051

64. Tse Sum Bui, B., Florentin, D., Fournier, F., Ploux, O., Méjean, A., and Marquet, A. (1998) *FEBS Lett.* **440**, 226-230

65. Ugulava, N. B., Sacanell, C. J., and Jarrett, J. T. (2001) *Biochemistry* **40**, 8352-8358

66. Jameson, G. N., Cosper, M. M., Hernandez, H. L., Johnson, M. K., and Huynh, B. H. (2004) *Biochemistry* **43**, 2022-2031

67. Wuebbens, M. M., and Rajagopalan, K. V. (2003) *J. Biol. Chem.* **278**, 14523-14532

68. Leimkühler, S., Wuebbens, M. M., and Rajagopalan, K. V. (2001) *J. Biol. Chem.* **276**, 34695-34701

69. Marquet, A. (2001) *Curr. Opin. Chem. Biol.* **5**, 541-549

70. Santamaria-Araujo, J. A., Fischer, B., Otte, T., Nimtz, M., Mendel, R. R., Wray, V., and Schwarz, G. (2004) *J. Biol. Chem.* **279**, 15994-15999

71. Wuebbens, M. M., and Rajagopalan, K. V. (1993) *J. Biol. Chem.* **268**, 13493-13498

72. Werst, M. M., Kennedy, M. C., Houseman, A. L., Beinert, H., and Hoffman, B. M. (1990) *Biochemistry* **29**, 10533-10540

73. Beinert, H., Kennedy, M. C., and Stout, C. D. (1996) *Chem. Rev.* **96**, 2335-2374

74. Auerbach, G., Herrmann, A., Bracher, A., Bader, G., Gutlich, M., Fischer, M., Neukamm, M., Garrido-Franco, M., Richardson, J., Nar, H., Huber, R., and Bacher, A. (2000) *Proc. Natl. Acad. Sci. U S A* **97**, 13567-13572.

75. Kaiser, J., Schramek, N., Eberhardt, S., Puttmer, S., Schuster, M., and Bacher, A. (2002) *Eur. J. Biochem.* **269**, 5264-5270

76. Rebelo, J., Auerbach, G., Bader, G., Bracher, A., Nar, H., Hosl, C., Schramek, N., Kaiser, J., Bacher, A., Huber, R., and Fischer, M. (2003) *J. Mol. Biol.* **326**, 503-516

**Figure 5.1** Multiple sequence alignments of the N- (*A*) and C-terminal (*B*) cysteine motifs of MOCS1A**.** From top to bottom (accession numbers in brackets): *Homo sapiens* (CAC44527), *Arabidopsis thaliana* (CAA88107), *Clostridium perfringens* (BAA76928), *Haemophilus influenzae* (P45311), *Mycobacterium tuberculosis* (CAB08366), *Escherichia coli* (P30745), *Arthrobacter nicotinovorans* (CAA71779), *Bacillus subtilis* (CAB03683), *Staphylococcus carnosus* (AAC8383), *Helicobacter pylorii* (P56414) and *Rhodobacter capsulatus* (Q9X5W3). The consensus sequences have been calculated with a threshold of 80%. Completely conserved amino acids show a "!" in the consensus sequence and are highlighted white on black. Highly conserved amino acids are shown with dark grey backgrounds (white letters) and low conserved amino acids with light grey backgrounds (black letters).

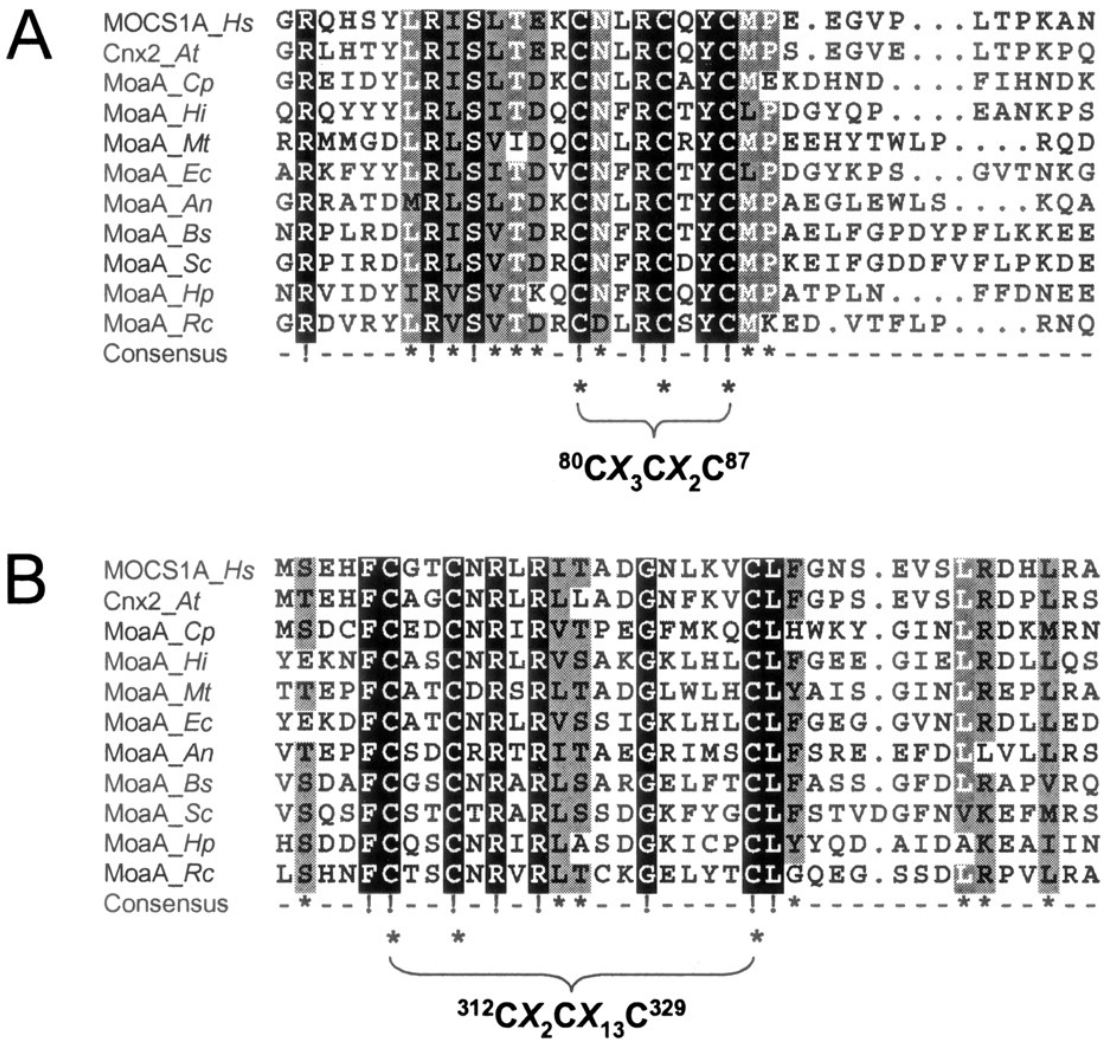
A
MOCS1A_Hs GRQHSYLRISLTEKCNLRCQYCMPE.EGVP...LTPKAN
Cnx2_At GRLHTYLRISLTERCNLRCQYCMPS.EGVE...LTPKPQ
MoaA_Cp GREIDYLRISLTDKCNLRCAYCMEKDHND....FIHNDK
MoaA_Hi QRQYYYLRLSITDQCNFRCTYCLPDGYQP....EANKPS
MoaA_Mt RRMMGDLRLSVIDQCNLRCRYCMPEEHYTWLP....RQD
MoaA_Ec ARKFYYLRLSITDVCNFRCTYCLPDGYKPS...GVTNKG
MoaA_An GRRATDMRLSLTDKCNLRCTYCMPAEGLEWLS....KQA
MoaA_Bs NRPLRDLRISVTDRCNFRCTYCMPAELFGPDYPFLKKEE
MoaA_Sc GRPIRDLRLSVTDRCNFRCDYCMPKEIFGDDFVFLPKDE
MoaA_Hp NRVIDYIRVSVTKQCNFRCQYCMPATPLN....FFDNEE
MoaA_Rc GRDVRYLRVSVTDRCDLRCSYCMKED.VTFLP....RNQ
Consensus -!----*!*!***-!*-!!-!!**--------------
* * *
$^{80}CX_3CX_2C^{87}$
B
MOCS1A_Hs MSEHFCGTCNRLRITADGNLKVCLFGNS.EVSLRDHLRA
Cnx2_At MTEHFCAGCNRLRLLADGNFKVCLFGPS.EVSLRDPLRS
MoaA_Cp MSDCFCEDCNRIRVTPEGFMKQCLHWKY.GINLRDKMRN
MoaA_Hi YEKNFCASCNRLRVSAKGKLHLCLFGEE.GIELRDLLQS
MoaA_Mt TTEPFCATCDRSRLTADGLWLHCLYAIS.GINLREPLRA
MoaA_Ec YEKDFCATCNRLRVSSIGKLHLCLFGEG.GVNLRDLLED
MoaA_An VTEPFCSDCRRTRITAEGRIMSCLFSRE.EFDLLVLLRS
MoaA_Bs VSDAFCGSCNRARLSARGELFTCLFASS.GFDLRAPVRQ
MoaA_Sc VSQSFCSTCTRARLSSDGKFYGCLFSTVDGFNVKEFMRS
MoaA_Hp HSDDFCQSCNRIRLASDGKICPCLYYQD.AIDAKEAIIN
MoaA_Rc LSHNFCTSCNRVRLTCKGELYTCLGQEG.SSDLRPVLRA
Consensus -*--!!---!-!-!**--!-----!!*--------**--*--
* * *
$^{312}CX_2CX_{13}C^{329}$

**Figure 5.2** UV-visible absorption spectra of MOCS1A**.** *A*, aerobically (solid line) and anaerobically (dashed line) purified MOCS1A (29 μM). The inset shows the spectra of anaerobically purified MOCS1A as isolated (solid line) and after reduction with 2.5 mM sodium dithionite (dashed line). *B*, aerobically purified MOCS1A (68 μM) in 50 mM Tris/HCl, pH 9.0, 300 mM NaCl, 10% (v/v) glycerol and 500 mM imidazole. From top to bottom: immediately after Ni-NTA purification and after 6 h, 12 h and 24 h of air exposure. Upper panel: MOCS1A as purified; Lower panel: MOCS1A after addition of 1 mM 5′-GTP. *C*, anaerobically reconstituted MOCS1A (8 μM) before (solid line) and after 5 min (dashed line) of air exposure. The inset shows a time dependence of air exposure. *D*, from top to bottom: anaerobically purified MOCS1A wild type, C-terminal Cys → Ser triple variant and N-terminal Cys → Ser triple variant. Spectra were normalized to equal amounts of protein (30 μM). The inset shows a time dependence of air exposure of wild type MOCS1A (▲) and mutants of the N- (•) and C-terminal (☐) cysteine motif. All spectra were recorded in 100 mM Tris/HCl, pH 9.0, with 300 mM NaCl with exceptions as indicated.

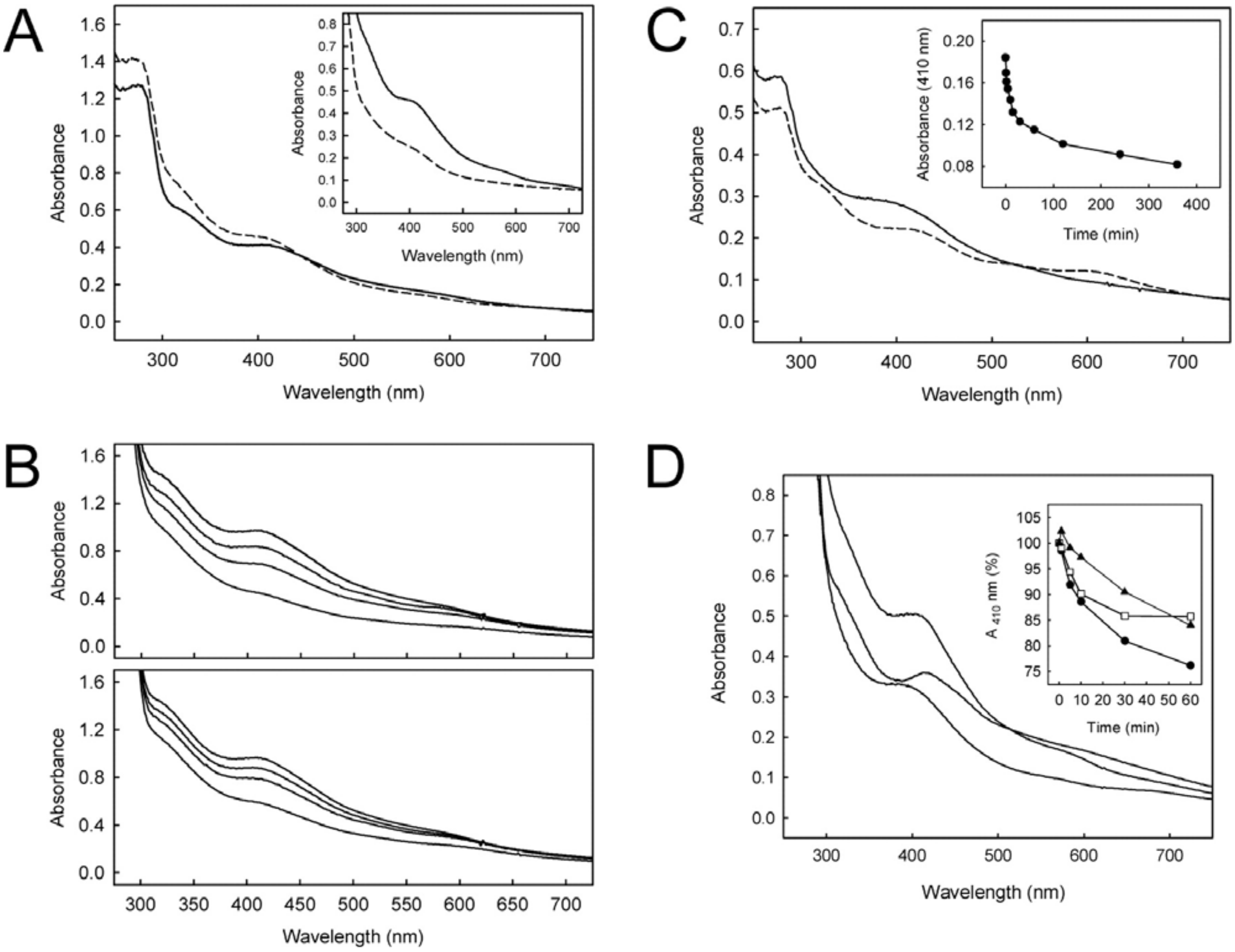
A
B
C
D
Absorbance
Wavelength (nm)
Absorbance (410 nm)
Time (min)
A 410 nm (%)
1.6
1.4
1.2
1.0
0.8
0.6
0.4
0.2
0.0
0.7
0.5
0.3
0.1
0.20
0.16
0.12
0.08
105
100
95
90
85
80
75
300
350
400
450
500
550
600
650
700
0
10
20
30
40
50
60
100
200

**Figure 5.3** Resonance Raman spectra of MOCS1A**.** *A*, aerobically purified MOCS1A. *B*, anaerobically purified MOCS1A. *C*, dithionite-reduced anaerobically purified MOCS1A. *D*, anaerobically purified MOCS1A after exposure to air for 10 min. *E,* anaerobically reconstituted MOCS1A. *F*, anaerobically purified MOCS1A N-terminal Cys → Ser triple variant. The spectra were recorded with 150 mW of 457 nm laser excitation incident on ~2-3 mM samples frozen at 17 K. Each scan involved photon counting for 1 s at 0.5 $cm^{-1}$ increments at 8 $cm^{-1}$ spectral resolution and the spectra are the sum of ~100 scans.

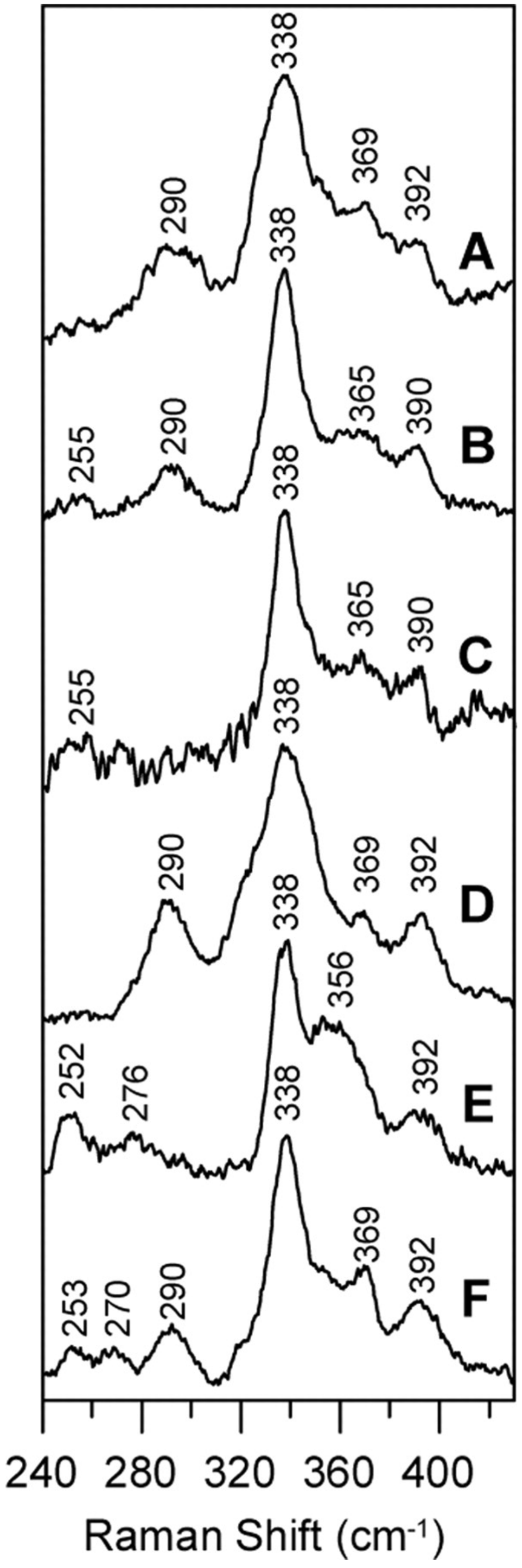
338
369
392
290
A
338
365
390
255
290
B
338
365
390
255
C
338
290
369
392
D
338
356
252
276
392
E
338
369
392
253
270
290
F
240
280
320
360
400
Raman Shift (cm-1)

**Figure 5.4** X-band EPR spectra of MOCS1A. Samples are indicated on the figure with the left panel as purified and the right panel after reduction with a 10-fold excess of sodium dithionite. Conditions of measurement: temperature, 20 K; microwave power, 5 mW; frequency, 9.59 GHz; modulation amplitude, 0.64 mT. Selected *g* values are indicated on the spectra. Sample concentrations were 0.43 mM for aerobically purified, 0.24 mM for anaerobically purified, 0.14 mM for anaerobically reconstituted, and 0.25 mM for the anaerobically purified N-terminal Cys → Ser triple variant.

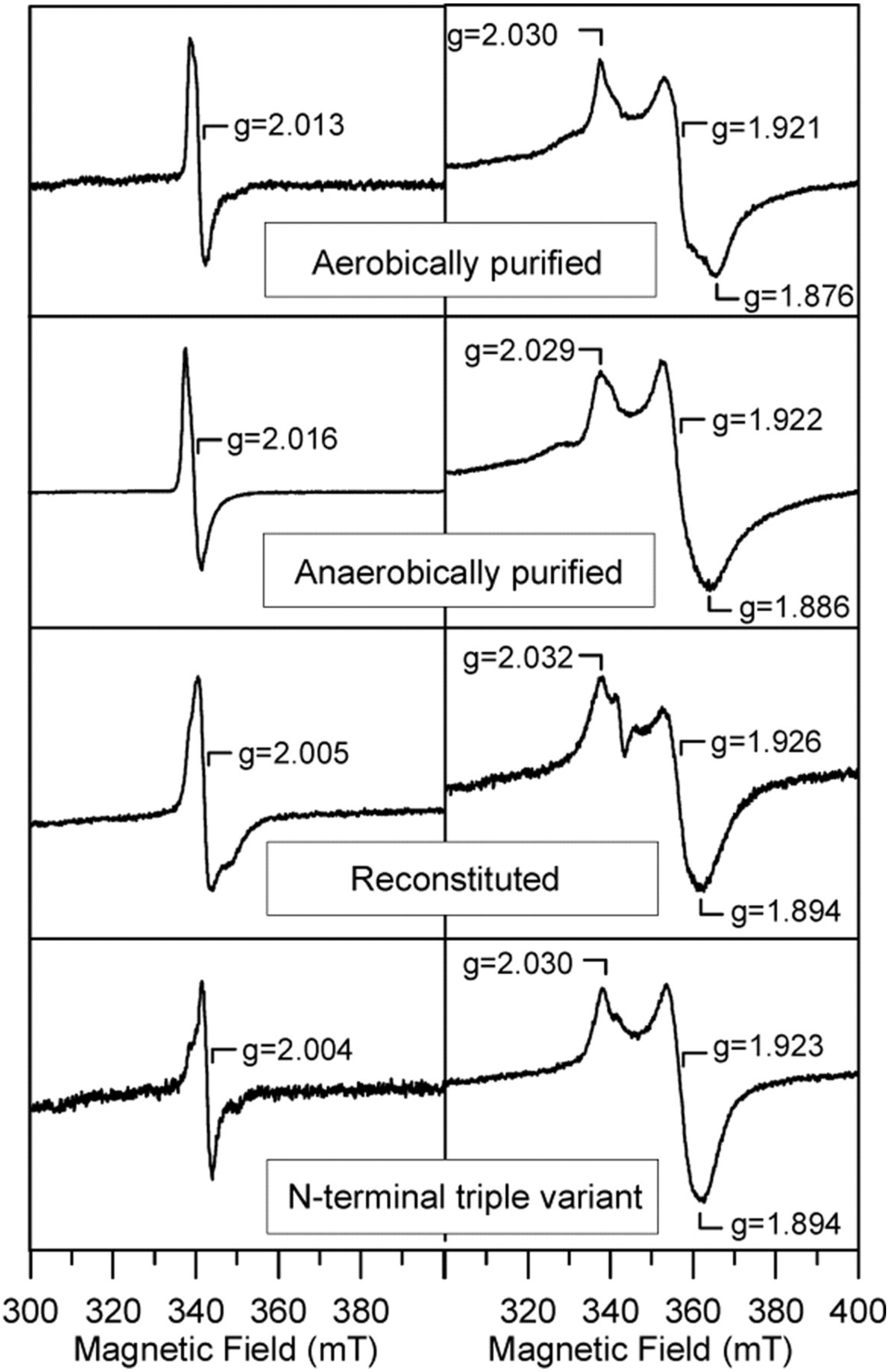
g=2.013
g=2.030
g=1.921
g=1.876
Aerobically purified
g=2.016
g=2.029
g=1.922
g=1.886
Anaerobically purified
g=2.005
g=2.032
g=1.926
g=1.894
Reconstituted
g=2.004
g=2.030
g=1.923
g=1.894
N-terminal triple variant
300
320
340
360
380
Magnetic Field (mT)
320
340
360
380
400
Magnetic Field (mT)

**Figure 5.5** Perpendicular and parallel-mode X-band spectra of anaerobically purified MOCS1A. EPR spectra recorded at 4 K and 50 mW microwave power with a modulation amplitude of 0.63 mT and a microwave frequency of 9.60 GHz (perpendicular mode) and 9.36 GHz (parallel mode). The sample is as described in Fig. 5.4. The data shown is for anaerobically purified MOCS1A, but identical spectra were observed for aerobically purified MOCS1A and the anaerobically purified N-terminal triple Cys → Ser variant of MOCS1A.

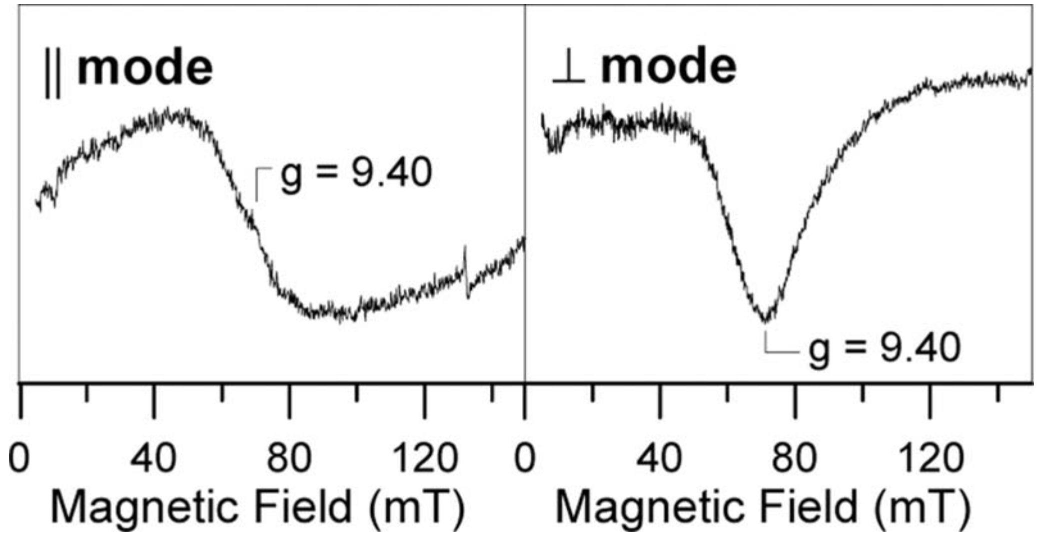
|| mode
g = 9.40
⊥ mode
g = 9.40
0
40
80
120
Magnetic Field (mT)
0
40
80
120
Magnetic Field (mT)

**Figure 5.6** VTMCD spectra of MOCS1A. *A,* as purified MOCS1A. From top to bottom: aerobically purified MOCS1A (0.11 mM) at 4.22 K; anaerobically purified MOCS1A (0.19 mM) at 1.77 K, 4.22 K, 10.0 K, 25.0 K, and 50.0 K; anaerobically purified MOCS1A N-terminal triple Cys → Ser variant (0.33 mM) at 1.80 K, 4.22 K, 10.0 K, 25.0 K, and 50.1 K. *B*, dithionite-reduced MOCS1A. From top to bottom: aerobically purified MOCS1A (0.26 mM) at 1.81 K, 4.22 K, 10.3 K, and 25.0 K; anaerobically purified MOCS1A (0.16 mM) at 1.93 K, 4.22 K, 10.2 K, and 25.0 K; anaerobically reconstituted MOCS1A (0.11 mM) at 1.84 K, 4.22 K, 11.5 K, and 24.6 K. MCD spectra were collected with an applied field of 6 T and all transitions increase in intensity with decreasing temperature. All samples were in 100 mM Tris/HCl buffer pH 9.0, with 300 mM NaCl and 50% (v/v) ethylene glycol, and samples were reduced anaerobically with a 10-fold stoichiometric excess of sodium dithionite.

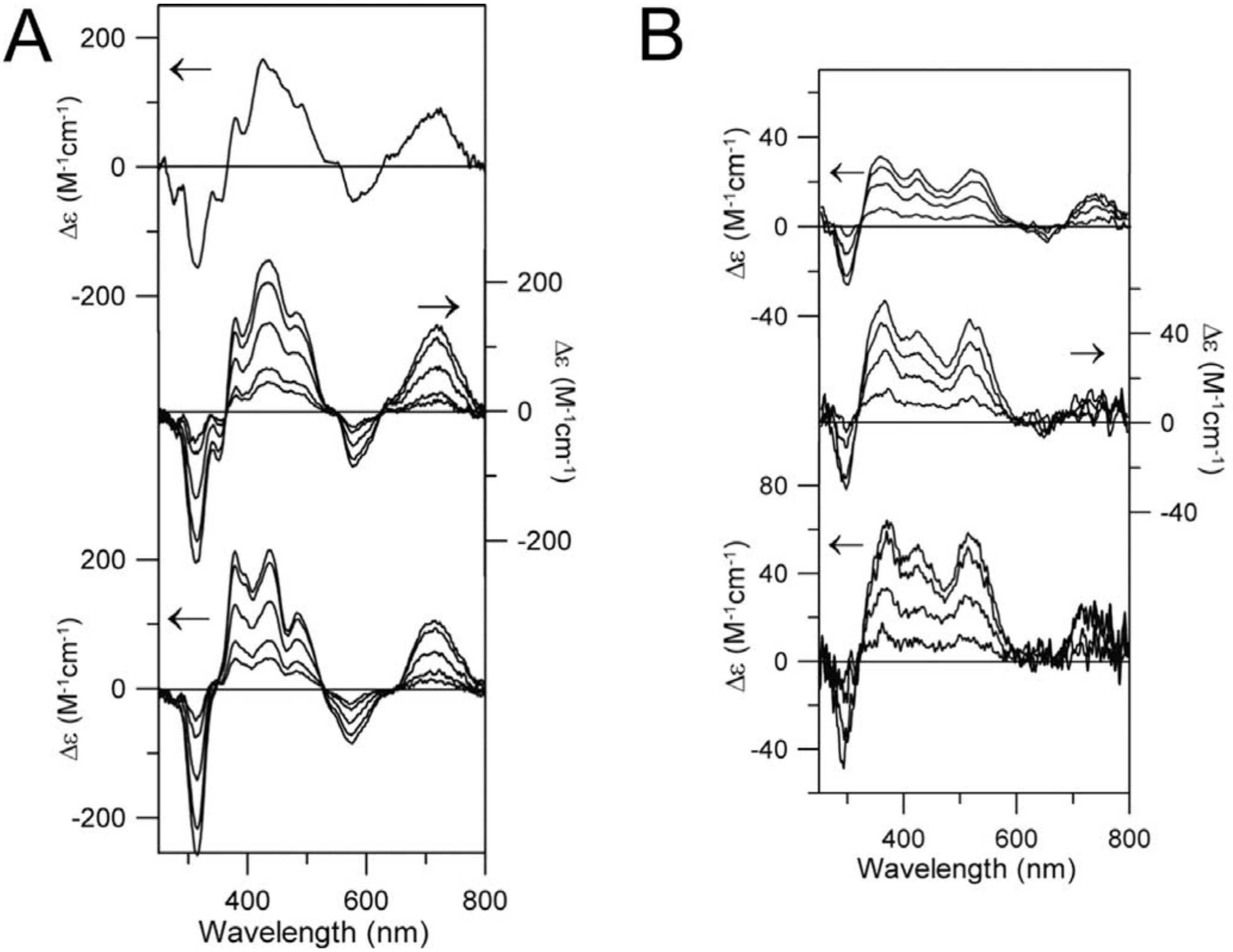
A
B
Δε (M-1cm-1)
200
0
-200
200
0
-200
Δε (M-1cm-1)
200
0
-200
400
600
800
Wavelength (nm)
40
0
-40
80
40
0
-40
Δε (M-1cm-1)
40
0
-40
400
600
800
Wavelength (nm)

**Figure 5.7** VHVT MCD saturation magnetization plots for MOCS1A. *A*, anaerobically purified MOCS1A at 720 nm. Data collected at 1.77 K (circles), 4.22 K (triangles), and 10.0 K (squares) for magnetic fields in the range 0-6 T. Solid line is simulated magnetization data for an xy-polarized transition from a $S = 2$ ground state ($g_{||} = 8.0$ and $g_{\perp} = 0.0$). Very similar VHVT MCD saturation plots were observed for aerobically purified MOCS1A and the anaerobically purified MOCS1A N-terminal triple variant. All samples are as described in Fig. 5.6A. *B*, aerobically purified MOCS1A at 520 nm. Data collected at 1.81 K (circles), 4.22 K (triangles), and 10.3 K (squares) for magnetic fields in the range 0-6 T. Solid line is simulated magnetization data for a $S = 1/2$ ground state with $g_{||} = 2.03$ and $g_{\perp} = 1.92$. Very similar VHVT MCD saturation plots were observed for anaerobically purified MOCS1A and the anaerobically reconstituted MOCS1A. The samples are as described in 5.6B.

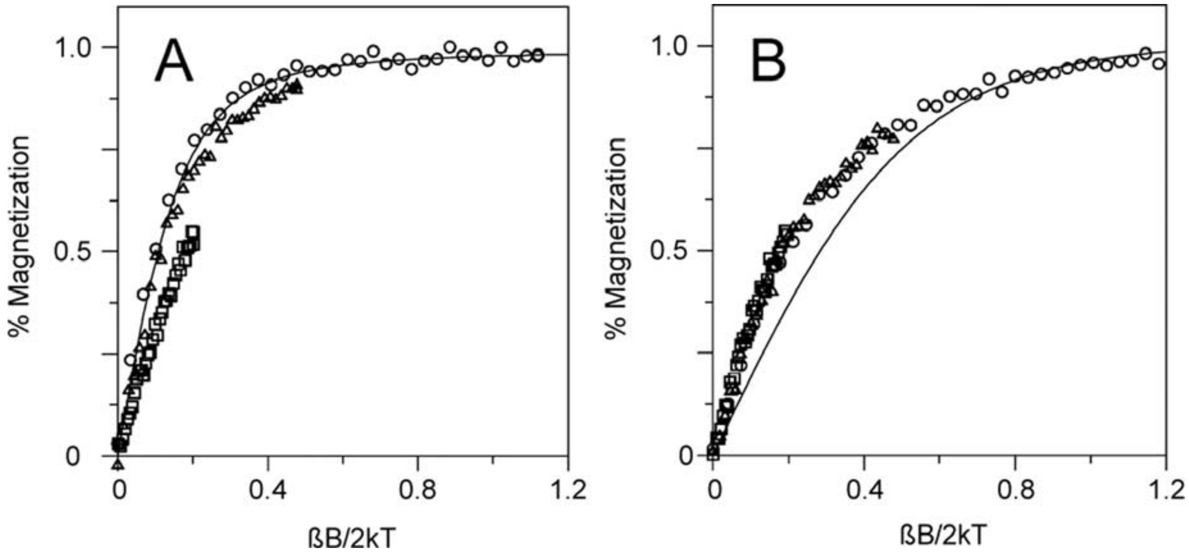
A
B
% Magnetization
1.0
0.5
0
ßB/2kT
0
0.4
0.8
1.2

**Figure 5.8** Mössbauer spectra of MOCS1A. Anaerobically purified MOCS1A N-terminal triple Cys → Ser variant (hatched marks) recorded at 4.2 K in zero-field (*A*) and in a field of 50 mT applied parallel to the γ-rays (*B*). The *solid line* shown in *A* is a least-squares fit of the data. The parameters are reported in the text. The spectrum of anaerobically purified MOCS1A recorded at 4.2 K in a parallel field of 50 mT is shown in *C* (hatched marks) overlaid with the spectrum of *B* (solid line), which is scaled to 60% of the total absorption of *C*. Removal of the contribution of spectrum *B* from spectrum *C* results in the spectrum shown in *D* (hatched mark). The *solid line* shown in *D* is a theoretical simulation of the superposition of two equal-intensity quadrupole doublets with the following parameters: $\Delta E_Q(1) = 1.26$ mm/s and $\delta(1) = 0.48$ mm/s; and $\Delta E_Q(2) = 0.93$ mm/s and $\delta(2) = 0.49$ mm/s.

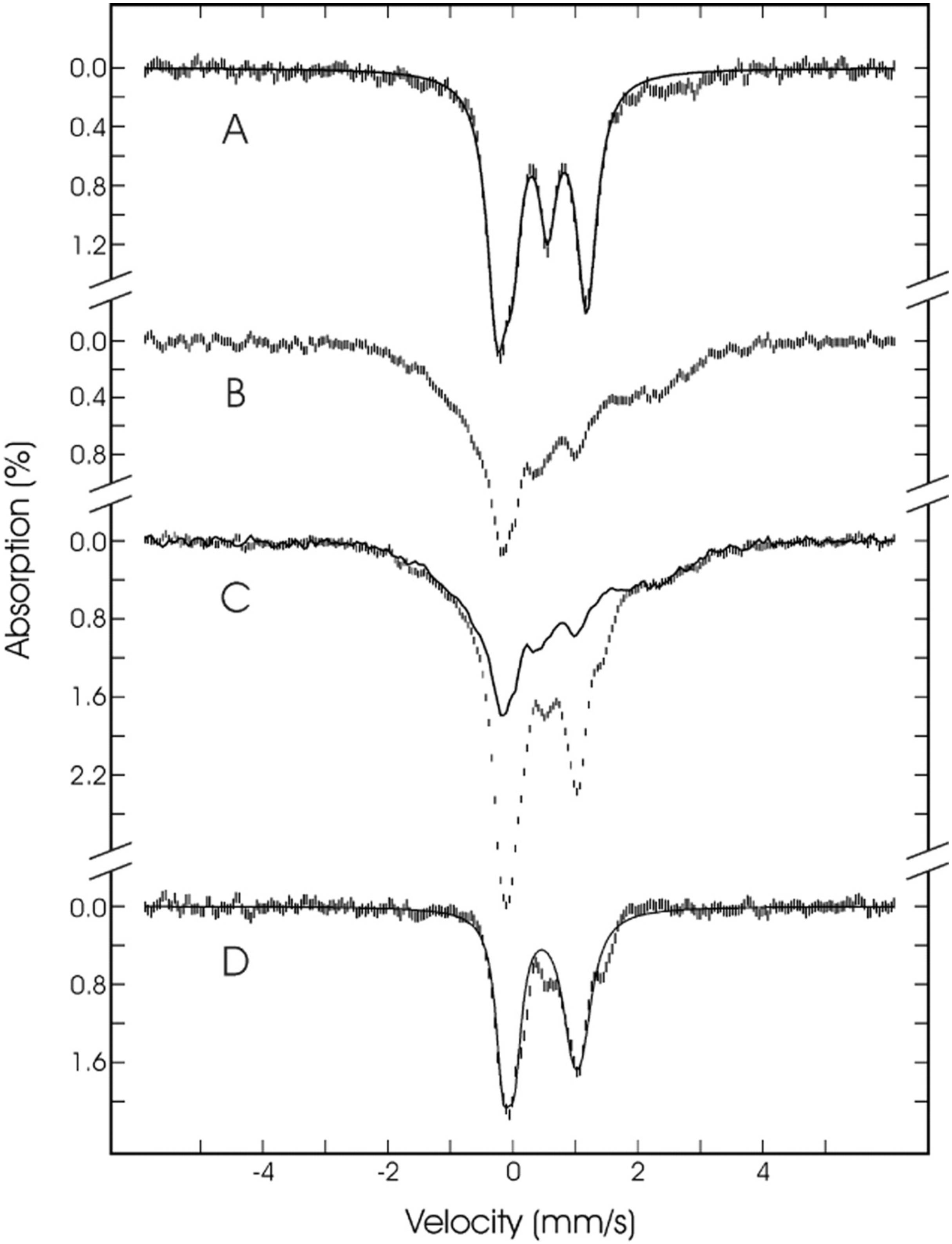
A
B
C
D
0.0
0.4
0.8
1.2
0.0
0.4
0.8
0.0
0.8
1.6
2.2
0.0
0.8
1.6
Absorption (%)
-4
-2
0
2
4
Velocity (mm/s)

**Figure 5.9** Functional and UV-visible absorption characterization of MOCS1A and single Cys → Ser mutants. *A*, complementation of an *E. coli moa* mutant strain (KB2037) with wild type full-length MOCS1A and Cys → Ser variants, and activity analysis with a nitrate reductase overlay assay. The lower panel shows the corresponding expression profiles. Equal amounts of the soluble fractions of *E. coli* crude cell extracts were separated by SDS-PAGE and immunoblotted with polyclonal MOCS1A antibodies: wild type MOCS1A (1), C80S (2), C84S (3), C87S (4), C312S (5), C315S (6) and C327S (7). *B*, purification and spectroscopic properties. UV-visible absorption spectra of MOCS1A and single Cys → Ser mutants purified under aerobic conditions. Spectra were recorded in 50 mM Tris/HCl, pH 9.0, 300 mM NaCl, 10% (v/v) glycerol and 500 mM imidazole and are normalized to the same protein concentration (22 μM). Upper panel, from top to bottom: wild type MOCS1A, C84S, C80S and C87S. Lower panel, from top to bottom: wild type MOCS1A, C329S, C312S and C315S. The insets show the corresponding Coomassie Blue stained SDS-PAGE analysis of purified wild type MOCS1A and single Cys → Ser mutants.

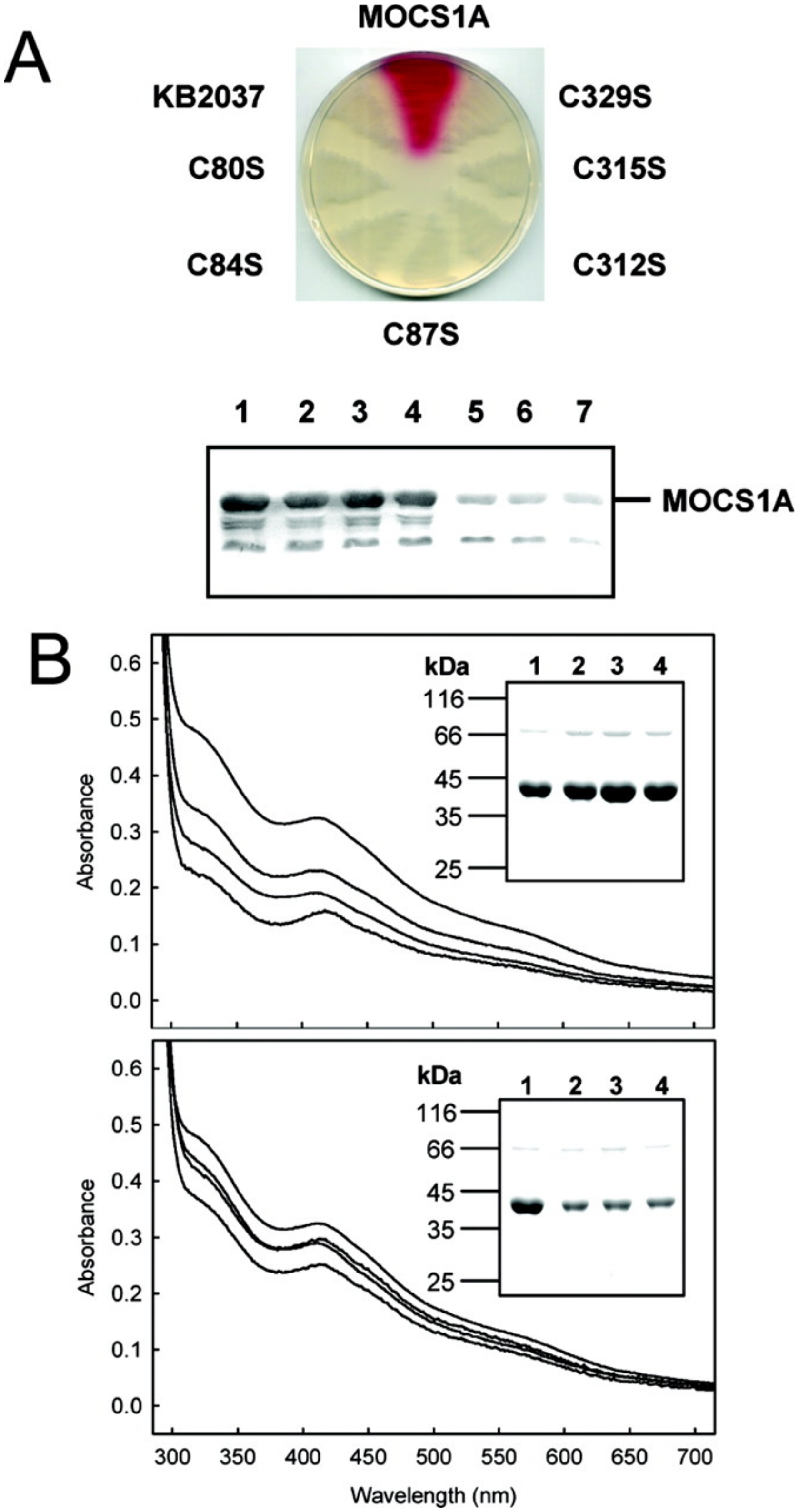
A
MOCS1A
KB2037
C329S
C80S
C315S
C84S
C312S
C87S
1
2
3
4
5
6
7
MOCS1A
B
Absorbance
0.0
0.1
0.2
0.3
0.4
0.5
0.6
kDa
1
2
3
4
116
66
45
35
25
Wavelength (nm)
300
350
400
450
500
550
600
650
700

# CHAPTER 6

# MIAB PROTEIN FROM THERMOTOGA MARITIMA. CHARACTERIZATION OF AN EXTREMELY THERMOPHILIC TRNA-METHYLTHIOTRANSFERASE[1]

---

[1] Pierrel, Fabien; Hernández, Heather L.; Johnson, Michael K.; Fontecave, Marc; Atta, Mohamed. *J. Biol. Chem*. **2004**, *278*, 29515-29524.

Reprinted here with permission of publisher.

**Abbreviations:** T. m., *Thermotoga maritima*; PCR, polymerase chain reaction; bp, base pair; ORF, open reading frame; $ms^2i^6A$-37, the modified nucleoside 2-methylthio-N6-isopentenyl adenosine at position 37; $s^4U$, 4-thiouridine; $mnm^5s^2U$, 5-methyaminomethyl-2-thiouridine; SDS-PAGE, sodium dodecylsulfate polyacrylamide gel electrophoresis; RR, resonance Raman; VTMCD, variable temperature magnetic circular dichroism; SAM, *S*-adenosylmethionine; Fe-S, iron-sulfur cluster; DTT, dithiothreitol; tRNA, transfer ribonucleic acid.

## Abstract

In *Escherichia coli*, the MiaB protein catalyzes the methylthiolation of N-6-isopentenyl adenosine in tRNAs, the last reaction step during biosynthesis of 2-methylthio-N-6-isopentenyl adenosine ($ms^2i^6A$-37). For the first time the thermophilic bacterium *Thermotoga martima* is shown here to contain such a MiaB tRNA-modifying enzyme, named MiaBTm, and to synthesize $ms^2i^6A$-37 as demonstrated by an analysis of modified nucleosides from tRNA hydrolysates. The corresponding gene, (*TM0653*), was identified by sequence similarity to the *miaB* gene cloned and expressed *E. coli*. MiaBTm was purified to homogeneity and thoroughly characterized by biochemical and spectroscopic methods. It is a monomer of 443 residues with a molecular mass of 50,710 kilodaltons. Its amino-acid sequence shares the Cys*XXX*Cys*XX*Cys sequence with MiaB from *E. coli* as well as with biotin synthase and lipoate synthase. This sequence was shown to be essential for chelation of an iron-sulfur center and for activity in these enzymes. As isolated, MiaBTm contains both iron and sulfide and an apoprotein form can coordinate up to 4 Fe and 4 S atoms per polypeptide chain. UV-visible absorption, resonance Raman, variable-temperature magnetic circular dichroism, and EPR spectroscopy of MiaBTm indicate the presence of a $[4Fe\text{-}4S]^{+2/+1}$ cluster under reducing and anaerobic conditions, whereas $[3Fe\text{-}4S]^{+1}$ and $[2Fe\text{-}2S]^{+2}$ forms are generated under aerobic conditions. The redox potential of the $[4Fe\text{-}4S]^{+2/+1}$ transition is –495 ±10 mV (*vs.* the normal hydrogen electrode). Finally, the expression of MiaBTm from *T. martima* in an *E. coli* mutant strain lacking functional *miaB* gene allowed production of $ms^2i^6A$-37. These results provide further information on the enzymes involved in methylthiolation of tRNAs.

## Introduction

Transfer RNAs (tRNAs) of all organisms contain a number of modified nucleosides, which are derivatives of the four ordinary nucleosides (1). They are formed by enzymatic modifications of the polynucleotide transcripts during the complex process of tRNA maturation (2). Changes in the degree of tRNA modification have been invoked as a possible global regulatory mechanism by which cells respond to certain environmental stresses (3). The importance of these modifications is well demonstrated by the fact that as much as 1% of the bacterial genome is devoted to tRNA modification (4). Modified bases are located throughout the tRNA molecule, but the greatest variety is found in the anticodon loop. Some of these reactions of modification consist in the introduction of a sulfur atom to generate thionucleosides in tRNAs. The chemistry of the biological reactions leading to the synthesis of sulfur-containing metabolites is still not well understood and remains a very active field of research for bio-inorganic and bio-organic chemists. Among the metabolic pathways requiring further elucidation are those leading not only to sulfur-containing bases in RNA but also to iron-sulfur clusters (5), biotin (6), molybdopterin (7), lipoic acid (8), and thiamin (9). Our laboratories are investigating several of these biosynthetic reactions, and we report here our results on sulfur atom insertion reactions in tRNAs.

In *Escherichia coli* four different thiolated nucleosides have been characterized. The best characterized biosynthetic pathway is that of 4-thiouridine, which is formed from uridine through a reaction catalyzed by the ThiI protein (10). The tRNA modification leading to 2-methylthio-N-6-isopentenyl adenosine (ms$^2$i$^6$A-37) involves a chemically intriguing and difficult aromatic C-H to C-S bond conversion, the mechanism of which has yet to be investigated. The modified nucleoside ms$^2$i$^6$A-37 is found at position 37, next to the anticodon on the 3’ position in almost all eukaryotic and bacterial tRNAs that read codons beginning with U except $\mathrm{tRNA}^{\mathrm{I,V}}$ Ser (11). The postulated pathway for the synthesis of $\mathrm{ms}^2\mathrm{i}^6\mathrm{A}$-37 and the proteins involved are shown in Figure 6.1 (2, 12, 13).

The biosynthesis of $\mathrm{ms}^2\mathrm{i}^6\mathrm{A}$-37 requires at least two enzymatic activities, and the corresponding genetic loci are designated *miaA* and *miaB*. A third gene, *miaC*, has been postulated but has not been identified (Figure 6.1). In *E. coli*, the first step of the biosynthesis of $\mathrm{ms}^2\mathrm{i}^6\mathrm{A}$-37 is the addition of the isopentenyl group to the N-6 nitrogen of adenosine. This reaction is catalyzed by the well-characterized tRNA-isopentenylpyrophosphate transferase enzyme, encoded by the *miaA* gene (14-16). The second step, which is dependent on iron, cysteine, *S*-adenosylmethionine (SAM), consists of both sulfur insertion and methylation at position 2 of the base moiety but it is still unknown whether each reaction is catalyzed by a single enzyme (MiaB + MiaC) or both by the same enzyme MiaB (17-19). However, tRNAs from mutant strains lacking a functional *miaB* gene have been shown to contain only $\mathrm{i}^6\mathrm{A}$-37, the product of the first step of the pathway, suggesting that the MiaB protein is involved at least in C-S bond formation (20).

The main feature of MiaB protein sequences, which has emerged from the first sequence determination (20) and has been strongly substantiated when significant comparisons became possible (21), is the presence of highly conserved motifs. The N-terminal half of all MiaB enzymes contains a strictly conserved canonical cysteine triad Cys*XXX*Cys*XX*Cys, which is also found in biotin and lipoate synthases. In these two enzymes, which also catalyze C-H to C-S bond conversion reactions, this motif was shown to provide cysteine ligands for a catalytically essential $[4\mathrm{Fe}\text{-}4\mathrm{S}]^{+2/+1}$ cluster. Furthermore, it is the signature for a superfamily of iron-sulfur enzymes involved in a great variety of biosynthetic pathways and metabolic processes that function via radical mechanisms (22). Because we recently showed that MiaB from *E. coli* was an iron-sulfur protein with one [4Fe-4S] cluster per polypeptide chain and that the three cysteines of the CysXXXCysXXCys motif were required for activity (23), it is very likely that MiaB, biotin synthase and lipoate synthase employ similar radical mechanisms for activation of sulfur and its insertion into their respective substrates.

*Thermotoga maritima* is a hyperthermophilic bacterium with an optimal growth temperature of 80 °C and is one of the deepest and most slowly-evolving eubacterial lineage (24). The genomic sequence of *T. maritima* shows an ORF (*TM0653*) encoding a putative MiaB tRNA-methylthiotransferase. Because MiaB from *E. coli* proved quite difficult to manipulate and characterize and to gain more insight into the structure of the MiaB enzymes, we have extended our work on thiolation of tRNAs by investigating the MiaB protein from *T. maritima*. We report its purification and characterization, and show that it displays some properties (stability and homogeneity of the iron-sulfur cluster) that have not been observed with other enzymes of the "radical-SAM" superfamily. Furthermore, we demonstrate that this protein in indeed a MiaB enzyme because its expression in an *E. coli* strain lacking its own *miaB* gene (20) results in the formation of $ms^2i^6A$ Finally, we show that the modified nucleoside $ms^2i^6A$ is actually present in tRNA from *T. maritima*.

## Materials and Methods

*Strains—E. coli* DH5α was used for routine DNA manipulations. *E. coli* BL21CodonPlus(DE3)-RIL$^{TM}$ (Stratagene) which contains extra copies of genes encoding tRNA with codons rarely used in *E.coli* (argU, ileY, leuW tRNA genes) was used to produce the recombinant protein. *Thermotoga maritima* (strain DSMZ3109) was a gift from the laboratory of

Professor Robert Huber, University of Regensburg, Germany. *E. coli* strain TX3346 *miaB*- was a gift of Professor Malcolm E. Winkler, University of Texas, Houston, United-States.

*General procedures*—All DNA manipulations were as described previously (25). Enzymes, oligonucleotides, and culture media were purchased from Invitrogen Cergy-Pontoise, France. T4 DNA ligase was from Promega, Inc. Bacterial alkaline phosphatase and plasmid DNA purification kit, Flexiprep$^{TM}$, were from Amersham-Pharmacia, Inc. DNA fragments were extracted from agarose gel and purified with High Pure PCR Product Purification Kit (Roche, Inc.), DNA sequencing was performed by Genome Express company (Grenoble, France).

*Cloning of the MiaB gene and construction of the overexpressing plasmid*—The *TM0653* gene, encoding the MiaB protein named MiaBTm was identified from the GenBank database using the BLAST search algorithm (26). The open reading frame was amplified by Polymerase Chain Reaction-based method (PCR) using genomic DNA of *T. maritima* as a template. The following primers were used : 5'-gggaggtcgcatATGagattttacataaag-3' (*Nde*I site underlined, ATG codon in upper case) hybridized to the non coding strand at the 5' terminus of the gene and 5'-gacaagggaagaaagcttgtccaccgtcgtg-3' (*Hind*III site underlined) hybridized to the coding strand, approximately 25 bp after the TGA stop codon. PCR was run on a Stratagene RoboCycler Gradient 40 machine as follows. Genomic DNA (0.5-1 μg) was denatured for 4 min at 95°C in the presence of the primers (0.5 μM each). The *Pwo* DNA polymerase (2 units) and deoxynucleotide mix (0.2 mM each) were added and 25 cycles (1 min at 95 °C, 1 min at 52 °C, 2 min at 72 °C) were then performed followed by a final 10 min elongation step at 72 °C. The PCR product was digested with *Nde*I and *Hind*III and then ligated with T4 DNA ligase into the pT$_7$-7 plasmid previously digested with the same restriction enzymes. The cloned gene was entirely sequenced to ensure that no error was introduced during PCR reaction. The plasmid was then named p$T_7$-MiaBTm.

*Overexpression of the recombinant protein MiaBTm*—The protein was overexpressed in *E. coli* BL21CodonPlus(DE3)-RIL$^{TM}$. The transformation of competent cells was carried out following the instructions of the manufacturer. Then a single colony from a LB plate was transferred into 100 mL of LB medium supplemented with ampicillin (100 μg/mL) and chloramphenicol (34 μg/mL). The bacteria were grown overnight at 37 °C and 50 mL of this culture were used to inoculate 10 L of fresh LB medium supplemented with the same antibiotics. Bacterial growth proceeds at 37 °C until $OD_{600}$ reached 0.4, the time at which protein expression was induced by adding 200 μM of IPTG. Cells were collected after 3 hours of culture at 37 °C by centrifugation at 5000 ×g at 10 °C, then resuspended in 50 mM Tris-Cl, pH 8 containing 200 mM NaCl and stored at –70 °C until use.

*Purification of MiaBTm*—The frozen cells were thawed, disrupted by sonication and centrifuged at 220,000 ×g at 4°C for 1h 30 min. The cell free extracts were heated at 75°C for 15 min and the denatured *E. coli* proteins were eliminated by centrifugation at 14,000 ×g at 4 °C for 15 min. The nucleic acids were partially eliminated by adding 0.04% of polyethylene imine. The proteins present in the supernatant were precipitated with 60% ammonium sulfate. The pellet was resuspended in 50 mM Tris-Cl, pH 8 and 50 mM Tris-Cl, pH 8, 1.5 M ammonium sulfate was added to reach a final concentration of 1 M ammonium sulfate. The solution was then loaded onto a Butyl-Sepharose column previously equilibrated with 50 mM Tris-Cl, pH 8, 1 M ammonium sulfate. The column was washed extensively with the same buffer and the adsorbed proteins were eluted by a linear gradient from 1 to 0 M ammonium sulfate. Fractions containing the protein were pooled and concentrated in an Amicon cell fitted with a YM30 (Spectrapor) membrane. The protein was then loaded on a Superdex 200 gel filtration column equilibrated with 50 mM Tris-Cl, pH 8, 200 mM NaCl, 5 mM DTT. The colored fractions, which contained the protein were pooled, DTT was removed from the protein solution by using Centricon 30 devices (Amicon). The pure protein was divided into aliquots and stored frozen at –70°C until use.

*Aggregation state analysis*—Fast protein liquid chromotography gel filtration with a Superdex 200 at a flow rate of 0.5 mL/min was used for size determination. The running buffer was 50 mM Tris-Cl, pH 8, 200 mM NaCl. The column was calibrated with a gel filtration calibration kit (calibration proteins II, Boehringer Inc.).

*Preparation of the apoprotein*—Protein-bound iron was removed by overnight exposure to EDTA (10 mM) under reducing conditions (10 mM sodium dithionite) at 4 °C. After incubation, the colorless protein was loaded onto a Sephadex NAP-25 gel filtration column equilibrated with 50 mM Tris-Cl, pH 8, 200 mM NaCl. The apoMiaBTm was then washed and concentrated with the same buffer using Centricon 30 devices (Amicon).

*Reconstitution of the iron-sulfur cluster of apoMiaBTm*—All the following procedures were carried out anaerobically inside a glove box containing less than 2 ppm $O_2$. The apoMiaBTm was treated with 2 mM DTT for 20 min and then a 6 molar excess of $Na_2S$ and $FeCl_3$, from a solution containing DTT, were added. The mixture was incubated for 3 hours and chromatographed on a Sephadex G-25 column. The dark brown fractions were collected and concentrated using an Amicon cell.

*Analytical methods*—Protein concentration was measured by the method of Bradford using bovine serum albumin as a standard (27) and also checked using Bicinchonic Acid Protein

Kit Assay (Sigma) with the same standard. Iron was determined by the method of Fish (28), and inorganic sulfide was quantified as described by Beinert (29).

*Analysis of T. maritima tRNA nucleosides composition by HPLC*—Total tRNA from *T. maritima* (strain DSMZ3109) was prepared essentially as described by Buck *et al.* (30). tRNA samples were digested to nucleosides by the method of Gehrke *et al.* (31) by using nuclease P1 and bacterial alkaline phosphatase. 50 -100 μg of tRNA was loaded onto LC-18 HPLC column (Vydac) connected to a HP-1100 HPLC system. The gradient profile developed by Gehrke and Kuo was used to separate the different nucleosides (31).

DNA and amino acid sequences were analyzed using the DNA Strider 1.3 software package. Sequence comparisons and homology searches implemented the BLAST program (26) at the NCBI server (http://www.ncbi.nlm.nih.gov). The amino acid sequences were aligned using ClustalW (32) at the EBI server (http://www.ebi.ac.uk/clustalW).

*Spectroscopic Measurements.*

*Light absorption*—UV-visible absorption spectra were recorded with a Cary 1 Bio (Varian) spectrophotometer.

*Electron Paramagnetic Resonance (EPR*)—X-Band EPR spectra were recorded on a Brucker Instruments ESP 300D spectrometer equiped with an Oxford Instruments ESR 900 flow cryostat (4.2-300 K). Spectra were quantified under non-saturating conditions by double integration against a 1 mM CuEDTA standard.

*Resonance Raman (RR)—*RR spectra were recorded using an Instruments SA U1000 spectrometer fitted with a cooled RCA 31034 photomultiplier tube with 90° scattering geometry. Spectra were recorded digitally using photon-counting electronics and improvements in signal-to-noise were achieved by signal averaging multiple scans. Band positions were calibrated using the excitation frequency and $CCl_4$ and are accurate to ±1cm$^{-1}$. Lines from a Coherent Sabre 10-W argon ion laser were used for excitation, and plasma lines were removed using a Pellin Broca prism premonochromator. For each sample, ~200 mW of incident laser power was used, and slit widths were adjusted for each excitation wavelength to give 8.0 cm$^{-1}$ spectral resolution. Scattering was collected from the surface of a frozen 18 μl droplet of sample using a custom-designed anaerobic sample cell (33) attached to the cold finger of an Air Products Displex model CSA-202E closed cycle refrigerator. This enables samples to be cooled down to 17 K, which facilitates improved spectral resolution and prevents laser-induced sample degradation. A linear ramp fluorescent background has been subtracted from each spectrum shown in this work.

*Variable-Temperature Magnetic Circular Dichroism (VTMCD)*—VTMCD measurements were made on samples containing 60% (v/v) ethylene glycol in 1-mm cuvettes using a Jasco J-715 (180-1000 nm) spectropolarimeter mated to an Oxford Instruments SM4000 split-coil superconducting magnet. The experimental protocols for measuring anaerobic MCD spectra over the temperature range 1.5-300 K with magnetic fields up to 6 T have been described elsewhere (34, 35). The MCD intensities are expressed as $\Delta\varepsilon(\varepsilon_{LCP}-\varepsilon_{RCP})$ where $\varepsilon_{LCP}$ and $\varepsilon_{RCP}$ are the molar extinction coefficients for the absorption of left and right circularly polarized light, respectively.

*Electrochemistry*—Electrochemical experiments were performed in a closed three-electrodes cell as described previously (36). The three-electrodes design included a saturated Ag/AgCl reference micro-electrode MI-401F from Microelectrode Inc, a platinum wire counter electrode from EG&G Instruments, and a gold working electrode from Radiometer. The three electrodes were connected to a EG&G Instruments model 273A potentiostat/galvanostat controlled with model software. The gold disc tip of the working electrode was hand-polished with $Al_2O_3$ and cleaned with distilled water before each analysis of sample. Reconstituted protein (200 µM) was prepared under anaerobic conditions in 50 mM Tris-Cl, pH 8, containing 200 mM NaCl. The solution (10-20 µL) was transferred with Hamilton gas-tight syringe on the working electrode, and other electrodes were positioned to contact the drop. The measurement was carried out at 25 °C, with a pulse height of 80 mV, a frequency of 20 Hz, and a potential increment of 2 mV.

## Results

*Amino acid sequence comparisons*—Using the BLAST search algorithm against the protein database with the sequence of MiaB from *E. coli* as a query, we were able to identify three putative MiaB proteins in the genome of *T. maritima* (37). We selected the protein encoded by the gene *TM0653*, which we named MiaBTm, because it displays the highest alignment score *E* value ($E = 3 \times 10^{-87}$) to MiaB from *E. coli*. As shown below, it proved to be catalytically competent for biosynthesis of $ms^2i^6A$. The function of the two other *miaB*-like genes, which display much lower *E* values, remains to be determined. MiaBTm contains the canonic cysteine residue pattern Cys*XXX*Cys*XX*Cys (Cys shown as *open triangles* in Figure 6.2), which has been shown to be important for the activity of the *E. coli* enzyme (23). The sequence alignment also shows that the three additional strictly conserved cysteines in the sequence of MiaB from *E. coli* and closely related organisms (Cys shown as *black triangles* in Figure 6.2) were present in the three proteins (21). These additional conserved cysteines occur near the beginning of the N-terminal region (~100 amino acids), which is highly conserved, and in the case of *E. coli* were shown to be also essential for activity (20 and our unpublished results). Furthermore, MiaBTm shares with the other MiaB enzymes a sequence of 60-80 residues, in the C-terminal part, which is proposed to form a domain reminiscent of the ß-barrel RNA-binding domains (21). The 5 predicted ß strands of this domain are marked with *black boxes* in Figure 6.2. This domain was named TRAM (for TRM2 and MiaB) and is most likely the domain of MiaB that binds the tRNA substrate. MiaBTm thus consists of 443 amino acids, and the molecular mass of the apoprotein as calculated from the sequence is 50,710 Da, comparable with that of the *E. coli* enzyme (53,600 Da).

*Analysis of tRNA nucleoside composition from T. maritima by HPLC*—Total tRNA from *T. maritima* cells was prepared and digested with nuclease P1 and phosphatase, and the released nucleosides were analyzed by HPLC. The elution profile of a tRNA hydrolysate is shown in Figure 6.3. A nucleoside with a retention time (84 min) corresponding to the one of $ms^2i^6A$ was detected. Moreover, this modified nucleoside has a UV-visible spectrum (Figure 6.3, *inset*) identical to that of $ms^2i^6A$ from *E. coli* (31). Thus, we conclude that the tRNA from *T. maritima* contains the $ms^2i^6A$ modified nucleoside and that as a consequence these bacteria have a MiaB enzyme for introduction of the sulfur atom.

*Cloning, overexpression and purification of the MiaB protein from T. maritima*—The open reading frame (ORF) *TM0653* was amplified from the genomic DNA by PCR reaction technology and cloned into a $pT_7$-7 vector. The *E. coli* BL21CodonPlus(DE3)-RIL$^{TM}$ strain was transformed with the resulting expression vector, named $pT_7$-MiaBTm, which establishes control over *TM0653* gene expression with the $T_7$ RNA polymerase promoter. Isopropyl-1-thio-β-D-galactopyranoside induction of the transformed *E. coli* cells resulted in the overproduction of a protein that migrates at ~50 kDa on SDS gels (Figure 6.4, *lane 2*) and was found mainly in the soluble fraction of cell free extracts (Figure 6.4, *lane 3*). After the final step of purification the purity was evaluated by SDS-PAGE to be over 95% (Figure 6.4, *lane 7*). Typical yields were

~40 mg of pure protein from a 10-liter culture. The apparent molecular mass of MiaBTm determined by analytical gel filtration chromatography (Superdex 200) showed that the protein is mainly a monomer in solution (data not shown). Indeed, whereas the pure protein eluted in different peaks corresponding to multimeric, dimeric, and monomeric states, the latter was by far the major one. When 5 mM DTT was added in the protein solution and in the eluting buffer, only the monomer was observed.

*The TM0653 gene from T. maritima complements the ms$^2$ deficiency of an E. coli miaB mutant strain*—The functionality of the MiaB protein from *T. maritima* was assayed *in vivo* using the *miaB*$^-$ TX3346 *E. coli* strain lacking a functional *miaB* gene (20). This strain was transformed with the plasmid pT$_7$-MiaBTm. Cells were first cultivated at 37 °C until $A_{600}$ reached 0.8. tRNAs were then isolated and their modified nucleoside content was analyzed by HPLC, as described (31). Under these conditions tRNAs from the control strain (TX3346) as well as the ones from the pT$_7$-miaBTm transformed strain showed an accumulation of the i$^6$A-37 with no evidence for the presence of ms$^2$i$^6$A-37 (Figure 6.5*A*). In a second experiment the control and the transformed cells were grown at 37 °C until $A_{600}$ reached 0.4 and then shifted to 45 °C for 3 hours. Whereas the tRNAs from the control strain still showed only an accumulation of i$^6$A-37, those from the MiaBTm-expressing strain showed both i$^6$A-37 and ms$^2$i$^6$A-37 (Figure 6.5*B*). These results demonstrate that the product of the *TM0653* gene is a functional MiaB enzyme even for modification of *E. coli* tRNAs, catalyzing the conversion of i$^6$A-37 to ms$^2$i$^6$A-37 *in vivo*. However, as expected for a thermophilic enzyme, this reaction requires a temperature higher than 37 °C. The fact that the enzyme is not working at the optimal temperature (80 °C) explains why the conversion of i$^6$A-37 to ms$^2$i$^6$A-37 is not total.

*Light absorption spectroscopy*—The bacterial pellets of induced cells as well as the soluble cell free extracts were dark brown. The color survived the heating step (75 °C) during purification. The UV-visible spectrum of the as-isolated recombinant MiaBTm protein was similar to that of the MiaB protein from *E. coli* (23). It displayed bands at 330, 416, 460 and a shoulder at 560 nm, a pattern characteristic for $[2Fe\text{-}2S]^{+2}$ clusters (Figure 6.6*A*, and *inset a*) (23). The iron and sulfur content of the as-isolated protein was low (0.7-1 iron and sulfur/protein). To reconstitute a full iron-sulfur cluster, the apoprotein was prepared by removing iron and sulfur (see "Materials and Methods") and the protein was incubated anaerobically with an excess of ferrous iron and sulfide in the presence of DTT. After desalting on a Sephadex-G25 column, MiaBTm was found to contain approximately 4 iron and 4 sulfur atoms per protein. The UV-visible spectrum of the reconstituted protein is shown in Figure 6.6*B*. It is different from that of the as-isolated protein and more consistent with a $[4Fe\text{-}4S]^{+2}$ cluster (23). Reconstitution of the cluster was also achieved by adding iron and sulfide to the as-isolated form. Its UV-visible spectrum was identical to that shown in Figure 6.5*B,* and, as shown below, its Raman resonance spectrum is very similar to that of the preparation reconstituted from the apo form. During anaerobic reduction of reconstituted MiaBTm with a 10-fold molar excess of sodium dithionite, a bleaching of the solution and a loss of the visible absorption bands were observed.

*EPR spectroscopy*—Both as-isolated and reconstituted proteins were analyzed by EPR spectroscopy. The EPR spectrum of the as-isolated protein is shown in Figure 6.7*A*. It exhibits an isotropic EPR signal centered at g = 2.01 accounting for only 5% of total iron. The relaxation properties and g-tensor of this signal are characteristic for the $S$ = 1/2 ground state of an oxidized $[3Fe\text{-}4S]^{+1}$ cluster. Upon anaerobic reduction with dithionite, the sample gave rise to a new $S$ =

1/2 species, characterized by an axial EPR signal with g values at 2.05 and 1.93, accounting for 40-50% of total iron (Figure 6.7*B*). It became broader at 30 K and could not be detected anymore above 40 K. Such a temperature dependence of the EPR signal and its microwave power saturation properties (data not shown) are characteristic for the $S$ = 1/2 ground state of [4Fe-4S]$^{+1}$ clusters. Furthermore, the g value of the low field feature is more consistent with a [4Fe-4S]$^{+1}$ than with a [2Fe-2S]$^{+1}$ cluster. Non-reduced reconstituted MiaBTm displayed a signal of [4Fe-4S]$^{1+}$ accounting for as much as 30% of total iron (Figure 6.7*C*). Upon reduction with 2 mM sodium dithionite, this signal increased and accounted for 60% of total iron (Figure 6.7*D*).

*Resonance Raman (RR) spectroscopy*—RR studies of proteins containing [2Fe-2S]$^{+2,+1}$, [3Fe-4S]$^{+1,0}$, and [4Fe-4S]$^{+3,+2,+1}$ clusters in the Fe-S stretching region provide a means of assessing cluster type and redox state (38-41). RR is particularly effective for discriminating between clusters with diamagnetic ground states, such as [4Fe-4S]$^{+2}$ and [2Fe-2S]$^{+2}$ clusters, which are not amenable to investigation by EPR or VTMCD spectroscopies, and for providing an initial assessment of the likelihood of partial non-cysteinyl ligation for both [4Fe-4S]$^{+2}$ (42) and [2Fe-2S]$^{+2}$ (43-45) clusters.

RR spectra of MiaBTm obtained with 457.9-nm excitation in the Fe-S stretching region, 200-450 cm$^{-1}$, are shown in Figure 6.8. In agreement with the UV-visible absorption spectrum, the resonance Raman spectrum of the as-isolated MiaBTm, (Figure 6.8*a*), is characteristic of a [2Fe-2S]$^{+2}$ cluster. The frequency of the lowest energy mode at 291 cm$^{-1}$, which corresponds to the out-of-phase symmetric stretching of the two tetrahedral ligated iron atoms, is consistent with ligation by four cysteines or three cysteines and one oxygenic ligand (44,46). Moreover, the spectrum of the as-isolated MiaBTm is very similar to those reported for [2Fe-2S]$^{+2}$ clusters generated via oxidative degradation of [4Fe-4S]$^{+2}$ clusters in other radical-SAM/Fe-S enzymes, *e.g.* anaerobic ribonucleotide reductase activating enzyme (47), pyruvate formate-lyase activating component (48), biotin synthase (49), and in the nitrogenase Fe protein (50), *i.e.* broad, poorly resolved bands centered at ~290, 340, and 395 $cm^{-1}$. In the spectrum of as-isolated MiaBTm, the trace of $[3Fe\text{-}4S]^{+1}$ clusters that are apparent in the EPR spectrum are likely to be responsible, at least in part, for the Raman intensity at 345 $cm^{-1}$ (see below).

The resonance Raman spectra of MiaBTm reconstituted anaerobically with iron and sulfide from the apo and as-isolated forms of the enzyme are shown in Figures 6.8 (*b* and *c*, respectively. Both spectra are very similar and characteristic of $[4Fe\text{-}4S]^{+2}$ clusters (38,39,51). Furthermore, because the resonance Raman spectra of $[2Fe\text{-}2S]^{+2}$ and $[3Fe\text{-}4S]^{+1}$ centers are generally 4-6 times more intense than those of $[4Fe\text{-}4S]^{+2}$ centers using 457.9-nm excitation (52, 53), and all the observed bands can be accounted for by a $[4Fe\text{-}4S]^{+2}$ center, the resonance Raman data indicate that $[4Fe\text{-}4S]^{+2}$ clusters are the sole type of oxidized cluster in reconstituted samples. Previous resonance Raman studies of biological $[4Fe\text{-}4S]^{+2}$ centers have shown that the frequency of the most intense band, which corresponds to the symmetric breathing mode of the $Fe_4S_4$ cube, provides an indication of cluster ligation (42, 54). The observed frequency of this mode in MiaBTm, 340 $cm^{-1}$, is at the boundary of the ranges of frequencies reported for $[4Fe\text{-}4S]^{+2}$ clusters with complete cysteinyl ligation (333-339 $cm^{-1}$) and those having oxygenic ligation at a specific iron site (340-343 $cm^{-1}$) and hence consistent with but not conclusive concerning the possibility of incomplete cysteinyl ligation.

Additional changes in the resonance Raman spectrum were apparent after reconstituted samples were thawed and exposed to air, Figure 6.8*d*. The bands associated with the $[4Fe\text{-}4S]^{+2}$ were no longer observable and the resulting spectrum is readily interpretable in terms of overlapping contributions from a $[2Fe\text{-}2S]^{+2}$ cluster analogous to that observed in as-prepared

MiaBTm and a $[3Fe\text{-}4S]^{+1}$ similar to those found in bacterial ferredoxins (41, 52). $[3Fe\text{-}4S]^{+1}$ clusters exhibit characteristic resonance Raman spectra with 457.9-nm excitation which are dominated by an intense band in the range 342-348 $cm^{-1}$ corresponding to symmetric stretching involving the $\mu_3$-S. This band is observed at 346 $cm^{-1}$ in air-exposed samples of reconstituted MiaBTm. Identical resonance Raman spectra were observed for samples of reconstituted MiaBTm that were exposed to air for 5 and 30 minutes, indicating that the oxidative cluster degradation occurs rapidly on exposure to air. Confirmation of $[3Fe\text{-}4S]^{+1}$ clusters in air-exposed samples of reconstituted MiaBTm was provided by EPR studies which revealed $S$ = 1/2 resonances analogous to those shown in Figure 6.7*A* corresponding to 25% of the total Fe in the sample. Because aerobically isolated MiaBTm contains predominantly $[2Fe\text{-}2S]^{+2}$ clusters with a minor component of $[3Fe\text{-}4S]^{+1}$ clusters accounting for 5% of the total iron (Figure 6.7*A*), we conclude that oxygen-induced degradation of the $[4Fe\text{-}4S]^{+2}$ in anaerobically reconstituted MiaBTm to yield a $[2Fe\text{-}2S]^{+2}$ cluster occurs via a stable $[3Fe\text{-}4S]^{+1}$ cluster intermediate.

*VTMCD spectroscopy*—Resonance Raman is of limited utility for assessing cluster type in reduced samples of MiaBTm, because $[4Fe\text{-}4S]^{+1}$ clusters exhibit negligible resonance enhancement with visible excitation (38, 39). Because $[4Fe\text{-}4S]^{+1}$, $[3Fe\text{-}4S]^{0}$ and $[2Fe\text{-}2S]^{+1}$, which are the one-electron-reduced forms of $[4Fe\text{-}4S]^{+2}$, $[3Fe\text{-}4S]^{+1}$ and $[2Fe\text{-}2S]^{+2}$ respectively, are all paramagnetic, VTMCD provides useful supplement to EPR for assessing the nature of the cluster in dithionite-reduced samples via the excited-state properties, as revealed by the complex pattern of temperature-dependent MCD bands in the UV/visible/near-IR region, and the ground-state properties as assessed via variable-field and variable-temperature MCD saturation magnetization studies (55). The VTMCD spectrum of a dithionite-reduced sample of anaerobically reconstituted MiaBTm is shown in Figure 6.9. Saturation magnetization measurements at 540 nm (data not shown) indicate that the MCD bands originate from an *S* = 1/2 ground state, and hence argue against any significant contribution from *S* = 3/2 $[4Fe\text{-}4S]^{+1}$ clusters or *S* = 2 $[3Fe\text{-}4S]^{0}$ clusters. Moreover, the pattern of bands is very similar to that observed for *S* = 1/2 $[4Fe\text{-}4S]^{+1}$ clusters (55, 56) and quite distinct from those observed for *S* = 1/2 $[2Fe\text{-}2S]^{+1}$ clusters (40, 55). Parallel EPR studies of the identical sample containing 60% (v/v) ethylene glycol revealed an axial *S* = 1/2 resonance with *g* = 2.05, 1.93, analogous to those shown in Figure 6.7 (*B-D*). All these results are consistent with (i) the reconstituted protein contains $[4Fe\text{-}4S]^{+2}$ and $[4Fe\text{-}4S]^{+1}$ exclusively and (ii) the reduced clusters being exclusively in the $[4Fe\text{-}4S]^{+1}$ state.

*Redox Potential*—The redox potential of the reconstituted MiaBTm protein has been measured by square wave voltammetry (Figure 6.10). The electrochemical response of the protein was found to be reversible and the measured redox potential of the $[4Fe\text{-}4S]^{+2/+1}$ was found to be –495 ±10 mV (*versus* the normal hydrogen electrode). The value determined here for MiaBTm protein is consistent with redox potential values determined for biotin synthase (57) and the activase of the anaerobic ribonucleotide reductase (58).

## Discussion

We demonstrate here for the first time that tRNAs in the thermophilic bacterium *Thermotoga maritima* contains the thionucleoside $ms^2i^6A$-37. A candidate for the *miaB* gene (*TM0653*) was identified in a BLAST peptide homology search using as a query the *E. coli* MiaB protein, which is responsible for the methythiolation step in this microorganism. The search revealed that the corresponding protein has a primary structure not only related to the tRNA-methylthiotransferase enzymes (20, 21), but also to the enzymes of the radical-SAM superfamily (22). In particular, analysis of the amino acid sequence shows that the protein shares the [4Fe-4S]-cluster-binding cysteine triad Cys*XXX*Cys*XX*Cys with MiaB from *E. coli* and with related radical-SAM [4Fe-4S] enzymes, such as biotin synthase and lipoate synthase, which also catalyze the formation of C-S bonds.

The results presented in this paper show that the product of the *TM0653* gene is a true functional MiaB enzyme, required for the biosynthesis of $ms^2i^6A$-37, as indicated by the ability of the corresponding gene to complement the *miaB* mutation in *E. coli.* We thus named this protein MiaBTm. The fact that the complementation was effective only at 45 °C is certainly in relation with the thermophilic origin of the MiaBTm protein. We also show that the purified MiaBTm protein is a monomer in solution and that it contains an iron-sulfur cluster. Obviously the MiaBTm protein displays some features already observed with the *E. coli* enzyme (23). However, in comparison with the *E. coli* enzyme, MiaBTm has several advantages that make this enzyme more suitable for future mechanistic studies. Indeed the *E. coli* enzyme did not allow the extensive characterization reported here for the first time for a MiaB enzyme. In particular, it proved difficult to get preparations of *E. coli* MiaB containing homogeneous iron-sulfur cluster composition and spectroscopic data obtained with the *E. coli* enzyme were hard to interpret. In fact, heterogeneity in cluster composition is currently observed with radical-SAM enzymes. In contrast, cluster in MiaBTm were more stable, as expected for a thermophilic protein, and amenable to thorough spectroscopic characterization which was the objective of the present work. Interestingly, we found conditions for obtaining preparations of MiaBTm containing exclusively either [4Fe-4S] or [2Fe-2S] clusters as clearly shown by resonance Raman spectroscopy.

Under anaerobic conditions, the purified apoprotein could bind up to four atoms of iron and four atoms of sulfur per polypeptide chain, assembled exclusively in a [4Fe-4S] center in both 2+ (oxidized; $S = 0$) and 1+ (reduced; $S = 1/2$) states, as shown by UV-visible absorption, resonance Raman and VTMCD spectroscopy. During reduction with sodium dithionite the proportion of the $[4Fe\text{-}4S]^{+1}$ reduced state increased and no evidence for the presence of reduced $[2Fe\text{-}2S]^{+1}$ or $[3Fe\text{-}4S]^{0}$ clusters could be observed. It is remarkable that the anaerobic reconstitution of the as-isolated form, which contains [2Fe-2S] and [3Fe-4S] clusters, with iron and sulfide also resulted in a preparation containing exclusively [4Fe-4S] clusters.

The spectroscopic studies reported herein show that the [4Fe-4S] cluster of MiaBTm is stable under anaerobic conditions but is degraded by oxygen. This explains why iron and sulfide are lost during purification and why the as-isolated protein contains substoichiometric amounts of iron and sulfur. Aerobically isolated MiaBTm contains mainly diamagnetic $[2Fe\text{-}2S]^{+2}$ clusters, as shown by resonance Raman spectroscopy, together, with very small amounts of paramagnetic $S = 1/2$ $[3Fe\text{-}4S]^{+1}$ clusters, as shown by EPR spectroscopy. Furthermore, during exposure of the reconstituted protein to air, the $[4Fe\text{-}4S]^{2+}$ cluster decomposes generating both $[2Fe\text{-}2S]^{+2}$ and $[3Fe\text{-}4S]^{+1}$ clusters as evidenced by resonance Raman and EPR spectroscopies.

Thus, it appears that the spectroscopic, redox, oxygen-sensitivity, and cluster conversion properties of the Fe-S center in MiaB are comparable with those previously reported for other members of the radical-SAM iron-sulfur enzyme family. The presence of essential cysteines within a Cys*XXX*Cys*XX*Cys sequence (Cys-150, Cys-154, Cys-157), as already mentioned, together with the requirement of SAM for the conversion of $i^6A$-37 to $ms^2i^6A$-37 are further similarities. We thus here confirm that MiaB proteins are members of that enzyme superfamily. Well studied members of this family are lysine 2,3-aminomutase (59), biotin synthase (60), the activating components of ribonucleotide reductase (61), and pyruvate formate-lyase (62). They all contain a [4Fe-4S] cluster chelated by a conserved Cys*XXX*Cys*XX*Cys sequence and absolutely require SAM for activity (63).

Oxidative degradation of $[4Fe\text{-}4S]^{+2}$ clusters that constitute the active sites for reductive cleavage of SAM in all radical-SAM Fe-S enzymes generally proceed via $[2Fe\text{-}2S]^{+2}$ cluster (45, 49, 59, 62). The spectroscopic studies presented herein suggest that this cluster transformation occurs via a $[3Fe\text{-}4S]^{+1}$ cluster. In support of this proposal, $[3Fe\text{-}4S]^{+1}$ clusters have been reported in oxygen damaged samples of pyruvate formate-lyase activating enzyme (62), anaerobic ribonucleotide reductase activating enzyme (61), lysine 2,3-aminomutase (59) and lipoic acid synthase (64). However, $[3Fe\text{-}4S]^{+1}$ clusters have yet to be observed in biotin synthase. If oxidative $[4Fe\text{-}4S]^{+2}$ cluster degradation proceeds by the same mechanism in all radical-SAM Fe-S enzymes, we conclude that the $[3Fe\text{-}4S]^{+1}$ intermediate is unstable and occurs only as a transient intermediate in biotin synthase.

The modification of adenosine leading to the thionucleoside $ms^2i^6A$ at position 37 in most bacterial and eukaryotic tRNAs is an intriguing and unique reaction in many aspects. First, it is very important for normal cell function, as shown from decreased growth rate and cell yield in the case of mutant strains lacking $ms^2i^6A$-37 (65). Second, it is still unknown whether MiaB participates in both sulfur insertion and methylation or only to the first process and a second putative enzyme MiaC catalyzes the methylation step. Third, from a chemical point of view the reaction consists in a highly difficult aromatic C-H to C-S bond conversion. In contrast to the reactions of sulfur insertion into uridine of tRNAs leading to $s^4U$ (10) and $mnm^5s^2U$ (66), which are not redox processes, formation of $ms^2i^6A$-37 is an oxidation reaction. However, because MiaB is a member of the radical-SAM enzyme superfamily, it is a very likely that its [4Fe-4S] cluster plays a role similar to that of the clusters of other radical-SAM enzymes. We thus speculate that the cluster of MiaB catalyzes a one-electron transfer to SAM for generating a 5’-deoxyadenosyl radical and that the methylthiolation reaction implies such a 5’-deoxyadenosyl radical as the oxidant for a radical activation of the tRNA substrate. Thus the most simple hypothetical mechanistic scenario for the methylthiolation reaction implies a 5’-deoxyadenosyl radical as the oxidant for a radical activation of the tRNA substrate. Fourth, also in contrast to the reactions leading to $s^4U$ (10) and $mnm^5s^2U$ (66), the sulfur donor during $ms^2i^6A$ biosynthesis is still unknown and its identification, via genetic studies, is complicated by the fact that sulfur is required both for synthesis of the iron-sulfur cluster and for thiomethylation of adenosine. In the case of the $s^4U$ and $mnm^5s^2U$, the sulfur donor is likely to be a cysteine persulfide generated by the action of the cysteine desulfurase IscS, since a deletion of the *iscS* gene in *E. coli* or *Salmonella enterica* resulted in non detectable levels of $s^4U$ and $mnm^5s^2U$ (67, 68). In contrast, the same studies showed that IscS was not absolutely required for the biosynthesis of $ms^2i^6A$-37 (68).

In the case of biotin synthase, the problem of the sulfur donor has been recently extensively investigated by us and others. These studies have resulted in two conflicting hypothesis. The first one, proposed by J. T. Jarrett, implies a second cluster, a [2Fe-2S] one, as the sulfur donor (69), whereas the second hypothesis implies a persulfide as the donor (70). It is important to note that no evidence for the presence in MiaB of two clusters, one [4Fe-4S] and one [2Fe-2S], could be found, even when cluster reconstitution was achieved from the as-isolated protein. This might suggest that Jarrett’s model does not apply to MiaB. We believe that the investigation of MiaB, in particular that from *T. maritima*, might provide in addition to specific information on formation of ms$^2$i$^6$A-37 new insights into the general question of the mechanism of biological C-H to C-S bond conversion.

## Acknowledgments

We thank Dr V. Artero, E. Mulliez, J. Rubach, and Professor G. R. Björk for informative discussion. The genomic DNA and cells of *T. maritima* were a gift of Professor Robert Huber (University of Regensburg, Germany). This work was supported by a grant from the National Institutes of Health (GM62542 to M.K.J.)

## References

(1) Björk, R. G., Ericson, J. U., Gustafsson, C. E. D., Hagervall, T. G., Jönsson, Y. H., and Wikstrom, P. M. (1987) *Ann. Rev. Biochem*. **56**, 263-287.

(2) Björk, R. G., (1995) in *tRNA: Structure, biosynthesis and function*. (Söll, D, and Rajbhandary, U., Eds. pp. 23-85, ASM Press, Washington: D.C.

(3) Björk, R. G., and Rasmuson, T. (1998) in *Modification and editing of RNA* (Grojean, H., and Benne, R., Eds.) pp. 471-491, ASM Press, Washington, D.C.

(4) Esberg, B., and Björk, R. G. (1995) *J. Bacteriol*. **177**, 1967-1975.

(5) Mühlenhoff, U., and Lill, R. (2000) *Biochim. Biophys. Acta*. **1459**, 370-382.

(6) Marquet, A., Tse Sum Bui, B., and Florentin, D. (2001) *Vitamins and Hormones*. **61**, 51-101.

(7) Leimkühler, S., and Rajagopalan, K. V. (2001) *J. Biol. Chem*. **276**, 22024-22031.

(8) Begley, T. P., Xi, J., Kinsland, C., Taylor, S., and McLafferty, F. (1999) *Curr. Opin. Chem. Biol*. **3**, 623-629.

(9) Baldwin, J. E., and Bradley, M. (1990) *Chem. Rev*. **90**, 1079-1088.

(10) Mueller, E. G., Palenchar, P. M., and Buck, C. C. (2001) *J. Biol. Chem*. **276**, 33588-33595.

(11) Grosjean, H., Nicoghosian, K., Haumont, E., Söll, D., and Cedergeron, R. (1985) *Nucleic. Acids. Res*. **13**, 5697-5706.

(12) Björk, G. R. (1992) in *Transfer in protein synthesis*. (Hatfield., D. L., Lee., B. J., and Pirtle., R. M., Eds.) pp. 23-85, CRC Press, Boca Raton. F. L.

(13) Björk, G. R. (1996) in Stable RNA Modification. In Neidhart, F. C. C. I., R. Ingraham., J. L. Lin., E. C. C. Low Jr., K. B. Magasanik., B. Reznikoff., W. S. Riley., M. Schaechter., M. Umbarger., H. U. Eds. *Escherichia coli* and *Salmonella typhimurium: Cellular and Molecular Biology* pp. 861-886, ASM Press, Washington, D.C.

(14) Moore, J. A., and Poulter, C. D. (1997) *Biochemistry* **36**, 604-614

(15) Leung, E. H.-C., Chen, Y., and Winkler, M. E. (1997) *J. Biol. Chem*. **272**, 13073-13083.

(16) Soderberg, T., and Poulter, C. D. (2000) *Biochemistry* **39**, 6546-6553.

(17) Rosenberg, A. H., and Gefter, M. L. (1969) *J. Mol. Biol*. **46**, 581-584.

(18) Gefter, M. L. (1969) *Biochem. Biophys. Res. Commun*. **36**, 435-441.

(19) Agris, P. F., Armstrong, D. J., Schäfer, K. P., and Söll, D. (1975) *Nucleic. Acids. Res*. **2**, 691-698.

(20) Esberg, B., Leung, E. H-C., Tsui, H-C. T., Björk, G. R., and Winkler, M. E. (1999) *J. Bacteriol.* **181**, 7256-7265.

(21) Anantharaman, V., Koonin, E. V., and Aravind, L. (2001) *FEMS Microbiol. Lett*, **197**, 215-221.

(22) Sofia, H. J., Chen, G., Hetsler, B. G., Reyes-Spindola, J. F., and Miller, N. E. (2001) *Nucleic Acids. Res.* **29**, 1097-1106.

(23) Pierrel, F., Björk, G. R., Fontecave, M., and Atta, M. (2002) *J. Biol. Chem.* **277**, 13367-13370.

(24) Boccheta, M., Gribaldo, S., Sanangelantoni, A., and Cammarano, P. (2000) *J. Mol. Evol.* **50**, 366-380.

(25) Ausubel, F. M., Brent, R., Kingston, R. E., Moore, D. D., Seidman, J. G., Smith, J. A., and Struhl, K. (1998) *Current Protocols in Molecular Biology,*. Wiley-Interscience, NewYork.

(26) Atschul, S. F., Madden, T. L., Schäffer, A. A., Zhang, J., Zhang, Z., Miller, W., and Lipman, D. J. (1997) *Nucleic. Acids. Res.*, **25**, 3389-3402.

(27) Bradford, M. M. (1976) *Anal. Biochem.* **72**, 248-254.

(28) Fish, W. W. (1988) *Meth. Enzymol.* **158**, 357-364.

(29) Beinert, H. (1983) *Anal. Biochem.* **131**, 373-378.

(30) Buck, M., Connick, M., and Ames, B. N. (1983) *Anal Biochem.* **129**, 1-13.

(31) Gehrke, C. W., and Kuo, K. C. (1990) in *Journal of Chromatography Library*, pp. A3-A71, Elsevier, Amsterdam, The Netherlands.

(32) Higgins, D. G., Thompson, J. D., and Gibson, T. J. (1996) *Meth. Enzymol.* **266**, 383-402.

(33) Drozdzewski, P. M., and Johnson, M. K. (1988) *Appl. Spectrosc.* **42**, 1575-1577.

(34) Johnson, M. K. (1988) in *Metal clusters in proteins* (Que, L., Jr., Ed.) pp 326-342, American Chemical Society, Washington,D.C.

(35) Thomson, A. J., Cheesman, M. R., and George, S. J. (1993) *Methods Enzymol.* **226**, 199-232.

(36) Hagen, W. R. (1989) *Eur. J. Biochem.* **182**, 523-530.

(37) Nelson, K. E., Clayton, R. A., Gill, S. R., Gwinn, M. L., Dodson, R. J., Haft, D. H., Hickey, E. K., Peterson, J. D., Nelson, W. C., Ketchum, K. A., McDonald, L., Utterback, T. R., Malek, J. A., Linher, K. D., Garrett, M. M., Stewart, A. M., Cotton, M. D., Pratt, M. S., Phillips, C. A.,

Richardson, D., Heidelberg, J., Sutton, G. G., Fleishmann, R. D., Eisen, J. A., White, O., Salzberg, S. L., Smith, H. O., Venter, J. G., and Fraser, C. M. (1999), *Nature* **399**, 323-329.

(38) Spiro, T. G., Hare, J., Yachandra, V., Gewirth, A., Johnson, M. K., and Remsen, E. (1982) in *Iron-sulfur proteins* (Spiro, T. G., Ed.) pp 407-423, Wiley-Interscience, New York.

(39) Spiro, T. G., Czernuszewicz, R. S., and Han, S. (1988) in *Resonance Raman spectra of heme and metalloproteins* (Spiro, T. G., Ed.) pp 523-554, John Wiley & Sons, New York.

(40) Fu, W., Drozdzewski, P. M., Davies, M. D., Sligar, S. G., and Johnson, M. K. (1992) *J. Biol. Chem.* **267**, 15502-15510.

(41) Johnson, M. K., Duderstadt, R. E., and Duin, E. C. (1999) *Adv. Inorg. Chem.* ***47***, 1-82.

(42) Conover, R. C., Kowal, A. T., Fu, W., Park, J.-B., Aono, S., Adams, M. W. W., and Johnson, M. K. (1990) *J. Biol. Chem.* **265**, 8533-8541.

(43) Kuila, D., Schoonover, J. R., Dyer, R. B., Batie, C. J., Ballou, D. P., Fee, J. A., and Woodruff, W. H. (1992) *Biochim. Biophys. Acta* **1140,** 175-183.

(44) Meyer, J., Fujinaga, J., Gaillard, J., and Lutz, M. (1994) *Biochemistry* **33**, 13642-13650.

(45) Duin, E. C., Lafferty, M. E., Crouse, B. R., Allen, R. M., Sanyal, I., Flint, D. H., and Johnson, M. K. (1997) *Biochemistry* **36**, 11811-11820.

(46) Crouse, B. R., Sellers, V. M., Finnegan, M. G., Dailey, H. A., and Johnson, M. K. (1996) *Biochemistry* ***35***, 16222-16229.

(47) Ollagnier, S., Meier, C., Mulliez, E., Gaillard, J., Schuenemann, V., Tratwein, A., Mattioli, T., Lutz, M., and Fontecave, M. (1999) *J. Am. Chem. Soc.* **121**, 6344-6350.

(48) Broderick, J. B., Duderstadt, R. E., Fernandez, D. C., Wojtuszewski, K., Henshaw, T. F., and Johnson, M. K. (1997) *J. Am. Chem. Soc.* **119**, 7396-7397.

(49) Johnson, M. K., Staples, C. R., Duin, E. C., Lafferty, M. E., and Duderstadt, R. E. (1998) *Pure Appl. Chem.* **70**, 939-946.

(50) Fu, W., Morgan, T. V., Mortenson, L. E., and Johnson, M. K. (1991) *FEBS Lett.* **284**, 165-168.

(51) Czernuszewicz, R. S., Macor, K. A., Johnson, M. K., Gewirth, A., and Spiro, T. G. (1987) *J. Am. Chem. Soc.* **109**, 7178-7187.

(52) Johnson, M. K., Czernuszewicz, R. S., Spiro, T. G., Fee, J. A., and Sweeney, W. V. (1983) *J. Am. Chem. Soc.* **103**, 6671-6678.

(53) Fu, W., Drozdzewski, P. M., Adams, M. W. W., Morgan, T. V., Mortenson, L. E., LeGall, J., Peck, H. D., Jr., DerVartanian, D. V., and Johnson, M. K. (1993) *Biochemistry* **32**, 4813-4819.

(54) Brereton, P. S., Duderstadt, R. E., Staples, C. R., Johnson, M. K., and Adams, M. W. W. (1999) *Biochemistry* **38**, 10594-10605.

(55) Johnson, M. K., Robinson, A. E., and Thomson, A. J. (1982) in *Iron-sulfur proteins* (Spiro, T. G., Ed.) pp 367-406, Wiley-Interscience, New York.

(56) Onate, Y. A., Finnegan, M. G., Hales, B. J., and Johnson, M. K. (1993) *Biochim. Biophys. Acta* **1164**, 113-123.

(57) Ugulava, N. B., Gibney, B. R., and Jarrett, J. T. (2001) *Biochemistry* **40**, 8343-8351.

(58) Mulliez, E., Padovani, D., Atta, M., Alcouffe, C., and Fontecave, M. (2001) *Biochemistry* **40**, 3730-3736.

(59) Frey, P. A. (2001) *Annu. Rev. Biochem.* **70**, 121-148.

(60) Hewitson, K. S., Ollagnier-de Choudens, S., Sanakis, Y., Shaw, N. M., Baldwin, J. E., Münck. E., Roach, P. L., and Fontecave, M. (2002) *J. Biol. Inorg. Chem.* **7**, 83-93.

(61) Tamarit, J., Mulliez, E., Meier, C., Trautwein, A., and Fontecave, M. (1999) *J. Biol. Chem.* **274**, 31291-31296.

(62) Külser, R., Pils, T., Kappl, R., Hütterman, J., and Knappe, J. (1998) *J. Biol. Chem.* **273**, 4897-4903.

(63) Fontecave, M., Mulliez, E., and Ollagnier-de Choudens, S. (2001) *Curr. Opin. Chem. Biol.* **57**, 506-511

(64) Miller, J. R., Busby, R. W., Jordan, S. W., Cheek, J., Henshaw, T. F., Ashley, G. W., Broderick, J. B., Cronan, J. E., and Marletta, M. A. (2000) *Biochemistry* **39**, 15166-15178.

(65) Ericson, J. U., and Björk, G. R. (1991) *J. Mol. Biol.* **218**, 509-516.

(66) Kambampati, R., and Lauhon, C. T. (2003) *Biochemistry* **42**, 1109-1117.

(67) Lauhon, C. T. (2002) *J. Bacteriol.* **184**, 6820-6829.

(68) Nilsson, K., Lundgren, H. K., Hagervall, T. G., and Björk, G. R. (2002) *J. Bacteriol.* **184**, 6820-6829.

(69) Ugulava, N. B., Sacanell, C. J., and Jarrett, J. T. (2001) *Biochemistry* **40**, 8352-8358.

(70) Ollagnier-de-Choudens, S., Mulliez, E., and Fontecave, M. (2002) *FEBS Lett* **532**, 465-468.

**Figure 6.1:** Biosynthesis of ms$^2$i$^6$A-37. The adenosine modification in tRNA is catalyzed by MiaA, MiaB and possibly MiaC (unknown) enzyme activities. *DMAPP*, dimethylallyl diphosphate; *SAM*, *S*-adenosylmethionine; *Cys*, cysteine; *R*, ribose; *PPi*, pyrophosphate.

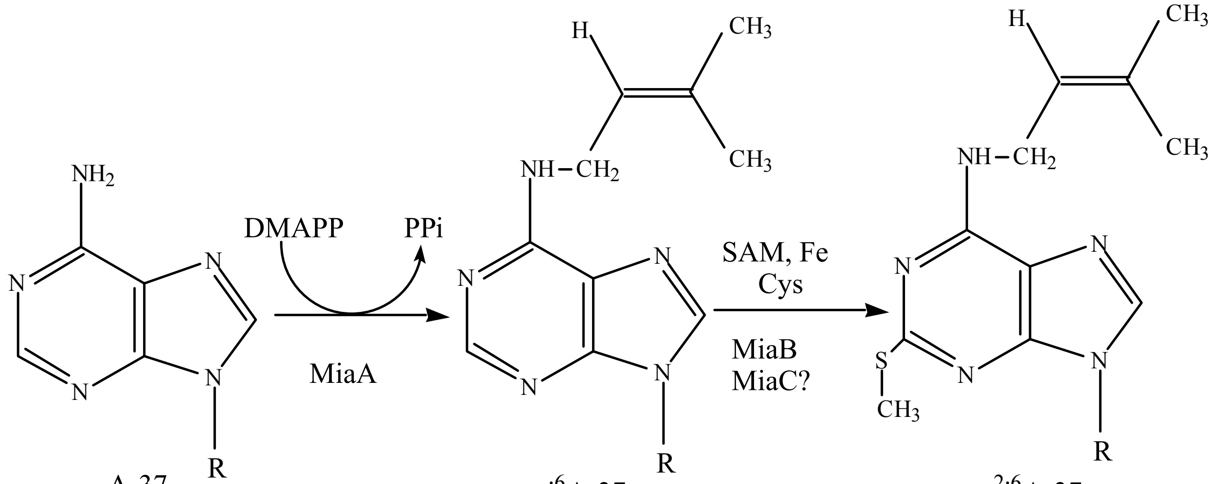
NH$_2$
N
N
N
N
R
DMAPP
PPi
MiaA
H
CH$_3$
CH$_3$
NH−CH$_2$
N
N
N
N
R
SAM, Fe
Cys
MiaB
MiaC?
H
CH$_3$
CH$_3$
NH−CH$_2$
N
N
N
N
S
CH$_3$
R

A-37
(Adenosine at tRNA
position 37)

i$^6$A-37
(N6-isopentenyl)-adenosine-37)

ms$^2$i$^6$A-37
(2-methylthio-N6-isopentenyl-
adenosine-37)

**Figure 6.2:** Amino acid alignments of MiaB proteins from *T. maritima* (*Tm*), *E. coli* (*Ec*), *Salmonella typhimirium* (*St*), *Yersina pestis* (*Yp*), *Vibrio cholera* (*Vc*), and *Aquifex aeolicus* (*Aa*). The alignments were performed with ClustalW (32). Totally conserved residues are indicated by *star*, conserved cysteine residues are in *bold face* and are marked with *open triangles* for the Cys*XXX*Cys*XX*Cys triad and with *black triangles* for others. The *five boxes* represent the five predicted β strands of the TRAM domain (21).

```
                   ▼                                    ▼                                 ▼
T.m     --MRFYIKTFGCQMNENDSEAMAGLLV-KEGFTPASSPEEADVVIINTCAVRRKSEEKAYSELGQVLKLKKKK-KIVVGVAGCV 80
E.c     MTKKLHIKTWGCQMNEYDSSKMADLLDATHGYQLTDVAEEADVLLLNTCSIREKAQEKVFHQLGRWKLLKEKNPDLIIGVGGCV 84
S.t     MTKKLHIKTWGCQMNEYDSSKMADLLDATHGYQLTDVAEEADVLLLNTCSIREKAQEKVFHQLGRWRLLKEKNPDLIIGVGGCV 84
Y.p     MTKKLHIKTWGCQMNEYDSSKMADLLASTHGYQLTTIPEEADLLLLNTCSIREKAQEKVFSLLGQWKLLKEKNPQLIIGVGGCV 84
V.c     MSKKLLIKTWGCQMNEYDSSKMADLLNAANGYELTEIPEEADVLLLNTCSIREKAQEKVFHQLGRWKTLKDKKPGVVIGVGGCV 84
A.a     MSKKFFIKTFGCQMNFNDSERIRGLLK-TIGYEQTDNWEEADLIILNTCTIREKPDQKVLSHLGEYKKIKEKNPKALIAVAGCL 83
           :: ***:*****  **. : .**    *:     :****:::***::*.*.::*    .**.    *.*:  ::. *.**:

                                                                                  ▽   ▽  ▽
T.m     AEKEREKFLEKG--ADFVLGTRAVPRVTEAVKKALEG-EKVALFEDHLDEYT--HELPRIRTSRHHAWVTIIHGCDRFCTYCIV 159
E.c     ASQEGEHIRQRAHYVDIIFGPQTLHRLPEMINSVRG--DRSPVVDISFPEIEKFDRLPEPRAEGPTAFVSIMEGCNKYCTYCVV 166
S.t     ASQEGEHIRQRAHYVDIIFGPQTLHRLPEMINSVRG--DRSPVVDISFPEIEKFDRLPEPRAEGPTAFVSIMEGCNKYCTYCVV 166
Y.p     ASQEGEQLRQRAPCVDVIFGPQTLHRLPEMINHVQG--TNSPVVDISFPEIEKFDRLPEPRAEGPTAFVSIMEGCNKYCTFCVV 166
V.c     ATQEGDSIRDRAPYVDVIFGPQTLHRLPEMIKQSQT--SDAPVMDISFPEIEKFDRLPEPRAEGPTAFVSIMEGCSKYCTYCVV 166
A.a     AQRTGWELVKKAPVIDIMFSSFNMHQLPELINQAQAGYKAIAILDELPQDEDKIWEYPVERDNKYCAYVTIIKGCDKNCTYCVV 167
        * :    : .:.   *.::..  : ::.* :: .:.:            :     . *  *   . *:*:*:.**.: **:*:*

T.m     PYTRGRERSRPMADILEEVKKLAEQGYREVTFLGQNVDAY-GKDLK-DGSSLAKLLEEASKIEGIERIWFLTSYPTDFSDELIE 241
E.c     PYTRGEEVSRPSDDILFEIAQLAAQGVREVNLLGQNVNAWRGENYDGTTGSFADLLRLVAAIDGIDRIRFTTSHPIEFTDDIIE 250
S.t     PYTRGEEVSRPSDDILFEIAQLAAQGVREVNLLGQNVNAWRGENYDGTTGTFADLLRLVAAIDGIDRIRFTTSHPIEFTDDIIE 250
Y.p     PYTRGEEVSRPSDDILFEIAQLAAQGVREVNLLGQNVNAYRGATYDGDICSFAELLRLVAAIDGIDRVRFTTSHPIEFTDDIID 250
V.c     PYTRGEEVSRPMDDVLFEIAQLAEQGVREVNLLGQNVNAYRGATHDGGICSFAELLRLVATIDGIDRIRFTTSHPLEFTDDIIA 250
A.a     PRTRGKERSRALHSILDEVKRLVDDGVREIHLLGQNVTAW-GKDFEKPIP-FSELLYQVSKIDGVERIRFTTGHPRDLTDDIIE 249
        * ***.* **.  .:* *: :*. :* **: :***** *: *   .     ::.**.:   *:*::*: * * .:*:::*::*

T.m     VIAKNPKVAKSVHLPVQSGSNRILKLMNRRYTKEEYLALLEKIRSKVPEVAISSDIIVGFPTETEEDFMETVDLVEKAQFERLN 325
E.c     VYRDTPELVSFLHLPVQSGSDRILNLMGRTHTALEYKAIIRKLRAARPDIQISSDFIVGFPGETTEDFEKTMKLIADVNFDMSY 334
S.t     VYRDTPELVSFLHLPVQSGSDRVLNLMGRTHTALEYKAIIRKLRAARPDIQISSDFIVGFPGETTDDFEKTMKLIADVNFDMSY 334
Y.p     VYRDTPELVSFLHLPVQSGSDRILTMMKRAHTALEYKAIIRKLRQARPDIQISSDFIVGFPGETQQDFEQTMKLVADIHFDTSY 334
V.c     VYEDTPELVSFLHLPVQSGSDRILTMMKRPHTAIEYKSIIRKLRKARPDIQISSDFIVGFPGETDKDFQDTMKLIRDVDFDMSF 334
A.a     AMADIPQVCNALHLPFQAGSNRILALMDRGYTKEEYLEKIEKLKEKVKDIAMSTDVIVGFPTETEEDFEHTLDVLKKVRFEQVF 333
         . . *:: . :***.*:**:*:* :* * :*  **   : .*::   :: :*:*.***** ** .** .*:.:: .  *:

                                                         ▬▬▬▬▬▬▬▬         ▬▬▬▬    ▬▬▬▬▬
T.m     LAIYSPREGTVAWKYYKDDVPYEEKVRRMQFLMNLQKRINRKLNERYRGKTVRIIVEAQAKNG--LFYGRDIRNKIIAFEGEDW 407
E.c     SFIFSARPGTPAAD-MVDDVPEEEKKQRLYILQERINQQAMAWSRRMLGTTQRILVEGTSRKSIMELSGRTENNRVVNFEGTPD 417
S.t     SFIFSARPGTPAAD-MVDDVPEEEKKQRLYILQERINQQAMAWSRRMLGTTQRILVEGTSRKNIMELSGRTENNRVVNFEGTPE 417
Y.p     SFIYSPRPGTPAAD-LPNNVSEEEKKQRLHILQQRISQQAMEISRKMVGTVQRVLVEGTSRKNVMELAGRTENNRVVNFEGSPD 417
V.c     SFIFSPRPGTPAAD-YPCDLSEEVKKERLYELQQQINSQAMRYSRLMLGTEQRILVEGPSKKDLMELRGRTENNRVVNFEGSPD 417
A.a     SFKFSPRPGTPAAE-MEGQIPDDVKTERMRRLLELQKSILSEIAKKYEGTVQEVLVEEEKNG---ELIGRTTTNKWASFKGDPS 413
           :*.* ** * .    ::. : * .*:  * :  .       .   *.  .::**   .     : **   *:   *:*

            ▬▬▬▬▬▬▬     ▬▬▬▬▬▬
T.m     MIGRFADVKVEKITAGPLYGKVVWVEKTPSPVSSSE--------------------- 443
E.c     MIGKFVDVEITDVYPNSLRGKVVRTEDEMGLRVAETPESVIARTRKENDLGVGYYQP 474
S.t     MIGKFVDVEITDVYPNSLRGKVVRTEDEMGLRVAETPESVIARTRKENELGVGFYQP 474
Y.p     MIGKFVDVEIVNVYASSLRGILLRTEDQMDLRTHESPQSVIARTRKENEIGVGIYQP 474
V.c     LIGQFVDVKIVDVFPNSLRGELLRTEQEMNLRIATSPSEMKAKTRREDELGVATFTP 474
A.a     LLGKIVKIKVIKSSPFSLEGELLEVIK------------------------------ 440
        ::*::..::: .  . .* * :: . .
```

**Figure 6.3:** HPLC chromatogram of modified tRNA nucleosides from *T. maritima*. tRNA preparation and hydrolysis are as described under “Material and Methods.” *Inset*, UV-visible spectrum of the peak eluting at 84 min.

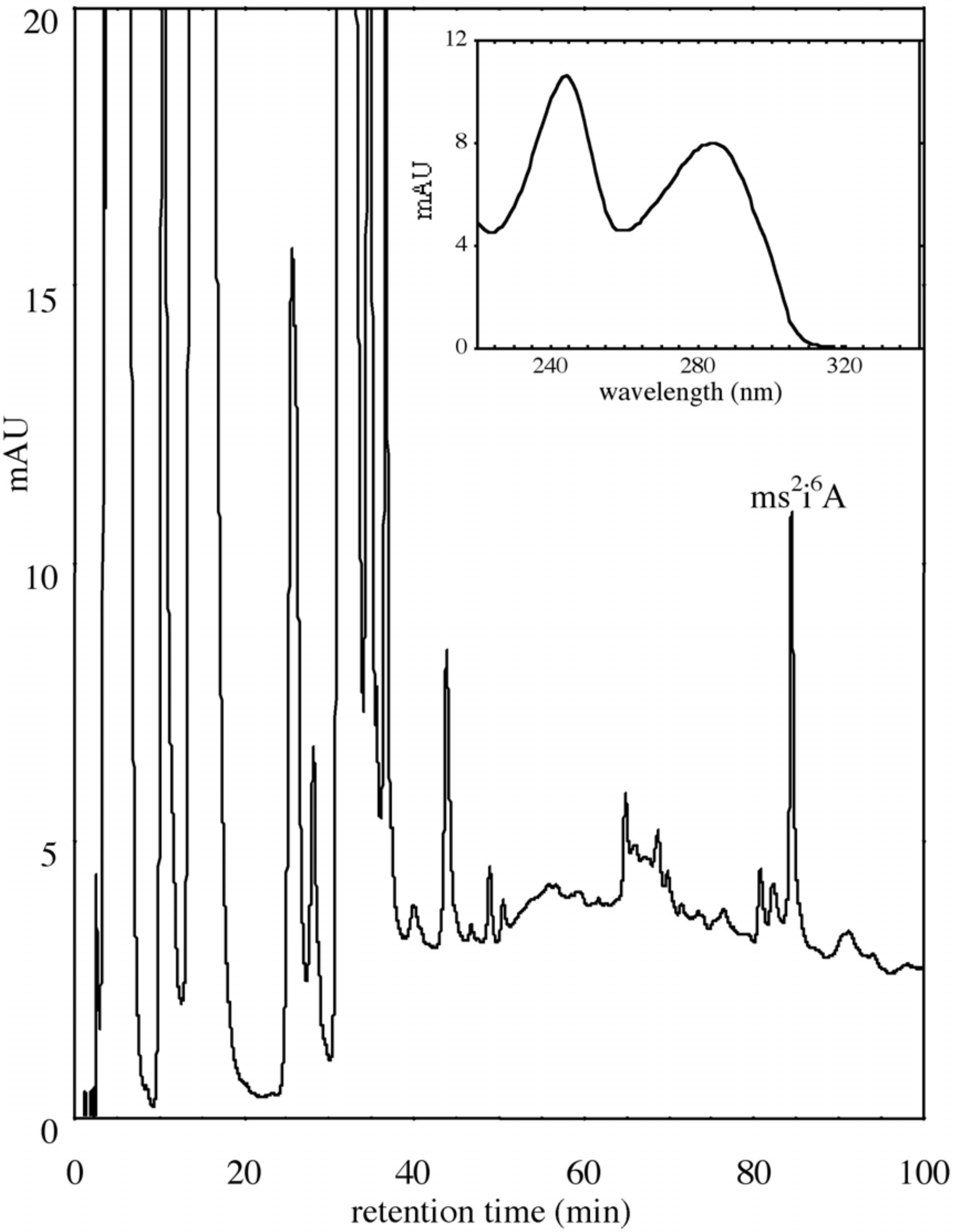
20
15
10
5
0
mAU
0
20
40
60
80
100
retention time (min)
$ms^{2}i^{6}A$
12
8
4
0
mAU
240
280
320
wavelength (nm)

**Figure 6.4:** Purification of MiaBTm. SDS-PAGE (12%) gel showing MiaBTm during different stages of purification: *lane MW*, size markers; *lane 1*, uninduced cells; *lane 2*, induced cells; *lane 3*, cell-free extracts; *lane 4*, soluble fraction after heating the extracts at 75 °C for 15 min; *lane 5*, 60 % ammonium sulfate precipitate; *lane 6*, MiaBTm-containing fraction after butyl-Sepharose chromatography; *lane 7*, MiaB-Tm-containing fraction after Superdex 200 chromatography.

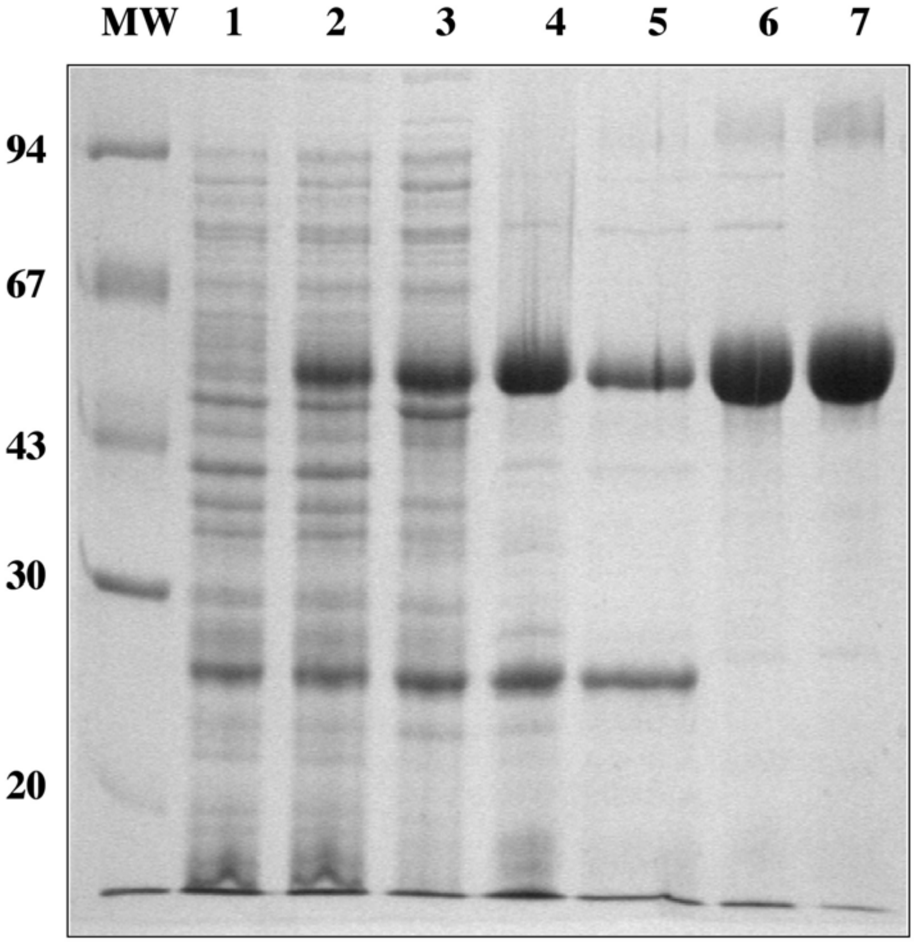
MW
1
2
3
4
5
6
7
94
67
43
30
20

**Figure 6.5:** HPLC chromatograms of tRNA hydrolysates for the *in vivo* complementation of miaB$^-$ TX3346 *E. coli* strain transformed with pT7-MiaBTm at 37 °C (*A*) and 45 °C (*B*). The identification is based on UV-visible spectra (data not shown) and retention times (i$^6$A elute at ~71 min and ms$^2$i$^6$A at ~84 min.

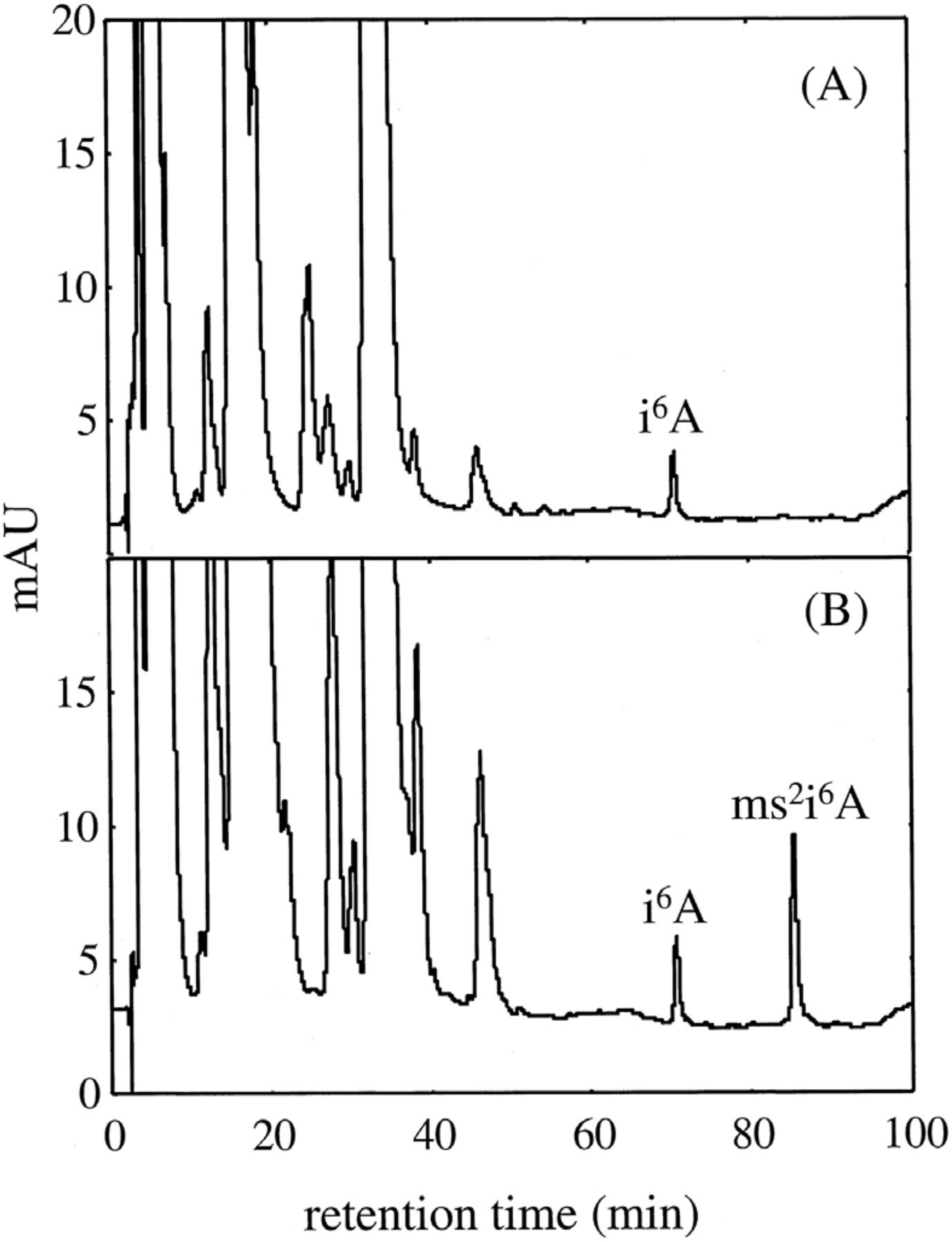
(A)
(B)
i$^6$A
i$^6$A
ms$^2$i$^6$A
mAU
20
15
10
5
0
0
20
40
60
80
100
retention time (min)

**Figure 6.6:** UV-visible absorption spectra of purified MiaBTm. *A*, as-isolated; *B*, after anaerobic reconstitution of the apoprotein with iron and sulfide. *Inset a*, expansion of the as-isolated protein spectrum. The protein concentrations were 240 μM and the buffer was 50 mM Tris-Cl, pH 8.0, with 200 mM NaCl.

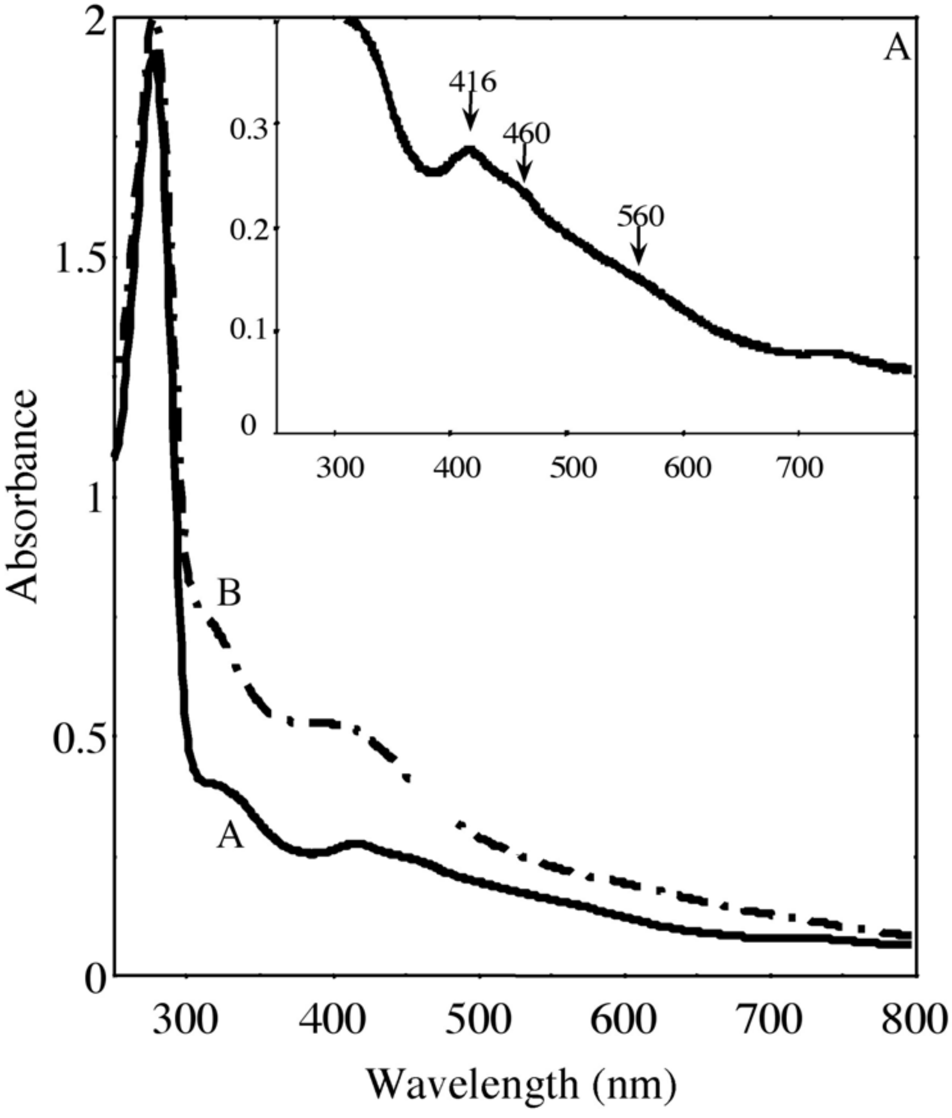
Absorbance
Wavelength (nm)
2
1.5
1
0.5
0
300
400
500
600
700
800
B
A
A
0.3
0.2
0.1
0
416
460
560

**Figure 6.7:** EPR spectra of MiaBTm. *A*, MiaBTm as isolated; *C*, MiaBTm after anaerobic reconstitution with iron and sulfide. The sample concentrations were 200 µM (*A*) and 100 µM (*C*), and the buffering medium was 50 mM Tris-Cl, pH 8.0, with 200 mM NaCl. The as-isolated and reconstituted samples were anaerobically reduced with 2 mM sodium dithionite in *spectra B* and *D*, respectively. The spectra were recorded under the same conditions: temperature, 10 K; microwave frequency, 9.655 GHz; microwave power, 0.2 mW; modulation amplitude, 1.0 mT.

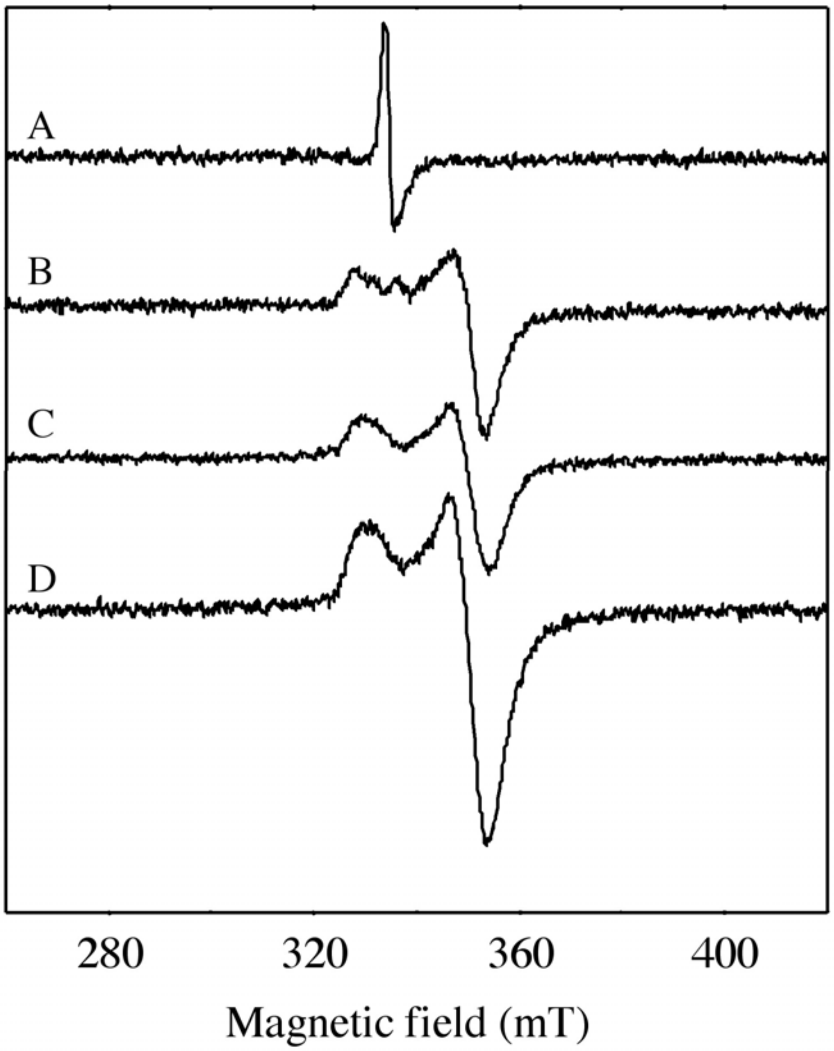
A
B
C
D
280
320
360
400
Magnetic field (mT)

**Figure 6.8:** Low-temperature resonance Raman spectra of MiaBTm as-isolated (*a*), reconstituted from the apoprotein (*b*), reconstituted from the as-isolated form before (*c*), and after (*d*) exposure to air for 30 minutes. The protein concentration was ~4 mM, and the buffering medium was 50 mM Tris-Cl, pH 8.0, with 200 mM NaCl. The spectra were obtained at 17 K using 457.9-nm excitation, and each is the sum of ~200 scans. Each scan involved advancing the spectrometer in 0.5 $cm^{-1}$ increments and photon counting for 1 s/point with 8 $cm^{-1}$ spectral resolution.

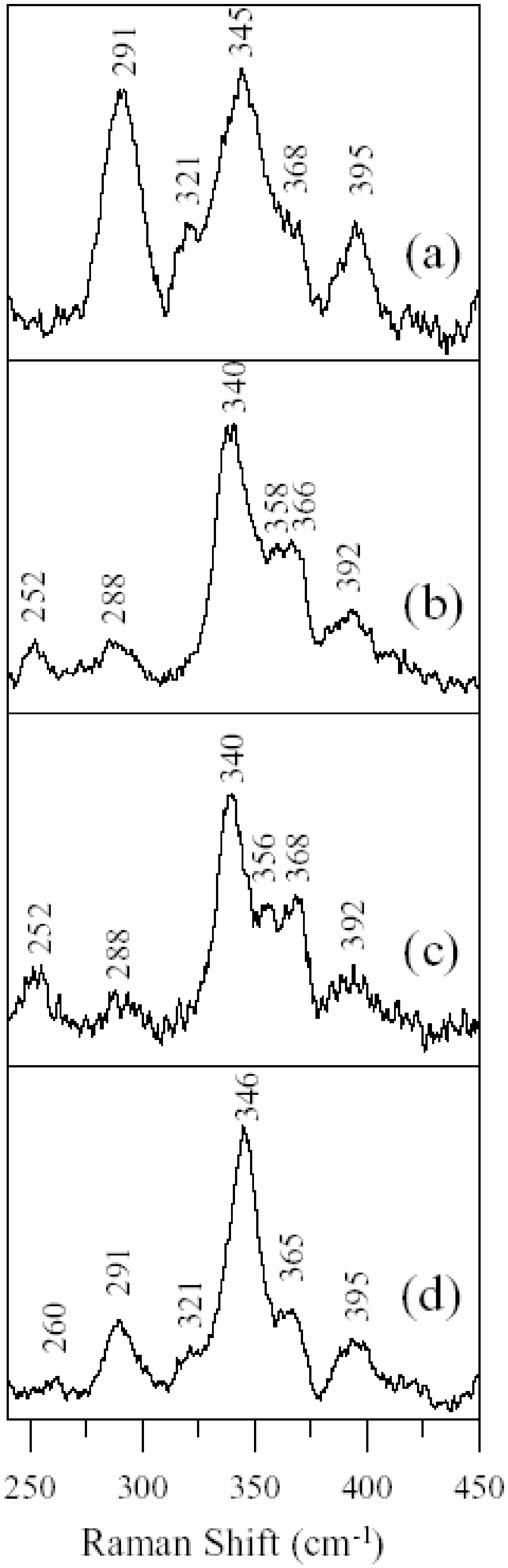
291
345
321
368
395
(a)
340
358
366
252
288
392
(b)
340
356
368
252
288
392
(c)
346
291
365
321
395
260
(d)
250
300
350
400
450
Raman Shift (cm-1)

**Figure 6.9:** VTMCD spectra of reconstituted MiaBTm reduced with a 6-fold excess of sodium dithionite. The buffering medium was 50 mM Tris-Cl, pH 8.0, 200 mM NaCl, with 60% (v/v) ethylene glycol to yield a final protein concentration of 450 μM. MCD spectra recorded with a magnetic field of 6.0 T at 1.82, 4.22, 10 and 35 K and the MCD intensity at all wavelengths increased in intensity with decreasing temperature. The MCD spectrum recorded at 50 K has been subtracted from each data set to ensure that the spectra shown originate exclusively from transitions associated with paramagnetic Fe-S clusters.

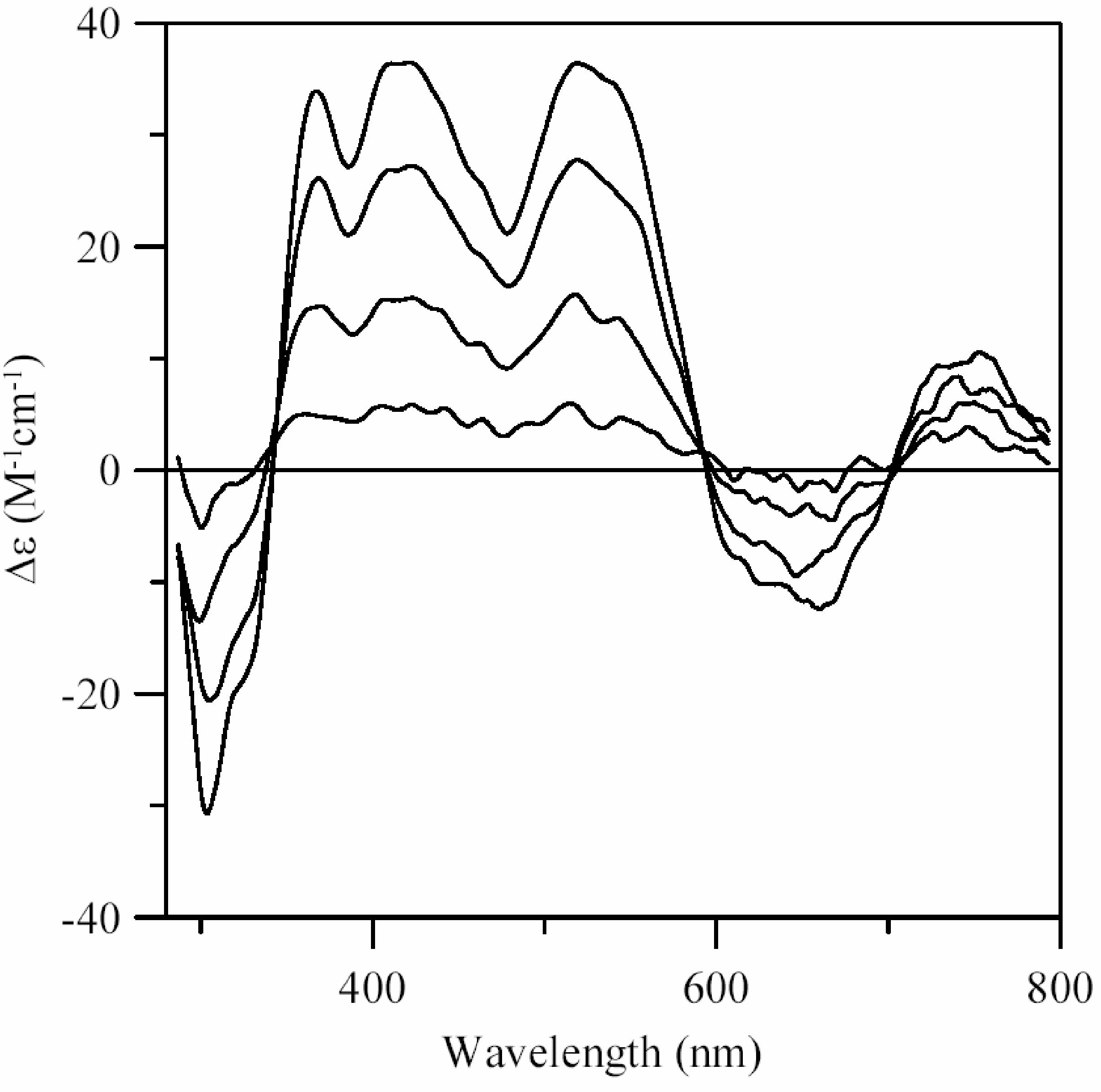
40
20
0
-20
-40
Δε (M-1cm-1)
400
600
800
Wavelength (nm)

**Figure 6.10:** Square wave voltammogram of reconstituted MiaBTm. Data were recorded anaerobically at the planar gold electrode. The protein concentration was 200 μM, and the solvent was 50 mM Tris-Cl, pH 8, containing 200 mM NaCl. The pulse frequency was 20 Hz, the scan increment 2 mV, and the pulse height amplitude 80 mV. The potential is *versus* the normal hydrogen electrode.

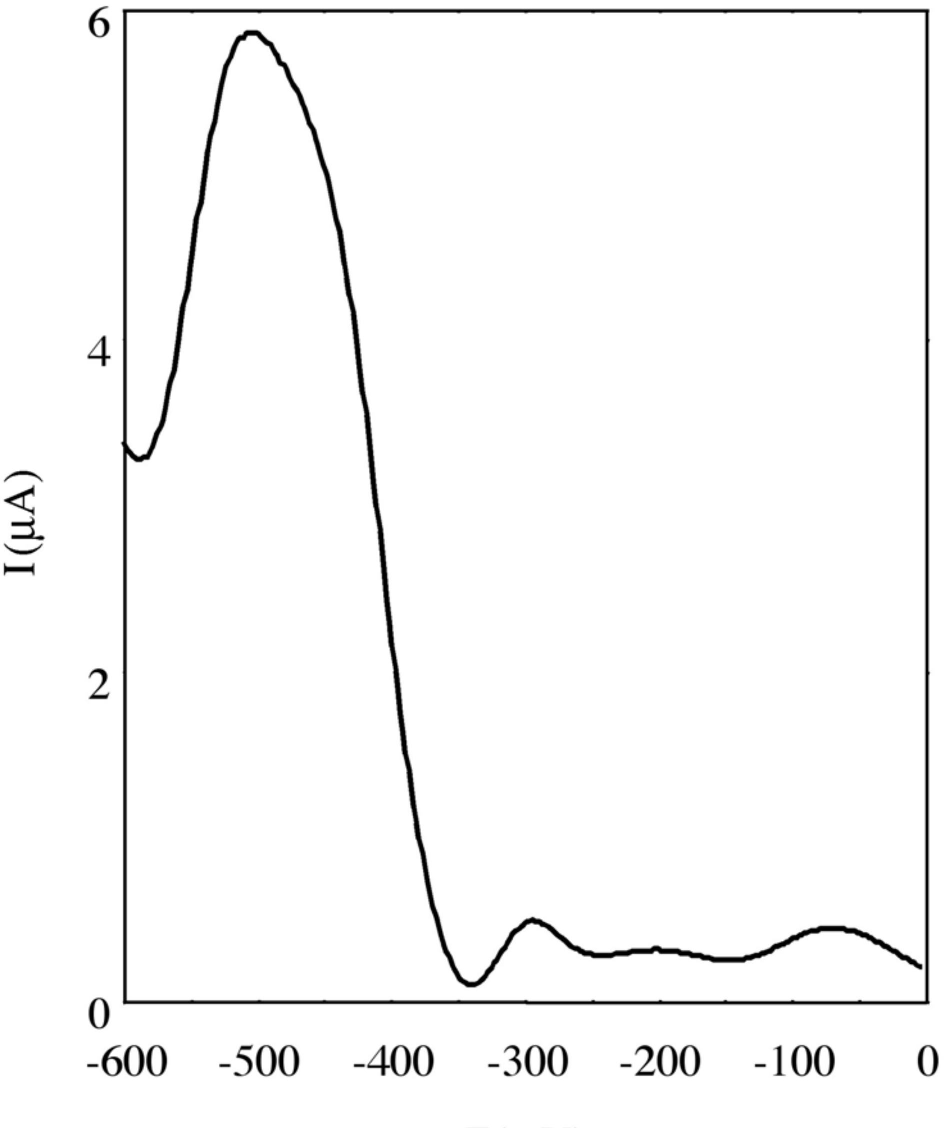

6
4
2
0
I (μA)
-600
-500
-400
-300
-200
-100
0
E(mV)

# CHAPTER 7

# MIAB, A BIFUNCTIONAL RADICAL-*S*-ADENOSYLMETHIONINE ENZYME INVOLVED IN THE THIOLATION AND METHYLATION OF TRNA, CONTAINS TWO [4FE-4S] CLUSTERS[1]

---

[1] Hernández, H. L., Pierrel, F., García-Serres, R., Huynh, B. H., Fontecave, M., Atta, M., and Johnson, M. K. To be submitted to *FEBS Letters*.

## Abbreviations

tRNA, transfer ribonucleic acid; SAM, *S*-adensoyl-L-methionine; ms$^2$i$^6$A-37, modified nucleoside 2-methylthio-*N*-6-isopentenyl-adenosine at position 37, DTT, dithiothreitol

## Abstract

MiaB catalyzes the post-transcriptional methylthiolation of *N*-6-isopentenyl adenosine in tRNAs. Spectroscopic and analytical studies of the reconstituted wild-type and C150/154/157A triple variant forms of *Thermotoga maritima* MiaB have revealed two distinct $[4Fe\text{-}4S]^{2+,+}$ clusters. One is coordinated by the three conserved cysteines in the radical-SAM motif (Cys150, Cys154, and Cys157) and the other is proposed to be coordinated by the three N-terminal conserved cysteines (Cys10, Cys46, and Cys79). The two $[4Fe\text{-}4S]^{2+}$ clusters have similar UV-visible absorption, resonance Raman and Mössbauer properties, but differ in terms of redox potentials and the EPR properties of the reduced $[4Fe\text{-}4S]^{+}$ clusters. Reconstituted forms of MiaB containing two [4Fe-4S] clusters have 3-fold higher activity than previously prepared forms containing approximately one [4Fe-4S] cluster, suggesting that both clusters are required for catalytic activity. The N-terminal $[4Fe\text{-}4S]^{2+,+}$ cluster does not interact with the tRNA substrate as judged by resonance Raman and EPR studies and a possible role as a sacrificial S-donor in the methylthiolation reaction is discussed.

## Introduction

Modified nucleosides are found in transfer RNAs (tRNAs) of all three domains of life and are crucial to their biological activity (*1;2*). Complex maturation processes have been shown to be involved in the post-transcriptional modification of tRNA nucleosides at a variety of different positions with the anticodon loop constituting the most heavily modified region (*3*). Several of these modifications involve thiolation of tRNA nucleosides and it appears that thiolation of tRNA nucleosides occurs via at least two distinct pathways (*4;5*). For example, the biosynthesis of 4-thiouridine is dependent on IscS which directly transfers sulfur to its tRNA modifying enzyme, ThiI (*6;7*). In contrast, the biosynthesis of 2-methylthio-*N*-6-isopentenyl-adenosine ($ms^2i^6A$-37) involves MiaB which utilizes an Fe-S center in the thiolation of nucleosides (*4*).

Located at position 37 next to the anticodon on the 3'-position, $ms^2i^6A$-37 is found in almost all eukaryotic and bacterial tRNAs that read codons beginning with U except $tRNA^{I,V}$Ser (*8*). The first step in $ms^2i^6A$-37 biosynthesis is catalyzed by MiaA and involves the addition of a isopentenyl group at the N-6 nitrogen of adenosine, converting adenosine-37 to $i^6A$-37, see scheme 7.1 (*9-11*). The second step, catalyzed by MiaB, consists of a chemically challenging H-abstraction followed by both sulfur insertion and methylation at position 2 of $i^6A$-37 forming $ms^2i^6A$-37. Initially, iron, cysteine and *S*-adenosyl-L-methionine (SAM) were implicated in the methylthiolation of $i^6A$ (*12;12-14*), but it was not until the *miaB* gene was identified and observed to contain the highly conserved C*XXX*C*XX*C motif that it was speculated to be a radical activating enzyme that binds iron (*15*). Fontecave and coworkers subsequently demonstrated that the MiaBs from *E. coli* and *Thermotoga maritima* were in fact radical-SAM enzymes requiring SAM and a [4Fe-4S] cluster bound by the C*XXX*C*XX*C motif for catalytic activity (*16;17*).

Radical-SAM enzymes are a super-family of proteins consisting of over 600 putative enzymes (*18*). These enzymes share a common mechanism that utilizes a $[4Fe\text{-}4S]^{2+,+}$ cluster to initiate a radical reaction by mediating reductive cleavage of SAM to yield a 5'-deoxyadenoxyl radical. This radical then abstracts a hydrogen from an appropriately placed substrate creating a substrate based carbon radical (*19-21*). In the formation of $ms^2i^6A$-37, the H-atom is abstracted at position 2 of the base moiety and then the activated carbon is thiolated and methylated. Recent studies revealed that MiaB is responsible for both the thiolation and methylation steps by using two molecules of SAM (*22*). The first SAM is used for radical generation and substrate carbon activation, while the second SAM is utilized in the more traditional role as the methyl donor (*22*).

Like MiaB, several other radical-SAM enzymes catalyze the thiolation of substrate, including biotin synthase (BioB) (*23;24*), lipoic acid synthase (LipA) (*25*), and possibly HydE or HydG (*26*). The source of the inserted sulfur has been the cause of much debate in the literature. Interestingly, BioB, LipA, and HydE have been shown to contain a second Fe-S cluster in addition to the radical-SAM [4Fe-4S] cluster: a [2Fe-2S] cluster in BioB (*27;28*) and an additional [4Fe-4S] cluster in LipA and HydE (*26;29*). These additional clusters have been implicated as the physiological S-donor in BioB and LipA. A recent 3.4 Å resolution crystal structure of BioB revealed a novel [2Fe-2S] cluster bound by three cysteine residues and one arginine residue and showed that a S of the [2Fe-2S] is positioned close to the S-insertion site of its substrate, dethiobiotin (*30*). When Se was introduced into BioB and MiaB or $^{34}S$ into LipA, forming $[2Fe\text{-}2Se/^{34}S]$ or $[4Fe\text{-}4Se/^{34}S]$ clusters, $Se/^{34}S$ was shown to be incorporated into the respective substrates (*22;31;32*). Thus far only one other radical-SAM enzyme, MOCS1A/MoaA, is known to contain a second cluster (*33;34*). MOCS1A/MoaA is not involved in thiolation of substrate and a recent crystal structure places its substrate, 5'-GTP, within binding distance of the non-radical-SAM cluster, implying that the cluster may act to position the substrate for H-abstraction by the 5'-deoxyadenosyl radical (*35*).

In this work, reconstituted *T. maritima* MiaB is also shown to contain two Fe-S clusters, an N-terminal [4Fe-4S]$^{2+,+}$ cluster in addition to the radical-SAM [4Fe-4S]$^{2+,+}$ cluster, and activity measurements indicate that both clusters are required for catalytic activity. The spectroscopic and redox properties of each [4Fe-4S] cluster have been investigated by comparing the UV/visible absorption, EPR, resonance Raman, and Mössbauer properties of wild-type MiaB, containing both clusters, and C150/154/157A MiaB, containing only the N-terminal, non-radical-SAM [4Fe-4S] cluster. Possible roles for the non-radical-SAM cluster are discussed.

## Materials and Methods

### *Construction, overexpression and purification of T. maritima MiaB*

Construction, overexpression and purification of wild-type MiaB and the C150/154/157A triple variant are described elsewhere (*17;22*). Both were purified under aerobic conditions and contained only trace quantities of Fe-S clusters as judged by UV-visible absorption spectroscopy. Apo-proteins were obtained by overnight exposure to EDTA (10 mM) under reducing conditions (10 mM sodium dithionite). Following purification using a Sephadex NAP-25 gel filtration column equilibrated with 50 mM Tris-HCl buffer, pH 8, with 200 mM NaCl, the protein was washed and concentrated using a Centricon with a 30 kDa membrane.

### *Reconstitution of as prepared and apo forms of wild-type and C150/154/157A T. maritima MiaB*

Fe-S cluster reconstitutions of wild-type and C150/154/157A *T. maritima* MiaB were carried out under strictly anaerobic conditions in a Vacuum Atmospheres glovebox containing less than 2 ppm $O_2$. Following incubation of the as-purified or apo-proteins with 10 mM DTT for 10 minutes, a 10-fold molar excess of $Fe^{II}(NH_4)_2(SO_4)_2$ was added, followed by the addition of a 10-fold molar excess of $Na_2S$. After 3 hours, the reconstitution mixture was loaded onto 10-mL HiTrap Q columns previously equilibrated with buffer A (50 mM Tris-HCl, pH 8.0 plus 50 mM NaCl) and eluted with a 0–100 % gradient of buffer B (100 mM Tris-HCl, pH 8.0 plus 1 M NaCl). The brown fractions were concentrated over an YM30 (Amicon) membrane and washed in buffer C (100 mM Tris-HCl, pH 8.0 plus 200 mM NaCl). Identical outcomes were achieved whether starting from apo or as-purified protein. The same procedure was used to prepare Mössbauer samples except that $^{57}$Fe-enriched $Fe^{II}(NH_4)_2(SO_4)_2$ was used. $^{57}$Fe-enriched $Fe^{II}(NH_4)_2(SO_4)_2$ was prepared from $^{57}$Fe metal (>95% isotopic enrichment) as previously described (*36*)

*Protein, Fe and activity assays*

Protein concentrations were determined by the *DC* protein assay (Bio-Rad), using BSA as a standard. All sample concentrations are based on protein determinations. Iron concentrations were determined colorimetrically using bathophenanthroline under reducing conditions, after digestion of the protein in 0.8% $KMnO_4$/0.2 M HCl (*37*). The $i^6$A-37-tRNA substrate was prepared and the activity assays were conducted as previously described (*22*).

*Spectroscopic characterization of Fe-S centers.*

UV-visible absorption spectra were recorded under anaerobic conditions in screw top 1 mm cuvettes using a Shimadzu UV-3101PC spectrophotometer. Resonance Raman spectra were recorded using an Instruments SA U1000 spectrometer fitted with a cooled RCA 31034 photomultiplier tube with 90° scattering geometry. Spectra were recorded digitally using photon-counting electronics and improvements in signal-to-noise were achieved by signal averaging multiple scans. Band positions were calibrated using the excitation frequency and are accurate to ±1cm$^{-1}$. Lines from a Coherent Sabre 10-W argon ion laser were used for excitation, and plasma lines were removed using a Pellin Broca prism premonochromator. For each sample, the laser power at the samples was ~200 mW, and slit widths were adjusted for each excitation wavelength to give 8.0 cm$^{-1}$ spectral resolution. Scattering was collected from the surface of a frozen 17 μl droplet of sample using a custom-designed anaerobic sample cell (*38*) attached to the cold finger of an Air Products Displex model CSA-202E closed cycle refrigerator. This enables samples to be cooled down to 18 K, which facilitates improved spectral resolution and prevents laser-induced sample degradation. X-band EPR spectra were recorded on a Bruker ESP-300E EPR spectrometer equipped with an ER-4116 dual-mode cavity and an Oxford Instrument ESR-9 flow cryostat. Resonances were quantified under non-saturating conditions by double integration against a 1 mM CuEDTA standard. Mössbauer spectra were recorded at 4.2 K in a weak (50 mT) applied field, using the spectrometer described in ref. (*39*), and analyzed with the program WMOSS (Web Research). The zero velocity of the spectra refers to the centroid of the room temperature spectrum of a metallic iron foil.

## Results and Discussion

Samples of wild-type *T. maritima* MiaB purified under aerobic conditions contain sub-stoichiometric amounts of [2Fe-2S]$^{2+}$ and [3Fe-4S]$^{+}$ clusters that are products of $O_2$-induced degradation of [4Fe-4S]$^{2+}$ clusters (*16;17*). However, the functional form containing [4Fe-4S]$^{2+,+}$ clusters can be prepared by standard anaerobic Fe-S cluster reconstitution procedures. Previous attempts to reconstitute Fe-S clusters in the apo form used excess $FeCl_3$ and $Na_2S$ in the presence of DTT and resulted in samples containing approximately one [4Fe-4S]$^{2+}$ cluster per MiaB (*17*).

However, more recent reconstitution attempts using $Fe(NH_4)_2(SO_4)_2$ in place of $FeCl_3$ and replacing gel-filtration purification with purification using anion exchange chromatography inside a glove box at < 2 ppm $O_2$ resulted in samples containing approximately two $[4Fe\text{-}4S]^{2+,+}$ clusters as judged by Fe determinations, UV-visible absorption and EPR. The resulting samples contained 8.3 ± 1.0 Fe per MiaB (average of three preparations) and had varying amounts of $[4Fe\text{-}4S]^{+}$ clusters as judged by EPR studies (0-0.3 $S = 1/2$ $[4Fe\text{-}4S]^{+}$ clusters based on EPR spin quantitations). The UV-visible absorption spectra of a fully oxidized sample, i.e. one that showed no evidence of reduced $[4Fe\text{-}4S]^{+}$ clusters as judged by parallel EPR studies, is shown in Figure 7.1. The visible spectrum comprises a broad shoulder centered at 400 nm that is characteristic of $[4Fe\text{-}4S]^{2+}$ clusters and has a $A_{400}/A_{280}$ ratio = 0.31. Moreover, the molar extinction coefficient at 400 nm ($\varepsilon_{400} = 34\ mM^{-1}cm^{-1}$) is characteristic of two $[4Fe\text{-}4S]^{2+}$ clusters per MiaB, as biological $[4Fe\text{-}4S]^{2+}$centers typically have $\varepsilon_{400} = 15\text{-}17\ mM^{-1}cm^{-1}$ on a per cluster basis.

Samples of MiaB containing two $[4Fe\text{-}4S]^{2+}$ clusters also showed enhanced activity compared to previous preparations which contained approximately one [4Fe-4S] cluster per MiaB. For both types of sample, HPLC monitored assays at 37°C showed that the reaction is slow and asymptotically approaches a maximal amount of $ms^2i^6A$ produced per MiaB after about 100 mins. MiaB samples containing approximately one [4Fe-4S] cluster maximally produced 0.18 $ms^2i^6A$ per MiaB (*22*), whereas as those containing two [4Fe-4S] clusters maximally produced 0.60 $ms^2i^6A$ per MiaB. While neither sample is capable of more than one turnover, the data clearly show that samples containing two $[4Fe\text{-}4S]^{2+}$ clusters are 3-times more effective in modifying tRNA in a single turnover experiment.

*T. maritima* MiaB has been shown to be a radical-SAM enzyme that converts one molecule of SAM into 5'-deoxyadenosine and has a radical-SAM [4Fe-4S] cluster binding motif. Hence one of the two [4Fe-4S] clusters is expected to be ligated by Cys150, Cys154, and Cys 157 and to be responsible for binding and reductive cleavage of one molecule of SAM to yield the reactive 5'-deoxyadenosyl radical that abstracts an H-atom from an unactivated substrate carbon atom to form 5'-deoxyadenosine. As there are only three other cysteines that are conserved in all MiaB proteins (*17*), Cys10, Cys46, and Cys79 in *T. maritima* MiaB, these residues are clearly the best candidates for the ligands to a second [4Fe-4S] cluster. To confirm the presence of a second [4Fe-4S] cluster and investigate the properties of a putative N-terminal [4Fe-4S] cluster in isolation, all three of the cysteine ligands to the radical-SAM [4Fe-4S] cluster were replaced with alanine. The C150/154/157A triple variant of *T. maritima* MiaB was expressed and purified aerobically primarily as an apo protein. However, anaerobic Fe-S cluster reconstitution yields a protein containing approximately one $[4Fe\text{-}4S]^{2+,+}$ cluster per MiaB based on Fe analyses, UV-visible absorption and EPR. Reconstituted C150/154/157A MiaB samples contained 3.2 ± 0.5 Fe per MiaB (average of three preparations) and had varying amounts of $[4Fe\text{-}4S]^{+}$ clusters as judged by EPR studies (0-0.5 $S = 1/2$ $[4Fe\text{-}4S]^{+}$ clusters based on EPR spin quantitations). The UV-visible absorption spectra of a fully oxidized sample, i.e. one that showed no evidence of reduced $[4Fe\text{-}4S]^{+}$ clusters as judged by parallel EPR studies, is shown in Figure 7.1. The visible spectrum is characteristic of a $[4Fe\text{-}4S]^{2+}$ cluster ($A_{400}/A_{280}$ ratio = 0.19) and the molar extinction coefficient, $\varepsilon_{400} = 13\ mM^{-1}cm^{-1}$, is indicative of ~0.8 $[4Fe\text{-}4S]^{2+}$ clusters per MiaB, in excellent agreement with the Fe determinations.

Resonance Raman and Mössbauer of reconstituted wild-type and C150/154/157A MiaB, see Figures 7.2 and 7.3, respectively, confirmed the presence of $[4Fe\text{-}4S]^{2+,+}$ clusters in both samples and facilitated more detailed comparison of the vibrational and electronic properties of the N-terminal and radical-SAM $[4Fe\text{-}4S]^{2+}$ centers. The resonance Raman of both samples in the Fe-S stretching region are uniquely characteristic of $[4Fe\text{-}4S]^{2+}$ clusters, see Figure 7.2, and are readily assigned based on the detailed vibrational studies that are available for $[4Fe\text{-}4S]^{2+}$ centers in ferredoxins and model complexes (*40;41*). Moreover, the near congruent resonance Raman spectra for both samples indicates structurally very similar $[4Fe\text{-}4S]^{2+}$ centers, each ligated by three cysteine ligands, in the N-terminal and radical-SAM binding sites. This is further supported by Mössbauer spectra of samples reconstituted using $^{57}Fe(NH_4)_2(SO_4)_2$, see Figure 7.3. The spectra of both wild-type and C150/154/157A MiaB are both dominated by quadrupole doublets from the $S = 0$ $[4Fe\text{-}4S]^{2+}$ clusters and both are well fit as two equal intensity valence delocalized pairs, one with $\delta = 0.46$ mm/s and $\Delta E_Q = 1.27$ mm/s and the other with $\delta = 0.44$ mm/s and $\Delta E_Q = 1.03$ mm/s. Hence the $[4Fe\text{-}4S]^{2+}$ centers in the N-terminal and radical-SAM domains also have analogous vibrational and electronic properties.

The Mössbauer spectra of the $^{57}Fe$-reconstituted wild-type and C150/154/157A MiaB samples as prepared also indicated that 29% and 42% of the $^{57}Fe$, respectively, is present as $S = 1/2$ $[4Fe\text{-}4S]^{+}$ clusters that are well simulated using the parameters reported for reduced *Bacillus stearothermophilus* [4Fe-4S] ferredoxin (*42*). This is supported by parallel EPR studies of the same samples, see Figure 7.4c, which revealed identical near-axial $S = 1/2$ resonances with $g_{\|} = 2.06$ and $g_{\perp} = 1.94$, accounting for 0.5 spins/MiaB for wild-type and 0.4 spins/MiaB for the C150/154/157A variant. In accord with the fast relaxation properties that are characteristic of $S = 1/2$ $[4Fe\text{-}4S]^{+}$ clusters, these resonances are only observable at temperatures below 50 K. The complete absence of low-field resonances in the $g = 5$ region indicative of $S > 1/2$ species, even at low temperatures (4.2 K) and high microwave powers (50 mW), and the ability to fit the corresponding Mössbauer resonance with the parameters expected for an $S$ = 1/2 [4Fe-4S]$^{+}$cluster, demonstrate that the [4Fe-4S]$^{+}$ clusters in reconstituted samples as prepared exclusively have $S$ = 1/2 ground states.

Differences in the properties of the reduced N-terminal and radical-SAM [4Fe-4S]$^{+}$ clusters in MiaB are apparent in EPR studies of dithionite-reduced samples, see Figures 7.4a and 7.4b. The N-terminal [4Fe-4S]$^{+}$ center in dithionite-reduced reconstituted C150/154/157A MiaB is exclusively $S$ = 1/2 and fully reducible by dithionite, as evidenced by spin quantitations and the absence of low field resonances in the $g$ = 5 region. The $S$ = 1/2 resonance ($g_{\|}$ = 2.06 and $g_{\perp}$ = 1.94) is identical to that observed in as prepared reconstituted samples of both wild-type and C150/154/157A MiaB, and corresponds to 0.7 ± 0.1 spins/MiaB, which translates to 0.9 ± 0.1 spins/[4Fe-4S] cluster based on the cluster content as determined by the Fe analyses and UV-visible absorption spectra discussed above. In contrast, dithionite-reduced reconstituted wild-type MiaB shows a broad low-field resonance centered at $g$ = 5.4 at low temperatures and high microwave powers that is indicative of a near-rhombic $S$ = 3/2 [4Fe-4S]$^{+}$ center and a significantly broadened resonance in the $S$ = 1/2 region that accounts for ~1.1 spins/MiaB. The $S$ = 1/2 resonance has similar principal g-values to those of the N-terminal $S$ = 1/2 [4Fe-4S]$^{+}$ center, but is broader and has developed ill-defined "wings" to lower and higher field. Such EPR characteristics are indicative of weak intercluster magnetic interactions between paramagnetic clusters separated by 12-20 Å (*43*). Hence in common with other radical-SAM [4Fe-4S]$^{+}$ clusters (*44;45*), the [4Fe-4S]$^{2+}$ cluster in the radical-SAM binding site of MiaB is at least partially reducible by dithionite at pH 8, and most likely is present as a mixed-spin species with both $S$ = 1/2 and 3/2 components. Hence the picture that emerges from the EPR studies of dithionite-reduced samples is that reconstituted wild-type MiaB contains two [4Fe-4S]$^{+}$ clusters separated by 12-20 Å. The N-terminal [4Fe-4S] cluster has a significantly higher redox potential resulting in partial reduction in the absence of dithionite and the reduced $[4Fe\text{-}4S]^+$ cluster is exclusively $S = 1/2$ with $g_{\|} = 2.06$ and $g_{\perp} = 1.94$. The radical-SAM [4Fe-4S] cluster has a lower redox potential, but is reduced at least partially by dithionite at pH 8, and the reduced $[4Fe\text{-}4S]^+$ cluster exists as a mixture of forms with $S = 1/2$ and 3/2 ground states.

The spectroscopic and analytical results unambiguously demonstrate the presence of two $[4Fe\text{-}4S]^{2+,+}$ clusters in MiaB and the activity studies suggest that both are required for methylthiolation of *N*-6-isopentenyl adenosine in tRNAs in a single turnover reaction. While the role of the radical-SAM [4Fe-4S] cluster clearly lies in generating the 5'-deoxyadenosyl radical and thereby activating the substrate for methylthiolation via H-abstraction, the role of N-terminal [4Fe-4S] cluster remains to be established.

By analogy with MoaA/MOCS1A (*35*), one possibility is that the N-terminal cluster plays a role in positioning the tRNA substrate for effective H-abstraction at position 2 of $i^6A$-37, see scheme 7.1. To investigate this possibility, the properties of the oxidized and reduced N-terminal $[4Fe\text{-}4S]^{2+,+}$ clusters in C150/154/157A MiaB were investigated by resonance Raman and EPR, respectively, in the presence and absence of a 6-fold stoichiometric excess of the $i^6A$-37-tRNA substrate, see Figure 7.5. The results clearly demonstrate that presence of the substrate has no significant effect on the resonance Raman spectrum of the $[4Fe\text{-}4S]^{2+}$ cluster or the EPR spectrum of the $[4Fe\text{-}4S]^+$ cluster and hence argue against a role for the N-terminal cluster in interacting with the substrate. In contrast, the available evidence does suggest that the N-terminal [4Fe-4S] cluster may function as a sacrificial S-donor during single turnover experiments; a role similar to that suggested for the [2Fe-2S] cluster in BioB (*30;46*) and the additional [4Fe-4S] cluster in LipA (*29*). Prior to the discovery of the N-terminal [4Fe-4S] in MiaB, wild-type MiaB was reconstituted with selenide in place of sulfide and the presence of approximately one [4Fe-4Se] cluster was inferred based on Fe analyses and UV-visible absorption data (*22*). This protein was functional in activity assays and the product was found to contain $\mathrm{mse}^2\mathrm{i}^6\mathrm{A}$ rather than $\mathrm{ms}^2\mathrm{i}^6\mathrm{A}$, indicating that the S atom in $\mathrm{ms}^2\mathrm{i}^6\mathrm{A}$ derives from the MiaB protein itself and is introduced into MiaB during reconstitution of the Fe-S clusters with iron and sulfide (*22*). The discovery of the N-terminal [4Fe-4S] cluster in MiaB and the conditions required to obtain MiaB with a full complement of Fe-S clusters, clearly lays the ground work for more detailed investigations to assess the fate of the N-terminal cluster under turnover conditions and the possibility that MiaB is able function as an enzyme capable of multiple turnovers, rather than suicide enzyme that degrades after one turnover.

*Acknowledgements*: This work was supported by grants from the National Institutes of Health (GM62542 to M.K.J., GM47295 to B.H.H.)

## References

1. Auffinger, P. and Westhof, E. (1998) Location and distribution of modified nucleotides in tRNA, in *Modification and Editing of RNA* (Grosjean, H. and Benne, R., Eds.) pp 569-576, ASM Press, Washington, D. C.

2. McCloskey, J. A., Graham, D. E., Zhou, S., Crain, P. F., Ibba, M., Konisky, J., Söll, D., and Olsen, G. J. (2001) Post-transcriptional modification in archaeal tRNAs: identities and phylogenetic relations of nucleosides from mesophilic and hyperthermophilic Methanococcales, *Nucleic Acids Res. 29*, 4699-4706.

3. Rozenski, J., Crain, P. F., and McCloskey, J. A. (1999) The RNA modification database: 1999 update, *Nucleic Acids Res. 27*, 196-197.

4. Leipuviene, R., Qian, Q., and Björk, G. R. (2004) Formation of thiolated nucleosides present in tRNA from *Salmonella enterica* serovar Typhimurium occurs in two principally distinct pathways, *J. Bacteriol. 186*, 758-766.

5. Lundgren, H. K. and Björk, G. R. (2006) Structural alterations of the cysteine desulfurase IscS of *Salmonella enterica* Serovar Typhimurium reveal substrate specificity of IscS in tRNA thiolation, *J. Bacteriol. 188*, 3052-3062.

6. Kambampati, R. and Lauhon, C. T. (1999) IscS is a sulfurtransferase for the *in vitro* biosynthesis of 4-thiouridine in *Escherichia coli* tRNA, *Biochemistry 38*, 16561-16568.

7. Mueller, E. G., Palenchar, P. M., and Buck, C. J. (2001) The role of the cysteine residues of ThiI in the generation of 4-thiouridine in tRNA, *J. Biol. Chem. 276*, 33588-33595.

8. Grosjean, H., Nicoghosian, K., Haumont, E., Söll, D., and Cedergren, R. (1985) Nucleotide sequences of two serine tRNAs with a GGA anticodon: the structure-function relationships in the serine family of *E. coli* tRNAs, *Nucleic Acids Res. 13*, 5697-5706.

9. Moore, J. A. and Poulter, C. D. (1997) *Escherichia coli* dimethylallyl diphosphate: tRNA dimethylallyltransferase: a binding mechanism for recombinant enzyme, *Biochemistry 36*, 604-614.

10. Leung, E. H. C., Chen, Y., and Winkler, M. E. (1997) Regulation of substrate recognition by the MiaA tRNA prenyltransferase modification enzyme of *Escherichia coli* K-12, *J. Biol. Chem. 272*, 13073-13083.

11. Soderberg, T. and Poulter, C. D. (2000) *Escherichia coli* dimethylallyl diphosphate:tRNA dimethylallyltrasferase: essential elements for recognition of tRNA substrates within the anticodon stem-loop, *Biochemistry 39*, 6546-6553.

12. Gefter, M. L. (1969) The in vitro synthesis of 2'-omethylguanosine and 2-methylthio $^6$N ($\gamma$,$\gamma$ dimethylallyl) adenosine in transfer RNA, *Biochem. Biophys. Res. Com. 36*, 435-411.

13. Rosenberg, A. H. and Gefter, M. L. (1969) An iron-dependent modification of several transfer RNA species in *Escherichia coli*, *J. Mol. Biol. 46*, 581-584.

14. Buck, M. and Griffiths, E. (1982) Iron mediated methylthiolation of tRNA as a regulator of operon expression in *Escherichia coli*, *Nucleic Acids Res. 10*, 2609-2624.

15. Esberg, B., Leung, E. H. C., Tsui, H.-C. T., Björk, G. R., and Winkler, M. E. (1999) Identification of the *miaB* gene, involved in methylthiolation of isopentenylated A37 derivative in the tRNA of *Salmonella typhimurium* and *Escherichia coli*, *J. Bacteriol. 181*, 7256-7265.

16. Pierrel, F., Björk, G. R., Fontecave, M., and Atta, M. (2002) Enzymatic modification of tRNAs. MiaB is an iron-sulfur protein, *J. Biol. Chem. 277*, 13367-13370.

17. Pierrel, F., Hernández, H., Johnson, M. K., Fontecave, M., and Atta, M. (2003) MiaB protein from *Thermotoga maritima*: Characterization of an extremely thermophilic tRNA-methylthiotransferase, *J. Biol. Chem. 278*, 29515-29524.

18. Sofia, H. J., Chen, G., Hetzler, B. G., Reyes-Spindola, J. F., and Miller, N. E. (2001) Radical SAM, a novel protein superfamily linking unresolved steps in familiar biosynthetic pathways with radical mechanisms: Functional characterization using new analysis and information visualization methods, *Nucleic Acids Res. 29*, 1097-1106.

19. Cheek, J. and Broderick, J. B. (2001) Adenosylmethionine-dependent iron-sulfur enzymes: versatile clusters in a radical new role, *J. Biol. Inorg. Chem. 6*, 209-226.

20. Frey, P. A. (2001) Radical mechanisms of enzymatic catalysis, *Annu. Rev. Biochem. 70*, 121-148.

21. Fontecave, M. and Pierre, J.-L. (2001) Mechanisms of formation of free radicals in biological catalysis, *C. R. Acad. Sci. Paris, Chimie 4*, 531-538.

22. Pierrel, F., Douki, T., Fontecave, M., and Atta, M. (2004) MiaB protein is a bifunctional radical-*S*-adenosylmethionine enzyme involved in thiolation and methylation of tRNA, *Biochemistry 46*, 47555-47563.

23. Jarrett, J. T. (2005) The novel structure and chemistry of iron-sulfur clusters in the adenosylmethionine-dependent radical enzyme biotin synthase, *Arch. Biochem. Biophys. 433*, 312-321.

24. Lotierzo, M., Tse Sum Bui, B., Florentin, D., Escalettes, F., and Marquet, A. (2005) Biotin synthase mechanism: an overview, *Biochem. Soc. Trans. 33*, 820-823.

25. Miller, J. R., Busby, R. W., Jordan, S. W., Cheek, J., Henshaw, T. F., Ashley, G. W., Broderick, J. B., Cronan, J. E., and Marletta, M. A. (2000) *Escherichia coli* LipA is a lipoyl synthase: *in vitro* biosynthesis of lipoylated pyruvate dehydrogenase complex from octanoyl-acyl carrier protein, *Biochemistry 39*, 15166-15178.

26. Rubach, J. K., Brazzolotto, X., Gaillard, J., and Fontecave, M. (2005) Biochemical characterization of the HydE and HydG iron-only hydrogenase maturation enzymes from *Thermotoga maritima*, *FEBS Lett. 579*, 5055-5060.

27. Ugulava, N. B., Surerus, K. K., and Jarrett, J. T. (2003) Evidence from Mössbauer spectroscopy for distinct $[2Fe\text{-}2S]^{2+}$ and $[4Fe\text{-}4S]^{2+}$ cluster binding sites in biotin synthase from *Escherichia coli*, *J. Am. Chem. Soc. 124*, 9050-9051.

28. Cosper, M. M., Krebs, B., Hernandez, H., Jameson, G., Eidsness, M. K., Huynh, B. H., and Johnson, M. K. (2004) Characterization of the cofactor content of *Escherichia coli* biotin synthase, *Biochemistry 43*, 2007-2021.

29. Cicchillo, R. M., Lee, K.-H., Baleanu-Gogonea, C., Nesbitt, N. M., Krebs, C., and Booker, S. J. (2004) *Escherichia coli* lipoyl synthase binds two distinct [4Fe-4S] clusters per polypeptide, *Biochemistry 43*, 11770-11781.

30. Berkovitch, F., Nicolet, Y., Wan, J. T., Jarrett, J. T., and Drennan, C. L. (2004) Crystal structure of biotin synthase, an *S*-adenosylmethionine-dependent radical enzyme, *Science 303*, 76-79.

31. Tse Sum Bui, B., Mattioli, T., Florentin, D., Bolbach, G., and Marquet, A. (2006) *Escherichia coli* biotin synthase produces selenobiotin. Further evidence of the involvement of the $[2Fe\text{-}2S]^{2+}$ cluster in the sulfur insertion step, *Biochemistry 45*, 3824-3834.

32. Cicchillo, R. M. and Booker, S. J. (2005) Mechanistic investigations of lipoic acid biosynthesis in Escherichia coli: Both sulfur atoms in lipoic acid are contributed by the same lipoyl synthase polypeptide, *J. Am. Chem. Soc. 127*, 2860-2861.

33. Hänzelmann, P., Hernández, H., Menzel, C., Garcìa-Serres, R., Huynh, B. H., Johnson, M. K., Mendel, R. R., and Schindelin, H. (2004) Characterization of MOCS1A, an oxygen-sensitive iron-sulfur protein involved in human molybdenum cofactor biosynthesis, *J. Biol. Chem. 279*, 34721-34732.

34. Hänzelmann, P. and Schindelin, H. (2004) Crystal structure of the *S*-adenosylmethionine-dependent enzyme MoaA and its implications for molybdenum cofactor deficiency in humans, *Proc. Natl. Acad. Sci. USA 101*, 12870-12875.

35. Hänzelmann, P. and Schindelin, H. (2006) Binding of 5'-GTP to the C-terminal FeS cluster of the radical S-adenosylmethionine enzyme MoaA provides insights into mechanism, *Proc. Natl. Acad. Sci. USA 103*, 6829-6834.

36. Cosper, M. M., Jameson, G. N. L., Eidsness, M. K., Huynh, B. H., and Johnson, M. K. (2002) Recombinant *Escherichia coli* biotin synthase is a $[2Fe\text{-}2S]^{2+}$ protein in whole cells, *FEBS Lett. 529*, 332-336.

37. Fish, W. W. (1988) Rapid colorimetric micromethod for the quantitation of complexed iron in biological samples, *Meth. Enzymol. 158*, 357-364.

38. Drozdzewski, P. M. and Johnson, M. K. (1988) A simple anaerobic cell for low temperature Raman spectroscopy, *Appl. Spectrosc. 42*, 1575-1577.

39. Ravi, N., Bollinger, J. M., Huynh, B. H., Edmondson, D. E., and Stubbe, J. (1994) Mechanism of assembly of the tyrosyl radical-diiron(III) cofactor of *E. coli* ribonucleotide reductase. 1. Mössbauer characterization of the diferric radical precusor, *J. Am. Chem. Soc. 116*, 8007-8014.

40. Czernuszewicz, R. S., Macor, K. A., Johnson, M. K., Gewirth, A., and Spiro, T. G. (1987) Vibrational mode structure and symmetry in proteins and analogues containing $Fe_4S_4$ clusters: Resonance Raman evidence for different degrees of distortion in HiPIP and ferredoxin, *J. Am. Chem. Soc. 109*, 7178-7187.

41. Spiro, T. G., Czernuszewicz, R. S., and Han, S. (1988) Iron-sulfur proteins and analog complexes, in *Resonance Raman spectra of heme and metalloproteins* (Spiro, T. G., Ed.) Ist ed., pp 523-554, John Wiley & Sons, New York.

42. Middleton, P., Dickson, D. P. E., Johnson, C. E., and Rush, J. D. (1978) Interpretation of the Mössbauer spectra of the four-iron ferredoxin from *Bacillus stearothermophilus*, *Eur. J. Biochem. 88*, 135-141.

43. Mathews, R., Charlton, S., Sands, R. H., and Palmer, G. (1974) On the nature of the spin coupling between the iron-sulfur clusters in the eight-iron ferredoxins, *J. Biol. Chem. 249*, 4326-4328.

44. Duin, E. C., Lafferty, M. E., Crouse, B. R., Allen, R. M., Sanyal, I., Flint, D. H., and Johnson, M. K. (1997) [2Fe-2S] to [4Fe-4S] cluster conversion in *Escherichia coli* biotin synthase, *Biochemistry 36*, 11811-11820.

45. Ollagnier-de-Choudens, S., Sanakis, Y., Hewitson, K. S., Roach, P., Baldwin, J. E., Münck, E., and Fontecave, M. (2000) Iron-sulfur center of biotin synthase and lipoate synthase, *Biochemistry 39*, 4165-4173.

46. Ugulava, N. B., Sacanell, C. J., and Jarrett, J. T. (2001) Spectroscopic changes during a single turnover of biotin synthase: Destruction of a [2Fe-2S] cluster accompanies sulfur insertion, *Biochemistry 40*, 8352-8358.

**Scheme 7.1**

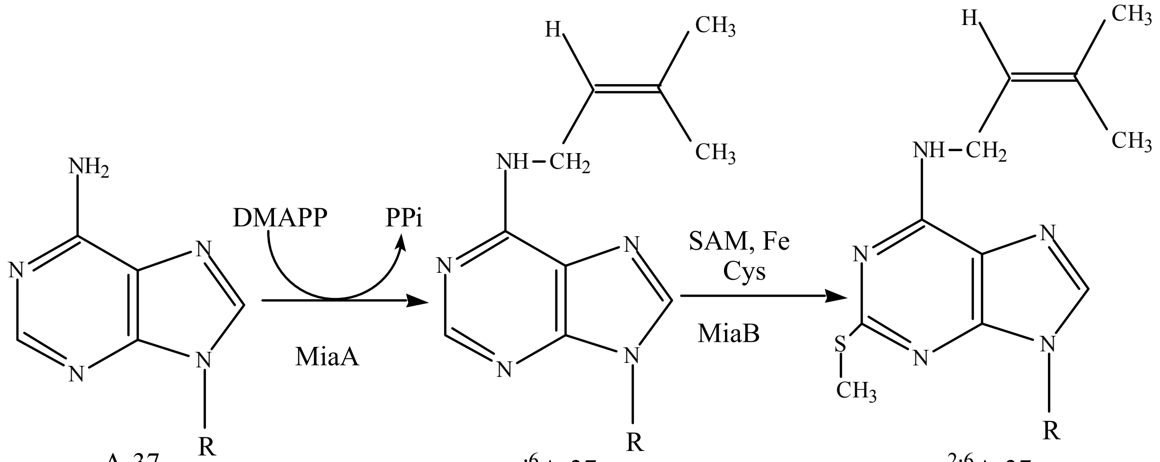
DMAPP
PPi
MiaA
SAM, Fe
Cys
MiaB

A-37
(Adenosine at tRNA
position 37)

$i^6$A-37
(N6-isopentenyl)-adenosine-37)

ms$^2$i$^6$A-37
(2-methylthio-N6-isopentenyl-
adenosine-37)

**Figure 7.1** UV/visible absorption spectra of reconstituted wild-type (black) and C150/154/157A (red) *T. maritima* MiaB. The buffering medium was 100 mM Tris, pH 8.0, with 200 mM NaCl and the sample concentrations were 108 μM and 194 μM for wild-type and the C150/154/157A variant, respectively. The spectra were recorded in 1-mm cuvettes and the molar extinction coefficients are based on protein concentrations.

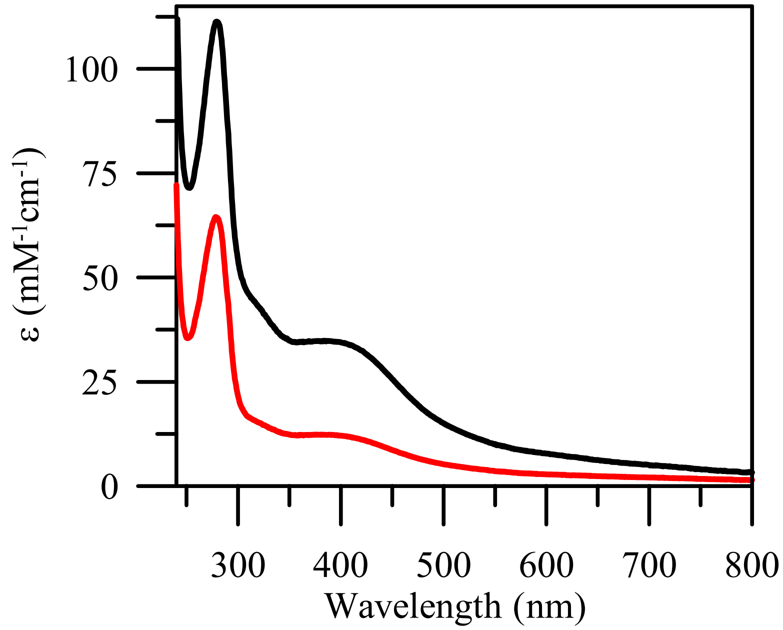
ε (mM$^{-1}$cm$^{-1}$)
100
75
50
25
0
300
400
500
600
700
800
Wavelength (nm)

**Figure 7.2** Resonance Raman spectra of reconstituted wild-type (black) and C150/154/157A (red) *T. maritima* MiaB. The resonance Raman spectra were recorded with 458-nm excitation, using samples in the form of frozen droplet at 17 K that were in 100 mM Tris-HCl buffer, pH 8.0, with 200 mM NaCl and ~3 mM in MiaB. Each scan involved photon counting for 1 s at 0.5 $\mathrm{cm}^{-1}$ increments with 8-$\mathrm{cm}^{-1}$ spectral resolution, and each spectrum is the sum of ~100 scans. Bands originating from lattice modes of ice and a linear ramp fluorescent background have been subtracted from each spectrum.

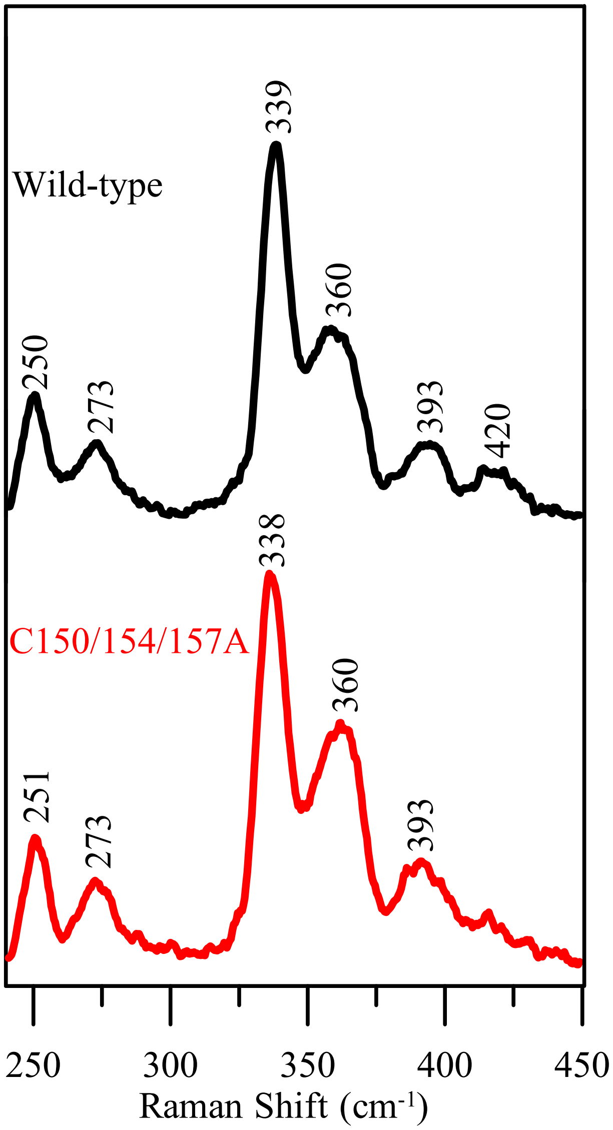
Wild-type
339
360
250
273
393
420
C150/154/157A
338
360
251
273
393
250
300
350
400
450
Raman Shift (cm-1)

**Figure 7.3** Mössbauer spectra (hatched marks) of reconstituted wild-type and C150/154/157A *T. maritima* MiaB. The samples were reconstituted from apo proteins with $^{57}Fe(NH_4)_2(SO_4)_2$ and were in 100 mM Tris-HCl buffer, pH 8.0, with 200 mM NaCl. The solid black lines are composite simulations constructed from $S$ = 0 $[4Fe\text{-}4S]^{2+}$ centers comprising two equal intensity valence delocalized pairs with $\delta$ = 0.46 mm/s and $\Delta E_Q$ = 1.27 mm/s and $\delta$ = 0.44 mm/s and $\Delta E_Q$ = 1.03 mm/s (green), $S$ = 1/2 $[4Fe\text{-}4S]^{+}$ simulated with the parameters reported for reduced *Bacillus stearothermophilus* ferredoxin (red), and an extraneous ferrous species (blue). (A) Reconstituted wild-type MiaB (109 μM) simulated with 29% of the $^{57}Fe$ in $[4Fe\text{-}4S]^{+}$ clusters and 71% of the $^{57}Fe$ in $[4Fe\text{-}4S]^{2+}$ clusters. (B) Reconstituted C150/154/157A MiaB (336 μM) simulated with 42% of the $^{57}Fe$ in $[4Fe\text{-}4S]^{+}$ clusters, 48% of the $^{57}Fe$ in $[4Fe\text{-}4S]^{2+}$ clusters and 10% of the $^{57}Fe$ in an extraneous Fe(II) species. The spectra were recorded at 4.2 K in a magnetic field of 50 mT oriented parallel to the γ-ray beam.

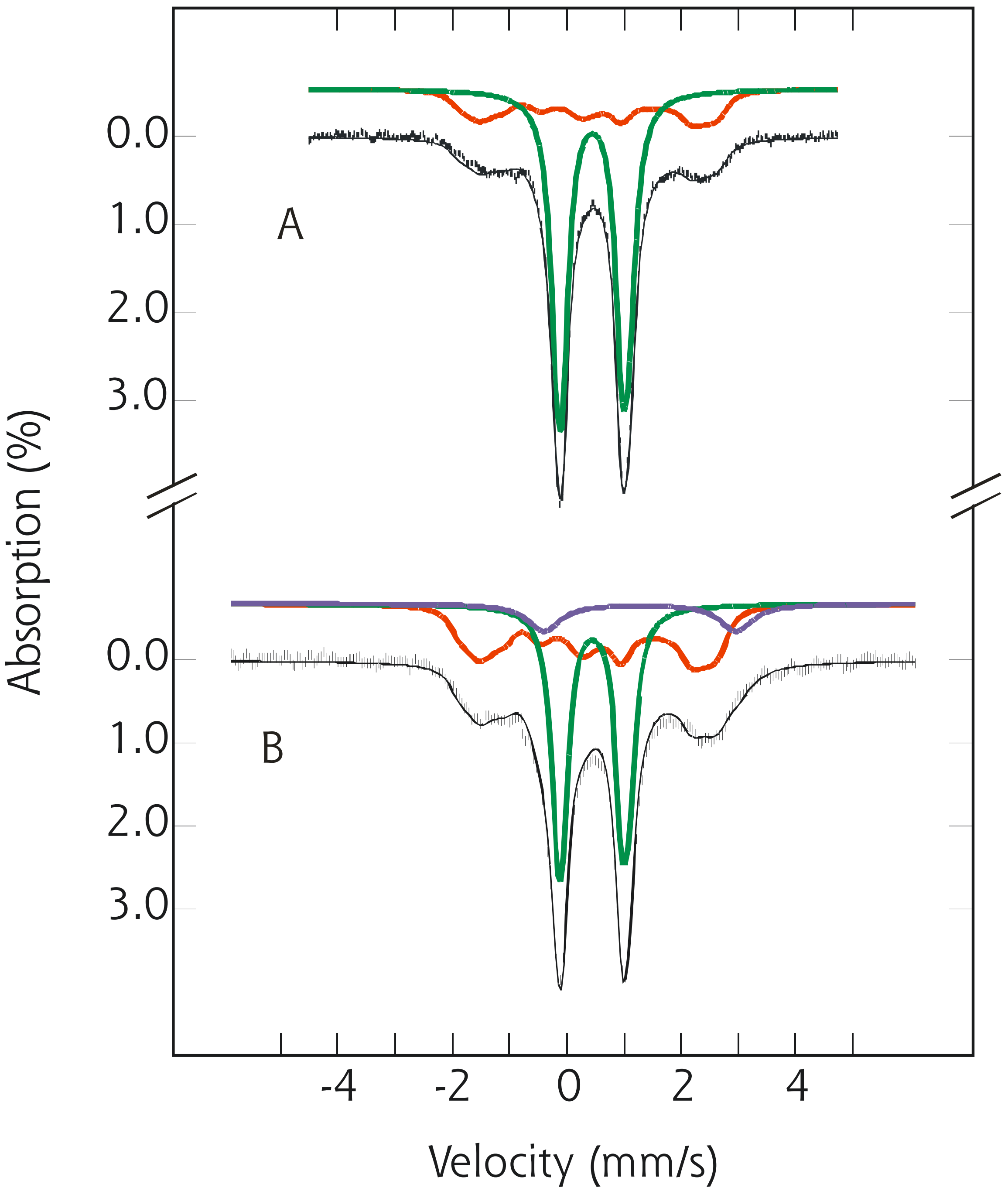
0.0
1.0
2.0
3.0
A
0.0
1.0
2.0
3.0
B
Absorption (%)
-4
-2
0
2
4
Velocity (mm/s)

**Figure 7.4** X-band EPR spectra of reconstituted wild-type (black) and C150/154/157A (red) *T. maritima* MiaB: (a) dithionite-reduced in the *S* = 3/2 region; (b) dithionite-reduced in the *S* = 1/2 region; (c) as prepared Mössbauer samples in the *S* = 1/2 region. The samples are described in Figures 7.1 and 7.3 and were reduced anaerob1cally with a 10-fold excess of sodium dithionite. Spectra were recorded at 20 K with a microwave power of 10 mW in the *S* = 1/2 region and at 4.2 K with a microwave power of 50 mW in the *S* = 3/2 region. The modulation amplitude was 0.64 mT and the microwave frequency was 9.59 GHz for all spectra.

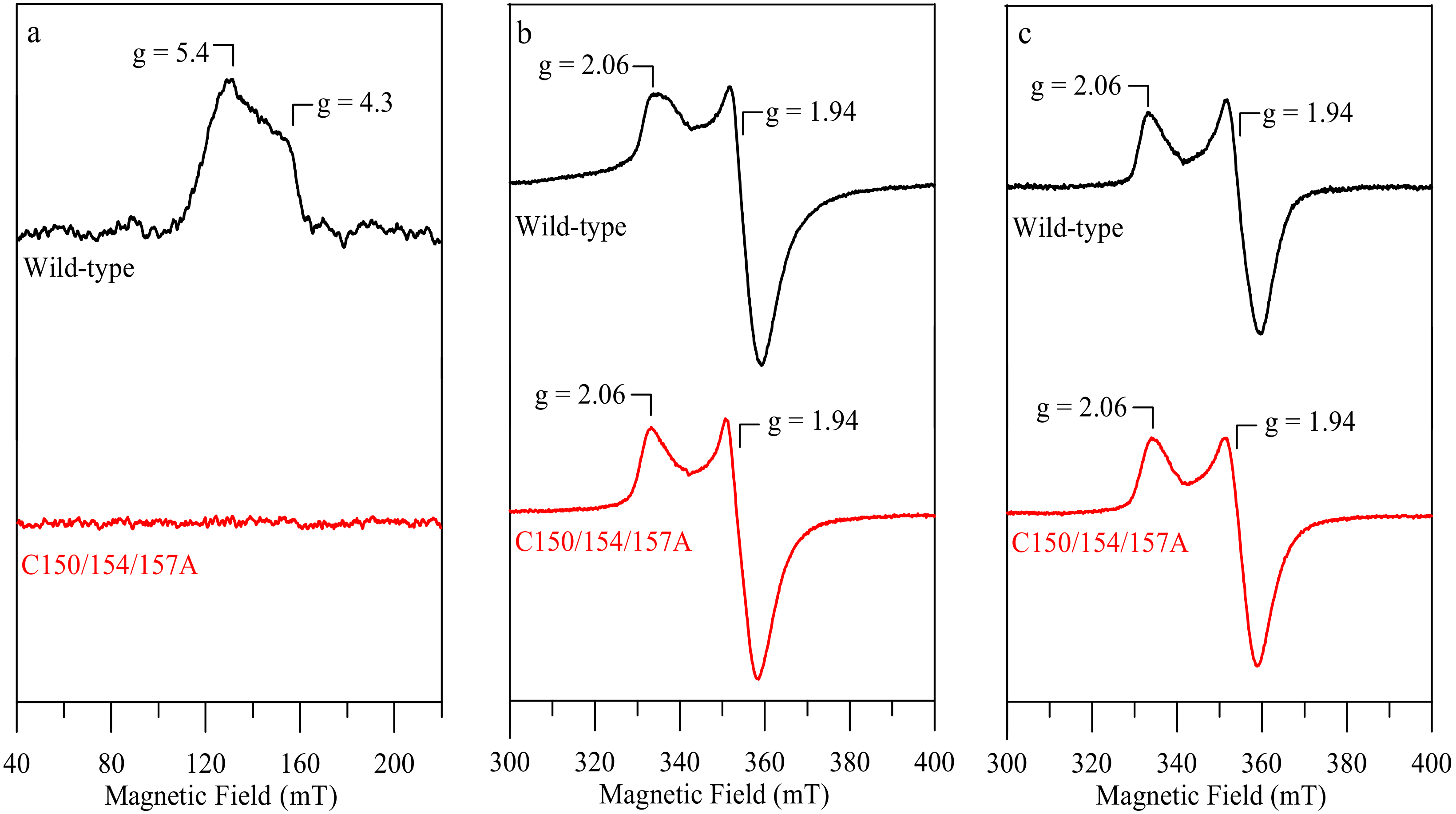
a
g = 5.4
g = 4.3
Wild-type
C150/154/157A
40
80
120
160
200
Magnetic Field (mT)
b
g = 2.06
g = 1.94
Wild-type
g = 2.06
g = 1.94
C150/154/157A
300
320
340
360
380
400
Magnetic Field (mT)
c
g = 2.06
g = 1.94
Wild-type
g = 2.06
g = 1.94
C150/154/157A
300
320
340
360
380
400
Magnetic Field (mT)

**Figure 7.5** Resonance Raman (*left panel*) and EPR (*right panel*) spectra of reconstituted C150/154/157A MiaB in the absence (a) and presence (b) of a 6-fold excess of the $i^6$A-37-tRNA substrate. The MiaB samples were 0.19 mM before addition of $i^6$A-37-tRNA and 0.16 mM after addition of $i^6$A-37-tRNA. The EPR samples were reduced with a 10-fold excess of sodium dithionite and the sample and measurement conditions used in recording the resonance Raman and EPR spectra are as described in Figures 7.2 and 7.4, respectively.

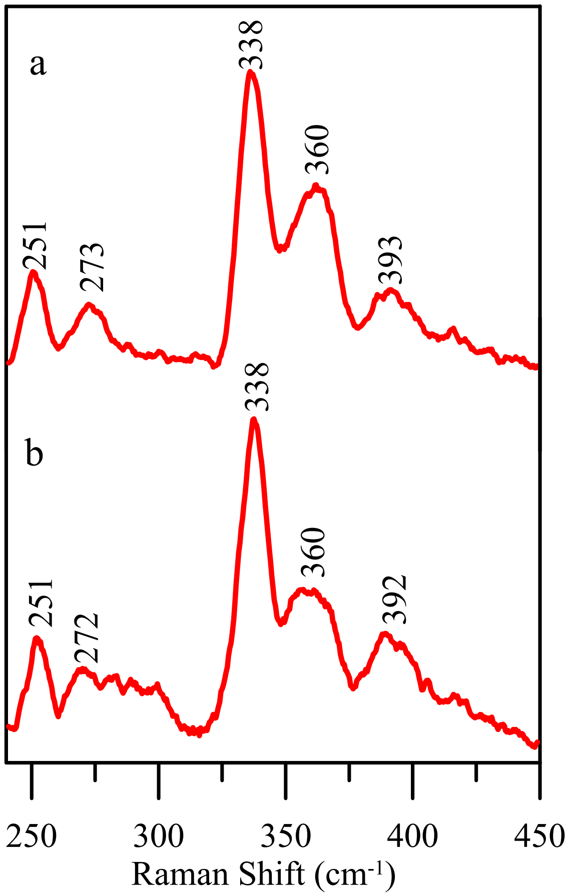
a
b
251
273
338
360
393
251
272
338
360
392
250
300
350
400
450
Raman Shift (cm$^{-1}$)

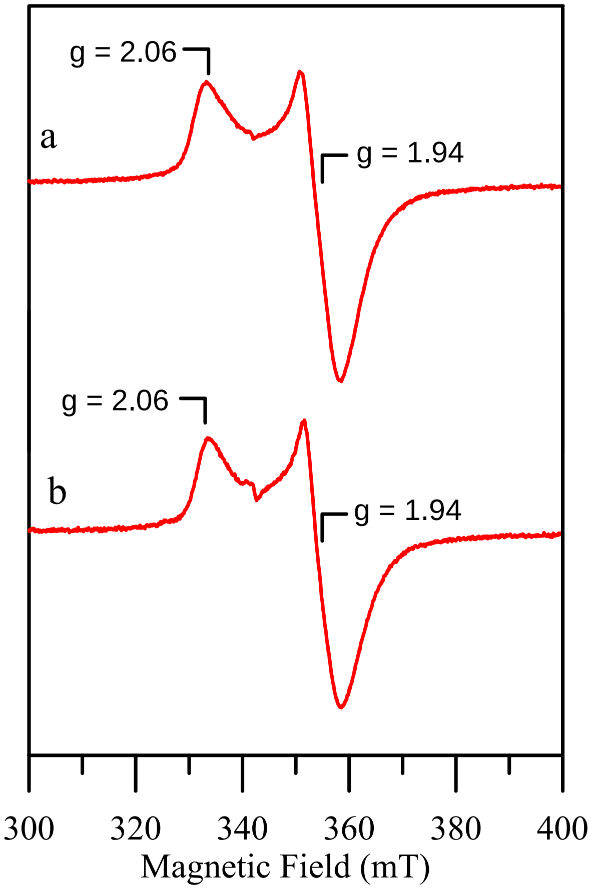
a
g = 2.06
g = 1.94
b
g = 2.06
g = 1.94
300
320
340
360
380
400
Magnetic Field (mT)